Biophysical and electrophysiological studies of transcranial electrical stimulation in human in-vivo using simultaneous stereoelectroencephalographic recordings in focal drug-resistant epilepsy and face recognition

Samuel Louviot

▶ **To cite this version:**

Samuel Louviot. Biophysical and electrophysiological studies of transcranial electrical stimulation in human in-vivo using simultaneous stereoelectroencephalographic recordings in focal drug-resistant epilepsy and face recognition. Human health and pathology. Université de Lorraine, 2022. English. NNT : 2022LORR0102 . tel-03827036

HAL Id: tel-03827036
https://hal.univ-lorraine.fr/tel-03827036

Submitted on 24 Oct 2022

HAL is a multi-disciplinary open access archive for the deposit and dissemination of scientific research documents, whether they are published or not. The documents may come from teaching and research institutions in France or abroad, or from public or private research centers.

L'archive ouverte pluridisciplinaire **HAL**, est destinée au dépôt et à la diffusion de documents scientifiques de niveau recherche, publiés ou non, émanant des établissements d'enseignement et de recherche français ou étrangers, des laboratoires publics ou privés.

UNIVERSITÉ DE LORRAINE | BIBLIOTHÈQUES UNIVERSITAIRES

AVERTISSEMENT

Ce document est le fruit d'un long travail approuvé par le jury de soutenance et mis à disposition de l'ensemble de la communauté universitaire élargie.

Il est soumis à la propriété intellectuelle de l'auteur. Ceci implique une obligation de citation et de référencement lors de l'utilisation de ce document.

D'autre part, toute contrefaçon, plagiat, reproduction illicite encourt une poursuite pénale.

Contact bibliothèque : ddoc-theses-contact@univ-lorraine.fr
(Cette adresse ne permet pas de contacter les auteurs)

LIENS

Code de la Propriété Intellectuelle. articles L 122. 4
Code de la Propriété Intellectuelle. articles L 335.2- L 335.10
http://www.cfcopies.com/V2/leg/leg_droi.php
http://www.culture.gouv.fr/culture/infos-pratiques/droits/protection.htm

Ecole Doctorale BioSE (Biologie-Santé-Environnement)

Thèse

Présentée et soutenue publiquement pour l'obtention du titre de

DOCTEUR DE l'UNIVERSITE DE LORRAINE

Mention : « Sciences de la Vie et de la Santé »

par **Samuel LOUVIOT**

Études biophysiques et électrophysiologiques de la stimulation électrique transcrânienne chez l'homme *in-vivo* à l'aide d'enregistrements stéréoélectroencéphalographiques simultanés dans l'épilepsie focale pharmacoresistante et en reconnaissance des visages

le 8 Juin 2022 à Nancy

Rapporteurs :	M. Jean-Pascal LEFAUCHEUR	Professeur des universités-Praticien hospitalier, Université de Paris-Est Créteil, Créteil, France
	M. Lucas PARRA	Professeur, City College Of New York, New York, USA
Examinateurs :	Mme. Isabelle MERLET	Chargée de recherche INSERM, Université de Rennes, Rennes, France
	Mme. Agnès TREBUCHON	Professeure des universités-Praticien hospitalier, Université de Aix-Marseille, Marseille, France (**présidente du jury**)
	M. Serge VULLIEMOZ	Professeur des universités-Praticien hospitalier, Université de Genève, Genève, Suisse
	Mme. Louise TYVAERT	Professeure des universités-Praticien hospitalier, Université de Lorraine, Nancy, France (**directrice de thèse**)
	M. Laurent KOESSLER	Chargé de recherche CNRS, Université de Lorraine, Nancy, France (**directeur de thèse**)
Membre invité :	M. Jacek DMOCHOWSKI	Professeur, City College of New York, New York, USA

CRAN UMR7039, CNRS-Université de Lorraine, Campus Sciences, Boulevard des Aiguillettes, 54506 Vandoeuvre-lès-Nancy, France

Remerciements

Avant toute chose, je tiens à adresser mes plus sincères remerciements aux personnes qui m'ont aidé, accompagné, qui ont été là pour moi durant ce très long périple.

Tout d'abord, je tiens à exprimer ma gratitude à mes directeurs de thèse : Louise Tyvaert pour ses analyses et points de vue intéressants sur certaines questions scientifiques et pour son aide pour le financement de mon déplacement à New York. Laurent Koessler pour m'avoir choisi pour ce projet de thèse, pour son aide, pour m'avoir enseigné les rouages et les règles du jeu de la science, le raisonnement, la rigueur scientifique et l'esprit critique. C'est grâce à vos enseignements que je peux désormais aborder le futur en science sans appréhension. Merci également pour la soumission du projet DrEAM et de l'ACI pour mon déplacement à New York.

Je remercie le laboratoire du CRAN et son directeur Didier Wolf pour m'avoir accueilli afin de mener cette thèse ainsi que pour le soutien financier pour mon déplacement à New York. Merci également à Bruno Rossion pour ses précieux conseils en cognition et notamment pour m'avoir permis de suivre les cours de neuroanatomie au King's College de Londres.

Je voudrais ensuite remercier l'équipe de l'unité d'épileptologie du Pr. Louis Maillard du CHRU de Nancy : merci à tous les médecins particulièrement au Pr. Louis Maillard lui-même pour ses conseils, pour avoir donné une place spéciale à la recherche au sein de l'unité. Merci au Dr. Olivier Aron pour sa gentillesse, sa grande disponibilité, pour avoir répondu à tant de questions et pour tous les services rendus, merci de m'avoir tant facilité la vie à l'hôpital !

Impossible de parler de l'unité d'épileptologie sans mentionner les infirmières, infirmiers, aides-soignantes et aides-soignants. Un immense merci à Julien Clabaut, Sylvie Claudel, Céline Demangeon, Karine Eigelthinger, Cecilia Florentin, Justine Glasse, Céline Grau, Emanuelle Maginot, Patricia Kern, André Paul, Christelle Piochaud, Christine Raoulx, Ludivine Rohrer, Jackie Valtin pour le travail que vous faites, votre bonne humeur à toute épreuve, merci de m'avoir soutenu dans les moments difficiles, merci pour ces pause-café. Venir vous voir était comme revenir à la surface pour prendre une bouffée d'oxygène. Merci pour les innombrables services que vous m'avez rendus, votre soutiens humain et logistique pour mes expérimentations, vous avez joué un rôle central dans cette thèse, encore merci.

À Jacek Dmochowski, pour m'avoir accueilli au sein de son laboratoire au City College of New York, pour m'avoir fait découvrir la recherche de l'autre côté de l'Atlantique, pour son aide en modélisation, pour les super moments passés avec son équipe. Merci notamment à Destiny Berisha et Duc Nguyen pour leur aide dans la jungle de New York, Prakhyat Sigh pour les moments de partage, Amilcar Malave pour les séances de débats, de sport et de basketball et à Andrea Corti (du labo voisin) pour les sorties en ville.

Un grand merci à Nelson Alves et à Yanis Menzer pour leur énorme travail et leur contribution à cette thèse. Merci à Radu Ranta et Steven Le Cam pour leurs conseils et leur aide en programmation et traitement du signal. À Denis Netter pour sa vision précieuse sur l'électromagnétisme et qui m'a enlevé une sacrée épine du pied !

À mes amis : Angélique Volfart et Harry Tran pour avoir répondu à toutes mes questions ! Merci Harry d'avoir aidé et accompagné le nouveau stagiaire perdu que j'étais. À Pierre Riff également pour son aide indispensable lors de mes expérimentations et analyses, pour les moments passés en pause-café/muffin à parler jeux vidéo. Merci pour ton soutien à tous les niveaux. Merci à Stéphanie Matt, Pauline Jurczynski, Viviana Del Rocio Hernandez Castanon, Natacha Forthoffer, Pierre Mirguet, pour avoir été là et pour votre soutien. Bien sûr merci à Fabien Bessière d'avoir été présent lors des moments difficiles, pour nos passionnantes discussions, pour tes appels pendant le confinement et pour nos péripéties à New York !

À ceux qui ont été présents depuis la prépa, à mes frères d'armes : Maxime Coccetta, Maxime Huther et Mike Holler. Force et honneur à vous.

Je remercie, évidemment ma famille, qui a joué un rôle essentiel : ma mère, mon père, ma sœur Joy et le beau-frère Florian, ma tante Mairead Louviot et mon oncle Vincent Louviot merci pour absolument tout le soutien moral, financier, humain, logistique, que vous m'avez apporté.

Et enfin, bien sûr, mon éternelle gratitude à ma fiancée, Marisa Aquino, sans oublier Nitty Nat et toute l'équipage, pour nos moments de rigolade, de Nittyoke, de partage. Merci Marisa notamment pour avoir relu cette thèse et la relecture de l'article. Merci pour ton aide sur absolument tous les aspects, il me faudrait plus de deux pages pour écrire tout ce que tu as fait pour moi. Donc, simplement merci du fond du cœur.

Acknowledgements

First and foremost, I would like to give my sincerest thanks to the people who helped me, accompanied me, who were there for me during this very long journey.

First, I would like to express my gratitude to my supervisors: Louise Tyvaert for her analyses, the interesting points of view on some scientific questions, and for her help in financing my trip to New York. Laurent Koessler for having chosen me for this project, for your help, for having taught me the workings and rules of science, reasoning, scientific rigor and critical thinking. It is thanks to your teachings that I can now approach the future in science without apprehension. Thank you notably for the submission of the DrEAM project, and the ACI for my trip to New York.

I would like to thank the CRAN laboratory and its director Didier Wolf for welcoming me to conduct this thesis, and for the financial support for my trip to New York. I would also like to thank Bruno Rossion for his precious advice in cognition, and especially for allowing me to attend the neuroanatomy courses at the King's College of London.

Thank you to the epileptology unit team of Pr. Louis Maillard at the CHRU of Nancy: to all the physicians, especially to Pr. Louis Maillard himself for his advice, and for giving me a special place to research within the unit. To Dr. Olivier Aron for his kindness, his great availability, for having answered so many questions and for all the services rendered -- thank you for making my life at the hospital so much easier!

It is impossible to talk about the epileptology unit without mentioning the nurses. With tremendous gratitude to Julien Clabaut, Sylvie Claudel, Céline Demangeon, Karine Eigelthinger, Cecilia Florentin, Justine Glasse, Céline Grau, Emanuelle Maginot, Patricia Kern, André Paul, Christelle Piochaud, Christine Raoulx, Ludivine Rohrer, Jackie Valtin for the work you do, your unfailing good humor, supporting me in difficult moments, and of course the coffee breaks. Coming to see you was like coming to the surface to take a breath of air. Thank you for the innumerable services, your human and logistical support for my experiments -- you played a central role in this thesis.

To Jacek Dmochowski, for having welcomed me in his laboratory at the City College of New York, for having made me discover research on the other side of the Atlantic, for his help in modeling, and the great moments spent with his team. Special thanks to Destiny Berisha and Duc Nguyen for their help in the New York jungle, Prakhyat Sigh for the moments of sharing, Amilcar Malave for the debates, gym, and basketball sessions and to Andrea Corti (from the nearby lab) for the city outings.

Many thanks to Nelson Alves and Yanis Menzer for their tremendous work and contribution to this thesis. To Radu Ranta and Steven Le Cam for their advice and help in programming and signal processing. Also, to Denis Netter for his precious vision on electromagnetism and who removed a thorn from my side!

To my friends: Angélique Volfart and Harry Tran for answering all my questions! Thank you, Harry, for helping and accompanying the new lost trainee that I was. Thanks to Pierre Riff for his indispensable help during my experiments and analyses, for the moments spent in coffee/muffin breaks talking about video games. Thanks for your support at all levels. To Stéphanie Matt, Pauline Jurczynski, Viviana Del Rocio Hernandez Castanon, Natacha Forthoffer, Pierre Mirguet, for being there and for your support. Of course, thank you to Fabien Bessière for being present during the difficult moments, for our exciting discussions, for your calls during the confinement and for our adventures in New York!

To those who have been present since prep school, to my brothers in arms: Maxime Coccetta, Maxime Huther and Mike Holler. Strength and honor to you.

My very heartfelt gratitude to my family, who played an essential role, my mother, my father, my sister Joy and my brother-in-law Florian, my aunt Mairead Louviot and my uncle Vincent Louviot, for absolutely all the moral, financial and human support that you have given me.

And finally, my eternal gratitude to my fiancée, Marisa Aquino, and Nitty Nat and the crew, for our precious moments shared, the laughter and of course Nittyoke. Thank you, Marisa, for proofreading this thesis and the article. I am forever grateful for your help with absolutely every aspect -- it would take me more than two pages to write everything you've done for me. Thank you from the bottom of my heart.

Table of contents

To my parents,
my sister and Marisa,
the stars guiding, at night,
the lost sailor I was

"*Ideas do not always come in a flash but by diligent trial-and-error experiments that take time and thought.*"

Charles K. Kao (1933-2018),
Physics Nobel Prize 2009

List of abbreviations

AC	Alternative Current
CSF	Cerebro-Spinal Fluid
CT	Computerized Tomography
DBS	Deep Brain Stimulation
DC	Direct Current
ECoG	Electrocorticography
EEG	Electroencephalography
EF	Electric Field
ERP	Evoked Related Potential
FEM	Finite Element Method or Finite Element Model
FFT	Fast Fourier Transform
FPVS	Fast Periodic Visual Stimulation
GND	Ground
IED	Interictal Epileptiform Discharges
iEF	intracerebral Electric Field
MEP	Motor Evoked Potential
MRI	Magnetic Resonance Imaging
PET	Positron Emission Tomography
ROI	Region Of Interest
SE	Standard Error
SEEG	Stereoelectroencephalography
SNR	Signal Noise Ratio
SSVEP	Steady State Visual Evoked Potential
tACS	transcranial Alternative Current Stimulation
tDCS	Transcranial Direct Current Stimulation
TES	Transcranial Electrical Stimulation
TL	Temporal Lobe
VOTC	Ventral Occipito-Temporal Cortex
VVS	Visual Ventral Stream

Résumé de la thèse en Français

I. Introduction et contexte scientifique

La stimulation électrique transcrânienne (TES pour *Transcranial Electrical Stimulation*) est une méthode de stimulation cérébrale non-invasive consistant à injecter un courant de faible amplitude via deux ou plusieurs électrodes placées sur le cuir chevelu. Sa dénomination change en fonction de la forme d'onde utilisée comme c'est le cas lors d'une stimulation à courant alternatif sinusoïdal (tACS pour *transcranial Alternative Current Stimulation*) ou lors d'une stimulation à courant continu (tDCS pour *transcranial Direct Current Stimulation*). La TES a connu ces vingt dernières années un engouement particulier de la part de la communauté scientifique. Sur PubMed le nombre de publications par an comprenant les mots-clefs « *Transcranial electrical stimulation* » est passé de 37 à 1181 en 21 ans (de 2000 à 2021).

Cependant, le fait d'appliquer un courant électrique sur le cuir chevelu dans un but thérapeutique ne date pas d'hier. On trouve des écrits datant de l'antiquité rapportant l'utilisation du poisson torpille de méditerranée dont la puissante décharge électrique permettait de guérir les migraines. C'est Scribonius Largus médecin de l'empire Romain qui, en l'an 43, fut le premier (ou du moins dont on possède la première trace écrite) à utiliser cette méthode. Il écrit dans son œuvre *Compositiones Medicae* que même les migraines chroniques les plus handicapantes parvenaient à être soignées par ce remède (Zago *et al.*, 2016). S'ensuit alors une longue tradition d'utilisation thérapeutique du poisson torpille durant le Moyen Âge par les médecins de l'empire Romain puis de l'empire Arabo-musulman dont Avicenna (Ou en francisé : Avicenne) (980–1037) qui utilisait ce remède dans le cas particulier de l'épilepsie. Enfin, l'utilisation maîtrisée de l'énergie électrique au XVIII^{ème} siècle a permis de procéder à des stimulations avec un contrôle sur l'intensité du courant. Depuis, l'exploration de la stimulation électrique s'est faite à tâtons jusqu'à la moitié du XX^{ème} siècle où l'on commença à voir apparaitre des études fondamentales, notamment celle de l'effet produit par un champ électrique sur un neurone (Terzuolo and Bullock, 1956).

Les résultats très mitigés découlant des études comportementales chez l'Homme ont entrainé petit à petit l'abandon de la stimulation électrique transcrânienne au profit de l'électro-convulsivothérapie (Priori, 2003; Zago *et al.*, 2016). C'est à la fin des années 1990 et au début des années 2000 que des études électrophysiologiques chez l'Homme ont montré des résultats encourageants (Priori *et al.*, 1998; Nitsche and Paulus, 2000, 2001; Antal, Nitsche and Paulus, 2001) ce qui entraîna la réapparition de la TES dans la littérature scientifique (Priori, 2003; Lefaucheur, 2016).

Les dix dernières années furent marquées par des débats concernant l'efficacité de la TES et ses effets neurophysiologiques et comportementaux dont les méta-analyses de Horvath, Forte et Carter en 2014 et 2015, immédiatement réfutées par Antal et al., 2015. Ces questionnements et débats traduisent l'existence d'une zone d'ombre au niveau des connaissances dans le domaine des champs électriques générés dans le cerveau lors d'une TES. Par la suite, il a été démontré, grâce à des mesures intracérébrales chez l'Homme *post-mortem*, que le champ électrique généré par la TES sur les populations de neurones ne pouvait atteindre des valeurs entraînant une potentielle neuromodulation (Underwood, 2016; Vöröslakos *et al.*, 2018).

Plusieurs questions se posent alors, la première concerne la mesure intracérébrale d'un champ électrique chez l'Homme *in-vivo* et s'il est possible d'atteindre une valeur permettant d'influer *a minima* sur l'activité neuronal (valeurs supérieures ou égales à 0,14 $V \cdot m^{-1}$ selon Francis, Gluckman and Schiff, 2003). La deuxième question concerne l'application de ce champ électrique généré par la TES dans le cadre de neuropathologies et la mesure intracérébrale des effets neurophysiologiques induits. La troisième question est l'évaluation de l'effet de la TES sur des réponses électrophysiologiques associées à des fonctions cognitives particulières sans avoir recours à des études comportementales pouvant facilement être biaisées. Ainsi, afin de répondre à ces questions, les travaux de recherche de cette thèse se répartirons sur 3 axes :

- Un axe biophysique permettant de répondre à la question des champs électriques intracérébraux chez l'Homme *in-vivo*, passage indispensable établissant les bases pour la suite des travaux de cette thèse.
- Un axe électrophysiopathologique permettant de répondre à la question de l'effet de la TES dans le cadre de pathologie neurologique plus précisément dans l'épilepsie focale pharmaco-résistante.
- Un axe cognition permettant de répondre à la question de l'effet de la TES sur des réponses électrophysiologiques associées à des fonctions cognitives particulières permettant de s'affranchir d'études comportementales dont les résultats sont sensibles aux perturbations extérieures. Cet axe fera l'objet d'investigation des réponses associé à la reconnaissance des visages mis en évidence grâce à de la stimulation visuelle périodique rapide (FPVS).

Les études se feront chez des patients atteint d'épilepsie focale pharmaco-résistantes et qui entrent dans le cadre d'un bilan pré-chirurgical et donc faisant l'objet d'exploration stéréo-électroencéphalographique (SEEG) permettant ainsi de réaliser des enregistrements intracérébraux simultanés lors d'une TES.

II. Champs électriques intracérébraux générés par la TES

La question de la mesure des champs électriques intracérébraux chez l'Homme *in-vivo* est fondamentale, car sa valeur permet d'évaluer le pouvoir neuromodulateur de la TES. Seulement quatre études publiées ont exploré cette question via l'investigation electrocorticographique (ECoG) couplé à la SEEG, ou via des électrodes de stimulation électrique profonde (DBS pour *Deep Brain Stimulation*) (Opitz *et al.*, 2016; Huang *et al.*, 2017; Chhatbar *et al.*, 2018; Ruhnau *et al.*, 2018). Cependant, ces études présentent plusieurs limites. Premièrement, l'exploration ECoG requiert une craniotomie qui modifie considérablement la géométrie du milieu et, par ce fait, la distribution des champs électriques. De plus, l'ECoG ne permet que de mesurer la distribution du courant de manière transversale au niveau de la surface cortical et non en profondeur. Deuxièmement, les études réalisées grâce à la DBS ne possèdent pas un nombre suffisant de point de mesures intracérébrales, le calcul du champ électrique est réalisé entre deux points très éloignés fournissant ainsi des résultats très approximatifs.

La méthode d'exploration SEEG, quant à elle, permet de réaliser des investigations en profondeur avec une bonne résolution (1,5 mm d'espacement entre contacts) et de manière mini-invasive (vis de 2,45 mm de diamètre implantés dans le crâne). Malgré les nombreux avantages qu'offre cette méthode, la totalité des études mentionnées n'incluent que deux patients avec la SEEG.

Les épilepsies temporales concernent la majorité des épilepsies focales pharmaco-résistante et les structures du système limbique (amygdales, hippocampes, gyrus cingulaire) sont donc majoritairement explorées en SEEG. De plus, le système limbique est un réseau d'une importance capitale dans de nombreux processus cognitifs (mémoire, émotions etc…) et, de ce fait, impliqué dans un grand nombre de pathologies neurologiques (maladie d'Alzheimer, schizophrénie, dépression, épilepsie…). Ainsi, obtenir un champ électrique modulateur au sein du système limbique est d'un intérêt non-négligeable. Cette étude des champs électrique intracérébraux générés par la TES s'est ainsi focalisé sur trois structures du système limbique : l'hippocampe, l'amygdale et le gyrus cingulaire. L'influence de plusieurs facteurs sur le champ électrique, comme les paramètres de stimulations (dont la fréquence, l'intensité et le placement des électrodes) et la profondeur ont également été explorée.

La méthodologie de cette étude repose sur la stimulation tACS (courant alternatif sinusoïdal) à une intensité et à une fréquence donnée. Les amplitudes générées par la stimulation ont été enregistrées sur les différents contacts intracérébraux SEEG. Ces valeurs d'amplitudes ont été mesurées sur le spectre fréquentiel à la fréquence à laquelle la stimulation a été réalisée. Les valeurs de champs électriques ont été calculées en faisant la différence deux à deux des amplitudes sur les contacts adjacents le tout divisé par la distance séparant deux contacts intracérébraux (1,5 mm). Ainsi,

sur une même électrode SEEG, la magnitude du champ électrique E_n a été calculée de la façon suivante : $E_n = \frac{V_n - V_{n+1}}{1,5}$

Avec V_n et V_{n+1} les amplitudes mesurées sur les contacts intracérébraux *n* et *n*+1.

Les paramètres étudiés sont :

- L'intensité de stimulation. Deux intensités étudiées (0,5 mA et 1 mA) chez 6 sujets.
- La fréquence de stimulation. Sept fréquences de stimulation étudiées (1 Hz, 3 Hz, 7 Hz, 35 Hz, 71 Hz, 140 Hz et 300 Hz) chez un sujet.
- La position des électrodes. Quinze différents montages (C3-FT10; C3-T8; C3-C4; Cz-FT10; Cz-T8; Cz-C4; Fz-FT10; Fz-T8; Fz-C4; Fz-Cz; Fz-C3; Fz-T7, T7-FT10; T7-T8; T7-C4) réalisés chez un sujet.

Lors d'une stimulation à 1 mA à la fréquence de 300 Hz, les résultats montrent, chez les 8 sujets inclus, une valeur moyenne de champs électrique dans l'hippocampe de 0,17 ± 0,06 $V \cdot m^{-1}$ (avec un maximum de 0,38 $V \cdot m^{-1}$), dans l'amygdale de 0,21 ± 0,08 $V \cdot m^{-1}$ (avec un maximum 0,49 $V \cdot m^{-1}$) et de 0,07 ± 0,02 $V \cdot m^{-1}$ (avec un maximum de 0,11 $V \cdot m^{-1}$) au niveau du gyrus cingulaire. Ce qui donne une moyenne de 0,14 ± 0,08 $V \cdot m^{-1}$ dans la totalité des structures du système limbique explorées.

Il a également été observé qu'il existe une relation linéaire quasi-parfaite entre l'intensité de stimulation et les champs intracérébraux induits, c'est-à-dire lorsque l'intensité est doublée, les valeurs de champs sont doublées également (le coefficient directeur de la distribution de valeur des champs lors d'une stimulation à 0,5 mA comparé à une stimulation 1 mA est égal à 2, son ordonnée à l'origine entre 0 et 0,01 avec un coefficient de détermination $R^2 \geq 0.98$). Les résultats montrent par ailleurs une influence négligeable de la fréquence de stimulation. Ensuite, il a été établi que le montage délivrant un champ électrique maximal dans les structures du système limbique concerne les électrodes placées au niveau des deux lobes temporaux (T7-T8). Inversement, le montage délivrant les champs électriques, les plus faibles concerne les électrodes placées les plus proche l'une de l'autre au niveau du lobe frontal (Fz-Cz). Cela met en exergue notamment le phénomène de *shunt* par la peau du courant et confirme la meilleure pénétration de celui-ci lorsque les électrodes de stimulation sont les plus éloignées l'une de l'autre.

Pour finir, les valeurs de champs électriques diminuent en fonction de la profondeur suivant la loi de l'inverse carré confirmant ainsi chez l'Homme *in vivo* en intracérébral, les fondamentaux de l'électromagnétisme.

Cette étude, qui a fait l'objet d'une publication dans le journal *Brain Stimulation* (Louviot *et al.*, 2022), est la première à explorer avec autant de sujets exclusivement en SEEG les champs électriques intracérébraux (8 sujets explorés exclusivement en SEEG contre un total de deux sujets dans la littérature) notamment dans les structures du système limbique. Il a été établi chez l'Homme

in-vivo grâce à des mesures modifiant de manière négligeable les milieux intracérébraux (Datta, Bikson, et Fregni 2010), qu'il est possible de générer, avec la TES, un champ électrique étant susceptible de générer des effets stochastiques sur l'activité électrique neuronale (Bruce J Gluckman *et al.*, 1996; Stacey and Durand, 2000; Francis, Gluckman and Schiff, 2003; van der Groen and Wenderoth, 2016; Liu *et al.*, 2018). De plus, il a également été démontré expérimentalement que les théories biophysiques des champs électriques dans les tissues intracérébraux (influence négligeable de la fréquence de stimulation, relation linéaire entre intensité de stimulation et champs électrique, décroissance des champs en fonction de la profondeur) sont bel et bien applicable. Il est attendu que ces données expérimentales fournissent des connaissances fondamentales sur les valeurs de champs électriques intracérébraux pour de futures applications de la TES dans le cadre de pathologies neurologiques touchant le système limbique comme l'épilepsie.

III. La TES appliquée à l'épilepsie

L'application de la TES (plus précisément la tDCS, étant une stimulation à courant continu) dans l'épilepsie a déjà fait l'objet de nombreuses études cliniques (San-Juan *et al.*, 2015; Lefaucheur, 2016; Lefaucheur *et al.*, 2017; Regner *et al.*, 2018; San-juan *et al.*, 2019; Fregni *et al.*, 2021). Les résultats rapportent notamment une baisse du nombre de crises après l'application d'une ou de plusieurs sessions de stimulations (Fregni *et al.*, 2006; Auvichayapat *et al.*, 2013; Tekturk *et al.*, 2016; San-Juan *et al.*, 2017). De plus, d'un point de vue électrophysiologique, une modification du nombre d'apparitions de décharges paroxystiques intercritiques a été observé à l'EEG de surface après stimulation. Cependant, la grande variabilité des méthodologies et des résultats ne permet pas d'établir des recommandations quant à l'effet thérapeutique de la tDCS (Lefaucheur *et al.*, 2017) montrant la nécessité d'explorer encore l'effet électrophysiologique de la tDCS dans l'épilepsie. L'étude proposée dans cette thèse s'appuie sur l'exploration SEEG afin d'investiguer cet effet électrophysiologique directement sur site. L'analyse a été réalisée sur des biomarqueurs épileptiques que sont les décharges paroxystiques intercritiques. Le nombre d'occurrences de ces grapho-éléments ainsi que leurs amplitudes ont été scrutés avant, pendant et après tDCS.

La méthodologie se divise en 3 parties :

- L'identification de la zone irritative, foyer de l'activité intercritique (Talairach and Bancaud, 1966a; Kahane *et al.*, 2006) qui a été réalisée de manière automatisée grâce à un algorithme de détection (Janca *et al.*, 2013, 2014, 2018).
- Le choix du placement optimal des électrodes de stimulation afin de cibler la zone irritative qui a été réalisé grâce à la modélisation réaliste des champs électriques (Huang *et al.*, 2019) et à une méthode d'optimisation (Dmochowski *et al.*, 2011).
- L'expérimentation de stimulation comprenant 3 phases de 20 minutes :

- Phase 1 : Stimulation *placebo* (dite stimulation *Sham*) consistant à injecter un courant d'amplitude croissante pendant 30 secondes suivi d'une amplitude décroissante pendant 30 secondes. Ce pattern de stimulation a été réalisé au début puis à la fin des 20 minutes de la phase. Cela est effectué dans le but de faire ressentir au sujet les sensations cutanées d'une stimulation et ainsi de lui faire croire à une stimulation.
- Phase 2 : Stimulation tDCS à 1 ou 2 mA.
- Phase 3 : Stimulation placébo (idem que phase 1).

Chez 12 patients inclus, les résultats montrent une modulation d'amplitude significative de l'activité paroxystique intercritique chez 7 patients lors d'une stimulation à − 1 mA. Cependant, la modulation présente une certaine variabilité vis-à-vis de la polarité, car l'amplitude est soit augmentée en moyenne de + 14 ± 17 % chez 4 patients, soit diminuée en moyenne de − 21 ± 4 % chez 2 patients. Concernant le nombre d'occurrences, aucune modulation significative n'a été observée.

Cas unique d'une crise d'épilepsie survenant lors d'une tDCS :

Chez une patiente souffrant d'une épilepsie de l'opercule supérieur de l'insula gauche, le protocole mentionné précédemment a été réalisé. Les électrodes de stimulation ont été placées de manière à cibler la zone irritative localisée au même endroit que la zone épileptogène, c'est-à-dire au niveau de l'opercule supérieur de l'insula gauche. Après 8 minutes de stimulation à + 1 mA, la patiente a prévenu la survenue d'une crise entrainant l'arrêt immédiat de la stimulation. La crise enregistrée durant la tDCS fut comparée, via une analyse fréquentielle, avec quatre autres crises enregistrées la même semaine sans tDCS. Les résultats montrent une grande similarité des 4 crises survenues la semaine, mais une différence significative comparée à celle survenue durant la tDCS. En effet, comparé aux autres crises, celle survenue pendant la tDCS montre une activité de plus haute amplitude dans les basses fréquences, mais de plus basse amplitude dans les hautes fréquences. La durée de la crise durant tDCS a également été réduite de moitié.

Les résultats préliminaires découlant de ces études montrent des effets de la tDCS sur les manifestations électrophysiologiques et cliniques de l'épilepsie. Cependant, ces résultats restent mitigés et des questions restent en suspens notamment concernant la variabilité de la modulation (à la hausse ou à la baisse) pour une même polarité de stimulation. Les études mentionnées restent une preuve de concept de la faisabilité d'études en intracérébrales des effets de la TES sur l'électrophysiologie d'une pathologie et devrait encourager d'autres études à plus grande échelle et/ou multicentrique.

IV. La TES appliquée à la reconnaissance des visages

La réhabilitation cognitive est également une des potentielles applications de la TES. Une des solutions permettant d'étudier un processus cognitif est de mesurer l'activité électrophysiologique associée à ce processus via des potentiels évoqués. L'étude de la tDCS dans le cadre de ces potentiels évoqués a notamment été réalisée dans le domaine de la vision (Antal, Nitsche and Paulus, 2001; Antal, Kincses, *et al.*, 2004). La tDCS a aussi été étudiée dans le domaine de la reconnaissance des visages via la mesure d'un potentiel évoqué en EEG qui est associé à cette fonction cognitive spécifique : la N170 (Lafontaine *et al.*, 2013; Yang *et al.*, 2014; Civile *et al.*, 2020). Cependant, le mauvais rapport signal à bruit (SNR) et sa mauvaise spécificité (pouvant être confondu avec d'autres ondes similaires) (Bruno Rossion 2014a; Jacques, D'Arripe, et Rossion 2007) font de la N170 un biomarqueur cognitif s'avérant complexe à étudier lors d'une tDCS. Une autre solution existe : la stimulation visuelle périodique rapide (ou FPVS pour *Fast Periodic Visual Stimulation*) et son approche fréquentielle qui fournit un meilleur SNR et une qualité des résultats bien supérieure (Rossion, 2014b, 2014a, 2014c). Ainsi, c'est en s'appuyant sur l'expertise et le savoir-faire de l'équipe du *Face Categorization Lab* au sein du laboratoire que les réponses électrophysiologiques associées à la tâche cognitive de reconnaissance ou de perception des visages vont être évaluées lors d'une tDCS.

L'investigation électrophysiologique se fera à plusieurs niveaux :

- En intracérébral grâce à l'exploration SEEG de la voie visuelle ventrale chez des patients atteints d'épilepsies pharmaco-résistantes.
- En surface grâce à l'exploration EEG chez des sujets sains.

La méthodologie reposera sur des sessions de FPVS avant, pendant et après tDCS suivant le protocole expérimental décrit en partie III : Phase 1 Stimulation placébo, Phase 2 stimulation tDCS à ± 2 mA, Phase 3 stimulation *placebo*. Deux différents paradigmes FPVS seront utilisés permettant de mettre en évidence deux fonctions cognitives distinctes que sont la perception des visages (Rossion *et al.*, 2015) et la perception du changement d'identité (Liu-Shuang, Norcia and Rossion, 2014). L'amplitude de la réponse associée à la fonction cognitive étudiée sera mesurée sur le spectre fréquentiel aux fréquences d'apparition dites « oddball ».

Les résultats montrent, en intracérébral, une modulation d'amplitude des réponses cognitives associées à des processus de bas niveau (activité visuelle de base) pouvant aller jusqu'à − 94.64 % pour l'ensemble des contacts intracérébraux explorant le lobe temporal. Mais pas de modulation significative des réponse associées à es processus de haut niveau (perception des visages).

En surface, il a été mesuré une modulation des réponses cognitives associées à des processus de bas niveau pouvant aller jusqu'à – 23,57 % au niveau de la zone occipito-temporale droite lors d'une stimulation anodale. Il a également été observé une diminution d'amplitudes des processus de

haut niveau associés à la fonction de discrimination d'identité pouvant aller jusqu'à − 32 % entre avant et pendant une stimulation anodale.

V. Conclusion générale

Dans cette dernière partie, les discussions issues des différentes parties de la thèse seront reprises et mis en perspective avec des propositions d'amélioration des méthodologies. D'autres approches développées dans la littérature seront par ailleurs explorées et analysées afin de tenter de fournir des indications à la lumière des résultats présentés dans cette thèse pour de potentielles futures directions

Chapter I
Introduction and Scientific Questions

Among Non-Invasive Brain Stimulation (NIBS), Transcranial electrical stimulation (TES), has shown promising results over the past 20 years but is still under debate. Classical TES consists of applying a weak electric current on the scalp through electrodes to modulate brain activity (Nitsche, Liebetanz, *et al.*, 2003). Depending on the stimulation waveform used, TES has several names (Figure 1):

- tACS for transcranial Alternative Current Stimulation which uses alternative sinewave current
- tDCS for transcranial Direct Current Stimulation which uses a direct current to polarize the brain for a specified amount of time.
- tRNS for transcranial Random Noise Stimulation which uses a white noise waveform.
- tPCS transcranial Pulse Current Stimulation which uses squared waveform

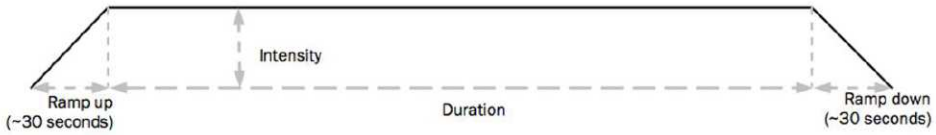

A. Active tDCS waveform

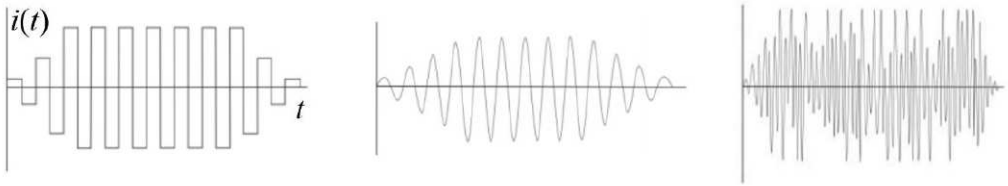

B. Active tPCS waveform (left). Active tACS waveform (middle). Active tRNS waveform (right). Waveforms are function $i(t)$ and are bipolar.

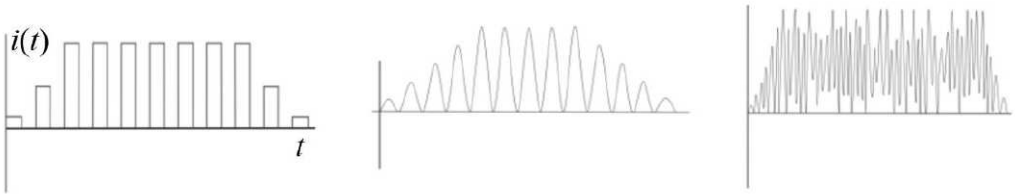

C. Active tPCS monopolar waveform (left). Active monopolar tACS waveform (middle). Active monopolar tRNS waveform (right). Waveforms are function $i(t)$

Figure 1: Different TES waveform from Soterix Medical

In this chapter introducing the thesis, the history of TES will be first discussed. Then some fundamentals about physics, neurophysiology and anatomy will be covered. Specific application of TES in neurological diseases and in cognition will conclude this chapter.

I. History of transcranial electric stimulation (TES)

1. From antiquity to the ages of enlightenment

Since the dawn of time, electricity and its effects have aroused the curiosity of human beings. The first written traces of electrical phenomena date back to the 7th century B.C., when Thales of Miletus tried to explain the effects produced when wool is rubbed with a rod of amber (in Greek "*êlektron*" (*ελεκτρον*) (Gardiol, 2002)). The latter, after friction, made strands of straw move thanks to an invisible force. Other written observations report the power of certain fish to inflict pain and to daze the fishermen who seize them. Hippocrates describes these mysterious creatures in the 5th century BC, in his (apocryphal) work *On Regimen* where he names these fish "*narke*" (*ναρκε*) the root of the word "narcosis", translating the state of numbness they can inflict (Kellaway, 1946). Among those cited by the father of medicine, we find the Mediterranean torpedo fish (or electric ray) which can deliver powerful shocks to stun, or even kill, its prey and its predators.

Scribonius Largus, a physician of the Roman Empire in 43 A.D., was the first to use the fish's electric discharges as a remedy against migraines. He advocates, in his work *Compositiones Medicae*, to put a living torpedo fish on a patient's head to get rid of their headaches. He mentions that even chronic migraines with unbearable pain disappeared completely with this remedy. Later, during the Middle Ages and until the renaissance, Marcellus Empericus (IV sec. d.C.), Aetius Amidenus (527–565), Alexander Trallianus (525–605), Paulus Aeginata (625–690), the notorious Avicenna (980–1037), Averroès (1126–1198), and Dawud al Antaki (1543–1599), practitioners who marked medicine's History, used the electric fish as a treatment for headaches, depression *etc*. (Zago *et al.*, 2016). Avicenna (or Ibn Sina) was considered as the first physician to treat epilepsy with electrical shock delivered by electric catfish placed on the frontal lobe. Thus, electric fish was used by physicians for a thousand year-long without knowing the true physiological mechanisms of electricity's healing properties.

2. The 18th century

The 18th century was the century of the craze for electricity in Europe. The aristocrats, and later the people, were fond of scientific demonstrations (which consisted of applying electricity to the human body) carried out by physicists during "*electrical soirée*" (Bertucci, 2007). Thanks to these experiments/shows, Johann Gottlob Krüger (1715-1759), professor of medicine and philosophy at Halle (Germany), and his student Christian Gottlieb Kratzenstein (1723-1795), noticed around 1744 that electricity can induce involuntary muscle contraction (Bertucci, 2007). They later suggested that electricity could be used for medical purposes.

The year 1746 marked a turning point in electricity's history when the Leyden Jar, the ancestor of the capacitor (Figure 2), was invented making possible the "storage" of the electricity. This

innovation will make easier the manipulation of this mysterious energy. Since then, the healing properties of electricity were studied with an increasing interest (Bertucci, 2007). Among the numerous scientists who used the Leyden Jar, one was particularly prolific and held a central role in the development of electricity to treat neurological and psychological disorders.

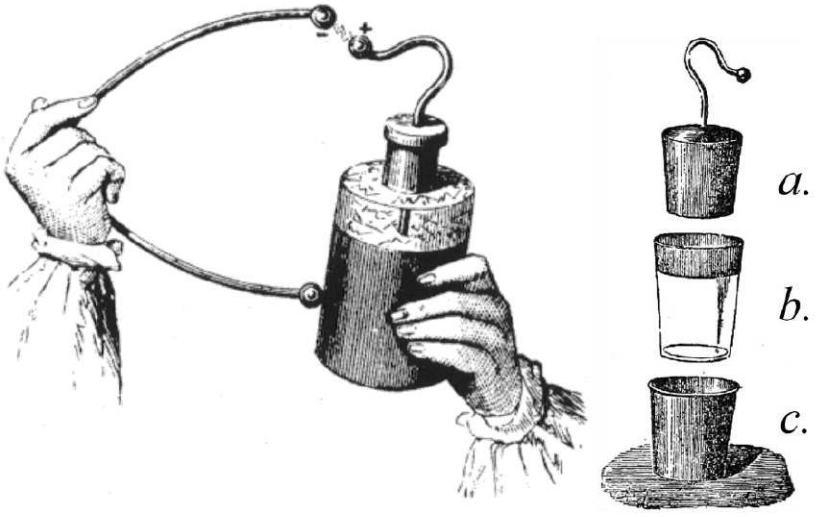

Figure 2: The Leyden Jar. On the right, the distinct part of the Leyden Jar: Two metallic parts (**a.** and **c.**) are separated by a glass insulating part (**b.**). This configuration works like a capacitor: the inner part (**a.**) can be charged and so elevated to a different potential than the outer part (**c.**). Then, when the inner part is connected to the outer part, the 2 potentials come into an equilibrium generating a spark: a circulation of charges (Left image).

Benjamin Franklin (1706-1790), who was qualified by Immanuel Kant as "The new Prometheus" or as "the father of modern electricity" by Joseph Priestley, found inspiration in Krüger's writing about the use of electricity in medicine and started to apply it on different parts of patients' body, such as the limbs, to heal diseases (Finger, 2007). Around 1750, after 2 accidents in which a strong electric discharge went through his head while he was treating a patient for paralysis, Franklin thought about applying electricity directly on the head to treat brain diseases. Then, in 1752, Franklin was asked to treat a patient with hysteria by this method of "head electrical stimulation". The patient who was completely healed reported in a letter:

> "*About this time there was a great talk of the wonderful power of electricity . . . Accordingly I went to Philadelphia, the beginning of September 1752, and apply'd to B. Franklin, who I thought understood it best of any person here. I receiv'd four strokes morning and evening... and indeed they were very severe... The symptoms gradually decreased, till at length they entirely left me. I staid in town but two weeks, and when I went home, B. Franklin was so good as to supply me with a globe and bottle, to electrify myself everyday for three months. The fits were soon carried off, but the cramp continued somewhat longer, tho' it was scarcely troublesome, and very seldom return'd. I now enjoy such a state of health, as I wou'd have given all the world for.*"(Evans, 1757).

In 1783 Jan Ingenhousz (1730-1799), a Dutch medical doctor who was living in Vienna, had the same accident as Franklin had 30 years earlier. He directly reported to Franklin in a letter about what he experienced and his suggestion about using head electrical stimulation for "mad men":

> "[...] *has induced me to advise som[e] of the London mad-Doctors, as Dr. Brook, to try a similar experiment o[n] mad men, thinking that, as I found in my self, my mental faculties impro[ved] and as the world well knows, that your mental faculties, if not improved [by] the two strooks you received, were certainly not hurt, by them, it might perhaps be[?] a remedie to restore the mental faculties when lost.*" (Ingenhousz, 1783).

Excited about the results presented in Ingenhousz's letter, Franklin (who was in France) communicated the recommendation to French physicians about the possibility of studying a new way to heal brain diseases, noticeably epilepsy, by applying electricity on patients' head. He wrote back to Ingenhousz:

> "*The Stroke you received, and its Consequences, are much more curious. I communicated that Part of your Letter to an Operator encourag'd by Government here to electrify epileptic and other poor Patients, and advis'd his trying the Practice on mad People according to your Opinion. I have not heard whether he has done it.*" (Franklin, 1785)

While French practitioners did not consider these recommendations serious enough to be further investigated, cranial electricity was explored in London by John Birch (1745? -1815), in New York State by T. Gale (c. 1800) and in Bologna by Giovanni Aldini the nephew of the electrophysiology pioneer: Luigi Galvani (1737-1798). In their research, most of the practitioners, who feared to harm their patients, purposefully used "low intensity cranial shocks" to not induce any loss of consciousness or full body convulsion and didn't report any of that. Finally, they communicated positive and encouraging results, notably for headaches, melancholia/depression, and madness (Birch, 1792; Gale, 1802; Aldini, 1803; Beaudreau and Finger, 2006; Finger, 2007).

3. The 19th century

For the writer Mary Sheley (1797-1851), the "modern Prometheus" wasn't the same one depicted by Kant: the good old Benjamin Franklin. At the opposite, Sheley's dark character, Dr. Frankenstein, was inspired by events people witnessed during the first years of the 19th century when a scientist was "resurrecting" cadavers by electrifying them. The scientist mentioned was Giovanni Aldini, well known in London in 1803, for his demonstration at the Royal College of Surgeon, on galvanic current (nowadays known as direct current) making a freshly hanged criminal corpse

convulsing. He also reported facial muscles contraction and even an eye opened when he applied the electric rods on mouths and ears of decapitated heads (Aldini, 1803; Parent, 2004).

Giovanni Aldini began his scientific adventure as an assistant of his uncle Luigi Galvani who was a physician and a scientist. Together, they worked on Galvani's theories about the so called "animal electricity" which came from Galvani's experiments when electricity was making frogs' legs contract. The results of Galvani's experiments are gathered in his book *De viribus electricitatis in motu musculari* (Galvani, 1791) where he established that electricity trigger muscles movements. Furthermore, he argues that animals and human have, intrinsically, electricity flowing inside the body and, outstandingly, he advocates that the brain is the source of this body electricity. Galvani found a novel approach to define brain diseases and principally to explain epilepsy (Parent, 2009) which led to a major revolution in science, philosophy, and medicine: electrophysiology was born.

After Galvanis' death, Giovanni Aldini pursued his uncle's works and strongly defended his theories against Volta's (1745-1827) attacks. He became known in Bologna in 1800 for his successful treatment to cure mental disorders with low intensity galvanic current after trying on his own head the effects of such therapy and reported:

> *"First, the fluid took over a large part of my brain, which felt a strong shock, a sort of jolt against the inner surface of my skull. The effect increased further as I moved the electric arcs from one ear to the other. I felt a strong head stroke and I became insomniac for several days."* (Aldini, 1804)

It is interesting to note, when Alberto Priori commented on the above excerpt, in 2003, he used the term of "activation" which lasted few days and can be considered as the first long-lasting activation described using galvanic current stimulation (Priori, 2003). Aldini's most famous result of galvanic current stimulation was when he treated a severe form of major depression of a 27-year-old farmer. He used (ironically) Volta's electric pile of disc (Figure 3) to perform repeated electrotherapy sessions during several weeks, which resulted in a considerable improvement of patient's mood.

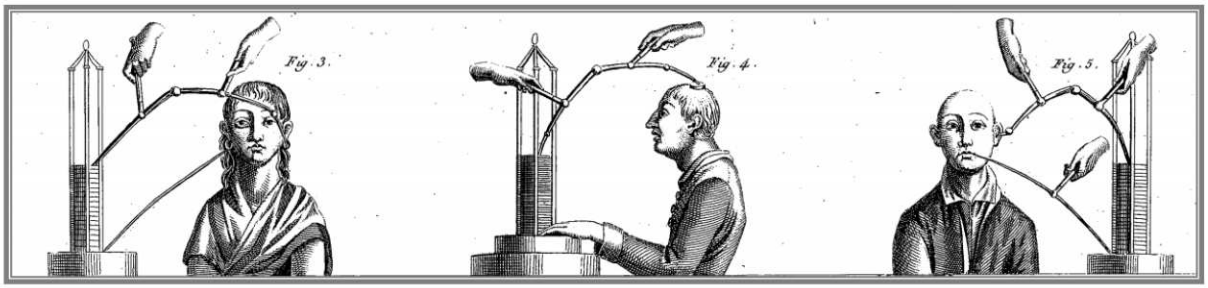

Figure 3: Aldini's electrotherapy using galvanic current (direct current) and Volta's pile (pile of metallic discs) on patient with depression. The rods (electrodes) were placed on each ear (left image) or on the parietal lobe with one hand on the pile's negative pole (middle image) or on one hear and the mouth (right image). Image from (Aldini, 1804).

After Aldini, low-intensity galvanic current was used by other scientists in Europe such as Friedrich Ludwig Augustin (1776–1854), Karl Johann Christian Grapeingiesser (1773–1813) and

Christian Heinrich Ernst Bischoff (1781–1861) to treat depression or sedate patients and reported successful results (Arndt, 1870; Priori, 2003). Also, during that time, the works of Michael Faraday (1791-1867) gave the opportunity to generate a current varying as a function of time (alternative current) which will be called "faradic current" as opposition to "galvanic current" (direct current). Since then, some scientists applied different types of stimulation in function of the pathology. At the end of the 19th century notorious French physicians, Jean Martin Charcot (1825–1893), and Joseph Babinski (1857–1932) reported the effect of electrotherapy on melancholia and epilepsy. However, because of inconsistent results, low-intensity stimulation became less and less used and totally forgotten until its reappraisal in the middle of the 20th century.

4. From the mid-20th century to now

It was in 1956 that low-intensity stimulation was reconsidered when Terzuolo and Bullock showed *in-vitro* the ability of a "weak" 1 $V \cdot m^{-1}$ voltage gradient (or electric field, explained in part II.1) to modulate neuronal firing frequency (Terzuolo and Bullock, 1956). Then, several animal *in-vivo* studies followed, investigating the effect of low-intensity stimulation such as Creutzfeldt *et al.* in 1962 who reported comparable results *in-vivo* when applying a small current and varying its intensity (Creutzfeldt, Fromm and Kapp, 1962). Later, in 1964 Bindman *et al.* reported an after-effect which can last over 3 hours after a one-minute stimulation only at an intensity as low as 3 µA (using 12 mm^2 saline cup electrodes resulting to a 0.25 $\mu A \cdot mm^{-2}$ current density) (Bindman, Lippold and Redfearn, 1964). Next, Purpura and McMurtry in 1965 reported *in-vivo* that stimulation polarity (positive current or negative currents named "anodal" or "cathodal" stimulation respectively) affected the modulation induced. These electrophysiological findings led to more systematic clinical studies of low intensity transcranial electric stimulation (TES) and mainly transcranial direct current stimulation (tDCS). Notably, Lippold and Redfearn in 1964 described effect on alertness, mood, and motor activity in 32 normal subjects under a 50-500 µA tDCS (Lippold and Redfearn, 1964). They also reported in depressed patients, mood improvement in more than the half of their cohort (26 patients) (Costain, Redfearn and Lippold, 1964). However, the described results remain indirect evidence of tDCS effect and was still difficult to reproduce: results were either confirmed (Costain, Redfearn and Lippold, 1964; Ramsay and Schlagenhauf, 1966; Carney, Cashman and Sheffield, 1970; Jaeger *et al.*, 1987) or failed to reproduce and even refuted (Dawson and Montagu, 1965; Lifshitz and Harper, 1968; Arfai *et al.*, 1970)).

It was in 1998 that the first direct electrophysiological evidence of a neuromodulation *in-vivo* in humans during tDCS measured on the scalp was reported by Priori and colleagues (Priori *et al.*, 1998). They modulated motor evoked potentials (MEPs) triggered by Transcranial Magnetic Stimulation and reported a "*slight but significant and consistent reduction*" of the MEPs amplitude. Then Nitsche and Paulus in 2000 measured the influence of the polarity of tDCS on MEPs and they found a reduction with cathodal and an increase with anodal stimulation which confirm in human *in-*

vivo what Purpura and McMurtry found 35 years earlier in animal *in-vivo* (Nitsche and Paulus, 2000). These studies mark the beginning of a new era for TES, which led to many clinical investigations in diverse neuropsychiatric and neuropsychological disorders (Lefaucheur, 2016). Since then, studies and scientific publications in the domain have grown exponentially going from 37 publications in 2000 to 1,183 publications in 2021 (source PubMed, keyword: Transcranial electrical stimulation), including clinical studies, but also fundamental *in-vitro* and animal *in-vivo* researches to deeper understand the basic mechanisms of transcranial electrical stimulation (TES) and to address crucial methodological TES parameters.

II. Fundamentals of transcranial electrical stimulation and the electric field

The effect of TES relies on the electric field (EF) generated on target. *In-vitro* experiments reported a modulation of the neuronal electrical activity when a neuron is placed in an EF. It is also demonstrated that the effects are not the same regarding the EF strength, the neuron's orientation to that EF or the cell type. Those *in-vitro* findings make up the cornerstone of our today's knowledge of TES's basic mechanisms making possible further *in-silico* and *in-vivo* studies. But before discussing the mentioned studies in more details, it is important for a complete understanding to recall the fundamentals of electromagnetism and neuroanatomy.

1. Basic principles of electromagnetism

Electromagnetism is based on the study of charged particle circulation occurring at atomic and subatomic level. An atom is composed of protons which have a positive charge, neutrons which have a neutral charge and electrons which have a negative charge (Figure 4). The entire atom possesses a neutral charge due to the same number of electrons (negative charge) and protons (positive charge). When the number of electrons differs from the number of protons, there is an imbalance between charges and the atom becomes an ion: a negatively or positively charged particle. If there are fewer electrons than protons, the atom becomes positively charged: it is a cation; if there are more electrons than protons, the atom becomes negatively charged: it is an anion. Charged particles such as anion, cations and electrons can attract or repel each other according to their charge and with a certain force. Indeed, in the vacuum, charged particles q_1 at a position r_1 will exert a force $\mathbf{F}$ on another charged particle q_2 at a position r_2 according to the Coulomb's law (Figure 5) (vector are written in bold characters):

$$\mathbf{F} = \frac{q_1 q_2}{4\pi\varepsilon_0} \frac{\boldsymbol{r_{12}}}{\|\boldsymbol{r_{12}}\|^3} \quad (1)$$

With $\mathbf{F}$ the force in Newton (N), q_1 and q_2 the signed magnitude of the charges in Coulomb (C), ε_0 the vacuum permittivity in Farad per meter ($F \cdot m^{-1}$) and $\boldsymbol{r_{12}}$ the vector distance between r_1 and

r_2 the positions of q_1 and q_2 respectively. Given $\frac{\boldsymbol{r_{12}}}{\|\boldsymbol{r_{12}}\|}$ the unit vector which could be expressed as: $\boldsymbol{u_{12}}$ the Coulomb's equation can be rewritten with more clarity:

$$\mathbf{F} = \frac{q_1 q_2}{4\pi\varepsilon_0 \|\boldsymbol{r_{12}}\|^2} \cdot \boldsymbol{u_{12}} \quad (2)$$

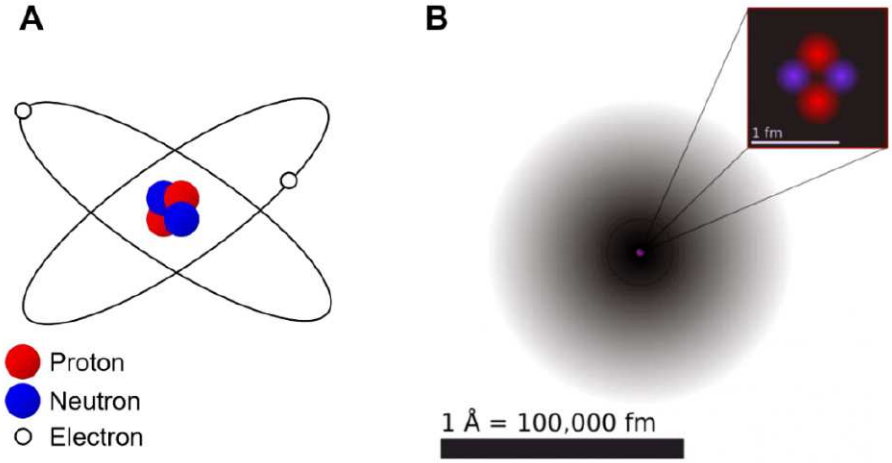

Figure 4: Helium atom models. A: Bohr model of helium atom which is an obsolete representation of the atomic architecture but more understandable because of the electron depiction which are considered as particles. B: Quantum model of the atomic architecture, which is a more realistic representation notably on how electrons are illustrated. An electron is actually both a wave and a particle. Its position is impossible to predict because of this duality. Its position follows a probabilistic distribution and is represented by a "cloud" of probability on the figure. Darker is the area, better is the chance to find the electron at a time *t*. The scale represents 1 Ångström which is 100,000 femto meter equal to 10^{-18} meter.

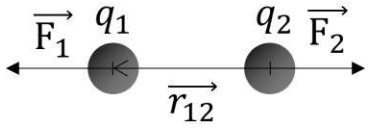

Figure 5: Coulomb's law representation, which describes the force F = F1 = − F2 applied on two charged particles q1 and q2 (in this case two same charges) separated by a distance ||r12||. If q1 has the same charge as q2, then q1q2 > 0: the particles repel from each other. In opposition, if the 2 particles have the opposite sign, then q1q2 < 0: the particles attract each other.

To express the force exerted only by q_1 on any other charge q_2 from anywhere in the space at a position r_2 it is possible to divide Coulomb's equation by q_2 which gives:

$$\mathbf{E} = \frac{\mathbf{F}}{q_2} = \frac{q_1}{4\pi\varepsilon_0 \|\boldsymbol{r_{12}}\|^2} \cdot \boldsymbol{u_{12}} \quad (3)$$

By simplifying the equation, we can express **E** as a function of one charge q at any distance r:

$$\mathbf{E} = \frac{q}{4\pi\varepsilon_0 r^2} \cdot \boldsymbol{u_r} \quad (4)$$

This new equation is a vector field from a charged particle called the electric field **E** expressed in Volt per meter ($V \cdot m^{-1}$) and decreases as a function of distance like Coulomb's force. The electric potential V in Volts (V) created at any point in the space is expressed as follows:

$$V = \int -\frac{q}{4\pi\varepsilon_0 r^2} \cdot \boldsymbol{dr} \quad (5)$$

$$V = \int -\mathbf{E} \cdot \boldsymbol{dr} \quad (6)$$

So, the electric field generated by a charged particle can be expressed as a function of the electric potential generated at every point r of the space:

$$\mathbf{E} = \frac{dV}{dr} \cdot \boldsymbol{u_r} \quad (7)$$

More generally, **E** can be expressed in function of the electric potential by:

$$\mathbf{E} = -\nabla V \quad (8)$$

Let's take 2 conductive plates separated by a distance $\boldsymbol{x}$ (Figure 6). One plate contains uniformly distributed positive charges, and the other has uniformly distributed negative charges. The positively charged plate is at a potential V_1 and the negatively charged plate is at a potential V_2. In other terms, the system is polarized. Between the two plates, the electric field is uniform and can be expressed simply by:

$$\mathbf{E} = \frac{V_1 - V_2}{|x|} \cdot \boldsymbol{u_x} \quad (9)$$

Now let's put a positively charged particle q with a mass m (in kg) in the media (vacuum) between the two plates (at an initial velocity of 0 meter per second ($m \cdot s^{-1}$)). The particle will move under the action of the Coulomb's force $\mathbf{F} = q\mathbf{E}$ toward the negatively charged plate. Knowing that $\mathbf{E} = m \cdot \boldsymbol{a}$ with $\boldsymbol{a}$ the acceleration in meter per second squared ($m \cdot s^{-2}$) the particle in an electric field **E** will move with an acceleration of $\boldsymbol{a} = \frac{q\mathbf{E}}{m}$.

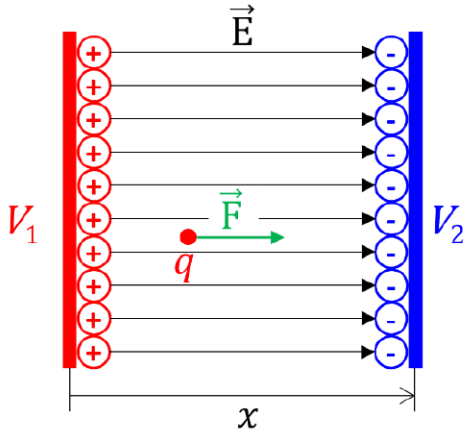

Figure 6: Charged particle in an external electric field between two charged conductive plates separated by a distance $\boldsymbol{x}$. Here, plates' surfaces are considered infinite to discard edges effects.

This case shows that an imbalance between charged particles distribution will create a potential difference ($V_1 - V_2$) expressed in Volt (V), an electric field **E** (in Volt per meter) and will

exert a force **F** in Newton (N) which will induce a movement to any charged particles in the electric field.

2. Neuroanatomy

Contrary to what is widely believed, the human brain is not constituted of 100 billion neurons with 10 times more glial cells. In fact, according to a new count the brain contains on average 86.1 ± 8.1 billion neurons and 84.6 ± 9.8 billion glial cells, which lower the ratio neuron/glial cells from 1:10 to 1:1 (Azevedo *et al.*, 2009; von Bartheld, Bahney and Herculano-Houzel, 2016).

In the human brain, neurons are organized and inter-connected in several layers. Axons are organized in a medium with 6 different cellular layers (Figure 7) forming the neocortex which is the superficial part of the brain also known as gray matter. Neurons' connection pathways form a complex axon network making fibrous tissues called the white matter. This complex connectivity is more and more studied and tends to challenge the well-established theory of functional location which postulates the brain is divided into functional zones. There are 3 parts in the human brain: the cerebrum, cerebellum, brain stem. The cerebrum is divided into two cerebral hemispheres and subdivided into 4 lobes: frontal lobe, parietal lobe, temporal lobe, and the occipital lobe. This thesis work will, in its major part, leverage on intracerebral investigation performed in the context of partial refractory epilepsy giving a unique opportunity to perform measurements directly within the brain. The most frequent form of refractory focal epilepsy affects the temporal lobe (Ladino and Moien-afshari, 2011) implicating notably the hippocampus, amygdala, cingulate gyrus, and fusiform gyrus (Maillard *et al.*, 2004; Kahane and Bartolomei, 2010). These structures are involved in numerous major cognitive processes (memory, emotions, vision *etc*.) implicating a lot of neurological pathologies (Alzheimer, depression, bipolar disorder, schizophrenia *etc*.). Being able to study TES in these structures could have an interesting impace offering the possibility to investigate either cognitive or therapeutic effects. Therefore, this thesis work will focus on the mentioned structures: The amygdala, hippocampus, cingulate gyrus, and fusiform gyrus.

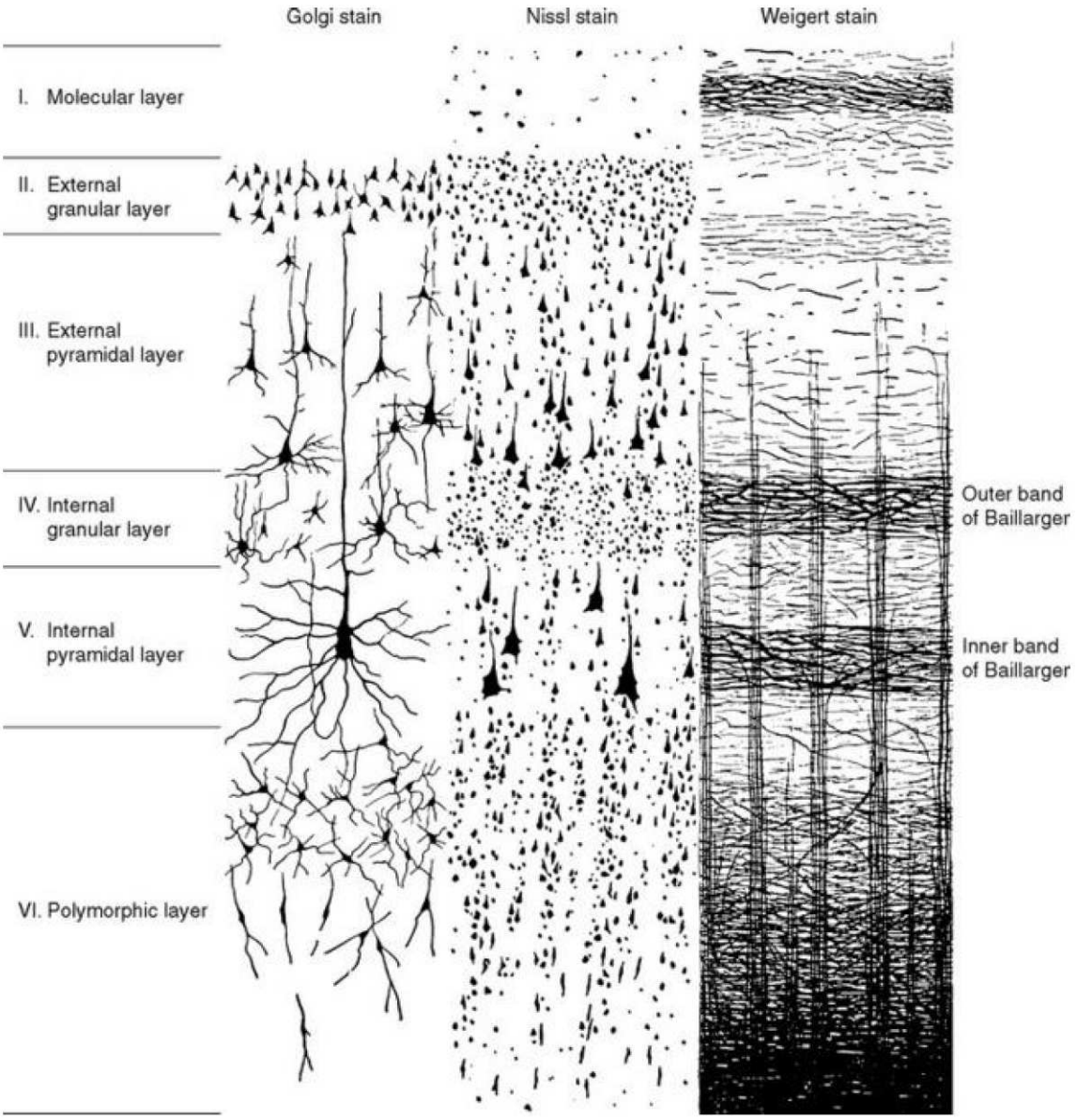

Figure 7: Representation of the neocortex cytoarchitecture and myeloarchitecture with different staining to highlight the distinct part of the cells: Golgi stain to make visible the entire cell, Nissl stain to reveal cells bodies only and Wiegert stain to reveal axons only from Brodmann K: *Vergleichende Lokalisation lehre der Grosshirnrinde in ihren Prinzipien dargestellt auf Grund des Zellenbaues*, Leipzig, 1909, JA Barth.

a. The amygdala or amygdaloid complex

The amygdala is not a cortical structure by itself but rather a region containing about 13 nuclei (Amaral *et al.*, 1992; Schumann, Bauman and Amaral, 2011; Ten Donkelaar *et al.*, 2020). It is also called amygdaloid nuclei, amygdaloid complex or amygdaloid bodies and are subdivided into 4 groups (Yilmazer-Hanke, 2012; Ten Donkelaar *et al.*, 2020): the basolateral nuclear group, centromedial nuclear group, the extended amygdala, and olfactory amygdala, which regroup 4, 4, 3 and 8 nuclei, respectively. The amygdaloid complex has many connections to the brainstem, the thalamus, hypothalamus, the basal forebrain, the striatum, the hippocampus and the neocortex and is involved in many function such as social interaction and communication (Jürgens, 1974; Kling, Steklis and Deutsch, 1979), social environment understanding (danger, warnings, submissive gestures (Kling and Brothers, 1992; Ten Donkelaar *et al.*, 2020), motivation, visual recognition (Aggleton, 1992; LeDoux, 1992) and memory (working mutually with the hippocampus).

Because of its central role in social behavior, alterations of the amygdala complex are the origins of some neurological and neurodevelopmental disorders. Indeed, several studies reported a pathological amygdala in autism, bipolar disorder, schizophrenia, depression and anxiety disorders, social phobia, Williams syndrome and Fragile X syndrome. Abnormal amygdala volume, structure alteration (such as a decrease in neuron population), or hyperactivation of the amygdaloid complex were found in the mentioned pathologies.

b. The hippocampus

The hippocampus contains only one cellular layer, which is called an allocortex by opposition to the neocortex which contains 6 cellular layers. This cellular organization has often earned it, wrongly, the name of “primitive cortex” or, “reptilian cortex”. The hippocampus is typically divided into 2 structures, which are the dentate gyrus and the cornu ammonis (or "Amon’s horn", CA). The dentate gyrus is subdivided into the fascia dentata and the hilus, and the CA is subdivided into 4 fields: CA1, CA2, CA3, and CA4 (Figure 9). The hippocampus is heavily connected to the other part (cortices) of the brain (Catani, Dell’Acqua and Thiebaut de Schotten, 2013; Schultz and Engelhardt, 2014) :

- The frontal lobe: the anterior eye fields (areas 8 and 9 in Figure 10), prefrontal cortex (areas 10 and 46), and lateral orbitofrontal cortex (area 47)
- The temporal lobe: the ventral and posterior lateral temporal cortex (areas 20,21,22), the temporal polar cortex (area 38 according to Schultz and colleague).
- The Insula (Figure 8)
- The cingulate gyrus: Anterior cingulate cortices (areas 24, 25, 32) and posterior cingulate gyrus (areas 23, 26, 29, 30)
- Parietal lobe: posterior parietal cortex (area7) and precuneus (area 31)

- Occipital lobe : dorsal occipital cortex (area 19).

Functionally, the hippocampus is involved in most memory tasks and spatial orientation. Structure alterations were found in Alzheimer's disease, amnesia and notably in temporal lobe epilepsy (see III.1.e page 52).

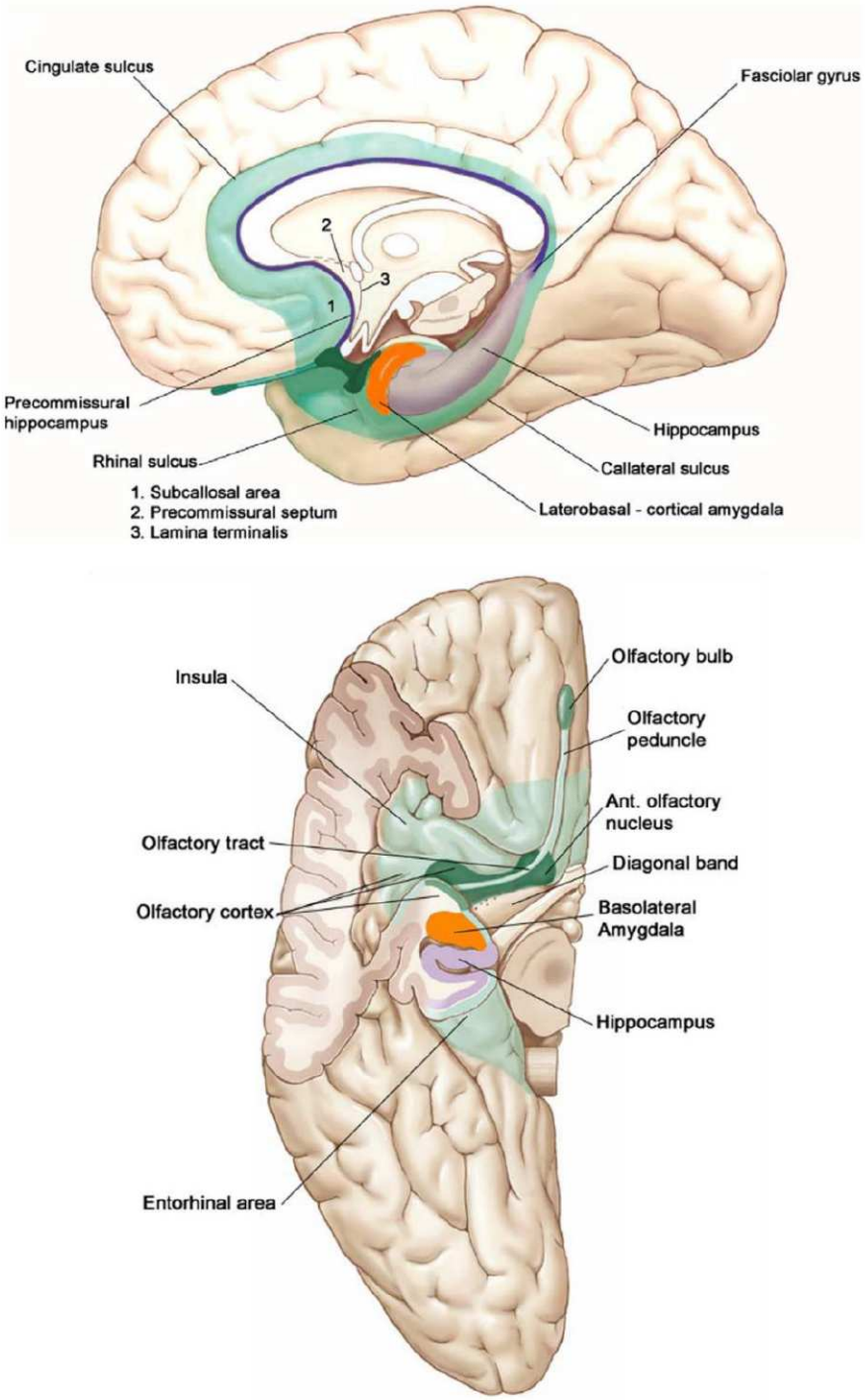

Figure 8: Anatomy of the limbic lobe. Top: sagittal view of the right hemisphere. Bottom: ventral view of the right hemisphere. From The limbic lobe and its output channels: Implications for emotional functions and adaptive behavior. *Neuroscience & Biobehavioral Reviews*, *30*(2), 126–147 by Heimer, L., & Van Hoesen, G. W (2006). © 2006 by Elsevier. Reproduced with permission of Elsevier under license number 5266980195944 in the format of print and electronic via Copyright Clearance Center.

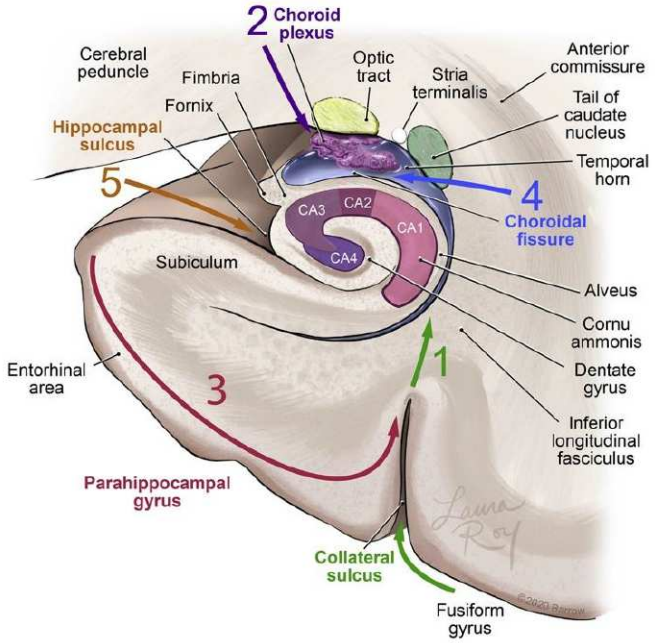

Figure 9: Artist's rendition of the surgical steps of anatomical hippocampectomy for tumor viewed in the coronal plane from (Przybylowski *et al.*, 2021), licensed under CC BY 4.0.

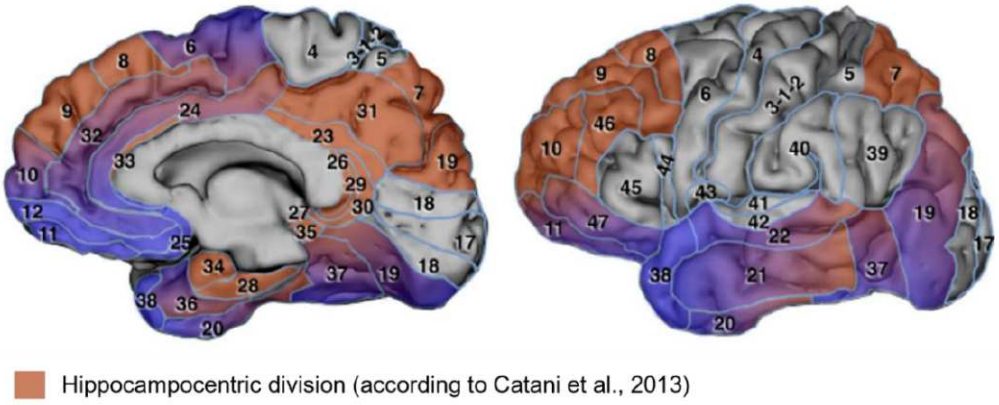

Figure 10: New proposition of the limbic system decomposition considering the complex functional connectivity with the Olfactory cortex (in blue) and the hippocampus (in red) according to Catani and colleague (Catani, Dell'Acqua and Thiebaut de Schotten, 2013). Adapted from A revised limbic system model for memory, emotion, and behaviour. Neuroscience & Biobehavioral Reviews, 37(8), 1724–1737 by Catani, M., Dell'Acqua, F., & Thiebaut de Schotten, M. (2013). © 2013 by Elsevier. Reproduced with permission of Elsevier under license number 5267121134314 in the format of print and electronic via Copyright Clearance Center.

c. The cingulate gyrus

The cingulate cortex, which includes the cingulate gyrus, is an area where numerous cognitive processes and emotions are transiting and can be associated as "a connecting hub of emotions, sensation, and action" and is subdivided into four parts (Vogt *et al.*, 1995; Strick, Dum and Picard, 1998; Vogt and Laureys, 2005; Leech and Sharp, 2014; Vogt, 2016; Jumah and Dossani, 2021):

- The anterior cingulate cortex which is involved notably in emotions regulation/responses, reward-based decision making.
- The midcingulate cortex involved in reward-based decision making, and conversion into motors responses from emotions inputs.
- The posterior cingulate cortex in charge of visuo-spatial orientation.
- The retrosplenial cortex participating in imagination and episodic memory.

d. The fusiform gyrus

The fusiform gyrus (or occipital gyrus) is the largest part of a wider anatomical zone known as the ventral temporal cortex (VTC) including the parahippocampal gyrus and their bounding sulci. It is involved in high level cognitive processing of visual tasks such as face, bodies, object and word perception, identification, and recognition (Peelen and Downing, 2005; Weiner and Grill-Spector, 2012; Roberts *et al.*, 2013; Grill-Spector and Weiner, 2014; Rangarajan *et al.*, 2014; Jonas *et al.*, 2016; Palejwala *et al.*, 2020). The lateral part is responsible to face perception (on the right hemisphere) and is located within a highly connected network in which we can also find the hippocampus (Kim *et al.*, 2000; Jonas *et al.*, 2016) and the amygdala (Lohse *et al.*, 2016; Palejwala *et al.*, 2020).

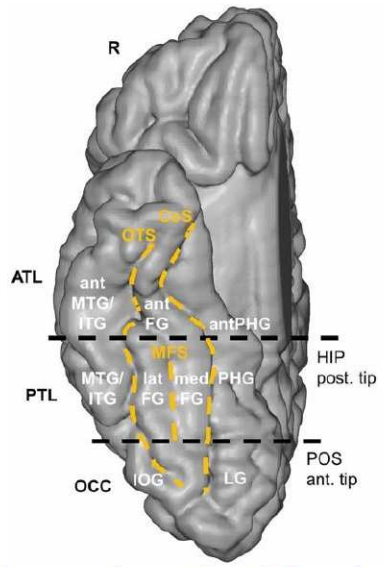

Figure 11: Anatomy of the ventral occipito-temporal cortex from A face-selective ventral occipito-temporal map of the human brain with intracerebral potentials. *Proceedings of the National Academy of Sciences of the United States of America*, *113*(28), E4088–E4097 by Jonas, J., Jacques, C., Liu-Shuang, J., Brissart, H., Colnat-Coulbois, S., Maillard, L., & Rossion, B. (2016). ATL: Anterior Temporal Lobe, PTL: Posterior Temporal Lobe, OCC: Occipital Lobe, CoS: Collateral Sulcus, OTS: Occipito Temporal Sulcus, MTG: Middle Temporal Gyrus, ITG: Inferior Temporal Gyrus, FG: Fusiform Gyrus, IOG: Inferior Occipital Gyrus, LG: Lingual Gyrus, PHG: Parahippocampal Gyrus.

As previously mentioned, the possibility of modulating these interconnected structures with TES could have interesting clinical and cognitive implications for therapeutic purpose or rehabilitation. For a long time, people applied electrical currents on the scalp ignoring the basic mechanisms of potential stimulation effects. TES induced neuromodulation is directly related to the electric field generated on the brain area of interest (neuron population). This basic knowledge of the electric field related neuromodulation comes from fundamental studies performed *in-vitro*. To study TES it is important to address first the basics of neuromodulation at the neuronal level.

3. Neuromodulation with an exogenous electric field

Neuron's basic electrophysiology as we know it today (membrane potential, action potential *etc*.) was studied by electric stimuli directly applied through electrodes in contact with the cell. It was Eduard Hitzig (1838-1907) and Gustav Fritsch (1837-1927) who first discovered in 1870 the neuron sensitivity to an electric current (Terzuolo and Bullock, 1956; Carlson and Devinsky, 2009). But typically, in the case of TES, neurons are not directly in contact with the stimulating electrode; and TES efficacy relies on the electric field (EF) generated on neurons. Thus, concerning the EF, Terzuolo & Bullock in 1956 were the first to quantify its effect on neurons by placing a lobster stretch receptor between 2 conductive plates (schematical representation in Figure 12, same principle as described in part II.1, Figure 6 page 35). They found that an EF as low as 1 $V \cdot m^{-1}$ can change the firing rate of a neuron between 5 % and 25 % (Terzuolo and Bullock, 1956).

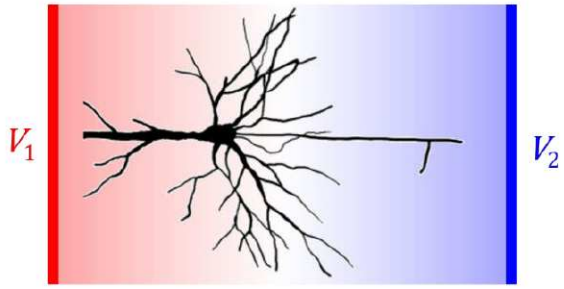

Figure 12: Representation of a neuron between two conductive plates at a different potential each (V1 and V2). The potential difference creates a uniform voltage gradient between the two plates, which is the electric field.

Then, in 1981, Jeffery and colleague studied the impact of an externally applied EF on the action potential amplitude (or amplitude of the spike: the fast neuron's depolarization-repolarization) of guinea pigs' hippocampal granule cells. They also studied the impact of the EF directionality at magnitudes from 5 $V \cdot m^{-1}$ to 10 $V \cdot m^{-1}$. They found that when the EF is perpendicular to the hippocampal cells layer (in other terms an EF parallel to the dendrosomatic axis: along the axon direction) population of neuron spikes amplitudes are modulated. However, for EF under 4 $V \cdot m^{-1}$ the study detected no modulation of spikes amplitude (Jefferys, 1981).

The two previous studies used only a constant EF. Using alternative EF (produced with an alternative current), neurons population spike amplitude can be modulated with a lower magnitude and the entrainment induced can last after the stimulation as Bawin and colleague have demonstrated in

1986. They used a sinusoidal EF in rats' CA1 cell layer from 0.5 $V \cdot m^{-1}$ to 5 $V \cdot m^{-1}$ and at frequencies ranging from 5 Hz to 60 Hz and found that the effect can last several minutes after a 20-second stimulation. They injected penicillin at a different concentration in rats' sliced hippocampi to reproduce epileptiform activity bursts and they found that above a certain amount of concentration (which increases the epileptiform activity), the EF induced long-term depression of epileptiform activity (Bawin *et al.*, 1986).

The previous studies constituted the cornerstone of the knowledge on exogenous EF cellular effect for in-vitro experiments, then several other studies on EF to investigate neuronal function followed (Chan and Nicholson, 1986; Wong and Stewart, 1992; Jefferys, 1995; Andreasen and Nedergaard, 1996). Also, potential clinical application of EF, notably in epilepsy, has been investigated *in-vitro* by (Bruce J. Gluckman *et al.*, 1996; Ghai, Bikson and Durand, 2000; Durand and Bikson, 2001; Bikson *et al.*, 2004). However, most of the mentioned works use electric strength over 5 $V \cdot m^{-1}$ which would be difficult to extrapolate to TES in Human. Indeed, in the context of TES, the stimulating current encounters several layers (skin, bone, meninges) before reaching neurons in the cortex and some claim that the EF generated is way lower than the magnitudes applied above and therefore generate no effects (see part V (Underwood, 2016; Vöröslakos *et al.*, 2018)*)*. Thus, studies which focus on weak EF ≤ 1 $V \cdot m^{-1}$ are more relevant for extrapolating to *in-vivo* TES experiments. Along these lines, Francis *et al*. 2003 studied low EF influence on hippocampal slices preparation and found EF as low as 0.14 $V \cdot m^{-1}$ (root mean square or RMS) in CA1 and CA3 produced a significant synchronization on network spike timing. They showed a higher EF sensitivity in CA1 cells than in CA3 cells. This value of 0.14 $V \cdot m^{-1}$ is the lowest magnitude known today which can induce a potential modulation and will be used as reference for this thesis work. They also advocated, as well as Jefferys in 1995, that neuron's length can modulate the sensitivity to an applied EF (Francis, Gluckman and Schiff, 2003). In the same vein, Deans *et al*., 2007 studied the effect of an alternative EF and its frequency on cell firing in rats' hippocampal slices (CA1). They found that a magnitude of 0.35 $V \cdot m^{-1}$ RMS at 50 Hz had significant effects in 71 % of slices and 0.18 $V \cdot m^{-1}$ RMS in 20 % of them. Their findings also show a frequency dependency on the transmembrane potential: higher was the frequency, lower was the EF effect on transmembrane potential with an exponential decay relationship between 1 Hz and 100 Hz (Deans, Powell and Jefferys, 2007).

EF effect on spike timing on CA1 cells previously described was confirmed by Radman and colleague in 2007. They generalized and quantified the spike timing modulation as a function of the external EF applied (for DC current and AC current) by extracting mathematical model from their experiments (Radman *et al.*, 2007).

The previous studies dealt mainly with hippocampal cells. Regarding neocortical cells, Radman and colleague demonstrated in 2009 that, interestingly, layer V cortical cells (Figure 7 page 37) are more sensitive to the EF even for magnitudes below 1 $V \cdot m^{-1}$. Setting systematically an EF

parallel to the dendrosomatic direction (along with the axon direction, see Figure 13A) to be in the best condition to modulate neurons constitutes one limit to the previously mentioned study. Typically, EF direction/orientation generated by TES wouldn't be only along the axons but flowing both tangentially and perpendicularly to the neuron direction. Considering brain geometry (Sulci and Gyri), Bikson and colleague hypothesized in 2006 that tangential EF, which would be the major direction, doesn't induce any cell polarization (Bikson, Radman and Datta, 2006). However, the team in 2013 (Rahman *et al.*, 2013) found experimentally, in a study which combines in-vitro and in-silico experiments, that a tangential EF could, in fact, modulate neuronal activity (Figure 13). They also demonstrated that cells are more sensitive when they have more afferents (other cells' axon connected to the dendrites)

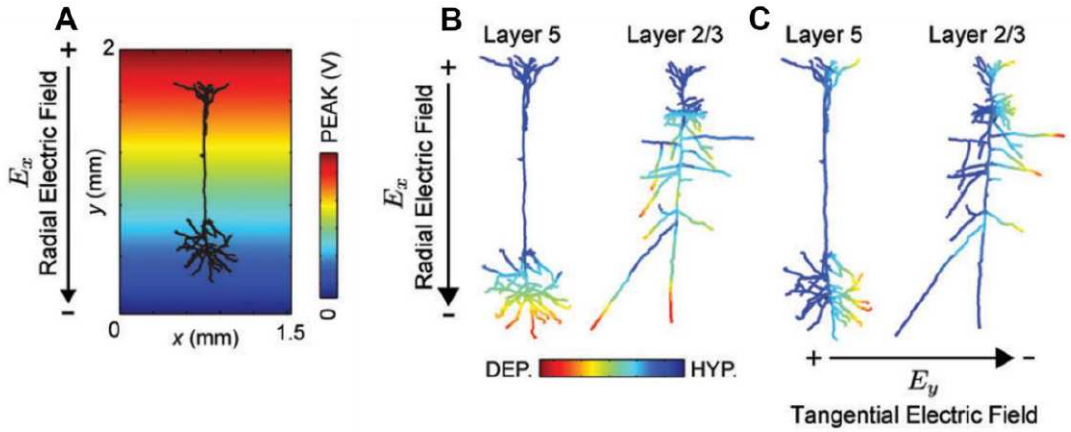

Figure 13: Compartment model simulations of morphologically reconstructed neocortical pyramidal neurons were used to provide a description of axon terminal polarization in a uniform EF. **A:** pyramidal neuron in a radial electric field. **B:** Polarization of layer 5 and layer 2/3 pyramidal neurons type in radial electric field. **C:** Polarization of layer 5 and layer 2/3 pyramidal neurons type in a tangential electric field. (DEP: depolarizing area, HYP: hyperpolarizing area.). From Cellular effects of acute direct current stimulation: Somatic and synaptic terminal effects. *Journal of Physiology*, *591*(10) by Rahman, A., Reato, D., Arlotti, M., Gasca, F., Datta, A., Parra, L. C., & Bikson, M. (2013). © 2013 by Elsevier. Reproduced with permission of Elsevier under license number 1198876-1 in the format of print and electronic via Copyright Clearance Center.

The basic relationship between EF strength (and its other parameters such as its directionality, its frequency *etc.*) and its electrophysiological effect has been widely studied. The question from now on is about the possibility of generating such EF during a TES in *in-vivo* experiments at the macroscopic level.

4. The electric field in the brain.

Findings about the electric field on a single neuron can't be extrapolated to a larger number of cells due to several factors such as network complexity, number of connection, orientation difference in the same area (Rahman *et al.*, 2013). Therefore, it is important to study and validate at the macroscopic level what was observed at the neuronal scale.

There are relatively few studies in the literature measuring electric field (EF) in *in-vivo* animals' brain during a TES. First, although findings in animals provide a good basic knowledge, the results are difficult to extrapolate to humans. Secondly, contrary to measuring a voltage which needs

only two physical measurement points, calculating an EF (which is a voltage gradient as mentioned in part II.1) requires many physical measurement points close to each other. To achieve this, invasive investigational methods are required and are complex to implement in living animals and even more in living humans.

a. Measuring the intracerebral electric field in animal *in-vivo*

Some studies have explored EF in animals (for a review see (Reato *et al.*, 2013; Liu *et al.*, 2018)) and its effect on spiking rate (Creutzfeldt, Fromm and Kapp, 1962; Ozen *et al.*, 2010) and on Low Frequency Potential (LFP) activities (Purpura and McMurtry, 1965). However, all these studies relied on *encéphale isolé* preparations, direct cortical stimulation, high intensities (more than 4 mA) or post-mortem EF measurement which are far from a classical TES configuration. To put the literature review in the context of classical TES, only studies which applied stimulation electrodes over the skin, using low intensities (< 4 mA) and did direct intracerebral *in-vivo* measurement were included in the following lines. Thus, in 2016 Alexander Opitz and colleagues, were the very first to measure successfully directly an intracerebral EF in a living animal during TES at low intensities (Opitz *et al.*, 2016). Using tACS simultaneously with intracranial electrodes implanted in 2 monkeys, they managed to measure maximum EF magnitudes from 0.35 $V \cdot m^{-1}$ to 1.17 $V \cdot m^{-1}$. Their methodology of stimulation combined with a mini-invasive intracerebral investigation provides accurate results in the most realistic conditions of TES. Also, since 1996, a recurrent scientific question about the signal propagation in function of its frequency has been raised in electrophysiology since Gabriel and colleagues explored tissues electric properties in function of the stimulation frequency (Gabriel, Lau and Gabriel, 1996). In the domain of TES, this question was addressed also by Opitz *et al.*, 2016 through the investigation of intracerebral voltage dependence in function of the stimulation frequency and found a maximum voltage drop of 10 % between 1 Hz and 150 Hz. Still in monkeys (2 monkeys), (Krause *et al.*, 2019) measured an electric field on micro-electrodes up to 0.28 $V \cdot m^{-1}$ and 0.35 $V \cdot m^{-1}$ in monkey 1 and 2, respectively. The strength of their study relies on the intracerebral EF measurement *in*-vivo combined with the measurement of its direct neuronal effect at the cellular scale. However, in rodents, Vörörslakos *et al.*, in 2018 and Asan *et al.*, in 2019 found that an EF of at least 1 $V \cdot m^{-1}$ is needed to induce an effect on neuronal spike timing (Vöröslakos *et al.*, 2018; Asan, Gok and Sahin, 2019).

From the above studies, it is possible to state that TES can generate an intracerebral EF in animals *in-vivo*. But discussions are still ongoing about the EF strength required to modulate neuronal activity. Despite the breakthrough provided by those *in-vivo* animal studies, the extrapolation to humans is not straightforward notably because of the difference between head geometries. Even results from non-human primates' studies can't pretend to apply to humans the same way. First, the monkey brain is smaller than the human brain and EF spatial distribution would be more spread out in monkeys. Second, because sensitivity to an EF depends also on the number of synaptic connections

(Reato *et al.*, 2010) a monkey's brain sensitivity wouldn't be the same as a human's brain because of their connectivity pattern difference. However, the complexity of obtaining intracerebral measurements in human *in-vivo* during a TES led the scientific community to elaborate and use computational models of the human head to calculate and simulate the intracerebral EF propagation.

b. Modelling the intracerebral electric field in human *in-silico*

In-silico experiments of intracerebral EF propagation from surface electrodes started with the handmade mathematical model of Rush and Driscoll in 1968 (Rush and Driscoll, 1968). They developed a model with 3 concentric spheres considering the human tissues resistivities of the scalp, the skull and the brain obtained in a previous study with monkeys. They experimentally validated their own model by putting a human skull in a water tank and measuring the EF resulting from 2 surface electrodes. Then, with the development of computer resources, Miranda *et al*. in 2006 used the same concentric spheres and implemented it numerically applying Finite Element Method (or Finite Element Model FEM) (Miranda, Lomarev and Hallett, 2006). They tested four different stimulation electrodes positions (montage) and sizes over the surface of a sphere. Their model exhibited a maximum EF of 0.22 $V \cdot m^{-1}$ on the cortex for a 2-mA stimulation. Wagner *et al*., 2007, used FEM derived from Magnetic Resonance Imaging (MRI) to obtain a more realistic model regarding the shape of the head/skull. They reported current density values generated on the cortex ranging from 0.77 $mA \cdot cm^{-2}$ to 2 $mA \cdot cm^{-2}$ for a 1 mA stimulation (Wagner *et al.*, 2007). Both previous studies also highlighted a phenomenon which will constitute the major argument used by a part of the community: the current shunted by the scalp. They found that a non-negligible amount of current doesn't penetrate the skull but circulated directly through the scalp's skin from one stimulating electrode to the other. Miranda *et al*., 2008 advocated that increasing distance between the stimulating electrodes would reduce scalp shunt and increase the amount of current going through the skull which will be confirmed a few years later by Faria and colleagues (Faria, Hallett and Miranda, 2011).

The purpose for computational modelling is to provide the most accurate simulation possible by using more computational power, implementing more anatomical features (such as gyri, sulci, meninges, hair, air, bones porosity), increasing segmentation precision and complexity *etc*.

The basic principle of intracerebral EF modeling is based on solving Laplace's equation in quasistatic condition to find the electric potential V:

$$\nabla \cdot (\sigma \nabla V) = 0 \qquad (10)$$

where σ is the medium electrical conductivity.

Then at every point of the head modelled EF and current density are calculated:

$$E = -\nabla V \qquad (11)$$

$$J = \sigma E \qquad (12)$$

Computational studies give the opportunity to perform many experiments and testing a lot of parameters in humans in a short amount of time, which would be impossible to execute in real life. For instance, it allows to investigate electrode placements (Huang *et al.*, 2017; Opitz *et al.*, 2018), shapes (Saturnino, Antunes and Thielscher, 2015), configuration and number influencing EF distribution and focality (Datta *et al.*, 2008, 2009; Dmochowski *et al.*, 2011; Edwards *et al.*, 2013; Ruffini *et al.*, 2014). Other models simulated the EF distribution in specific conditions such as with a skull defect (Datta, Bikson and Fregni, 2010), in stroke patients' brains (Datta *et al.*, 2011; Dmochowski *et al.*, 2013), in pediatry (Minhas *et al.*, 2012) or in depression (Csifcsák *et al.*, 2018). Also, studies on inter-individual variation and anatomical differences highlight the importance of accurate and individualized modelling (Datta *et al.*, 2012; Opitz *et al.*, 2015; Parazzini *et al.*, 2015) based on MRI segmentation and tissues distribution. The typical framework of such a method relies first on MRI-segmentation algorithm which determines tissues from MRI image (Ashburner and Friston, 2005). Secondly, a sorting into tissues compartments is performed: usually 3 (brain, cerebral spinal fluid (CSF), skull) to 6 compartments (white matter (WM), gray matter (GM), CSF, skull, air cavities and skin (Figure 14)) are defined. Then, tissues conductivities are set for each compartment (based on values obtained from the literature, for a review see (Koessler *et al.*, 2017)). Next, tissue volumes are discretized into a set of finite elements (Figure 14) ((Geuzaine and Remacle, 2009; Huang *et al.*, 2013; Windhoff, Opitz and Thielscher, 2013) each with uniform previously set conductivities, finally Laplace equation (10) is solved at each element.

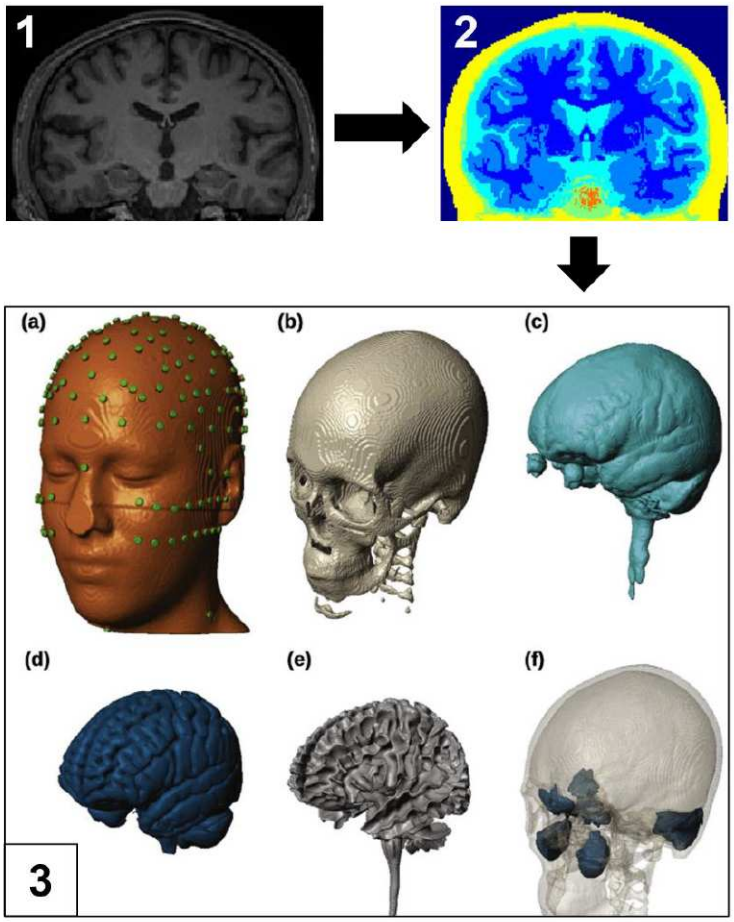

Figure 14: (previous page) Example of an MRI segmentation and modelling into 6 tissues compartment in Finite Element from ROAST (Huang *et al.*, 2013, 2019). **1**. Patient's MRI in coronal view. **2.** Image segmentation into different tissues. **3.** Segmentation of the ICBM-NY head into six different tissue types by (Huang, Parra and Haufe, 2016) is licensed under **CC BY 4.0**. (a) Scalp and surface electrodes (in that case 231 electrodes visible), (b) skull, (c) cerebro-spinal fluid, (d) gray matter, (e) white matter, (f) air cavities.

Models became more and more detail oriented, some studies used 40 and even 62 tissue types (Sadleir *et al.*, 2010; Parazzini *et al.*, 2011) but despite their complexity and their high precision displayed in literature, no one really knew how accurate models were compared to reality. Scientists struggled for a long time to validate their model in human *in*-vivo due to technical limitations until 2017 (Huang *et al.*, 2017).

The most popular algorithms workflow which automatically computes intracerebral EF from MRI images are:

- **ROAST** (**R**ealistic v**O**lumetric **A**pproach to **S**imulate **T**ranscranial electric stimulation (Huang *et al.*, 2019)). Using automatic segmentation (SPM12), it is the first model validated with empirical human *in-vivo* data (Huang *et al.*, 2017). This workflow is based on one Matlab command in which it is possible to set different parameters. It has the advantage of being easy to use and fast to compute.
- **SimNIBS** (**Sim**ulation of **N**on-**I**nvasive **B**rain **S**timulation (Thielscher, Antunes and Saturnino, 2015)). Using automatic segmentation (SPM12, CAT12, FreeSurfer) and has

been recently validated with data from Huang *et al.,* 2017 (Puonti *et al.*, 2020). This workflow has a user interface and has the advantage of modeling the white matter anisotropy, which provides a more realistic simulation of current propagation. However, the cost in computing resources for such precision is quite high and the computing time is therefore longer. Also, extracting data from the simulation is not straightforward and other software or Matlab codes are required for the analysis.

Overall, from models and studies previously described, electric field computed on the cortex varied from 0.22 $V \cdot m^{-1}$ (Miranda, Lomarev and Hallett, 2006) to 1.57 $V \cdot m^{-1}$ (Parazzini *et al.*, 2011) for a 1 mA stimulation depending on the electrode size and the method used. About electrode size, (Mikkonen *et al.*, 2020) showed that the smaller the stimulating electrode are, higher is the electric field magnitude on the neocortical surface. Indeed, smaller is the area under the electrode, higher is the current density and, therefore, higher is the electric field (equation 12).

Precise simulations give a view of EF propagation in the brain, which helps for optimized and personalized use of TES in function of patient individual anatomy and the area to target in a clinical routine. Yet, in a more fundamental point of view, it is important to know how the electric field behaves inside a real human living brain and it is technically the most complex study to perform.

c. Measuring the intracerebral electric field in human *in-vivo*

Opitz and colleague in 2016 were the first to measure an intracerebral EF in human *in-vivo*. They performed these intracerebral measurements in 2 epileptic patients with 2 different investigational methods: one patient with stereoelectroencephalography (SEEG see part III.1.3 page 56) the other with electrocorticography (ECoG see also part III.1.3 page 56). They reported an EF magnitude up to 0.36 ± 0.008 $V \cdot m^{-1}$ in the patient with SEEG and 0.163 ± 0.007 $V \cdot m^{-1}$ in the patient with ECoG for a 1 mA stimulation. Then, Huang *et al.*, (2017) (as mentioned previously, who were the first to validate a computational model with empirical EF measurement in human *in-vivo*) measured EF in a larger cohort: 10 patients, 9 of them with ECoG investigation, and 1 with SEEG only. They found a cortical EF up to 0.4 $V \cdot m^{-1}$ for a 2-mA stimulation. In the two studies, a total of 12 patients were included (10 patients with EcoG, 2 patients with SEEG). They both performed a stimulation with alternative current (tACS) using two saline-soaked sponge electrodes (25 cm^2 (Opitz *et al.*, 2015)) or two rubber electrodes (4 cm^2 (Huang *et al.*, 2017)) and measured that deterministic signal on the subdural or intracerebral electrodes. Next, they quantified the electric potential attenuation from one measurement point to another ($V1 - V2$) and calculated the electric field by dividing the result by the distance separating the two measurement points. The strength of their studies relies on the use of SEEG in 2 patients (one patient each study) allowing a good sampling of the depth. The weakness of these two studies lies in the ECoG exploration in most patients (10 patients out of 12) in which the craniotomy performed for the investigation significantly modifies the head geometry and conductivities inducing a modification of the EF distribution (current passage can be facilitated on the

cortex surface at the craniotomy site) which was demonstrated by (Datta, Bikson and Fregni, 2010). Using a direct current, (Chhatbar *et al.*, 2018) measured intracerebral EF on Deep Brain Stimulation (DBS) electrodes during tDCS at 2 mA and 4 mA with 2 sponge pads (35 cm^2) in 3 patients with movement disorder. They calculated the electric field based on the offset generated by the direct current injection recorded on DBS electrodes. Then, they divided these values by the distance separating the two DBS electrodes. They reported an electric field up to 0.13 $V \cdot m^{-1}$ in subthalamic nuclei. The strength of the study is the use of direct current which could confirm directly tDCS studies without assumptions and extrapolations. The second strength is the use of only mini-invasive methods like DBS electrodes that have a minimal impact on head geometry. However, electric field values calculated on a few intracerebral contacts and the relatively long distance between them can't be consider as accurate. Therefore they reported a *"crude estimate of the generated electric field with 2 mA bitemporal tDCS was 0.12± 0.13 mV/mm."* (Chhatbar *et al.*, 2018). In the same idea, using DBS electrodes, (Ruhnau *et al.*, 2018) reported a single case with whom they recorded a sinusoid signal coming from a tACS (using bilateral montage with sponge electrodes 35 cm^2) but didn't report any EF magnitude values.

Overall, considering techniques that have the least impact on head geometry (SEEG and DBS), 6 patients were included (n = 1 (Opitz *et al.*, 2016) ; n = 1 (Huang *et al.*, 2017) ; n = 3 (Chhatbar *et al.*, 2018) ; n = 1 (Ruhnau *et al.*, 2018)) in whom EF magnitude reported ranged from 0.13 $V \cdot m^{-1}$ to 0.38 $V \cdot m^{-1}$. Despite their weakness (small number of patients included, lack of precision of the techniques used (DBS)), these studies constitute the cornerstone of knowledge about human *in-vivo* intracerebral EF distribution during a TES.

Still, more experimental studies need to be done on electric field distribution in human *in-vivo* using mini-invasive techniques in a larger cohort. This thesis will attempt to do so by taking the advantage of SEEG investigation performed in refractory focal epilepsy patients. Subsequently, the effects of such electric field applied in epilepsy will be studied.

III. TES applied to refractory focal epilepsy

1. The epilepsy

Epilepsy (*επιληεψία*), deriving from the Greek term *epilambanein* (*επιλαμβυειυ*) which means "to seize, to possess, or afflict" (Magiorkinis, Sidiropoulou and Diamantis, 2010), has been known for millennia, and people have had many theories about its origin: from a godlike touch to a demonic possession. The first written description of epilepsy date from a 4000-year-old tablet found in Mesopotamia reporting the symptoms:

> *"his neck turning left, hands and feet are tense, and his eyes wide open, and from his mouth froth is flowing without him having any consciousness"* (Labat, 1951)

In 1700 B.C, from an experiment on a wounded patient with an opened skull, Egyptians proved that epilepsy originates from the brain instead of coming from gods or spirits as the Mesopotamians believed. However, during the following centuries, theories of epilepsy's spiritual origin took over the rational Egyptian's explanation notably when the Babylonians studied the disease. Symptoms and diagnostics of epilepsy were written on tablets of the Neo-Babylonian period (ca. 626-539 BC). They used terms like miqtu (fall), hayyatu (fit), and sibtu (seizure) and advocated also coming from *"the Hands of several supernatural entities"* (Wilson and Reynolds, 1990). The Greeks also believed on the spiritual origin of epilepsy by naming it *seliniasmos*, sacred disease, Herculian disease (Hercules was affected by the disease) or demonism. During the 5th century B.C Hippocrates brought back rational explanations saying that the brain might be the root cause of the seizures and qualified as charlatan practitioners who believe in the disease's spiritual causes (Magiorkinis, Sidiropoulou and Diamantis, 2010):

> *''My own view is that those who first attributed a sacred character to this malady were like the magicians, purifiers, charlatans and quacks of our own day, men who claim great piety and superior knowledge. Being at a loss, and having no treatment which would help, they concealed and sheltered themselves behind superstition, and called this illness sacred, in order that their utter ignorance might not be manifest"* (Hippocrates 1849)

In his work, he also described and interpreted with an astonishing precision the clinical manifestation of the pathology, notably the aura:

> *''[The people who] are habituated to their disease have a presentiment when an attack is imminent, and run away from men, home, if their house be near, if not, to the most deserted spot, where the fewest people will see the fall, and immediately hide their heads. This is the result of shame at their malady, and not, as the many hold, of fear of the divine"* (Hippocrates 1849; Magiorkinis, Sidiropoulou, and Diamantis 2010)

Despite the tremendous work emanating from Hippocrates' prodigious scientific mind, most people still believed that epilepsy comes from gods and/or demons. Then, during millennia, these beliefs lasted and have even been enforced from the misunderstanding and/or the wrong translation of scriptures from the New Testament:

> *"Teacher, I brought You my son, who has a mute spirit. And wherever it seizes him, it throws him down; he foams at the mouth, gnashes his teeth, and becomes rigid.* […] *And when he saw Him, immediately the spirit convulsed him, and he fell*

> *on the ground and wallowed, foaming at the mouth."* The Bible, Mark 9:17-18,20 (New King James Version)

The spectacular manifestation of the pathology and the difficulty of finding its origin elicited fear in people, which led to misinterpretation and irrational theories. The idea of an evil spirit invading the body brought society to the practice of exorcism on epileptic patients, then to their discrimination and even persecution. For thousands of years, until recent time, epileptic patients have been oppressed by people in addition to their own disease. For instance, in 1956, 17 states of the USA prohibited people with epilepsy from getting married and 18 states sterilized epileptic people for eugenic purposes. Nowadays, epilepsy stigmatization, mainly resulting from religion and superstitions, is as prevalent in developing countries as they are, surprisingly, in Western countries. Even nowadays in western countries it exists a non-negligible amount of people "who claim great piety and superior knowledge" accusing epilepsy patients to be possessed by demons "in order that their utter ignorance might not be manifest" as Hippocrates said. Thus, still today epileptic patients must deal with societal outcomes in addition to the burden of their own disease.

d. Epidemiology

Today, the estimated number of epileptic people in the world is around 50 million (WHO, 2018). A large metadata study reported that the overall lifetime prevalence of epilepsy was 7.60 per 1,000 persons and was higher in low to medium income countries (8.75 per 1,000) than in high income countries (5.18 per 1,000) (Fiest *et al.*, 2017), or according to the WHO, 80 % of epileptic patients live in low-income countries (WHO, 2018). Prevalence can vary according to ethnicity, health quality, gender, and preexisting disabilities (Kaiboriboon *et al.*, 2013). Indeed, the prevalence is higher in men than women and the incidence is higher in the youngest and oldest populations, but lower in the mid-aged population (Fiest *et al.*, 2017). Epilepsy costed 8.6 billion dollars in USA in 2016 (Dieleman *et al.*, 2020) and 0.2 % of the gross domestic product for European countries (Baulac *et al.*, 2015).

e. Semiology and Physiopathology

The main clinical manifestation of epilepsy is the epileptic seizure, of which there are two types: generalized seizures and focal seizures (psychogenic non-epileptic seizures are not disclosed here). Cognitive impairment, sleep or language disorders are also part of the epilepsy syndrome.

Generalized seizures

In generalized seizures, epileptic ictal discharges (electrophysiologic discharge during a seizure) are immediately propagated to both hemispheres, and thus involve simultaneously the entire brain. The clinical characteristics of these seizures do not include any sign that could link them to an anatomical and functional system located in the two hemispheres. The motor manifestations, when they exist, are immediately bilateral and symmetrical. The critical EEG manifestations are characterized by spikes, poly-spikes, spike-waves, or poly-spikes-waves discharges that are bilateral,

synchronous, and symmetrical on both hemispheres. They associate a transient loss of consciousness (absence of a few seconds to a few minutes) with tonic (muscle contractions), myoclonic (muscle jerks), tonic-clonic (combining of both) or atonic (without muscle tone) motor signs.

They are two types of generalized seizures according to the 2017 ILAE classification:

- The first one, the most impressive, corresponds to a motor seizure affecting the whole skeletal musculature (sudden stiffening then shaking), associated with a loss of consciousness and vegetative manifestations (respiratory, urinary...). They are subdivised into 8 groups according to the new ILAE 2017 classification (Scheffer *et al.*, 2017; Sarmast, Abdullahi and Jahan, 2020): Tonic-clonic, Clonic, Tonic, Myoclonic, Myoclonic Tonic-clonic, Myoclonic Atonic, Atonic, Epileptic Spasm.
- The second one, called "absence", is characterized by a brutal rupture of consciousness, sometimes accompanied by slight muscular contractions of the limbs or the eyelids, or by a fall of the muscular tone. They are subdivided into 4 groups according to the new ILAE 2017 classification (Scheffer *et al.*, 2017; Sarmast, Abdullahi and Jahan, 2020): Typical, Atypical, Myoclonic, Eyelid Myoclonia.

Focal seizures

Only a specific brain area is involved in the excitation and hypersynchronization, which led to various clinical manifestations. For instance, a discharge in the motor cortex may cause finger stiffening or twitching which may spread to the arm and then to the rest of the body. In the same way, epileptic seizures can generate tingling in a limb, auditory or visual hallucinations according to the area where the electric discharge occurs. There are many various clinical manifestations of focal epilepsy such as language impairments, manifestations of *déjà vu*/*déjà-vécu*, emotional signs (fear, laughter, ecstasy...), pain, vegetative signs (salivation, apnea, tachycardia...) automatic gestures or motor behaviors. A loss of consciousness (or loss of contact with the surrounding environment) is also often observed. The first clinical signs are thus very important for localizing the epileptogenic zone. Focal seizure can spread and therefore, generate a secondary generalized seizure.

Epilepsy may have distinct etiologies. It can be of genetic, infectious, immune metabolic, or structural causes (Scheffer *et al.*, 2017).

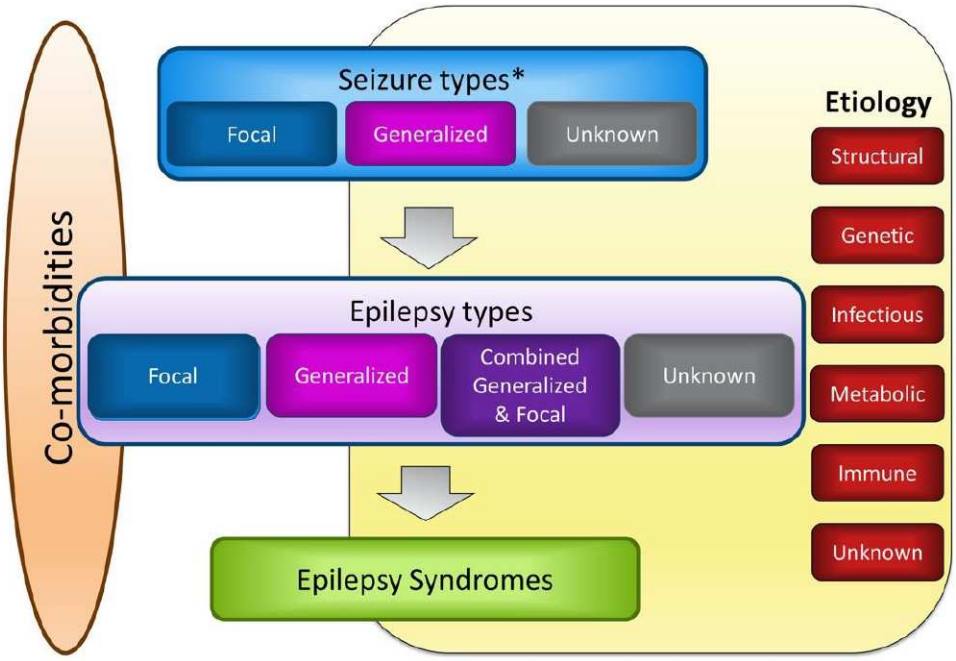

Figure 15: Framework for Classification of the Epilepsies. * Denotes onset of seizure. From ILAE classification of the epilepsies: Position paper of the ILAE Commission for Classification and Terminology. *Epilepsia*, *58*(4), 512–521 by Scheffer, I. E. *et al.*, (2017). © 2017 by Blackwell publishing inc. Reproduced with permission of Blackwell publishing inc. under license number 1199810-1 in the format of print and electronic via Copyright Clearance Center.

2. Investigational method: the electroencephalography (EEG)

To establish a diagnosis, the electroencephalogram (EEG) (Figure 16) is one of the most important diagnostic tools among Positron Emission Tomography (PET scan), MRI and biological exams. Physicians will detect potential electrophysiological abnormalities, mainly inter-ictal epileptic discharges (or IEDs Figure 18) or seizures (ictal discharges Figure 21). IED are paroxysmal asymptomatic (without any obvious clinical manifestation) pathological patterns of activity occurring between seizures (ictal) which frequency of occurence oscillates with the circadian rhythm (Baud *et al.*, 2018). This pathological activity is produced in the "irritative zone" (Talairach and Bancaud 1966a; Kahane et al. 2006). Detection of such activity is necessary (but not sufficient) to establish the diagnosis of epilepsy.

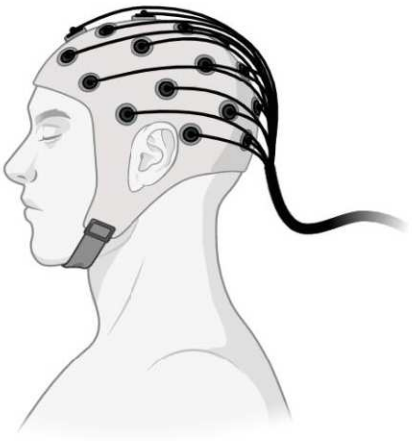

Figure 16: Schematic view of an electroencephalography created from BioRender.com.

There are 2 types of conventional EEG: short EEG recording (several hours) and long EEG recording (several days). Both EEG examinations are coupled with video recording to correlate clinical manifestation to electrophysiological activity of a potential seizure. Indeed, the first clinical symptoms are very important to localize the pathological brain area. EEG clinical investigation implies also "activation tasks" like intermittent photic stimulation (using a strobe light which can activate pathological activity on the trace), hyperpnea or sleep deprivation.

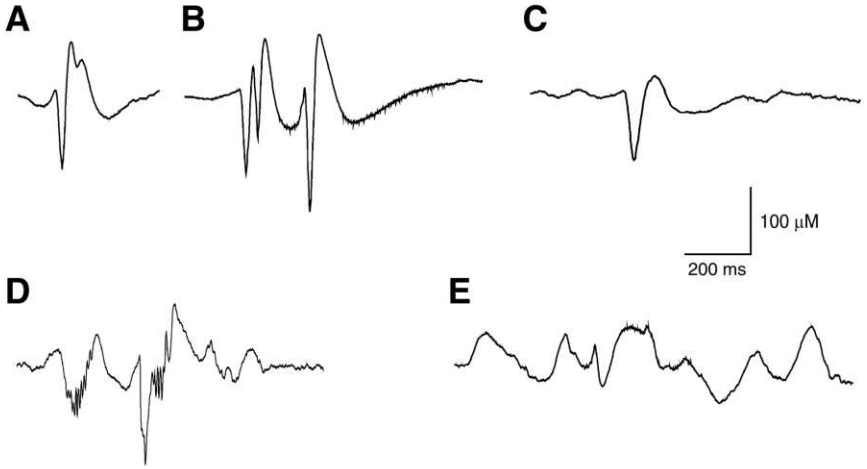

Figure 17: Interictal epileptic discharge (IED) patterns recorded in human partial epilepsies with intracranial electrodes from Jasper's Basic Mechanisms of the Epilepsies 4th edition Chapter: Interictal Epileptiform Discharges in Partial Epilepsy (de Curtis, Jefferys and Avoli, 2012) licensed under **CC BY 3.0**. **A** Interictal spike; **B** group of interictal spikes from neocortical dysplasia, **C** sharp wave from a lesional partial epilepsy; **D** fast activity (brushes) riding on a spike recorded from a Taylor type II focal cortical dysplasia; **E** paroxysmal slow activity superimposed to slow spikes recorded in a lesional partial epilepsy.

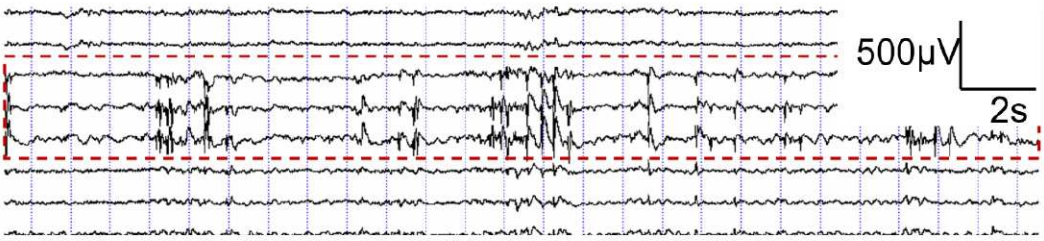

Figure 18: Interictal discharges recorded on SEEG (CHRU Nancy)

After the diagnosis, a pharmacological treatment is usually proposed. The aim is to reverse the alterations in the excitatory or inhibitory synaptic transmission and to limit seizures' electrical propagation. With these treatments, seizures can be controlled (reduction of seizures occurrence or total seizure suppression) in 60 to 70 % of cases (Thomas and Arzimanoglou, 2003). Sometimes, despite several lines of antiepileptic drug treatment, seizures can't still be controlled: the epilepsy becomes a "refractory epilepsy".

In the case of focal refractory epilepsy, if a unique epilepsy focus is located in a non-eloquent brain area, the patient could be eligible to surgery to try to remove the pathological area. But before the surgery, patients need to undergo into a presurgical evaluation including notably intracerebral electrophysiological recording with stereotactic-EEG (stereoelectroencephalography or SEEG).

3. The reference method for the investigation of refractory focal epilepsy: the stereoelectroencephalography (SEEG)

The presurgical evaluation must precisely identify the epileptogenic zone and the highly functional cerebral areas which must be spared during the intervention (Thomas and Arzimanoglou, 2003). This assessment should ideally be carried out in an epilepsy center and by a multidisciplinary team. The standard presurgical evaluation includes neuropsychological tests and long-term (5-day period) high-resolution electroencephalographic (EEG) video recordings combined with electrical source imaging analysis, Positron Emission Tomography (PET) and high-resolution Magnetic Resonance Imaging (MRI). Finally, an accurate topological electrophysiological identification of the epileptogenic zone via an intracerebral investigation (Figure 21). To do so, there are 2 current methods:

- Sub-dural or epidural investigation with sensors grids or strips placed on cortical surface after performing a craniotomy: ElectroCorticography (ECoG). (Figure 19 A and B)
- A depth cortical and sub-cortical investigation with sensors placed with a stereotactic method: stereoelectroencephalography which was invented in France (Talairach, Bancaud, and Szikla 1974; Talairach and Bancaud 1966a) (Figure 19 C and D).

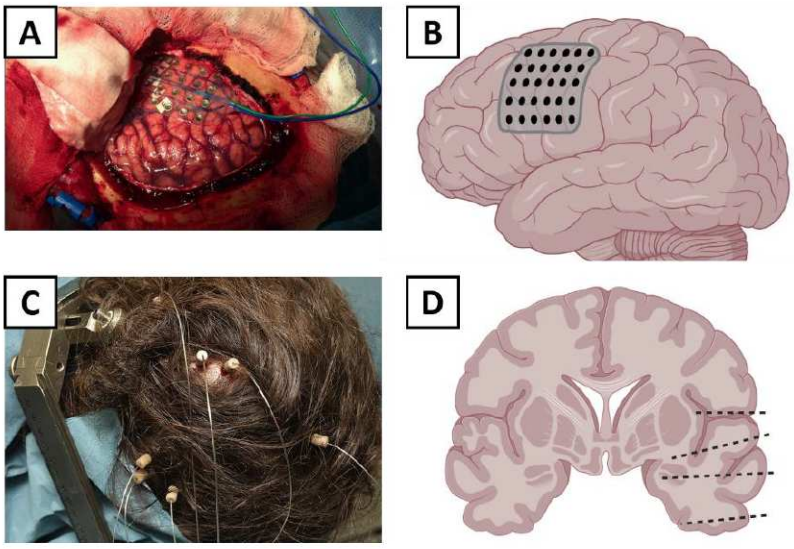

Figure 19: The two invasive investigational methods for refractory focal epilepsy. **A**. Picture of an ongoing ECoG investigation in the surgery room from Utility of electrocorticography in the surgical treatment of cavernomas presenting with pharmacoresistant epilepsy. In *Epileptic Disorders* (Vol. 16, Issue 3, pp. 245–260) by San-Juan *et al*., (2014). © 2014 by John/Libey eurotext. Reproduced with permission of John/Libey eurotext under license number 1201189-1 in the format of print and electronic via Copyright Clearance Center. **B**. Schematic view of an ECoG grid over the cortex created from BioRender.com. Each black dot represents an electrophysiological measurement point (metallic contact). **C**. Picture of an ongoing SEEG implantation. **D**. Schematic view of an SEEG implantation. Each black segment represents a metallic contact on which electrophysiological activity is recorded. created from BioRender.com.

SEEG consists of implanting multi-contact intracerebral electrodes (Figure 19 C and D) in and around the epileptogenic zone with a stereotactic frame (Figure 20). This is done in a surgical room under general anesthesia (for a more detailed method see Chapter 2, Method). Compared to ECoG, SEEG has several advantages: firstly, this mini-invasive method doesn't require a heavy and traumatic surgical intervention like a craniotomy which carries the risk of hemorrhage, infection, and cerebrospinal fluid leak and is therefore a safer procedure (Salado *et al.*, 2018). Secondly, it is possible to explore deep brain structures such as the hippocampus, cingulate gyrus, and amygdala contrary to ECoG which records only cortical surfaces areas. Thirdly, it is possible to record intracerebral electrophysiological activity for a long period (1 or 2 weeks) which produces a large amount of electrophysiological data for an accurate targeting and diagnosis. Fourthly, if one or several SEEG electrodes are placed exactly in the epileptogenic zone, it is, in some case, possible to perform a thermocoagulation to burn the pathological area.

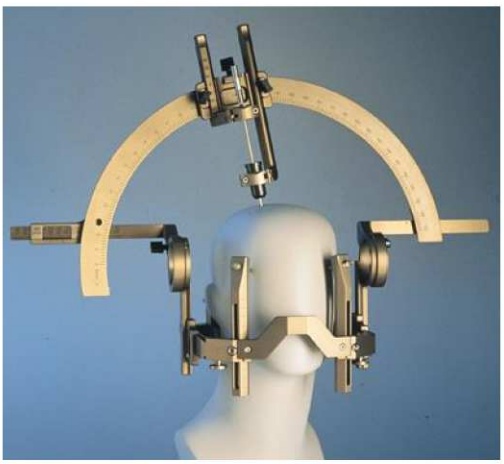

Figure 20: Stereotactic frame (G-frame Leksell Stereotactic System) to perform Stereoelectroencephalography electrodes implantation.

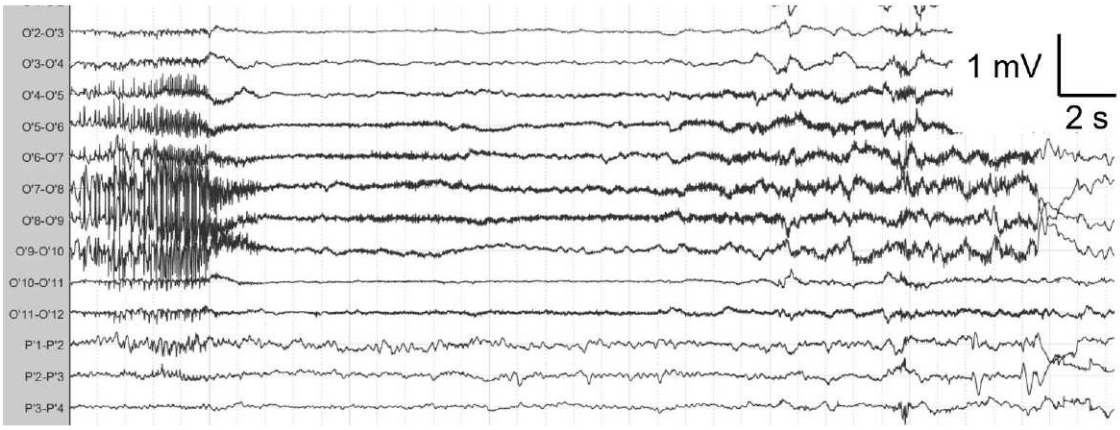

Figure 21: Example of a seizure recorded on a SEEG electrode in the insula (CHRU Nancy).

4. TES applied to refractory focal epilepsy

Sometimes patients are not eligible to epilepsy surgery because the epileptic network is too complex, it involves highly functional areas (memory, language, and other complex functions) or several epileptogenic zones are detected. For those patients other therapeutic methods exist which are used in clinical routine or under scientific research and clinical trials. Among them, there are the vague nerve stimulation (invasive method), Transcranial Magnetic Stimulation (TMS, non-invasive) and TES (non-invasive).

For the last 15 years, tDCS were explored in epilepsy (San-Juan *et al.*, 2015) and a few controlled clinical studies investigated focal refractory epilepsy (Lefaucheur, 2016). They mainly used tDCS to induce long polarization on the cortex to impact the inhibitory/excitatory imbalance of the epilepsy. They usually performed a cathodal stimulation (negative polarity) to try to inhibit the neuronal hyperexcitability on the cortex. In the following lines, only clinical trials are reported in accordance with the review provided by (Lefaucheur, 2016). Case reports are discarded.

Fregni et al., 2006 started to investigate TES (with direct current: tDCS) in a control randomized clinical study in 19 refractory epileptic patients. They applied sham (placebo) stimulation

in 9 patients and a 20-min cathodal DC stimulation at − 1 mA tDCS through saline soaked sponge electrodes (35 cm^2) in 10 patients. Patients were asked to report any seizure within the month before and the month after the DC stimulation. Patients underwent EEG protocol 20 min before and after stimulation to record IEDs. They measured a significant decrease of 64.3 % of IEDs activity for patients who had the stimulation active and of 5.8 % for patients who had a sham stimulation. They also reported a reduction trend (but not significant) in seizure frequency.

Another team reported the same effect in 2013 in 36 children with refractory epilepsy (27 of them had an active stimulation and 9 had a sham stimulation) (Auvichayapat *et al.*, 2013). They showed a significant IEDs decrease recorded on EEG after a 20 min cathodal stimulation at − 1 mA (with saline soaked electrodes 35 cm^2) which can last 48 hours. They also noticed a slight decrease (but not significant) of seizure frequency.

The effects of repetitive tDCS session were also investigated in 28 patients with mesial temporal lobe epilepsy and hippocampal sclerosis in a randomized placebo-controlled, double-blinded clinical trial (San-Juan *et al.*, 2017). They performed several daily sessions (one group 3 days and one group 5 days) of a 30min tDCS at − 2 mA, cathode placed on the irritative zone with saline soaked sponges' electrodes (35 cm^2). They reported a significant reduction in seizure frequency in the 2 following months (− 43.4 % for 3 days sessions and − 54.6 % for 5 days sessions) and a significant decrease of IEDs measured on EEG immediately post stimulation.

(Tekturk *et al.*, 2016) reported a similar effect on seizure frequency (a reduction of 50 %) for repetitive tDCS session (3 session of 20min at 2 mA with saline soaked sponge electrodes 35 cm^2) in a crossover study.

A clinical trial explored tDCS effect in Lennox-Gastaut syndrome, in which 22 children were included (15 active stimulation, 7 sham, (Auvichayapat *et al.*, 2016)). They performed consecutive daily tDCS sessions (5 days) at 2 mA with saline soaked sponges (35 cm^2). They reported a significant seizure reduction from 53.4 % (day 1) to 99.8 % (day 5) during the treatment. Then, after the treatment, a slight increase of seizure frequency was noticed (from 89.7 % reduction at week 1 to 81.1 % reduction at week 4). For the IEDs they measured a decrease of 76.4 % immediately after the treatment. During the following weeks, IEDs reduction went from − 63.1 % to − 8.5 % from week 1 to week 4, respectively.

Assenza and colleague in 2017 also reported a significant seizure frequency reduction (of − 71 % compared to sham − 25 %) after tDCS. They performed several tDCS sessions of 1 mA for 20 mA through saline-soaked sponges electrodes (35 cm^2) (Assenza *et al.*, 2017)

Overall, according to clinical studies, cathodal tDCS reduces systematically and significantly seizure frequency and IEDs measured on EEG. Also, repetitive sessions seem to increase the beneficial effect of tDCS. The strengths of these studies are the number of patients included, the

electrophysiological biomarker studied (IED) and the study design (most of them are blinded studies, some are crossover and/or double blinded). Despite these encouraging results, the previous studies present some weakness such as the number of seizures reported by patients in some studies, the manual IED counting which can be biased, the EEG recording which is very sensitive to environmental electromagnetic pollution and electrophysiological artifacts. Moreover, there is still a lack of knowledge about the tDCS effect on pathological biomarkers directly measured on pathological area.

This thesis work will tackle this topic by studying tDCS effects on epileptic biomarkers through intracerebral measurement performed with SEEG. As mentioned in part II.2 the majority of refractory focal epilepsy affect the temporal lobe. Among the structures explored with SEEG in temporal lobe epilepsy we can find the ventral occipito-temporal cortex which is responsible for high level visual cognitive functions such as facial perception. Recording electrophysiological activity in the ventral occipito-temporal cortex made possible studies in face perception notably the mapping of face responsive areas (Jonas *et al.*, 2016).

SEEG investigation in temporal lobe epilepsy patients can give a unique opportunity to also study TES effects on cognition by measuring intracerebral electrophysiological activity associated to the cognitive function of face perception.

IV. TES applied to facial perception and recognition.

Some behavioral studies have been conducted with TES applied to face perception (tDCS, tACS, tRNS) with various sample sizes (from 16 to 114 participants). They reported diverse effects on behavior during or after TES such as face perception, face memory and, humor detection enhanced (Manfredi *et al.*, 2017), learning effect decreased (Renzi *et al.*, 2015) or even no effect at all (Willis *et al.*, 2019). But the sensitivity of some behavioral protocols to external factor (fatigue of the subject, mood, events, attention which is hard to quantify *etc*.) can add variability to results. Also, the behavior studied to assess a specific cognitive function, involves several other cognitive processes which can deliver false positive results, or “drawn” the information. More generally, behavioral studies assessing TES have been challenged by some excellent critiques pointing out some poor experimental designs (Parkin, Ekhtiari and Walsh, 2015) or oversimplifications made by some authors when interpreting results (Bestmann, de Berker and Bonaiuto, 2015).

This encourages to study more fundamental quantities of cognitive processes such as electrophysiological biomarkers. In face perception, the N170 is a known evoked related potential (ERP) and there are a few studies investigating this ERP with surface EEG combined with tDCS. They all measured TES effects on ERP’s amplitude and timing and reported variable results. While some reported a non-significant amplitude difference between active stimulation and sham (Lafontaine *et*

al., 2013), others observed the opposite by measuring an amplitude increase of the ERP during and/or after TES (Yang *et al.*, 2014; Civile *et al.*, 2018, 2020).

From these results it is possible to state that TES has an effect. However, results still present a high variability and the low signal noise ratio of the N170 could weaken even more their conclusions. Another approach exists to study the electrophysiological response of the face perception function which is the Fast Periodic Visual Stimualtion (FPVS) (Rossion, 2014c), synchronizing neuron population responsible of the cognitive function desired (in that case face perception) thanks to fast periodic visual stimuli. The amplitude of the cognitive response is quantified on the amplitude spectrum at the exact frequency of the visual stimulus after a fast Fourier transform of the EEG and/or SEEG signal. This interesting approach make possible the discrimination and quantification of two different visual cognitive processes: low level basic visual responses and high-level face perception responses. Also, this method delivers a high SNR and very reproducible responses (Rossion, 2014c, 2014a). To date there are no study investigating TES effects on cognitive responses using this method. Therefore, this thesis will adresse the question of TES effects in face recognition by leveraging on this paradigm combined with intracerebral investigation of the visual ventral stream.

V. Objectives of this thesis

Despites the encouraging results in biophysics, in epilepsy and in face recognition, TES effects are still debated (Horvath, Forte and Carter, 2014, 2015; Bestmann, de Berker and Bonaiuto, 2015; Parkin, Ekhtiari and Walsh, 2015; Medina and Cason, 2017). This debate increased when results from a post-mortem study challenged conventional TES saying it can't generate a sufficient electric field in the brain (Underwood, 2016). But it is important to note that the mentioned presentation suggested to reconsider conventional stimulation methodologies by proposing other interesting solutions to increase the intracerebral electric field. In the meantime, Opitz and colleague reported an intracerebral electric field *in-vivo* with conventional TES and then pointed out *ex-vivo* studies limitations providing an answer to the ongoing debates (Opitz *et al.*, 2016, 2017). This marked a new era in biophysics of TES investigation. Several studies followed then demonstrating an electric field in human *in-vivo* during a TES (see part II.4.c page 49 "Measuring the intracerebral electric field in human *in-vivo*"). Nonetheless the mentioned studies present some weaknesses such as the use of ECoG in most patients. There are too few patients included in SEEG exclusively (n = 2) which represent an interesting approach for exploring EF *in-vivo* with a minimum modification of the head geometry. This technique is used in this thesis as an approach to answer the following questions:

1. Is it possible to generate and measure systematically an intracerebral electric field in the limbic system with values superior to 0.14 $V \cdot m^{-1}$ (minimum value inducing a neuronal entrainment reported by (Francis et al., 2003)) during a TES in human *in-vivo*?

2. What is the impact of different parameters such as the stimulation frequency, intensity, electrode placement, and depth of measurement on EF magnitude in human *in-vivo*?

These questions will be addressed in the first study (Chapter II). TACS at several frequencies, using different montages and at different intensities were performed and intracerebral EF calculated from the voltage values recorded on each intracerebral contact. The term "systematically" mean that an intracerebral EF on SEEG was measured in every patients in a bigger cohort than the previous mentioned studies altogether.

Then, once the basis of intracerebral EF will have been studied, a second study (Chapter III:) will address the question of its application as a therapeutic tool in epilepsy by attempting to answer the question:

"Is tDCS able to modulate the epileptic activity measured directly on the pathological zone?"

It will be organized into 2 sub-studies:

- The investigation of tDCS effects on inter-ictal activity (before, during and after stimulation) in 12 refractory focal epileptic patients who are implanted with SEEG electrodes. The inter-ictal evaluation will be performed with an automated spikes detection tool.
- The investigation of tDCS effect on ictal activity in a single patient who had an epileptic seizure during a tDCS.

Finally, because a major part of focal epilepsy implicates the temporal lobe, SEEG often explores the ventral occipito-temporal cortex. Therefore, a third study addressing the question of TES applied in cognitive processes of face perception will be performed (Chapter IV:) to answer the question: "Is it possible to modulate, the electrophysiological activity induced by face perception tasks?". The methodology will use a robust cognitive task (Fast Periodic Visual Stimulation) mastered by the team. Electrophysiological responses associated to the cognitive function of face perception and identity discrimination were measured and quantified before, during and after tDCS. This third study is also subdivided into 2 parts:

- Intracerebral investigation in 4 refractory focal epileptic patients who are implanted with SEEG electrodes.
- Scalp EEG investigation in 15 healthy subjects.

A fifth part will discuss the results and address the limits of the presented studies. Then, a focus will be done on some solutions to overcome the mentioned limits and to give ideas for future perspectives.

Chapter II

Human *in-vivo* investigation of intracerebral electric field induced by TES

Neuromodulatory effects of TES are directly related to the electric field (EF) strength generated on the neuron population. Numerous publications have reported neuromodulation with TES, but the lack of knowledge regarding the causes (i.e., the electric field) has led some researchers to question the technique's effects. Many computational methods attempted to simulate with great precision in humans the EF distribution induced by a TES. Despite the numerous computational models existing, there is still a need of establishing a ground truth. To that end it is fundamental to measure the intracerebral EF (iEF) empirically in humans. But the complexity of these investigations (especially the availability of intracerebral investigations) has refrained the community from performing studies on this specific topic. Only recently, a few teams managed to obtain results and/or publish proof of concept for intracerebral EF investigation in humans.

This chapter will attempt to treat the question of empirical intracerebral EF measurement in human *in-vivo* by using a different approach. Results from this chapter will also form the basis for the work presented hereafter in this thesis.

A part of the work described in this chapter was published in the journal of *Brain Stimulation*:

Louviot S, Tyvaert L, Maillard LG, Colnat-Coulbois S, Dmochowski J, Koessler L. 2022 "Transcranial Electrical Stimulation generates electric fields in deep human brain structures" *Brain Stimulation*; 15 (1) :1–12. https://doi.org/10.1016/j.brs.2021.11.001.

I. State-of-the art and scientific context

1. Human *post-mortem* study

Buzsáki's team post-mortem study presented in 2016 has been widely discussed in the past years and in the previous lines of this thesis. It was published only 2 years later, in 2018 along with an *in-vivo* iEF investigation in rodents providing, nonetheless, important, and interesting basic knowledge on TES biophysics in humans (Vöröslakos *et al.*, 2018) which has been cited 332 times (source Google Scholar). In their study, they included 11 cadavers with brain *in situ* and subdural space filled with physiological saline solution (0.9 % Na-Cl) to replace cerebrospinal fluid (CSF) lost during their implantation. They investigated electric stimulation in different configurations:

- Epidural (stimulation was applied on the meninges).
- Subcutaneous (the scalp was removed, and stimulation was applied directly on the skull)
- Transcutaneous (scalp was not removed, and stimulation was applied on the skin).

Transcutaneous electrical stimulation, which was the closest configuration to conventional TES, was performed on 6 cadavers. In these cadavers, they implanted 4 intracerebral electrodes (distributed in a same plane) containing 7 recording contacts each, which represent 168 intracerebral contacts.

In their article, they used "intensity" for the two physical quantities of current and voltage. In the following lines, to avoid any confusion and to use physics' proper terminology, voltage V (in Volts [V]) and intensity I (or current in Ampere [A]) will be used.

They investigated the effect of TES voltage applied on iEF in transcutaneous stimulation (6 cadavers, 5 different voltages from 1 V to 5 V. They applied 2 to 3 different voltages to each cadaver, making a sample size of 14 experiments). To do so, they performed tACS at 200 Hz and found a "nearly perfect" linear correlation between the voltage applied and the current measured (with the indirect measure of the voltage drop) with a Pearson's correlation of $R = 0.86$. They concluded that Ohm's law can be applied and from that finding established a relationship between iEF measured and stimulus current (derived from estimations).

They found a linear relationship between the current estimated and measured iEF, with a Pearson's correlation of $R = 0.80$ (calculated on 28 intracerebral contacts in 6 cadaver). A mathematical relationship was extracted from that experiment:

$$E_{transcutaneous} = 0.13 \cdot I + 0.04$$

Where $E_{transcutaneous}$ is the intracerebral electric field for a transcutaneous stimulation in milli-Volts per milli-meter ($mV \cdot mm^{-1}$) which can directly be expressed into Volts per meters ($V \cdot m^{-1}$) (1 $mV \cdot mm^{-1} = 1\ V \cdot m^{-1}$); I the stimulation amplitude in milli Ampere (mA). By another extrapolation, they concluded that a 6 mA TES applied on the scalp is needed to generate 1 $V \cdot m^{-1}$ in a living brain.

They also studied the effect of the stimulation frequency (9 frequencies: 5 Hz; 10 Hz; 20 Hz; 50 Hz; 100 Hz; 200 Hz; 500 Hz; 1000 Hz; 2000 Hz) and the electrode size in only subcutaneous and epidural configuration. They reported a *"minor effect"* of the frequency on the iEF ($p = 0.99$, one-way ANOVA test).

Finally, in their transcutaneous stimulation study, they reported that 58 % of the current is shunted by the skin and the soft tissues (and not 90 % as reported Underwood in 2016).

2. Pioneers *in-vivo* studies in human

a. Opitz et al., 2016 - Spatiotemporal structure of intracranial electric fields induced by transcranial electric stimulation in humans and nonhuman primates

As mentioned in chapter I, Opitz and colleague in 2016 were the first to investigate iEF during a TES in human in-vivo (Opitz *et al.*, 2016). They included 2 patients with focal refractory epilepsy who were included into a presurgical evaluation protocol. One patient had a bilateral SEEG implantation of 11 electrodes containing 8 to 12 intracerebral contacts each, for a total of 110 intracerebral contacts. The other patient had 64 ECoG electrodes, and 10 subdural/depth EEG electrodes containing from 4 to 10 contacts for a total of 134 measurement points. They performed a

1 mA tACS at 1 Hz with saline soaked sponges (25 cm^2) placed on both temples (to obtain the main iEF component along intracerebral electrodes directionality) and recorded the voltage on intracerebral contacts (channels). Then, they obtained amplitudes (or voltage in V) by calculating absolute values of the Fast Fourier Transform (FFT) at the frequency of 1 Hz. After that, they calculated the voltage gradient to obtain iEF magnitude values. They also evaluated the spatial distribution of the iEF by measuring the spatial distance for values above 25 % and 50 % of the maximum.

For the SEEG patient, they reported a median iEF of 0.098 $V \cdot m^{-1}$ and a maximum iEF of 0.36 ± 0.008 $V \cdot m^{-1}$. The longest distance for iEF magnitude above 50 % of the maximum was 39.6 mm and above 25 % was 45.7 mm. For the ECoG patient, they reported a median iEF of 0.059 $V \cdot m^{-1}$ and a maximum iEF of 0.16 ± 0.007 $V \cdot m^{-1}$. The longest distance for iEF magnitude above 50 % of the maximum was 47 mm and above 25 % was 74.6 mm.

The authors concluded that head tissues can be as resistive with a small capacitive component. This conclusion derived from the frequency investigation in monkeys where they found a 10 % decrease in the measured voltage for a stimulation frequency over 15 Hz and negligible phase-shift (from 1 to 2 degree). This precious information needed to be confirmed in human *in-vivo*.

b. Huang *et al.*, 2017 - Measurements and models of electric fields in the in vivo human brain during transcranial electric stimulation

Huang and colleagues in 2017 aimed to validate their computational model by human *in-vivo* experiments in 10 focal refractory epilepsy patients who underwent into a presurgical evaluation (Huang *et al.*, 2017). The following line will focus on the iEF measured and the influence of different parameters such as the frequency and the intensity. Comparisons between computational model and empirical values are not in the scope of this chapter.

Nine patients with ECoG and depth electrodes were included and one patient with only SEEG electrodes (5 mm spacing between each intracerebral contact). They performed tACS at various frequencies (from 1 Hz to 10 Hz with 1 Hz step and from 10 Hz to 100 Hz with 10 Hz step) and at various intensities (from 0.5 mA to 2 mA) with rubber electrodes and gel (4 cm^2) placed on the frontal (Pz) and occipital (Oz) lobes. They measured the intracerebral voltages induced by tACS on a total of 1,380 intracranial/intracerebral contacts (80 intracerebral contacts for the patient with SEEG-only). They discarded contacts with strong 60 Hz interference and clipping (example of sine wave clipped, Figure 34). Thus, 175 contacts were discarded, and analysis was done on 1,205 intracranial/intracerebral contacts (78 intracerebral contacts for the patient with SEEG-only investigation). They measured voltage values by fitting a sinusoid to the signal recorded on each contact. Then, they obtained iEF values by subtracting voltages on adjacent contacts and dividing by the distance separating them.

Their main finding was a maximum iEF of 0.4 $V \cdot m^{-1}$ for a 2-mA stimulation. In their discussion, they considered this result rather weak under the light of the previous study (0.36 $V \cdot m^{-1}$ (Opitz et al.., 2016)) They explained this value by the remote position of stimulation electrodes purposefully placed far from craniotomy sites to avoid modification in the current flow. They observed qualitatively a linear relationship between stimulation intensity and measured intracerebral voltage. Concerning the frequency investigation, they reported a 25 % decrease in voltage measured from 1 Hz to 100 Hz. They observed the same phenomenon in saline solution and concluded to a non-uniform gain of the recording equipment and electrodes.

This important study is the only one validating computational model for simulating TES-generated iEF in humans *in-vivo*. Furthermore, all their raw data are provided to help the community validate their own model and, doing so, building the biggest published database about iEF in humans *in-vivo* during a TES. Recently, this database was used to publish a comparison between several computational modeling methods (Puonti *et al.*, 2020).

c. Ruhnau *et al.*, 2018 Sailing in a sea of disbelief: In vivo measurements of transcranial electric stimulation in human subcortical structures

In a letter strongly denouncing the TES critics, Ruhnau and colleagues showed in a single case that intracerebral voltages induced by tACS can reach subthalamic nuclei. They performed 1 mA tACS at 10 Hz and 130 Hz with 2 saline-soaked sponge electrodes (35 cm^2) (Ruhnau *et al.*, 2018). They recorded voltage induced on intracerebral contacts of Deep Brain Stimulation (DBS) electrodes. The patient had 2 DBS electrodes containing 4 intracerebral contacts each. They calculated iEF between each intracerebral DBS contact (green arrow in Figure 23) by subtracting voltages measured between 2 adjacent contacts and dividing by the distance separating them.

They reported an iEF max of 0.08 $V \cdot m^{-1}$ which is rather weak compared to previous studies. This is explained by the orientation of the iEF calculated (vector along the DBS electrode which are positioned vertically Figure 23) regarding to its main component (horizontal for a bitemporal stimulation see Figure 23).

d. Chhatbar et al,. 2018 Evidence of transcranial direct current stimulation-generated electric fields at subthalamic level in human brain in vivo

So far, iEF were measured in humans *in-vivo* with AC stimulation. But an interesting approach was proposed by Chhatbar and colleague in 2018 by using tDCS with Deep Brain Stimulation (DBS, Figure 23). This methodology could directly validate the use of tDCS itself and not by extrapolation as it was done with tACS (Chhatbar *et al.*, 2018).

They included three patients with movement disorders who were eligible for a DBS implantation. In a surgical room, during DBS implantation or replacement, they applied tDCS at 2 mA

and 4 mA through saline-soaked sponge electrodes (35 cm^2). They measured on DBS intracerebral contacts the signal (voltage) offset induced by the DC injection (To illustrate, Figure 22 **A** shows an electrophysiological activity recorded on an intracerebral contact and Figure 22 **B** shows the same signal but with a DC injection). Two DBS electrodes (called lead in the paper) were implanted in two patients and one DBS electrode in one patient (each DBS electrode containing 4 intracerebral contacts). For patients who had two DBS electrodes, voltage was recorded with an intracerebral reference, and for the patient with one electrode, measurements were referenced to an electrode put on the chest wall. Two stimulation electrode positions (montage) were tested with patients who had 2 DBS electrodes: bitemporal and occipitofrontal. They calculated an iEF between the reference (voltage measured on DBS contact 5 (V5 in Figure 23) considered as the reference voltage) and the highest voltage value (voltage measured on DBS contact 1 (V1 in Figure 23). So, in that case, the iEF is expressed as:

$$|\mathrm{E}| = \frac{\mathrm{V1} - \mathrm{V5}}{d} = \frac{\mathrm{V1}}{d}$$

With *d* the distance between two DBS electrodes (Blue arrow in Figure 23).

They reported an iEF between 0.19 and 0.26 $\mathrm{V \cdot m^{-1}}$ in the subthalamic nuclei for patient 2 and patient 3, respectively. This was the first time that an iEF during a tDCS was measured in deep brain structures and provides valuable knowledge for studies using tDCS. They also reported a decrease in the body resistance when a 4 mA tDCS was applied perhaps due to polarizing tissues.

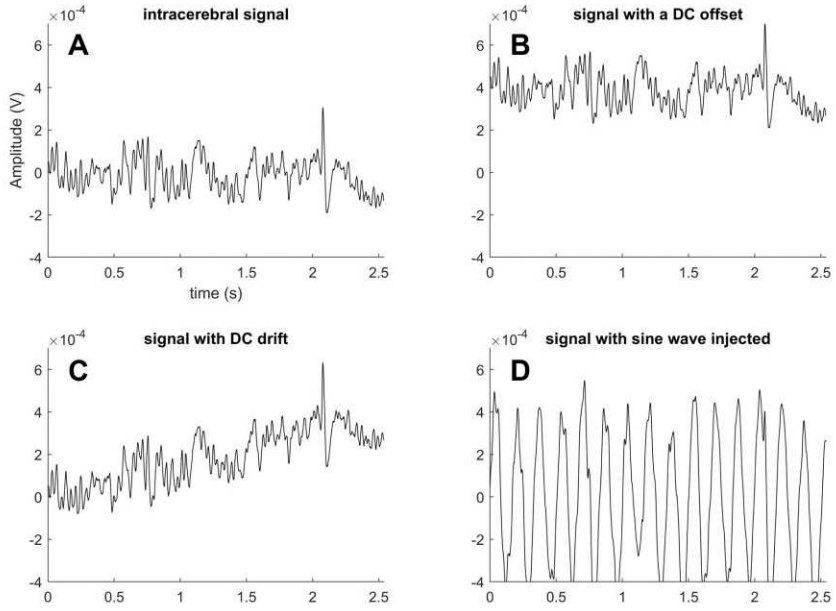

Figure 22: Example of an intracerebral signal with theoretical DC and AC current injection (all DC and AC components were added artificially on a pre-existing intracerebral recording. This is not the result of an intracerebral signal during a TES) (CHRU Nancy). **A**: Original intracerebral signal without alteration. **B**: Same intracerebral signal displayed in **A** affected by a DC offset. **C**: Intracerebral signal affected by a DC drift. **D**: intracerebral signal affected by a sine wave.

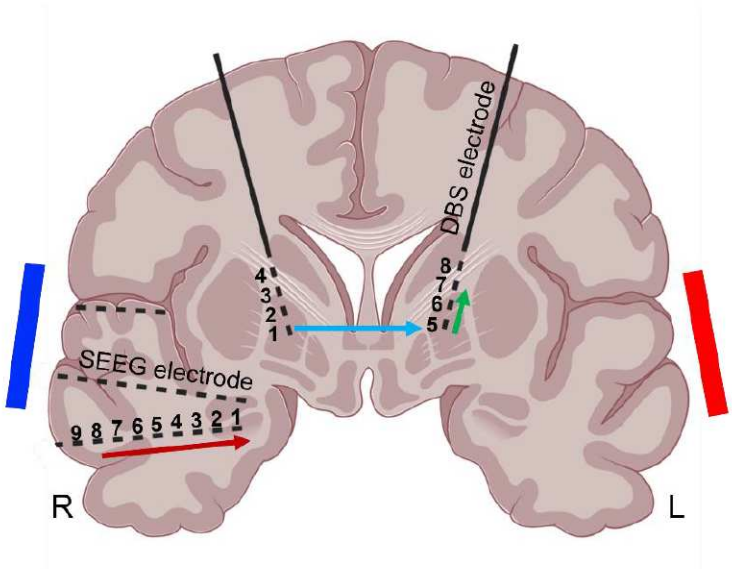

Figure 23: Schematic representation of different techniques used to calculate *in-vivo* iEF during a TES in literature. SEEG are represented as horizontal dashed lines in the right hemisphere: every black dot is a metallic intracerebral contact where voltages are measured. DBS electrodes are represented in vertical mixed plain and dashed lines. All black dots represent a metallic intracerebral contact where voltages are measured (for the specific context of Rhunau *et al.*, and Chhatbar *et al.*, studies). Colored arrows represent how iEF (during a TES, stimulation electrodes represented by blue and red rectangles) are calculated in literature. **Red arrow** iEF calculation method used by Opitz *et al.*, 2016 and Huang *et al.*, 2017: Voltages measured on SEEG intracerebral contacts are subtracted to each other (V1−V2; V2−V3…) and then divided by the distance separating 2 contacts. **Green arrow** calculation method used by Ruhnau *et al.*, 2018: Voltages measured on DBS intracerebral contacts are subtracted to each other (V5−V6; V6−V7…) and then divided by the distance separating 2 contacts. **Blue arrow** iEF calculation method used by Chhatbar *et al.*, 2018: Voltage measured on one electrode (V1 or V2 or V3) is divided by the distance separating the two DBS electrodes. In that case, voltage measured on one electrode is the potential difference between one DBS electrode and the other where the reference (0 V) is set considering V5 = 0 V. Created with BioRender.com

3. Scientific questions

The presented studies provide basic knowledge and constitute the cornerstone of iEF in humans. However, their limitations leave some questions unanswered.

a. About the *post-mortem* study

The first limitation is about the model of study used. It has been explained by Opitz *et al.*, (2017) that results obtained from *ex-vivo* studies are difficult to extrapolate to *in-vivo*. Secondly, the subdural medium has been modified, replacing the CSF with salted water. According to Spector et al. (2015), the human CSF is composed of (Spector, Robert Snodgrass and Johanson, 2015):

- Ions (Na^+ ; HCO_3^- ; K^+ ; Cl^- ; Ca^{++} ; Mg^{++} ; Mn^{++})
- Vitamins (C, folate, thiamine monophosphate, pyridoxal phosphate…)
- Peptides and proteins (leptin, proclatine, transthyretin, albumin, immunoglobulins …)

So, it is challenging to conclude when CSF has been replaced. The third limitation is about the spatial sampling of the iEF measurement. Indeed, iEF measurement for transcutaneous stimulations relied only on 28 intracerebral contacts (distributed in the same plan) in 6 cadavers. This number is quite low to establish reliable conclusions about iEF spatial distribution. The fourth limitation is about the frequency investigation: it was not done in transcutaneous configuration and conclusions from

results obtained without the skin layer can't be extrapolated to conventional TES use on living humans. To conclude, despite knowledge provided on iEF in human, conclusions from this study are built on too many assumptions to be deduced for humans *in-vivo* brains.

b. About humans *in-vivo* studies

Considering that SEEG (or DBS) is the most suitable configuration for an intracerebral measurement of an IEF in living humans, the focus will be on subjects included with SEEG (or DBS) only (without ECoG) among the cited papers. Thus, meeting this criterion, there are overall six subjects included in the literature (n = 1 subject for Opitz et al (2016), Huang et al (2017), and Ruhnau et al (2018); n = 3 for Chhatbar et al (2018)), and iEF was calculated in only five subjects (iEF in patient 1 of Chhatbar et al (2018) was not calculated).

In addition, although neo-cortical iEF has been extensively studied with hybrid ECoG/SEEG investigation (12 subjects), iEF in deep brain regions has only been studied in two subjects and in two structures (subthalamic and thalamic nuclei).

Moreover, results obtained in deep structures lack precision: some measured iEF cannot be considered *within* a single structure but rather *across* multiple structures (Chhatbar *et al.*, 2018). These same results were considered by authors as *"a crude estimate"* due to the distance (up to 4.35 cm) with which the iEF calculation was performed. Other results come from a measurement performed perpendicular (vertical vector following DBS electrode orientation) to the iEF main component (horizontal vectors for a bitemporal TES) (Ruhnau *et al.*, 2018).

Particularly, for the article investigating DC stimulation, the strength and the first weakness of this study was the use of DC current. This interesting approach is double-edged: conclusions resulting from this method directly apply to tDCS studies without assumption and extrapolation. On the other hand, it is challenging to measure a DC induced signal because the recording system can have "naturally" polarized channels and, therefore, show an offset. Also, DC drift can occur during recording, and for that reason recording devices usually have a high-pass filter which removes all DC pollution from the signal. Indeed, electromagnetic pollution in low frequencies is quite strong and it could be difficult to tell the difference between a stimulation induced signal or a pollution induced signal. Moreover, DC is not a deterministic signal (like a "pure" sine wave injected at a known frequency (Figure 22 **D** for more detail please refer to part II)). To process their data, they had to subtract the initial baseline of their signal (because of the initial DC offset, for an example of this phenomenon see Figure 22 **B**) and then detrend it (because of DC drift, for an example of a DC drift compared to a zero-centered intracerebral signal see Figure 22 **C**). All these post-processing operations lower the accuracy and the quality of the signal analyzed.

Huang et al., 2017 explored different factors which can influence the electric field measured such as intensity, stimulation frequency, or distance were explored but, unfortunately, not quantitatively.

c. About this thesis work

From what was described before, it has been identified that there is still a need for further study investigating iEF in humans *in-vivo* by resorting to SEEG investigation only. This chapter will tackle this topic by attempting to answer two major questions:

1. Is it possible to generate an electric field in the limbic system with TES?
2. What is the influence of different factors such as TES intensity, frequency, electrode placement and depth on iEF measured?

The focus will be on the iEF generated in the limbic system for several reasons: (1) the high prevalence of temporal lobe epilepsy SEEG investigation (2) the potential clinical outcomes due to the numerous neurological diseases affecting the limbic system (3) the potential TES application to cognition. The mathematical relationship of some factors (intensity, frequency, and depth) will be extracted from the results in order to quantify their influence on iEF generated by a TES.

Table 1: Summary of the presented study investigating intracerebral electric field during a TES in human

Study	Size	Investigational method	Intracerebral contacts	TES protocol	TES electrodes	Investigations	Results
Vöröslakos 2018	6 cadavers	Custom-made intracerebral multi-contacts electrode	28 in each cadaver, total 168	tACS 200Hz from 1V to 5V	Ag/AgCl EEG electrodes, 0.78 cm^2	iEF as a function of the voltage applied, scalp shunt	E = 0.13 × I + 0.04
Opitz 2016	2 patients	1 SEEG, 1 ECoG	110 SEEG 244 total	tACS 1Hz at 1mA	Saline soaked sponges 25cm^2	iEF magnitude and spatial distribution	Max 0.36 ± 0.008 $V.m^{-1}$ (median 0.098$V.m^{-1}$) Max 0.16 ± 0.007 $V.m^{-1}$ (median 0.059$V.m^{-1}$)
Huang 2017	10 patients	9 ECoG, 1 SEEG	78 SEEG 1205 total	tACS 1Hz to 100Hz, 0.5mA to 2mA	Rubber + gel 4cm^2	iEF magnitude and comparison with model	Max 0.4 $V.m^{-1}$ at 2mA
Chhatbar 2018	3 patients	DBS	20 (4 on each electrode)	tDCS 2mA and 4mA	Saline soaked sponges 35cm^2	iEF magnitude	0.12 $V.m^{-1}$ to 0.13 $V.m^{-1}$ at 2mA. 0.19 $V.m^{-1}$ to 0.26 $V.m^{-1}$ at 4mA.
Ruhnau 2018	1 patient	DBS	8 (4 on each electrode)	tACS 10Hz & 130Hz at 1mA	Saline soaked sponges 35cm^2	iEF magnitude	Max 0.08 $V.m^{-1}$

II. A new *in-vivo* investigation of TES induced intracerebral electric field in humans' limbic system: Method

1. Materials and experimental design

a. Intracerebral investigation

Eight patients (4 females and 4 males; age: 30 ± 11 years old) with focal drug-resistant epilepsy candidates for a presurgical evaluation were prospectively included in this study.

Their standard presurgical evaluation included: neuropsychological tests and long-term (5-day period) high-resolution electroencephalographic (EEG) video recordings combined with electrical source imaging analysis, positron emission tomography (PET) and 2 high-resolution magnetic resonance imaging (MRI at 1.5 Tesla. Including one with gadolinium injection to map the vascular network) (Rikir *et al.*, 2020).

Then, the individual SEEG implantation scheme was defined in accordance with the presurgical evaluation and electro clinical hypotheses to better localize the epileptogenic zone and the surrounding functional area (Isnard *et al.*, 2018). Once intracerebral targets were defined, SEEG electrodes coordinates and trajectory were calculated thanks to the gadolinium injected MRI to avoid the vascular network and, therefore, hemorrhage.

SEEG electrodes are multi-contact electrodes (Figure 24) of 16 mm to 80.5 mm length and 0.8 mm-diameter containing from 5 to 18 Platinum/Iridium contacts of 2 mm length separated by 1.5 mm insulator (Dixi Medical®, Besançon, France).

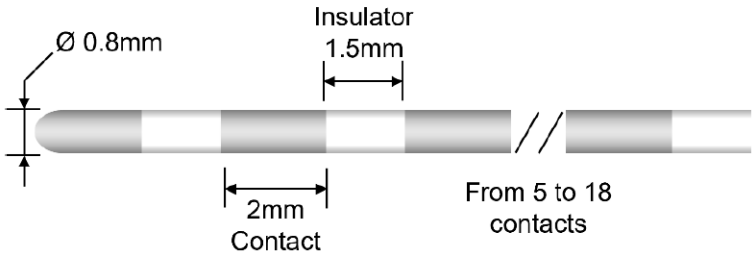

Figure 24: Schematic representation of a SEEG electrode Dixi Medical. One SEEG electrode has a typical length varying from 16 mm to 80.5 mm and contains from 5 to 18 Platinum/Iridium contacts (in gray) where the intracerebral electrophysiological activity is recorded. Contacts are separated by a 1.5 mm plastic insulator.

Under general anesthesia, SEEG electrodes were implanted according to a standard stereotactic procedure (Salado *et al.*, 2018) (Figure 26). SEEG electrodes were inserted into a screw (2.45 mm-diameter) and secured with a tight seal to prevent cerebrospinal fluid leak (Figure 25 A). Immediately after the implantation, patients underwent a postoperative CT-scan to check SEEG electrodes trajectories. Then, thanks to a CT-scan/MRI co-registration (voxel-based registration; SPM

8 toolbox for Matlab; MathWorks, Natick, Massachusetts), precise coordinates (*x*,*y*,*z*) of each electrode's contacts in the MRI volume were determined (software developed in the lab: ICEM (Hofmanis *et al.*, 2011) with potential error under 1 mm (Almukhtar *et al.*, 2014)), and potential surgical complications were inspected (Figure 27). Also, SEEG minimally invasive procedure prevents from brain anatomy modification, CSF leakage and parenchymal swelling.

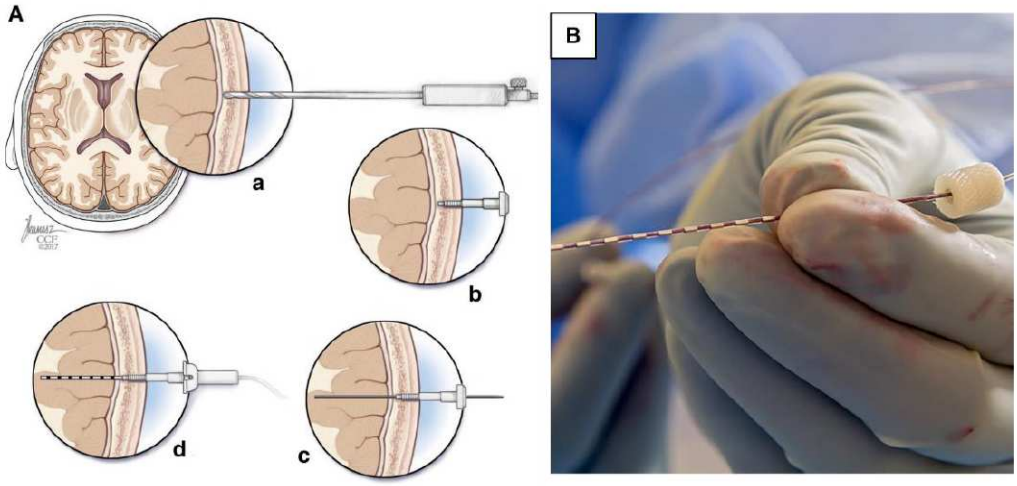

Figure 25: SEEG implantation procedure and real size of an SEEG electrode. **A**: Schematic representation of an SEEG electrode implantation procedure. **a.** Once the calculated coordinates are reported on the stereotactic frame, the skull is drilled thanks to the frame's guided system (see Figure 26). **b.** Then a guide is screwed into the skull through the burr hole previously made. **c.** Next, a stylet is passed through the cranially fixed guide to make a passage for the SEEG electrode through tissues. **d.** Finally, the SEEG electrode is implanted, and a cap seals it all to prevent from CSF leaking and bacteria going into the intracranial medium. From Techniques for placement of stereotactic electroencephalographic depth electrodes: Comparison of implantation and tracking accuracies in a cadaveric human study. *Epilepsia*, *59*(9), (2018) by Jones, J. C., Alomar, S., McGovern, R. A., Firl, D., Fitzgerald, Z., Gale, J., & Gonzalez-Martinez, J. A. © 2018 by Blackwell publishing inc. Reproduced with permission of Blackwell publishing inc. under license number 1201191-1 in the format of print and electronic via Copyright Clearance Center. **B.** real view of a SEEG electrode with its multiple contacts (grey).

In addition, 27 scalp electrodes were placed in accordance with the international 10/20 system (Koessler *et al.*, 2015; Seeck *et al.*, 2017) 5 days minimum, patients were monitored and recorded thanks to combined video-EEG-SEEG recording. In the meantime, neurologists checked for unusual electrophysiological activity such as breach rhythms, which are defined as focal increases in the amplitude activity of alpha, beta, and mu rhythms (Brigo *et al.*, 2011). This type of activity tends to occur close to a skull defect such as a craniotomy or cranial surgery, which can bias electric field measurement because of the electric current flow modification. In the current study, no breach rhythms were detected.

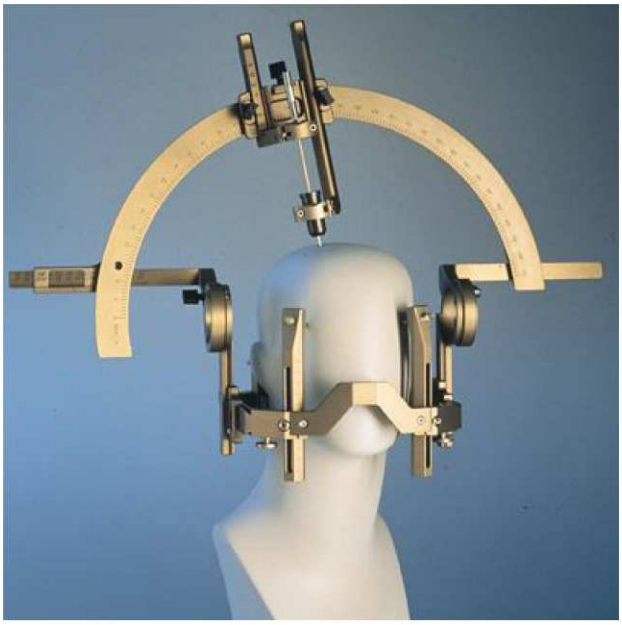

Figure 26: Stereotactic frame used for SEEG implantation. Coordinates previously calculated (from gadolinium injected MRI) for electrode trajectory are set on the frame. Then, the position of the guide is locked, and electrode implantation can begin (see Figure 25)

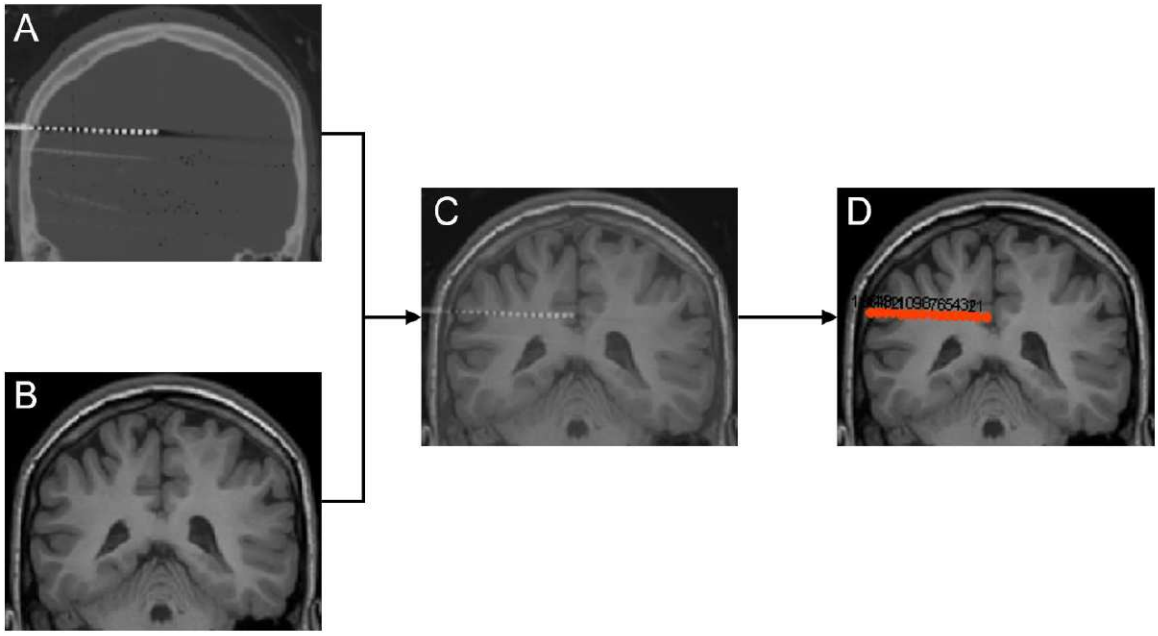

Figure 27: Automated SEEG electrode localization. **A**: post-surgical CT-scan in which one SEEG electrode is visible by its multiple intracerebral contacts (white dots). **B**: pre-surgical MRI in which the cerebral parenchyma is clearly distinct. **C**: Multimodal CT-scan/MRI co-registration in which the intracerebral contact positions are visible inside the brain parenchyma. **D**: Electrode modeling and coordinate generation to make visible only the intracerebral contacts (orange dots) in the brain parenchyma to better visualize their position in the precise anatomy. All intracerebral coordinates in the brain volume are then exported in an Excel file. (Hofmanis *et al.*, 2011)

b. Recording device

EEG-SEEG signals were recorded with a 256-channel (2x128 channels) amplifier. The analog/digital converter had a sampling rate of 10 kHz, 16 bits resolution at 0.25 µV/bit, a high-pass filter 1st order at 0.3 Hz (and 3rd -order low-pass at 7,500 Hz), an input impedance superior to 10 GΩ

and a maximum input signal range of ± 8.191 mV (NeuroPort™ System by Blackrock® Microsystems, Salt Lake City, UT, USA).

Recording device ground (GND)

During SEEG clinical evaluation, the device's ground (GND) is set as far as possible to the brain electric sources (0V required) i.e., a SEEG contact located in the skull. Bones tissues' high resistivity provides a good medium to set an electrical pseudo-neutral point for the amplifier circuit. One of the GND roles is the protection against environmental electromagnetic pollution by rejecting signal components common to all contact: it is the common mode rejection (CMR). Therefore, the GND location close to the head surface is important (compared to the other intracerebral contacts).

During a TES, GND (which is supposedly a neutral point of the circuit) is one of the most exposed contacts to the electric current (because of its proximity to the scalp). First, the high current amplitude injected on GND can radiate inside the device's Printed Circuit Board (PCB) and bias signal measured by inducing an amplitude modulation or a phase shift. Second, because of the common mode rejection, the intracerebral signal amplitude can also be altered. Therefore, the recording device's ground must be the farthest possible to TES-induced current flow. In this study, GND was set on the right foot (to imitate a driven right leg configuration).

Recording device reference

As Opitz *et al.*, (2106) reported, the reference's position doesn't change iEF calculation. Indeed, theoretically, assuming that EF is constant between two contacts, its magnitude is expressed by:

$$\mathrm{E} = \frac{\mathrm{V_2} - \mathrm{V_1}}{d} \tag{13}$$

In a context in which an instrumentation amplifier is involved, voltages are measured by subtracting the intracerebral contact electric potential to a reference potential V_{ref}:

$$\mathrm{U_1} = \mathrm{V_1} - \mathrm{V}_{ref} \tag{14}$$

$$\mathrm{U_2} = \mathrm{V_2} - \mathrm{V}_{ref} \tag{15}$$

Where V is the electric potential and U the voltage measured. So, the electric field magnitude is calculated as follows:

$$\mathrm{E} = \frac{\mathrm{U_2} - \mathrm{U_1}}{d} \tag{16}$$

By using equation (14) and (15) we obtain:

$$\mathrm{E} = \frac{\mathrm{V_2} - \mathrm{V}_{ref} - \mathrm{V_1} + \mathrm{V}_{ref}}{d} \tag{17}$$

So:

$$E = \frac{V_2 - V_1}{d} \quad (18)$$

with d the distance between the two contacts. This is the theoretical proof that the reference's potential value V_{ref} doesn't interfere with iEF magnitude calculation: wherever the reference electrode is put, iEF magnitude is unchanged. To empirically assess and confirm this, a subsidiary study was performed in one subject with whom stimulations were executed with 2 different references' positions: on the scalp (Fpz), and on an intracerebral contact. This study was performed on a recording device used in a clinical routine, which was an amplifier at 1,024 Hz sampling rate with 256-channel (SD LTM 128 Headbox; Micromed, Italy) with a maximum input signal range of ± 3.2 mV. A 1-mA tACS at 6Hz was done for each references' positions. Results from the experiment (page 92) confirmed the choice of the NeuroPort™ System by Blackrock® Microsystems recording device which has better precision and a wider maximum input signal range (± 8.191 mV) described above. It shows how important it is to carefully choose the right amplifier and the right reference to measure TES-generated intracerebral voltage without saturating the amplifiers (Figure 34) and therefore, biasing iEF calculations.

Then, according to the results obtained from the reference study, the device's (Blackrock® Microsystems) reference was set on one of the deepest intracerebral contacts for the other subjects. First, because the reference is within the same medium as the other intracerebral contacts: the difference between potentials would not induce a saturation of the amplifiers. Secondly, in accordance with physics' inverse squared law, potential value generated by TES would have a minimum impact on the reference.

Recording device accuracy

The acquisition chain accuracy (stimulation/recording devices) was evaluated by injecting a current from the stimulation device through known precise variable resistors and measuring the output voltages with the recording device (Figure 28).

Firstly, the tolerance interval was calculated by considering the recording device resolution (0.25 µV; 16 bits), stimulation device resolution (1 %), variable resistor resolution (1 %), and input reference noise on the full bandwidth: maximum 3 µV.

Tolerance interval for negative extrema was calculated as follows:

$$U_{extremes-} = (I - I \cdot 0.01)(R - R \cdot 0.01) \quad (19)$$

Tolerance interval for positive extrema was calculated as follows by adding the maximum input reference noise (3 µV in the worst case):

$$U_{extremes+} = (I + I \cdot 0.01)(R + R \cdot 0.01) + 3 \quad (20)$$

Secondly, voltage values measured by the recording device as a 16 bits analog/digital converter were calculated:

$$U_{measured} = \min\left|U_{extremes\pm} - U_{measurable}\right| \quad (21)$$

With $U_{measurable}$ the full range of measurable voltage values between 0 and 2^{16} with a step of 0.25

Thirdly, the stimulation device (Soterix Medical®, New York, NY, USA) and the EEG-SEEG recording system (Blackrock® Microsystems, Salt Lake City, UT, USA) were connected to a variable resistor in parallel. The injected current has the same characteristic as a typical human *in-vivo* experiment: 1min at 1 mA at the frequency of 300 Hz. Voltages were measured for 15 different impedances values (from 2 Ω to 16 Ω) to verify if the measured voltages were within the tolerance range.

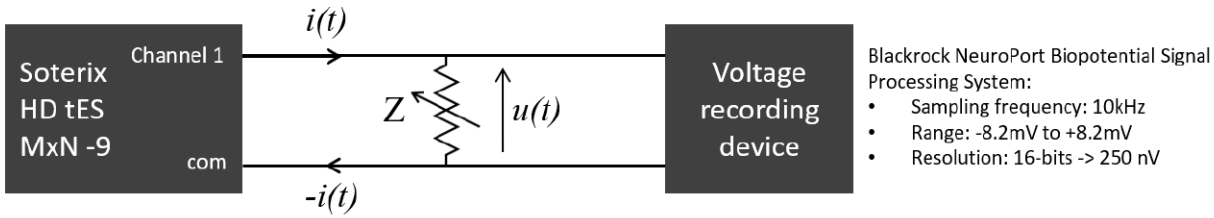

Figure 28: Experimental design for evaluating the accuracy of the acquisition chain and to quantify potential errors.

A 1st degree polynomial was fitted to the measured voltage values. Fitted values slope was p1 = 0.99, intercept p2 = − 0.006 and coefficient of determination $R^2 = 1$. So, measured voltages were close to theoretical values derived from Ohm's law and within the tolerance range (estimated in the first step, the yellow area in Figure 29). Thus, the acquisition chain was considered accurate for human *in-vivo* TES experimentations.

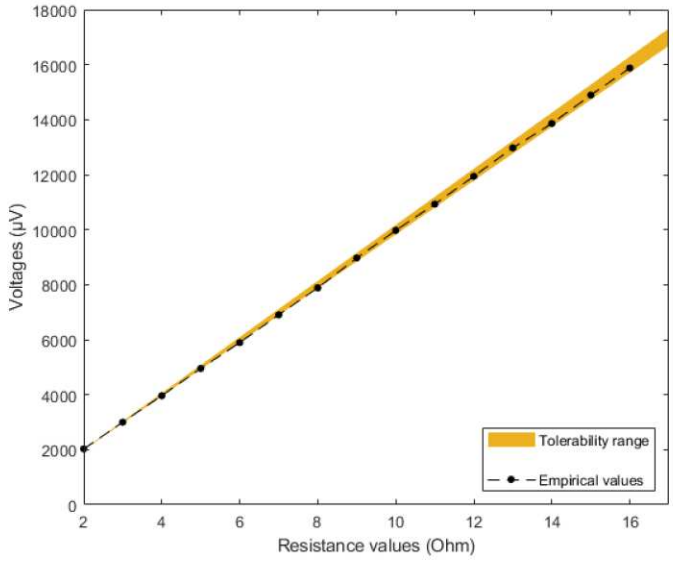

Figure 29: Measured voltages from the acquisition chain (black dots). Current injected was 1mA, resistor values range from 2 Ω to 16 Ω and tolerance interval (or tolerability range) displayed in yellow.

c. TES experiment

The last day, prior to the SEEG electrodes withdrawal, TES experiments were executed in sterile condition. TES consisted in the application of a bipolar transcranial alternating current stimulations (tACS).

Stimulation electrodes

Two HD ring electrodes (12 mm outer diameter; Soterix Medical®, New York, NY, USA) inserted into a HD electrode holder (24 mm diameter) filled with conductive gel were placed on the scalp at least 5 cm away from the SEEG implantation sites to ensure aseptic condition. The area under each stimulation electrode was 4.52 cm^2, which generates current densities of 0.11 $mA \cdot cm^{-2}$ and 0.22 $mA \cdot cm^{-2}$ for 0.5 mA and 1 mA stimulation intensities, respectively.

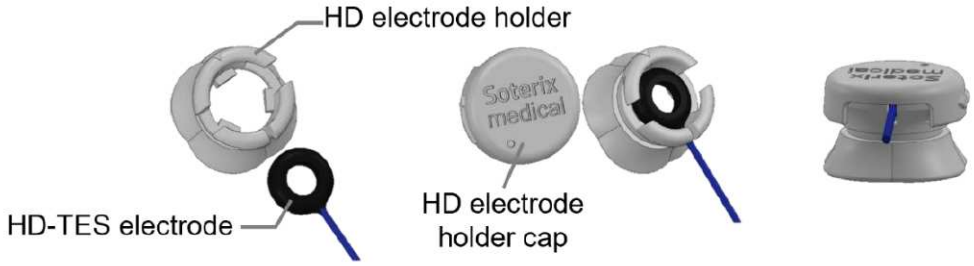

Figure 30: TES HD-Electrode and HD electrode holder used in tACS experiments

TES electrodes positions were arranged (1) to generate EF's major component along the intracerebral electrodes orientation (2) to be the most distant from each other to maximize the current flowing into the brain (Datta *et al.*, 2008; Faria, Hallett and Miranda, 2011) while respecting the standard 10-10 international system position. Positions were defined thanks to the MRI-CT co-

registration showing the SEEG electrodes trajectories (Salado *et al.*, 2018) and thus allowing cranio-anatomical correlations (Koessler et al. 2009). To target the hippocampus/amygdala complex and the cingulate gyri, stimulation electrodes were put on FT9-FT10 or T7-C4 or C3-FT10. Stimulating electrode's spatial coordinates were computed by fitting, in Brainstorm (Tadel *et al.*, 2011), a Colin27 generic 10-10 EEG cap on individual patient's head model.

Stimulation parameters

Stimulation was delivered from a multichannel TES stimulator MxN-9 (Soterix Medical®, New York, NY, USA) by injecting a bipolar sinusoidal waveform which can be expressed by:

$$s(t) = I \cdot \sin(2\pi f t) \quad (22)$$

where $s(t)$ is the stimulation signal as a function of the time t, I the stimulation intensity (0.5 mA or 1 mA) and f the stimulation frequency (Hz). Experiment design is displayed in Figure 31. A typical session was a 2-minute stimulation (30-second ramp up, 1-minute full intensity, 30-second ramp down) at a given intensity and frequency (Figure 32).

Four different protocols were performed:

- To study the influence of the intensity, two tACS at 300 Hz were executed: one session at 0.5 mA and the other at 1 mA with TES electrodes placed on FT9-FT10 (6 subjects: named Subject #1 to Subject #6)
- To study the influence of the frequency, seven tACS at 1 mA, at a different frequency were completed: 1 Hz; 3 Hz; 7 Hz; 35 Hz; 71 Hz; 140 Hz and 300 Hz with TES electrodes placed on FT9-FT10 (1 subject: named Subject #0).
- To study the influence of the electrode position, a 1-mA tACS at 300 Hz were executed fifteen time, each time for a different electrode position (montage): C3-FT10; C3-T8; C3-C4; Cz-FT10; Cz-T8; Cz-C4; Fz-FT10; Fz-T8; Fz-C4; Fz-Cz; Fz-C3; Fz-T7, T7-FT10; T7-T8; T7-C4 (1 subject: named Subject #7).
- To study the influence of the recording reference, a 1-mA tACS session at 6 Hz (electrode placed on FT9-FT10) was performed twice, each session with a different reference position: Fpz and on a lateral intracerebral contact (1 subject)

Each stimulation was separated by a break of 1 minute to settle down the potential neural entrainment. During all sessions, patients were in a resting state with eyes open. Impedance between the two tACS electrodes was checked before, during, and after each stimulation and were always inferior or equal to 5 kΩ.

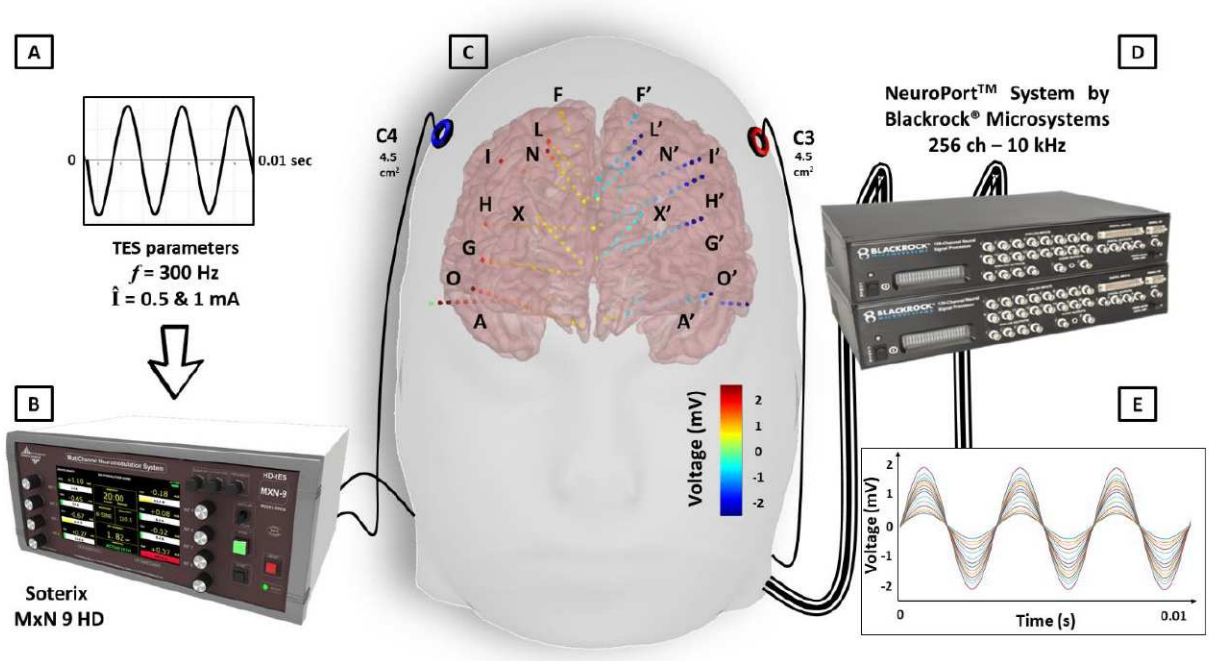

Figure 31: Simultaneous combination of transcranial alternative current stimulations (tACS) and SEEG recordings. Bipolar sinusoidal signals at 300 Hz (**A**) were delivered using a Soterix MxN stimulator (**B**), and two HD ring electrodes (4.5 cm^2, active electrode in red, neutral electrode in blue) (**C**). A 256-channel amplifier (NeuroPortTM System by Blackrock® Microsystems, Salt Lake City, UT, USA) (**D**) was used to record the sinusoidal signals in all intracerebral multi-contact electrodes (superimposed SEEG signals are represented in colored lines) (**E**). In part C, colors represent the in-vivo measured voltage in all intracerebral contacts (n = 140; colored dots) using a realistic head model (Subject # 7) with a C3-C4 stimulation at 300 Hz and 1 mA intensity.

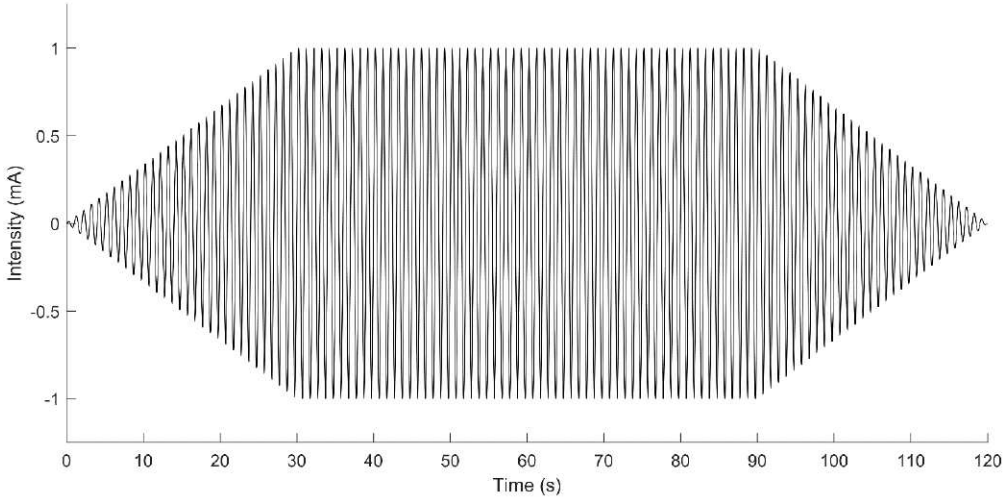

Figure 32: Output current from the stimulation device for a 1 mA tACS at 1 Hz set for 2 minutes. From 0 to 30 seconds, the intensity increases progressively, then reaches the preset value (1 mA) until the intensity started a ramp down of 30 before the end of the preset time.

2. Measurement and data processing to obtain the electric field

a. Empirical voltages measurement and electric fields calculation (single component calculation)

Output data were read and converted using Matlab (The MathWorks®) from .ns format (Blackrock®) to Matlab matrices ($m \times n$) time-series, where n is the number of intracerebral contacts (channel) and m the length of the signal (number of samples for t seconds recording multiplied by the sampling rate).

Preprocessing and saturated signal detection

The first step was to plot the intracerebral signals and manually select the time when stimulation is in a steady state (Figure 33). Most superficial SEEG contacts (outside of the brain) were systematically discarded to avoid aberrant values.

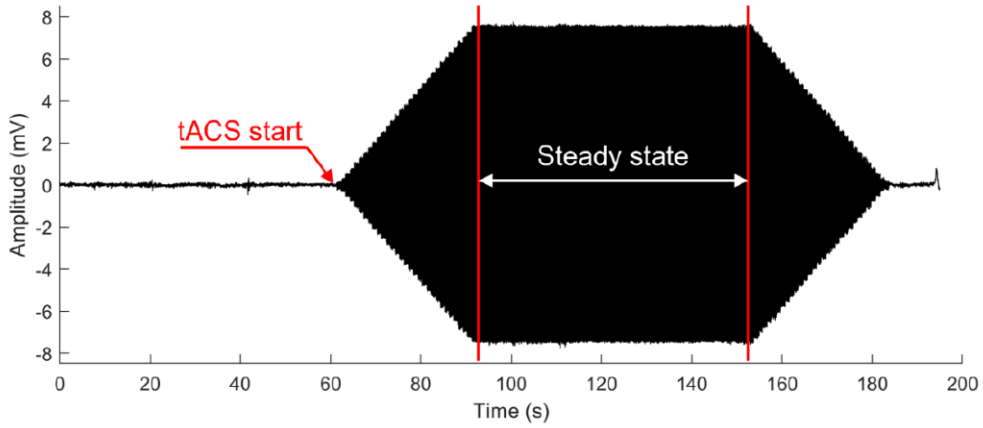

Figure 33: Intracerebral signal recorded on one SEEG contact during a 1 mA tACS at 300 Hz. Electrophysiological activity is visible before when tACS starts. The steady state is when tACS is at the pre set intensity (no transient state). The beginning of the steady state is visually selected, and the end is automatically calculated by the algorithm to obtain exactly the same number of samples for every subject and every parameter.

Sometimes, intracerebral voltages still reach values over the amplifiers' maximum input range and a few channels are saturated. Therefore, an algorithm was developed that automatically detects saturated channels. For the algorithm, a saturated channel was defined as a channel where the maximum device's input range (± 8.191 mV) is reached more than 10 % of a period time. More precisely, for an intracerebral signal $ics(n)$ where n a sample of the discretized signal:

$$ics(n) = \mathrm{U}_{tACS}(n) + \mathrm{U}_{\Phi}(n) + \mathrm{U}_{w}(n)\,;\ \forall\, n \in \mathbb{N}^{*} \qquad (23)$$

$ics(n)$ is a composit signal with the tACS-generated voltage $\mathrm{U}_{tACS}(n) = \mathrm{U} \cdot \sin(2\pi \mathrm{f} n)$ (where f is the stimulation frequency) the electrophysiological signal $\mathrm{U}_{\Phi}(n)$ and other background and hum noises $\mathrm{U}_{w}(n)$. Then, a signal noise ratio (SNR) was calculated with Matlab (function `SNR`) at the stimulation frequency (only the fundamental: 300 Hz) on every intracerebral contact for the lowest stimulation intensity (0.5 mA) to evaluate the signal quality in the worst case:

$$SNR = 20 \cdot \log_{10}\left(\frac{\mathrm{U}_{tACS}(n)}{\mathrm{U}_{\Phi}(n) + \mathrm{U}_{w}(n)}\right) \quad (24)$$

Because of remarkably high SNR values (see Results section), it is possible to simplify equation 24 by removing $\mathrm{U}_{\Phi}(n) + \mathrm{U}_{w}(n)$, considered as negligible. Thus, $ics(n) = \mathrm{U}_{tACS}(n)$.

Finally, a channel is considered saturated if, in a period T:

$$\left(\sum_{i=1}^{\mathrm{T}-1} ics(i) - ics(i+1)\right) > \frac{\mathrm{T}}{10} \; ; \; \forall \, i \in \mathbb{N}^* \quad (25)$$

Where T is the sinus period $\mathrm{T} = \frac{\mathrm{sf}}{\mathrm{f}}$, sf the sampling frequency and f the tACS frequency.

Fast Fourier Transform (FFT) and TES-generated intracerebral amplitude calculation

After marking and removing saturated channels, a Discrete Fourier Transform (DFT) is calculated on the discretized intracerebral signal $ics(n)$ (with a length of M samples):

$$\mathbf{ICS}(N) = \sum_{n=0}^{\mathrm{M}-1} ics(n)\, e^{\frac{-i2\pi Nn}{\mathrm{M}}} ; \forall \, n, N, \mathrm{M} \in \mathbb{N}^* \quad (26)$$

Numerically, the DFT is calculated through an FFT on Matlab based on the algorithm of (Frigo and Johnson, 2005).

Each value of $\mathbf{ICS}(N)$ is defined on $\mathbb{Z}$ and represents one complex sinusoidal component properties of the signal $ics(n)$, its amplitude at $N = S$ (where S an integer representing a discretized frequency sample of the sinusoidal component) is:

$$\frac{1}{\mathrm{M}}|\mathbf{ICS}(S)| = \frac{1}{\mathrm{M}}\sqrt{\mathrm{Re}[\mathbf{ICS}(S)]^2 + \mathrm{Im}[\mathbf{ICS}(S)]^2} \quad (27)$$

For all frequencies, $\frac{1}{\mathrm{M}}|\mathbf{ICS}(N)|$ gives the amplitude spectrum of the signal $ics(n)$.

So, to extract only the intracerebral tACS-generated amplitude U, the absolute value of $ics(n)$ DFT is calculated at the tACS frequency f (so at the sample $S = \frac{\mathrm{f}\cdot\mathrm{M}}{\mathrm{f}_s}$, with f_s the sampling frequency) and, divided by its length M (Equation 27). However, because frequencies are discretized by steps of $\frac{\mathrm{f}_s}{N\cdot\mathrm{M}}$ (where $N \in \mathbb{N}^*$), it is impossible to obtain amplitude values at the exact tACS frequency. To overcome this difficulty, the amplitude is defined as the maximum value on the spectrum within a window of $[\mathrm{f}-2; \mathrm{f}+2]$. Frequency window width (5 Hz) can be considered as quite wide at first sight but there is no risk of confusion with other electrophysiological activity within the same frequency band because of the excellent signal quality (High SNR measured on the fundamental, see Results section)

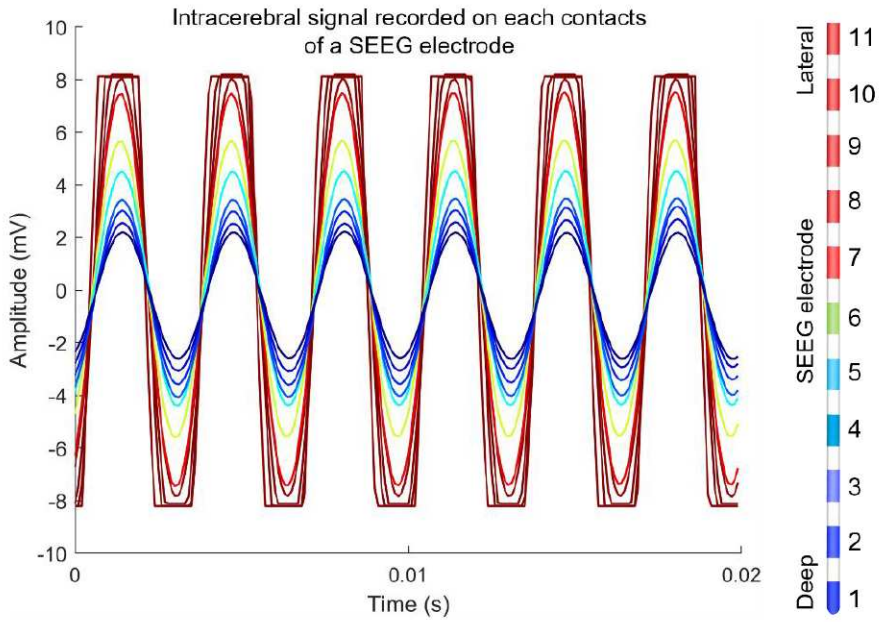

Figure 34: Intracerebral signal recorded on each contact of one SEEG electrode (represented on the right) during a 1 mA tACS at 300 Hz. Colors correspond to the signal amplitude (mV) measured for each intracerebral contact represented on the right. On the signal, one can notice 3 saturated contacts (9,10,11) (signal clipped) meaning that the difference of potential Ucontact = Vcontact-Vref has a higher value than the amplifier's maximum signal input range (± 8.191 mV). Saturated contacts are automatically detected by the algorithm and discarded from the study.

Electric field calculation

Between two adjacent contacts of an SEEG electrode, the medium is assumed uniform, homogeneous, isotropic and the electric field is constant in space and time. By making these assumptions, the intracerebral electric field (iEF) between 2 adjacent contacts can be calculated as follows:

1. In the three directions of a Cartesian coordinate system (*x,y,z*) the general expression of the electric field is:

$$\mathbf{E}_{x,y,z} = -\nabla V = -\left(\frac{\partial V}{\partial x}\cdot \boldsymbol{u_x} + \frac{\partial V}{\partial y}\cdot \boldsymbol{u_y} + \frac{\partial V}{\partial z}\cdot \boldsymbol{u_z}\right) \quad (28)$$

Where $\boldsymbol{u_x}$; $\boldsymbol{u_y}$ and $\boldsymbol{u_z}$ are the unit vector along the axis *x, y,* and *z*, respectively.

2. Because the calculation was done between 2 adjacent intracerebral contacts, it restricted the estimation to only one iEF component which is along the SEEG electrode orientation and characterized by the unit vector $\boldsymbol{u_p}$. Thus, equation 28 becomes:

$$\mathbf{E}_p = -\nabla V = -\frac{dV}{dp}\cdot \boldsymbol{u_p} \quad (29)$$

Its magnitude gives the "single-component electric field magnitude", in opposition to the "multi-component electric field magnitude" detailed in section b page 88.

Numerically, there are two solutions to calculate the voltage gradient:

Let **U** a ($m \times 1$) voltage vector, which contains voltage value on each intracerebral contact of one SEEG electrode.

1. The first solution consists of doing a basic voltage subtraction between two adjacent contacts and dividing them by the distance *d* separating them:

$$\mathbf{E} = \frac{\mathbf{U}(i+1,1) - \mathbf{U}(i,1)}{d} \quad (30)$$

2. The second solution consists of calculating the central difference of the interior data point by doing:

$$\mathbf{E} = \frac{0.5\cdot\left(\mathbf{U}(i+1,1) - \mathbf{U}(i-1,1)\right)}{d} \quad (31)$$

At the matrix's edges, for the first step:

$$\mathbf{E} = \frac{\mathbf{U}(i+1,1) - \mathbf{U}(i,1)}{d} \quad (32)$$

For the final step:

$$\mathbf{E} = \frac{\mathbf{U}(m,1) - \mathbf{U}(m-1,1)}{d} \quad (33)$$

Because intracerebral contacts are regularly spaced and because the voltage gradient is not a purely linear function, the second solution (using Matlab function `gradient()`) offers a better approximation of local variations considering neighbors' values instead of doing a simple linear interpolation.

Anatomical classification of brain structures:

With the CT/MRI co-registration, intracerebral contacts within structures of interest (*i.e.,* amygdala, cingulum and, hippocampus) were selected visually. Electrophysiological activity recorded on select contacts, were reviewed by a neurologist to confirm the anatomical selection. SEEG trace review also grants a precise discrimination between white matter and gray matter (Koessler *et al.*, 2017):

- Contacts on which an electrophysiological activity is recorded are located within the gray matter
- Contacts on which no electrophysiological activity is recorded are located within the white matter

Finally, mean iEF values were calculated on selected contacts within the structures of interest: The hippocampus, amygdala, and cingulate gyrus.

b. Computing the electric field tensor in the limbic system (multi-component electric field magnitude)

Empirically, iEF calculation is done along only one component (single component iEF magnitude). To overcome this limitation, it is interesting to compute an estimate of the full iEF tensor (multi-component magnitude) to verify and complete empirical measurement. This was done by interpolating scattered amplitude V on the MRI.

MRI automated segmentation and anatomical labeling

Using CAT12 (Gaser and Dahnke, 2016), individual MRI images underwent several processes:

First, the MRI was segmented into 5 compartments using voxel-based morphometry (Ashburner and Friston, 2005): skin, skull, cerebro-spinal fluid (CSF), gray matter and white matter (Figure 35).

Second, anatomy was labeled using a probabilistic cytoarchitectonic mapping (Eickhoff *et al.*, 2005, 2006, 2007) with CAT12 (Gaser and Dahnke, 2016). Because the empirical study focused on hippocampi, amygdalae and cingulate gyri, these structures were selected for the following analysis.

Masks generation

As previously mentioned, individual MRIs were automatically segmented, and anatomy labeled generating two 3D matrices ($m \times n \times o$) (same size as the MRI matrix) containing integer values for each tissue or each label. Then, by extracting values from those matrices, masks were

created for each tissue and each region of interest (ROI): scalp mask (**SC**) skull mask (**SK**) CSF mask (**CSF**) gray matter mask (**GM**) white matter mask (**WM**) hippocampus mask (**H**) amygdala mask (**A**) cingulum mask (**C**) (in red in Figure 36). To avoid edge effects during EF tensor calculation, a spheric dilatation with a radius of 10 voxels was applied on each ROI mask. Then, masks were cropped, and results were displayed (for visualization purpose) on non-dilatated masks (Figure 42).

Voltage interpolation and electric field calculation

Interpolation of amplitudes using the natural neighbor method (Sibson, 1981; Amidror, 2002) was calculated from scattered data **U** ($m \times 1$) measured on intracerebral contacts at positions **x** ($m \times 1$) **y** ($m \times 1$) **z** ($m \times 1$) (obtained from CT-MRI co-registration). The natural neighbor method was chosen among the other interpolation methods for the compromise it offers between robustness, accuracy and ease of use and knowing the theoretical iEF behavior as a function of the distance (Amidror, 2002).

Dilatated ROI masks were applied on interpolant matrix **F** giving a 3D matrix **V** ($m \times n \times o$) which is the voltage amplitudes in the three directions of space (*i.e* in each mask's voxels). Therefore, full EF vector can be calculated:

$$\mathbf{E} = -\nabla \mathbf{V} \tag{34}$$

And its magnitude:

$$|\mathbf{E}| = \sqrt{(\mathbf{E} \cdot \mathbf{u}_x)^2 + \left(\mathbf{E} \cdot \mathbf{u}_y\right)^2 + (\mathbf{E} \cdot \mathbf{u}_z)^2} \tag{35}$$

Where $\mathbf{u}_x = (1\ 0\ 0)^{\mathrm{T}}$; $\mathbf{u}_y = (0\ 1\ 0)^{\mathrm{T}}$ and $\mathbf{u}_z = (0\ 0\ 1)^{\mathrm{T}}$

Finally, non-dilatated ROI masks were applied to obtain only iEF magnitude in these areas:

$$|\mathbf{E}|_{amygdala} = |\mathbf{E}| \cap \mathbf{A} \tag{36}$$

$$|\mathbf{E}|_{cingulum} = |\mathbf{E}| \cap \mathbf{C} \tag{37}$$

$$|\mathbf{E}|_{hippocampus} = |\mathbf{E}| \cap \mathbf{H} \tag{38}$$

With **A**, **C** and **H** the non-dilatated masks of the amygdala, cingulate gyrus and hippocampus, respectively.

Comparison between single component and multi-component iEF magnitudes

To evaluate the accuracy of the single component iEF calculation, it was compared to the multi-component iEF mean magnitudes, structures by structures, by performing a student *t*-test. This statistical test was chosen by assuming that iEF values in the same structures (regarding their size) and in the same tissue follow a Gaussian distribution centered around the mean value.

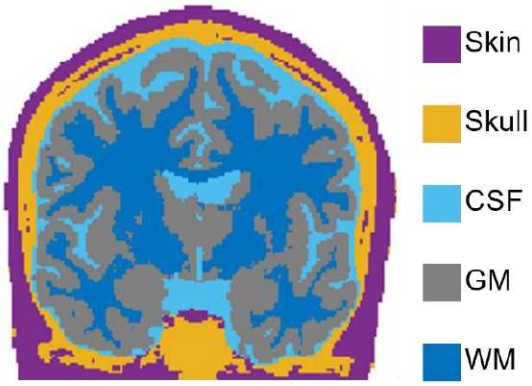

Figure 35: Tissue segmentation based on individual MRI with CAT12. Tissues are segmented based on voxel-morphometry method (Ashburner and Friston, 2005) and divided into 5 classes: Skin, Skull, cerebro-spinal fluid (CSF), gray matter (GM) and white matter (WM).

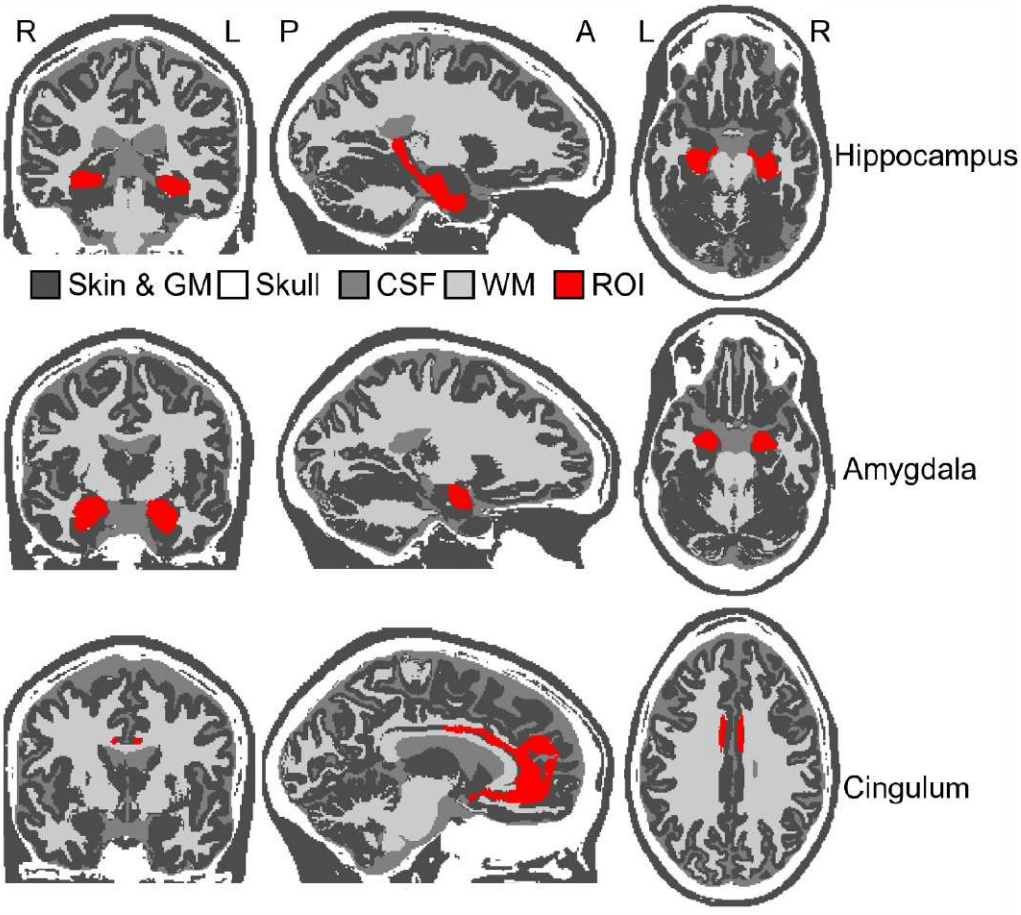

Figure 36: Superimposed segmented tissue masks (shades of gray) and the regions of interest (red ROI) masks. ROI displayed are the hippocampus, the amygdala and the anterior cingulum.

c. Influence of tACS parameters on iEF magnitudes

Three different tACS parameters were investigated: stimulation frequency, stimulation intensity and tACS electrodes placement (montage).

Influence of tACS frequency:

The objective of this sub-study was to quantify the influence of the stimulation frequency on the iEF magnitude. The hypothesis was that the frequency has a negligible linear relationship with the iEF magnitude.

iEF magnitude obtained for a 300 Hz-stimulation were compared to those obtained for other stimulation frequencies (1 Hz; 3 Hz; 7 Hz; 35 Hz; 71 Hz; 140 Hz). This was done by calculating the mean percentage variation (MPV):

$$MPV = \frac{1}{n}\sum_{i=1}^{n}\left(\frac{\mathrm{E}_i(\mathrm{f}) - \mathrm{E}_i(\mathrm{f}=300)}{\mathrm{E}_i(\mathrm{f}=300)} \cdot 100\right) \quad (39)$$

With f the frequency tested, n the total number of intracerebral contacts. This variation was first calculated on all intracerebral SEEG contacts and, secondly only on the SEEG contacts within the deep cortical structures.

Assuming that iEF would have a linear relationship with the frequency, and assuming that this progression is negligible (almost flat), a 1st degree polynomial curve was fitted to the mean iEF values in the deep structures of interest.

Influence of tACS intensity:

The objective of this sub-study was to quantify the relationship between iEF magnitude and stimulation intensity. The hypothesis was that iEF magnitudes has a perfect linear relationship with stimulation intensity:

$$\mathrm{I}_2 = \lambda\,\mathrm{I}_1 \Longrightarrow \mathrm{E}_2 = \lambda\,\mathrm{E}_1 \quad (40)$$

Before studying the influence of the intensity (i.e. comparing 0.5 mA *versus* 1 mA) an outlier detection was executed. To do so, the mean absolute error (MAE) was calculated:

$$MAE = \frac{1}{n}\sum_{i=1}^{n}\left|\mathrm{E}_{1j} - \widehat{\mathrm{E}_{1j}}\right| \quad (41)$$

Where E_{1j} is the empirical iEF magnitude for a 1 mA stimulation and $\widehat{\mathrm{E}_{1j}}$ the theoretical iEF magnitude for a 1 mA stimulation obtained by multiplying by 2 the empirical iEF magnitude for a 0.5 mA stimulation. Then, contacts on which iEF was over three times MAE's standard deviation were considered as outliers and discarded.

Next, a first-degree polynomial curve was fitted to $\mathrm{E}_1 = f(\mathrm{E}_{0.5})$ distribution with $\mathrm{E}_{0.5}$ and E_1 the electric field at 0.5 mA and at 1 mA, respectively.

Influence of tACS montages:

The single subject included in this study (Subject #7) had a symmetric implantation (see Figure 31, nine SEEG electrodes in each hemisphere). SEEG electrodes sampled mainly frontal lobe structures (cingulate gyri, supplementary motor areas, superior, middle, and inferior frontal gyri *etc*.) and both amygdalae. The objective was to investigate the impact of different tACS montages on iEF values in the amygdala and cingulum. Then, montages were sorted from the lowest to highest iEF magnitude delivered on targets. Fifteen montages were performed: C3-FT10; C3-T8; C3eC4; Cz-FT10; Cz-T8; Cz-C4; Fz-FT10; Fz-T8; Fz-C4; Fz-Cz; Fz-C3; Fz-T7, T7-FT10; T7-T8; T7-C4. These montages were tested to find which one delivers the strongest iEF in the limbic structures: hippocampus, amygdala, and cingulate gyrus (the anterior cingulate gyrus due to the patient implantation). The choice was also constrained by the SEEG implantation sites.

d. Influence of the depth

As mentioned in part II.1.c, tACS electrode's coordinates were computed by fitting, in Brainstorm (Tadel *et al.*, 2011), a Colin27 generic 10-10 EEG cap on an individual patient's head model. Therefore, the Euclidean distances between intracerebral contacts and the nearest TES electrode were calculated. The maximum value of the distance measured (of the entire cohort) was then divided into similarly sized segments of 1.5 cm and iEF magnitudes were grouped according to these segments. Mean, and median iEF within each segment were calculated. Next, assuming mean and median values would decrease as a function of the distance according to the inverse-squared law, a non-linear regression was performed by fitting a power curve expressed by:

$$f(d) = a \cdot \frac{1}{d^b} + c \qquad (42)$$

Where a, b and c are the coefficients and d the distance from the nearest TES electrode.

III. Results

1. On the importance of hardware choice and reference position

The experiment investigating the reference's position included one subject who had 160 intracerebral contacts. Signal recorded on more than 90 % of the intracerebral contacts was saturated in both cases allowing an iEF calculation only on the deepest SEEG electrode's contact (when reference is put on the scalp) or close to the reference (when the latter is set on an intracerebral contact on the contralateral SEEG electrode (yellow arrow in Figure 37)). This was because tACS-generated voltages were above the recording device admissible input values (± 3.2 mV). Those results can't be included in the study but shows the importance of the recording device choice (mainly the amplifier

maximum input signal range) and its reference position prior to any electric field investigation experiments.

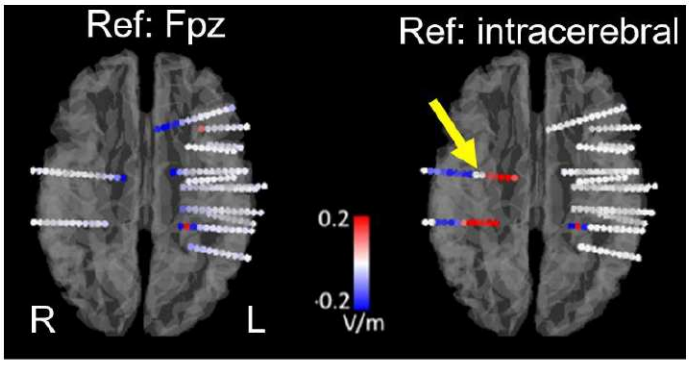

Figure 37: Intracerebral electric field (iEF) distribution for a 6 Hz tACS at 1 mA with TES electrodes on FT9-FT10 from voltage measured with a clinical recording device (SD LTM 128 Headbox; Micromed, Italy) with an input signal range of ± 3.2 mV. Left: iEF calculation from signal recorded with reference set on the scalp (Fpz). Right: iEF calculation from signal recorded with reference set on an intracerebral contact of a contralateral SEEG electrode (yellow arrow).

2. Intracerebral electric field in structures of the limbic system

As expected, during tACS, patients reported mild skin sensations (tickling) at both 0.5 mA and 1 mA intensities. No other side effects were noticed, and no epileptic seizure was induced by the tACS experiments. Altogether, patients had 1,360 intracerebral SEEG contacts. The most superficial SEEG contacts, in addition to 21 SEEG contacts (which were detected as outliers) were discarded (n = 215). Therefore, this intracerebral EF study relied on 1,145 SEEG contacts (average: 143 contacts per patient).

Overall, 102 SEEG contacts sampled the deep cortical structures: 42 were in the hippocampi, 28 in the amygdalae and 32 in the cingulate gyri. On all contacts, for all patients, mean SNR measured was 60 ± 9 dB, with a minimum of 20 dB and a maximum of 77 dB (maximum value conditioned by material limitation (saturation)) for the lowest stimulation intensity: at 0.5 mA. Thus, based on the SNR equation (24):

$$60 = 20 \cdot \log_{10}\left(\frac{\mathrm{U}_{tACS}(n)}{\mathrm{U}_{\Phi}(n) + \mathrm{U}_{w}(n)}\right) \quad (43)$$

$$\Leftrightarrow 3 = \log_{10}\left(\frac{\mathrm{U}_{tACS}(n)}{\mathrm{U}_{\Phi}(n) + \mathrm{U}_{w}(n)}\right) \quad (44)$$

$$\Rightarrow \frac{\mathrm{U}_{tACS}(n)}{\mathrm{U}_{\Phi}(n) + \mathrm{U}_{w}(n)} = 1000 \quad (45)$$

This mean tACS-generated signal amplitude recorded on intracerebral contact is, in average, a thousand times stronger than the noise (electrophysiological activity, environmental electromagnetic pollution *etc.*).

In the entire brain, the highest mean iEF value calculated was 0.36 ± 0.58 $V \cdot m^{-1}$ (Subject #1

Table 2 and Figure 38).

In the entire limbic system, a global mean iEF of 0.14 ± 0.08 $V \cdot m^{-1}$ was measured. More specifically, a mean of 0.17 ± 0.06 $V \cdot m^{-1}$ with a maximum of 0.38 $V \cdot m^{-1}$ in hippocampi for a 1 mA stimulation. In amygdalae, mean iEF measured was 0.21 ± 0.08 $V \cdot m^{-1}$ with a maximum of 0.49 $V \cdot m^{-1}$ for a 1 mA stimulation. In cingulate gyri, mean iEF measured was 0.07 ± 0.02 $V \cdot m^{-1}$ with a maximum of 0.11 $V \cdot m^{-1}$ for a 1 mA stimulation (Figure 39). Full tensors iEF magnitude calculated were 0.16 ± 0.14 $V \cdot m^{-1}$, 0.19 ± 0.09 $V \cdot m^{-1}$ and 0.10 ± 0.07 $V \cdot m^{-1}$ for the hippocampi, amygdalae, and cingulate gyri, respectively. These full tensors iEF magnitude values were not significantly different from the empirical mean iEF values (paired student's *t*-test $p = 0.88$) (Table 3 and Figure 42). tACS-induced voltage amplitude and iEF magnitudes distribution for Subject #0 to #6 (For a 1 mA tACS at 300 Hz with stimulation electrodes placed on FT9-FT10) are displayed on an MNI-normalized brain in Figure 40 and Figure 41, respectively.

Table 2: Means and standard deviations of the electric field magnitudes during tACS at 0.5 and 1 mA (EF: Electric field; SEEG: stereoelectroencephalography)

Subjects	**Nb of SEEG contacts**	**Mean EF at 0.5 mA** ($V \cdot m^{-1}$)	**Mean EF at 1 mA** ($V \cdot m^{-1}$)
0	172	NA	0.16 (±0.19)
1	162	0.18 (±0.29)	0.36 (±0.58)
2	101	0.13 (±0.11)	0.24 (±0.22)
3	151	0.09 (±0.1)	0.17 (±0.20)
4	89	0.14 (±0.29)	0.26 (±0.58)
5	155	0.08 (±0.14)	0.16 (±0.29)
6	149	0.04 (±0.02)	0.08 (±0.04)
7	166	NA	0.13 (±0.27)

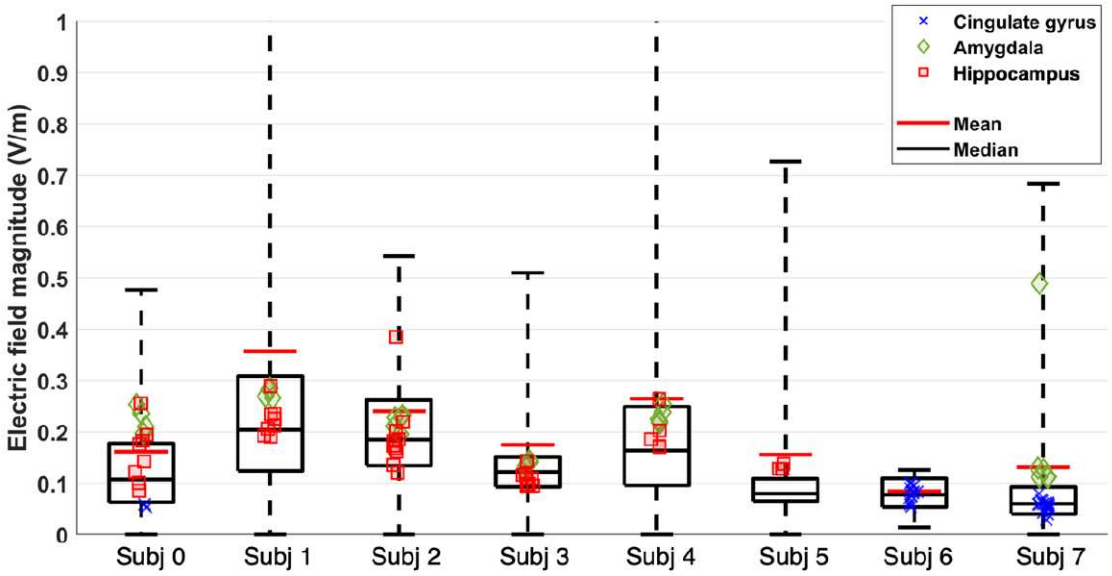

Figure 38: Intracerebral EF magnitudes for all subject during a 1-mA tACS at 300 Hz with stimulation electrodes placed on FT9-FT10 (Pat 0 to Pat 6) or T7-T8 (Pat 7). Boxes represent the 25th and 75th percentiles, whiskers represent minimum and maximum values (2.5 standard deviation for each distribution). Black bars inside boxes are median values. Additional red bar represents mean iEF values from the distribution and icons represent the deep structures explored.

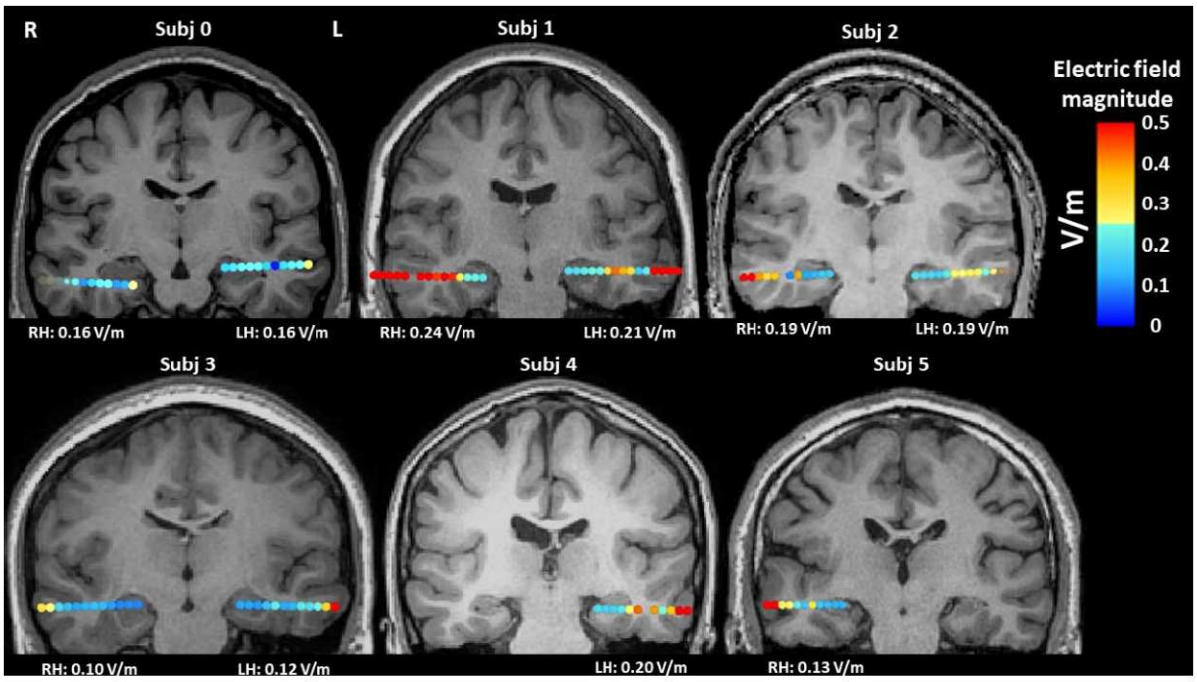

Figure 39: Empirical electric fields (EF) in the hippocampi for a 1-mA tACS at 300 Hz electrodes placed on FT9-FT10. Below each individual MRI with the reconstructed SEEG electrodes, the mean EF values of SEEG contacts within the deep structures are indicated. (L: left, R: right, H: Hippocampus)

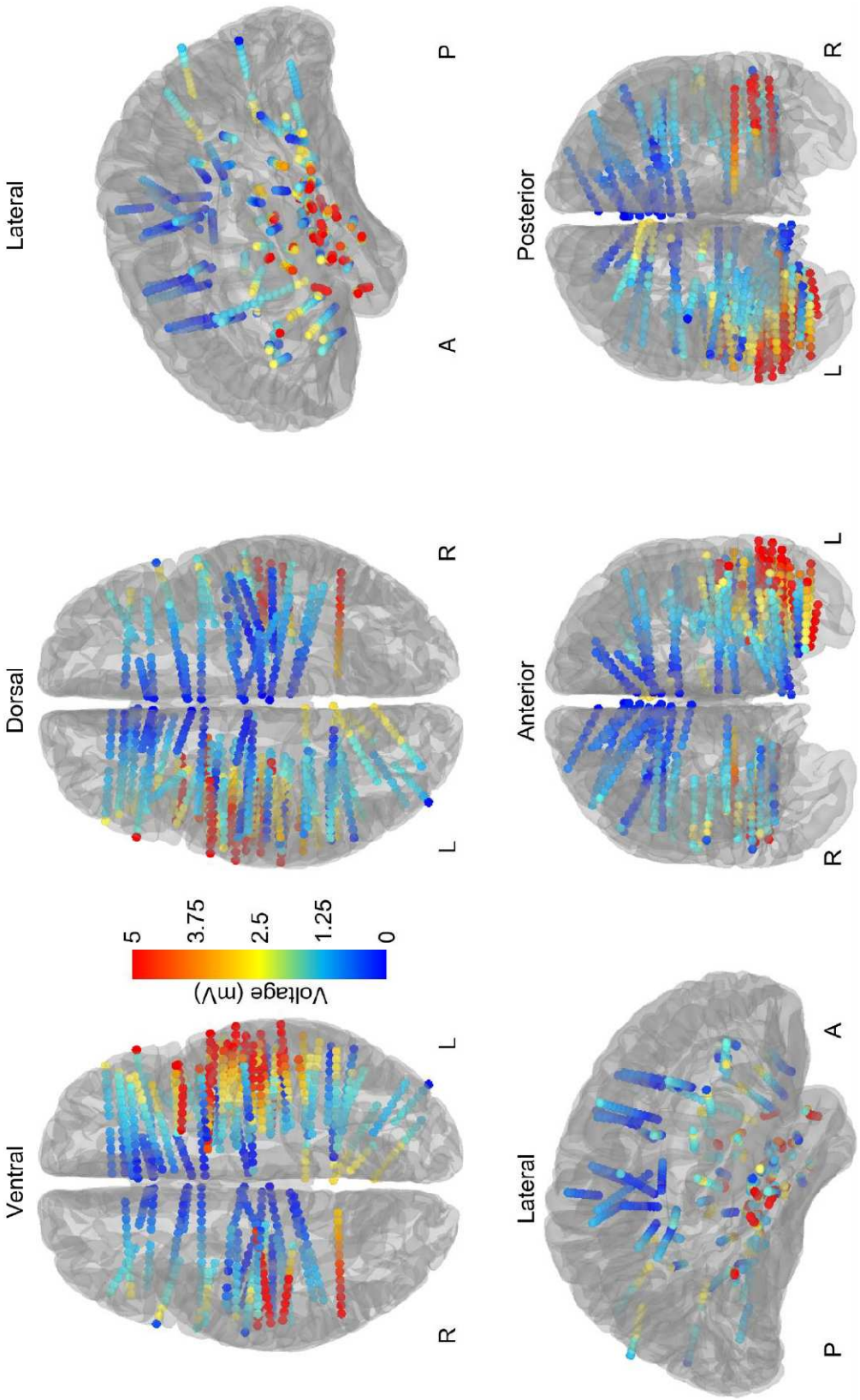

Figure 40: Voltage amplitude distribution for Subject #0 to #6 on an MNI-normalized brain. Voltage amplitude displayed are for a 1-mA tACS at 300 Hz with stimulation electrode placed on FT9-FT10.

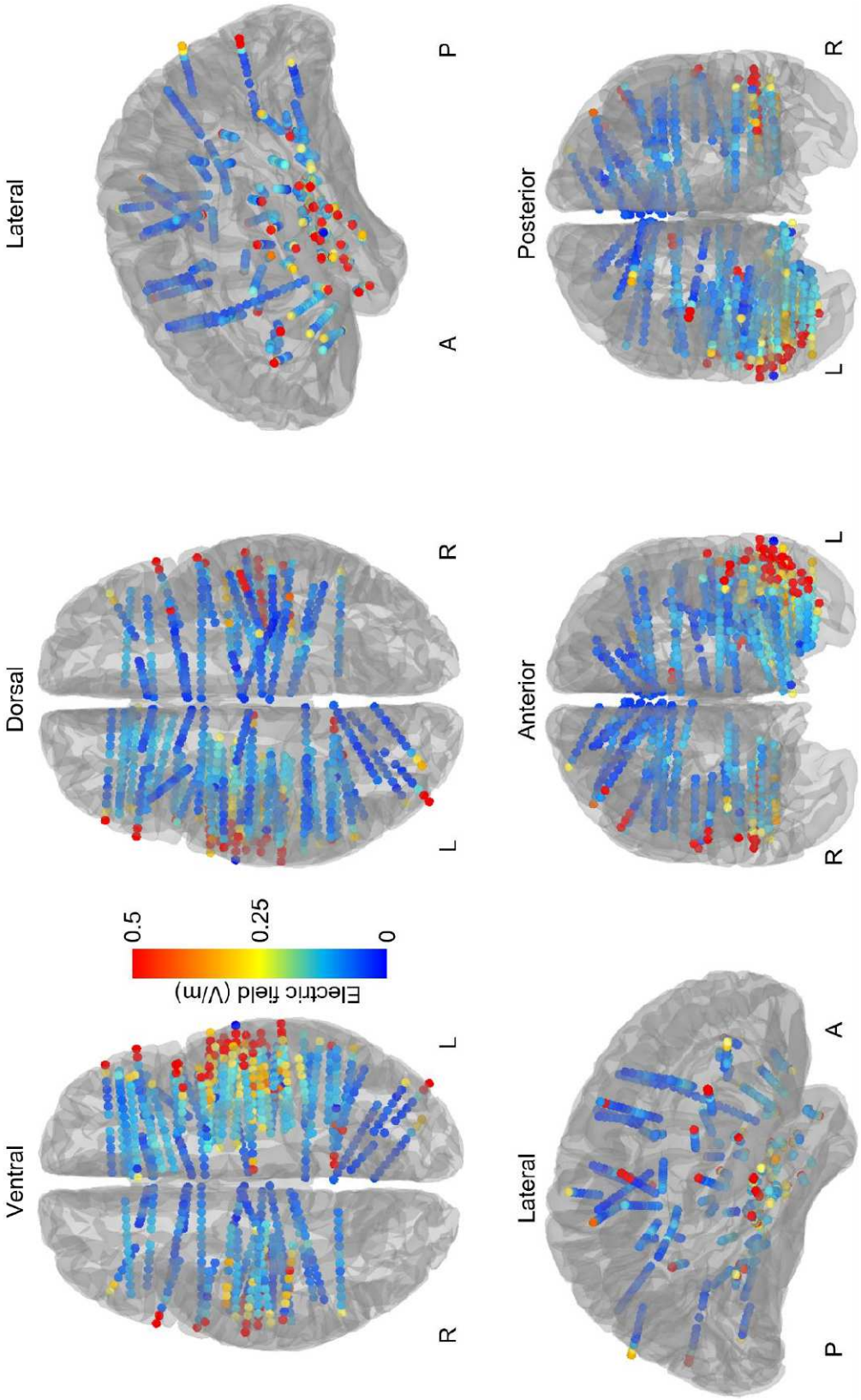

Figure 41: Electric field magnitude distribution for Subject #0 to #6 on an MNI-normalized brain. iEF magnitude displayed are for a 1-mA tACS at 300 Hz with stimulation electrode placed on FT9-FT10.

Table 3: Electric field magnitude in deep brain structures

Subjects	Deep brain structures	Nb of SEEG contacts	Mean EF at 1 mA ($V \cdot m^{-1}$)	Max EF at 1 mA ($V \cdot m^{-1}$)	Tensors ($V \cdot m^{-1}$)	EF Value 1 ($V \cdot m^{-1}$)	EF Value 2 ($V \cdot m^{-1}$)	EF Value 3 ($V \cdot m^{-1}$)	EF Value 4 ($V \cdot m^{-1}$)	EF Value 5 ($V \cdot m^{-1}$)
0	R Hippocampus	4	0.16	0.09	0.26	0.26	0.10	0.09	0.19	*NA*
	L Hippocampus	4	0.16	0.06	0.18	0.12	0.14	0.18	0.18	*NA*
	L Amygdala	4	0.22	0.09	0.25	0.25	0.24	0.21	0.20	*NA*
1	R Hippocampus	4	0.24	0.29	0.47	0.21	0.23	0.24	0.29	*NA*
	L Hippocampus	4	0.21	0.23	0.11	0.19	0.19	0.21	0.23	*NA*
	L Amygdala	4	0.28	0.29	0.30	0.28	0.29	0.27	0.27	*NA*
2	L Hippocampus	5	0.19	0.22	0.07	0.20	0.19	0.18	0.17	0.22
	R Hippocampus	5	0.19	0.38	0.28	0.17	0.16	0.14	0.12	0.38
	L Amygdala	5	0.22	0.23	0.34	0.23	0.23	0.21	0.20	0.23
3	L Hippocampus	4	0.12	0.14	0.07	0.12	0.12	0.11	0.14	*NA*
	R Hippocampus	4	0.10	0.11	0.28	0.10	0.10	0.10	0.11	*NA*
	L Amygdala	4	0.14	0.14	0.10	0.14	0.14	0.14	0.13	*NA*
4	L Hippocampus	5	0.20	0.26	0.13	0.19	0.17	0.17	0.20	0.26
	L Amygdala	5	0.23	0.25	0.13	0.25	0.24	0.22	0.22	0.23
5	R Hippocampus	3	0.13	0.14	0.07	0.13	0.13	0.14	*NA*	*NA*
6	L. Ant Cingulate gyrus 1	2	0.09	0.1	0.08	0.08	0.10	*NA*	*NA*	*NA*
	L. Ant Cingulate gyrus 2	3	0.08	0.9		0.09	0.08	0.08	*NA*	*NA*
	L. mid Cingulate gyrus	2	0.06	0.06		0.05	0.06	*NA*	*NA*	*NA*
	R ant. Cingulate gyrus 1	2	0.10	0.1		0.09	0.10	*NA*	*NA*	*NA*
	R ant. Cingulate gyrus 2	2	0.09	0.09	0.08	0.08	0.09	*NA*	*NA*	*NA*
	R. mid Cingulate gyrus	2	0.07	0.06		0.06	0.07	*NA*	*NA*	*NA*
	L ant. Cingulate gyrus	3	0.06	0.07		0.07	0.06	0.06	*NA*	*NA*
	L mid. Cingulate gyrus 1	3	0.07	0.08	0.18	0.07	0.07	0.08	*NA*	*NA*
	L mid. Cingulate gyrus 2	2	0.06	0.07		*NA*	0.05	0.07	*NA*	*NA*
7	R ant. Cingulate gyrus	3	0.05	0.07		0.04	0.05	0.07	*NA*	*NA*
	R mid. Cingulate gyrus 1	3	0.07	0.07	0.14	0.07	0.06	0.07	*NA*	*NA*
	R mid. Cingulate gyrus 2	3	0.09	0.11		0.11	0.09	0.07	*NA*	*NA*
	L Amygdala	3	0.13	0.13	0.20	0.13	0.13	0.12	*NA*	*NA*
	R Amygdala	3	0.24	0.49	0.18	0.11	0.11	0.49	*NA*	*NA*

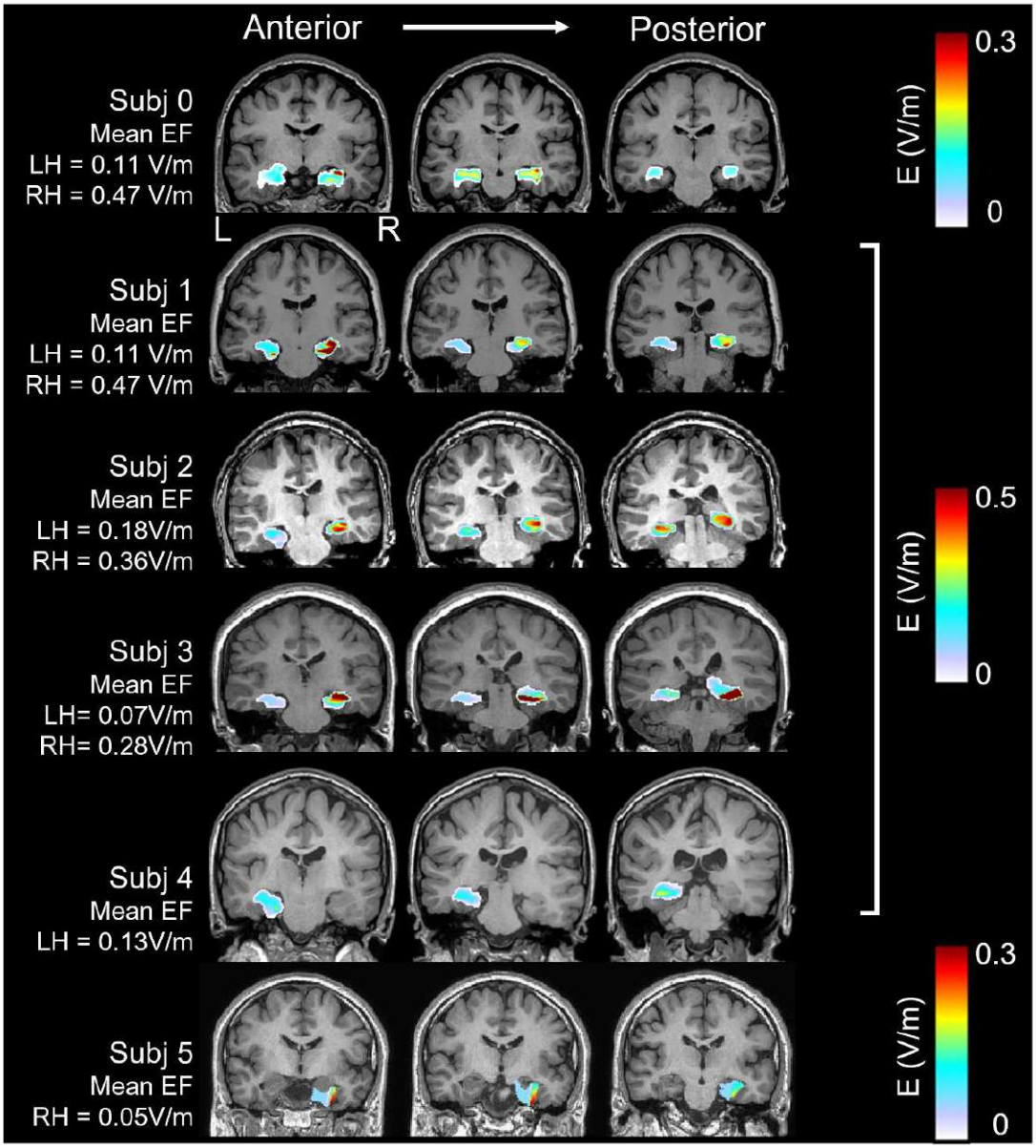

Figure 42: Coronal view of the electric field magnitudes spatial distribution in hippocampi after calculating the full electric field (EF) tensor overlayed on individual patients' MRI. EF tensors were computed from the empirical values measured in SEEG contacts within the hippocampus. For each patient, three slices of interest and the mean iEF within the slices are displayed (From left to right: anterior to posterior). (L: left, R: right, H: Hippocampus)

3. Influence of tACS parameters

a. Influence of tACS Frequency

TACS frequency was investigated in one subject. Mean MPV (Mean Percentage Variation which is the mean for all frequencies calculated with equation 39) calculated in the limbic system was 5 ± 7 %. MPV of 11 % was calculated between 1 Hz and 300 Hz (equation 39). It corresponded to a decrease of 0.03 $V \cdot m^{-1}$ from low (1 Hz) to high (300 Hz) frequencies (Figure 43).

Coefficients from the linear fitting were p1 (slope) = $-9 \cdot 10^{-5}$ and p2 (the intercept) = 0.2 with a determination coefficient R^2 of 0.5.

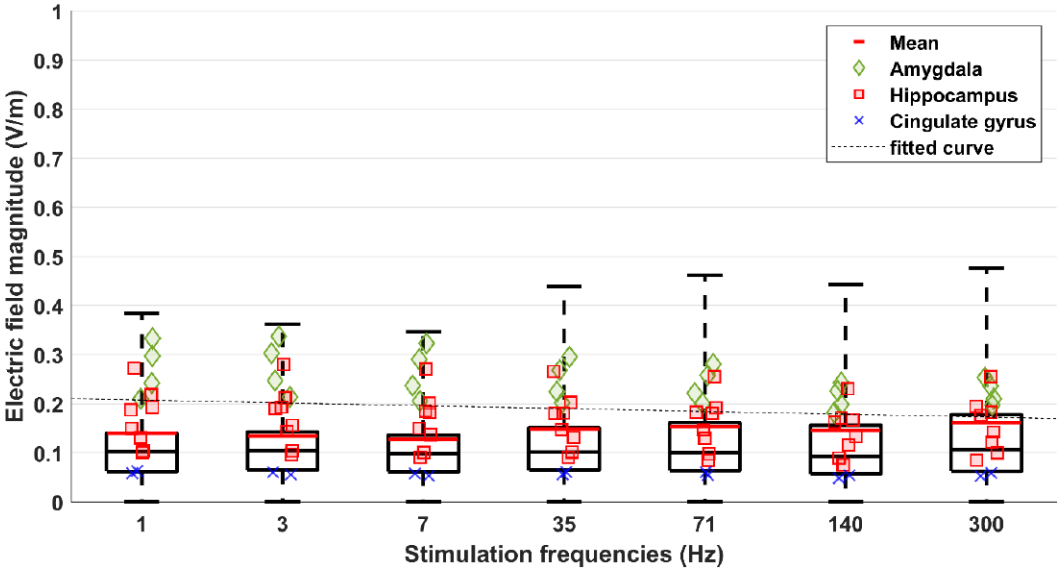

Figure 43: Intracerebral EF magnitudes for a 1 mA tACS at all frequencies tested in one subject with stimulation electrodes placed on FT9-FT10. Boxes represent the 25th and 75th percentiles, whiskers represent minimum and maximum values (2.5 times standard deviation for each distribution). Black bars inside boxes are median values. Additional red bar represents mean iEF values from the distribution and icons represent the deep structures explored. Black dashed lines represent the fitted polynomial curve calculated on mean iEF values in deep brain structures explored.

b. Influence of tACS intensity

TACS intensity was investigated in 6 subjects. Comparison between iEF magnitude for stimulation at 0.5 mA and 1 mA exhibited a slope (p1) from 2 (Subjects #1-5) to 2.2 (Subject #6), and a determination coefficients R^2 from 0.98 (Subject #6) to 1.00 (Subjects #3-5) (see Figure 44). Finally, comparison between empirical values $\mathbf{E}_1$ and expected values $\widehat{\mathbf{E}_1} = 2\mathbf{E}_{0.5}$ (equation 41) gave a MAE from 0.0003 (Subject #6) to 0.0174 (Subject #1).

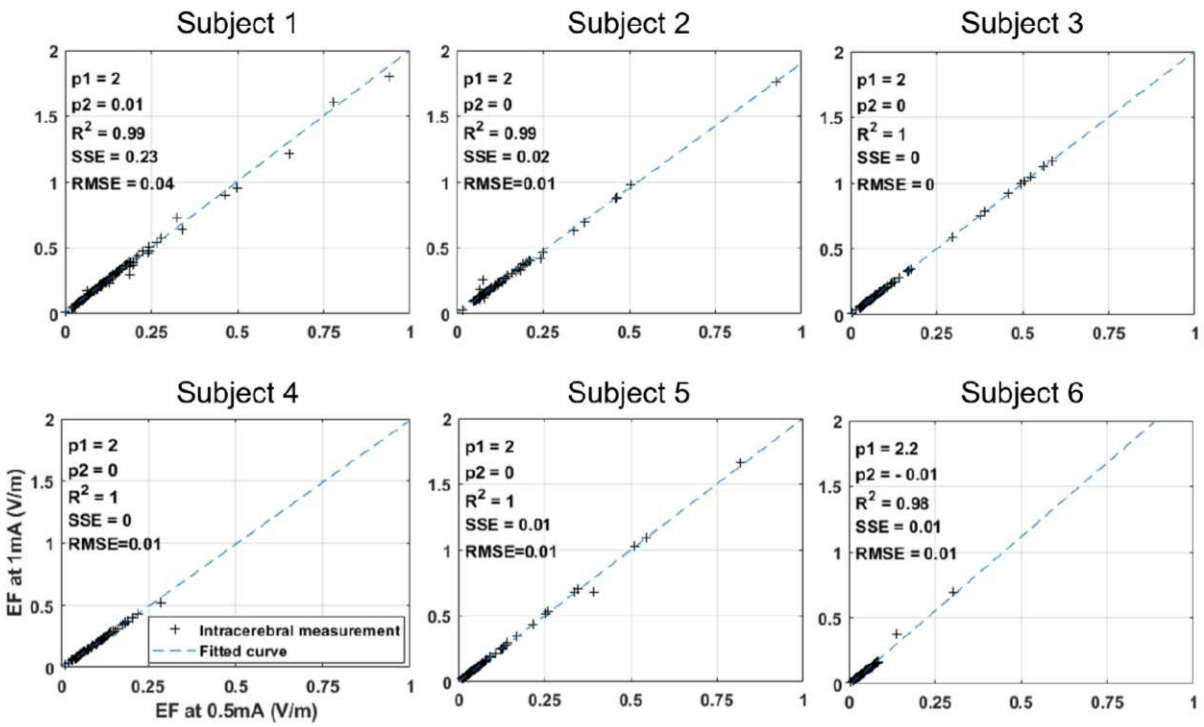

Figure 44: Intracerebral EF magnitudes for a 0.5 mA (*x*-axis) and a 1 mA (*y*-axis) tACS at 300 Hz on each intracerebral contact (black crosses) in 6 subjects with stimulation electrodes placed on FT9-FT10. Blue dashed lines are the fitted curve with p1 its slope, p2 its intercept, SSE the sum of squared error value and RMSE the root mean squared error.

c. Influence of tACS montage

Influence of tACS montage on iEF was investigated in one subject (Subject#7) and analysis performed on 166 SEEG contacts. On 15 montages tested, one was discarded (Fz-T7) because of uncommonly high amplitude white noise. Concerning limbic system structures, 17 SEEG contacts were in the cingulum and 6 in the amygdalae, but no contact in the hippocampus. TES montage, which yielded the highest mean iEF in the amygdalae was T7-T8 (0.24 $V \cdot m^{-1}$) and in the cingulum was T7-C4 (0.09 $V \cdot m^{-1}$) (Table 4). The TES montage, which yielded the lowest mean iEF was Fz-Cz. Figure 45 displays global EF distributions of Subject #7 according to tACS montages.

iEF magnitude issued from the full tensor calculation exhibited extremes values for the same montages: (T7-T8) for the amygdalae (0.41 $V \cdot m^{-1}$), Fz-C4 for the cingulate gyri (0.42 $V \cdot m^{-1}$), and the minimum for Fz-Cz (Table 5).

Table 4: Empirical (single component) electric field magnitude in deep brain structures for different tACS montages for Subject # 7 (ALCG: Anterior Left Cingulate Gyrus; MLCG: Middle Left Cingulate Gyrus; ARCG: Anterior Right Cingulate Gyrus; MRCG: Middle Right Cingulate Gyrus; RA: Right Amygdala; LA: Left Amygdala)

Mean EF (V/m)	Cz-FT10	Cz-T8	Cz-C4	C3-FT10	C3-T8	C3-C4	T7-FT10	T7-T8	T7-C4	Fz-FT10	Fz-T8	Fz-C4	Fz-Cz	Fz-C3
ALCG	0.03	0.03	0.06	0.06	0.05	0.04	0.06	0.05	0.05	0.05	0.04	0.05	0.01	0.01
MLCG1	0.04	0.04	0.07	0.07	0.07	0.04	0.06	0.06	0.05	0.05	0.05	0.05	0.02	0.01
MLCG2	0.03	0.03	0.06	0.06	0.06	0.02	0.04	0.05	0.05	0.04	0.05	0.04	0.02	0.00
ARCG	0.01	0.02	0.04	0.03	0.04	0.01	0.04	0.05	0.05	0.01	0.02	0.01	0.00	0.02
MRCG1	0.02	0.03	0.06	0.05	0.06	0.01	0.05	0.06	0.07	0.01	0.02	0.01	0.01	0.04
MRCG2	0.00	0.02	0.05	0.04	0.08	0.02	0.05	0.06	0.09	0.02	0.00	0.02	0.00	0.05
RA	0.11	0.09	0.18	0.12	0.17	0.05	0.17	0.24	0.22	0.05	0.11	0.05	0.00	0.08
LA	0.05	0.04	0.10	0.11	0.09	0.06	0.13	0.12	0.11	0.06	0.05	0.06	0.00	0.05

Table 5: multi-component electric field magnitude (from the full tensor calculation) in deep brain structures for different tACS montages for Subject # 7 (LCG: Left Cingulate Gyrus; RCG: Right Cingulate Gyrus; RA: Right Amygdala; LA: Left Amygdala)

Mean EF (V/m)	Cz-FT10	Cz-T8	Cz-C4	C3-FT10	C3-T8	C3-C4	T7-FT10	T7-T8	T7-C4	Fz-FT10	Fz-T8	Fz-C4	Fz-Cz	Fz-C3
LCG	0.10	0.08	0.17	0.18	0.13	0.11	0.10	0.09	0.08	0.09	0.31	0.31	0.23	0.23
RCG	0.18	0.08	0.13	0.17	0.13	0.20	0.11	0.13	0.14	0.09	0.36	0.42	0.32	0.28
LA	0.21	0.10	0.26	0.24	0.17	0.18	0.32	0.41	0.35	0.04	0.21	0.19	0.05	0.12
RA	0.15	0.08	0.19	0.18	0.12	0.13	0.19	0.23	0.18	0.02	0.18	0.16	0.05	0.05

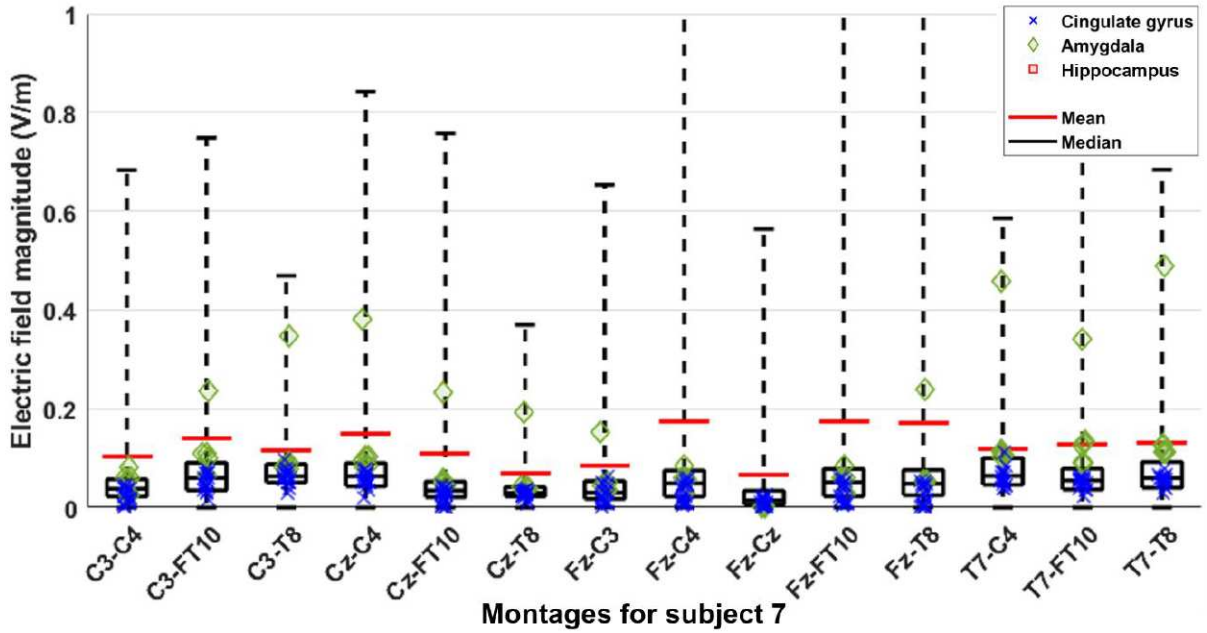

Figure 45: Intracerebral EF magnitudes for a 1 mA tACS at 300 Hz for one subject for the 14 different montages tested. Boxes represent the 25th and 75th percentiles, whiskers represent minimum and maximum values (2.5 times standard deviation for each distribution). Black bars inside boxes are median values. Additional red bar represents mean iEF values from the distribution and icons represent the deep structures explored. Black dashed lines represent the fitted polynomial curve calculated on mean iEF values in deep brain structures explored.

4. Influence of depth

iEF magnitudes, as a function of the distance from the nearest stimulation electrode on all intracerebral contacts, are displayed in Figure 47

The maximum distance from the nearest stimulation electrode and a SEEG contact was 14.6 cm. Thus, the full distance range (from 0 to 15 cm) was divided by 10 segments of 1.5 cm each. Between 0 cm and 1.5 cm there were no SEEG contacts (so no iEF magnitudes calculated within the first segment), therefore 9 groups were plotted in the violin plot (Figure 46).

a. Non-linear regression on median values

Measured coefficients from the non-linear regression on median values of iEF groups (black dashed line in Figure 46) were $a = 1.28$ (with 0.92 and 1.63 as the 95 % confidence bounds), $b = -1.76$ (-2.13 and -1.39), $c = 0.03$ (0.01 and 0.05) and a determination coefficient R^2 of 0.99.

b. Non-linear regression on mean values

Measured coefficients from the non-linear regression on mean values of iEF groups (red dashed line in Figure 46) were $a = 2.8$ (2.1, 3.51); $b = -1.65$ (-1.99, -1.31); $c = 0.03$ (-0.02, 0.07) and a determination coefficient R^2 of 0.99.

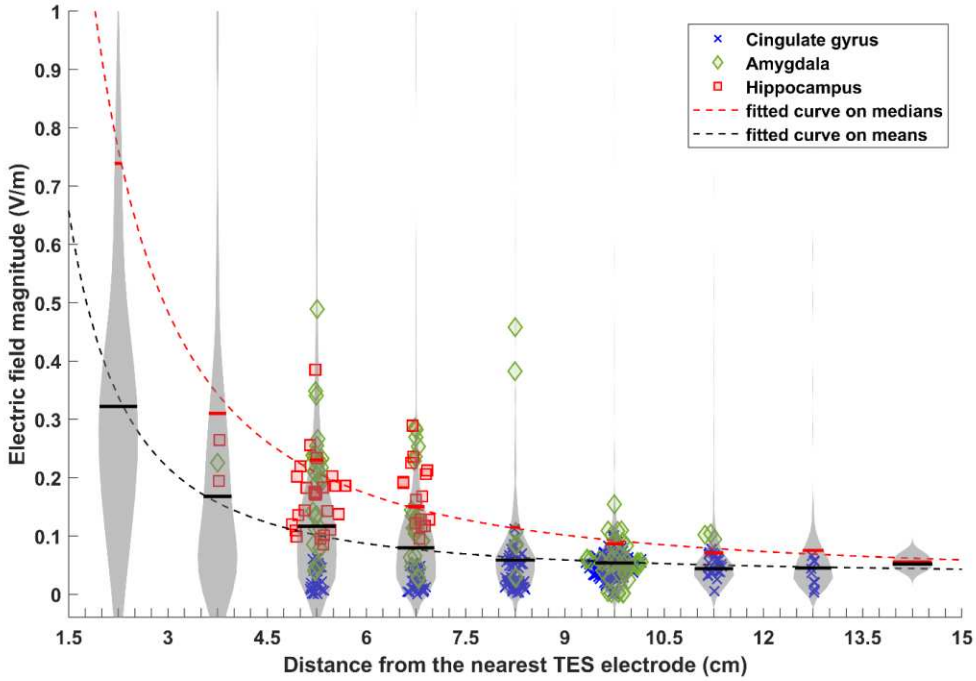

Figure 46: Violin plot displaying electric field magnitude as a function of the distance with values grouped into 9 distance segments (from 1.5 cm to 15 cm) for all patients for a 1 mA tACS at 300 Hz and for all montages. Black bars inside violins represent median iEF magnitude and red bars represent mean iEF magnitude. Red and black dashed lines represent the fitted values from the non-linear regression on mean and median values, respectively. Icons represent deep structures explored.

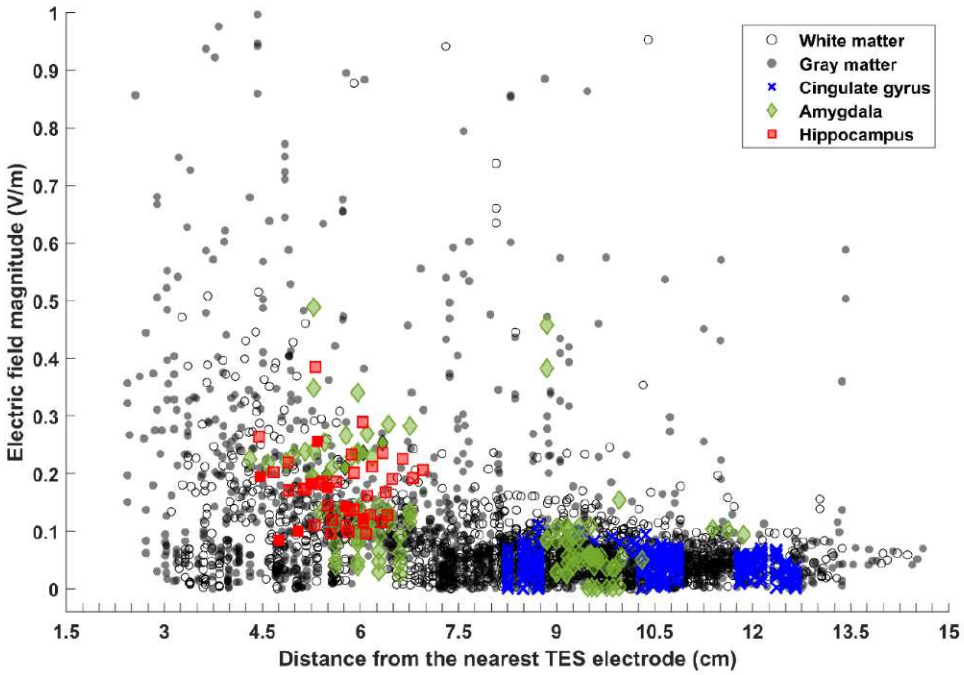

Figure 47: Raw intracerebral electric field values on each intracerebral contact for a 1 mA tACS at 300 Hz for all patients and all montages. Gray dots represent intracerebral contacts within the gray matter, white circles represent intracerebral contacts within the white matter and icons represent the deep structures explored.

IV. Conclusion and discussion

1. The measurement of an intracerebral electric fields

Measuring iEF in human *in-vivo* can be difficult due to the complex combination of simultaneous SEEG and TES. First, few patients a year are explored with SEEG, and only few centers perform this clinical investigation. Second, experiments need to be performed in a brief time window and in a complex environment: experiments on humans in asepsis condition.

Studies which already explored iEF in human *in-vivo* relied on ECoG investigation, hybrid ECoG/SEEG investigation or exclusive depth electrodes (SEEG or DBS) investigation (Opitz *et al.*, 2016; Huang *et al.*, 2017; Chhatbar *et al.*, 2018; Ruhnau *et al.*, 2018). Results from subjects involved in an ECoG or hybrid ECoG/SEEG investigations should be nuanced. Indeed, craniotomy performed for an ECoG substantially modify the skull geometry and conduction. This usually needs to be considered for brain stimulations (Datta, Bikson, and Fregni et al., 2010) or sources localizations (Benar and Gotman, 2000; Lau et al.., 2016). Moreover, craniotomies induce breach rhythms, defined as "*an increase in the amplitude of alpha, beta, and mu rhythms*" (Brigo *et al.*, 2011) which can also bias iEF calculation when performing low frequency tACS.

Exclusive SEEG investigation has the advantage of being minimally invasive by drilling small punctures in the skull (2.45 mm diameter in the study conducted in this chapter) (Salado *et al.*, 2018) which are considerably smaller than ECoG's skull defects. Also, SEEG offers the best spatial sampling in depth and allows electrophysiological measurements of specific deep structures such as the limbic system. Exclusive SEEG investigation offers a good tradeoff between a high spatial resolution and a minimal impact on the skull geometry and is, therefore, the best approach to study, in more realistic conditions, iEF during a TES. By making this statement, only exclusive SEEG (or DBS) investigation are considered in the literature.

Thus, among the 4 studies which explored iEF in human in-vivo, 5 patients with exclusive SEEG (or DBS) investigations were included overall (Opitz *et al.*, 2016; Huang *et al.*, 2017; Chhatbar *et al.*, 2018; Ruhnau *et al.*, 2018). Contrary to tDCS, tACS provides an extremely high signal quality (mean SNR of 60 ± 9 dB for a 0.5 mA stimulation) and the use of combined tACS and exclusive SEEG investigation is, therefore, a very robust methodology. Yet, in literature, only 3 subjects were included with the mentioned methodology. In the present study, 8 subjects were included using tACS with exclusive SEEG investigation, which is more than the cumulated number of subjects in the 4 studies.

Also, the current study is the first that focused on the limbic system, which plays an important role in many neurological disorders (Epilepsy, Alzheimer's, depression, schizophrenia, bipolar disorders *etc.*). IEF magnitudes measured within these deep brain regions are within a subthreshold

range ($0.14\ V{\cdot}m^{-1} < iEF < 1\ V{\cdot}m^{-1}$) susceptible to induce a modulation of spike timing, neural firing (Francis, Gluckman and Schiff, 2003; Kar, Duijnhouwer and Krekelberg, 2017) or other stochastic effects (Liu et al. 2018).

One limitation of the present study is that the findings rely mainly on the single component iEF magnitude calculation which are along imposed direction constrained by the clinical context (structures explored and trajectory regarding the vascular network). The variability of SEEG electrodes' relative angles (compared to each other) led to incomplete iEF magnitude information and approximation (averaging iEF magnitude within the same structure but calculated along different angles). However, differences between empirical (single component) and tensor calculated (multi-component) mean iEF magnitudes are not significant, meaning that information carried by the empirical (single component) iEF magnitudes are quite close to the "real" electric field generated.

Another limitation is regarding the method on how multi-component iEF are calculated. Despite the use of an accurate interpolation method, the calculation is still far from a realistic approach. A "simple" interpolation was performed assuming that all scattered points were in a uniform, homogeneous and isotropic medium. Moreover, multi-component iEF values in the limbic system results from interpolation executed on all intracerebral contact and not only on the few contacts within the structures of interest. This was done to include the maximum measurement point to obtain a more precise results of the electric field distribution within the structures of interest. Nonetheless, the presented multi-component iEF results should encourage further studies in computational TES modeling by using, for instance, FEM methods (from MRI segmentation and by applying tissues conductivity values) to solve the iEF propagation between intracerebral contacts and weighting the solution with the empirical values at the measurement points. It is also possible to think about modelling SEEG implantation in MRI-based model for future validation and comparing iEF distribution with and without intracerebral investigation.

2. On the importance of hardware choice

The experiment investigating the reference position with hardware used in clinical routine shows that iEF can't be studied on every recording device. The tACS-generated signal has values outside the amplifiers maximum input range and are saturated. For the clinical recording device, the number of saturated contacts was too important and made impossible the potential iEF investigation. Even with a higher quality amplifier used for scientific research purpose (with an input range of ± 8.191 mV) 18 % of intracerebral contacts were still saturated and thus discarded (most lateral contacts). For an optimal iEF investigation it is suggested to use amplifier with input range of ± 100 mV (Liu *et al.*, 2018). However, the use of such technology can represent substantial expenses that only the wealthiest research centers are able to cover. In order to avoid such investment of expensive electrophysiological recording equipment, it is possible to overcome the signal saturation issue by:

1. Carefully place the device's reference on a deep intracerebral contact close to the structure explored while investing in more affordable amplifiers (between ± 5 mV and ± 10mV): only the signal recorded far from the structure of interest will be saturated and therefore will allow iEF study within the desired structure.

2. Using lower tACS intensities (< 1 mA) with deep intracerebral recording reference. Then, it would be possible to extrapolate iEF magnitudes which would have been obtained at higher intensities just by multiplying iEF values by the desired factor. This can be done thanks to the linearity between tACS intensity and iEF magnitude demonstrated (Louviot *et al.*, 2022).

Human *in-vivo* intracerebral data for TES investigation are too precious given the scarcity of SEEG inclusions. Therefore, consideration of hardware and reference position (which can appear trivial) are too important to be overlooked. Indeed, this can avoid an unnecessary waste of data, time, and money.

3. What influences the intracerebral electric field?

a. The tACS frequency

To date, the presented study is the first to report and quantify iEF at several tACS frequencies in human *in-vivo* in the limbic system. The reported decrease of iEF magnitude (from the lowest to the highest frequency) in the limbic system is in line with the previous study in non-human primates (Opitz *et al.*, 2016). Indeed, because conductivity can increase as a function of the frequency (Gabriel, Lau and Gabriel, 1996), voltages measured in the same tissue-type will decrease with a same factor when frequency changes and, therefore, induce a decrease of iEF magnitude calculated. This highlights a small capacitance effect of brain tissues. Nonetheless, the mentioned decrease implies that all voltage values are recorded in the same tissue-type because conductivities don't change the same way regarding the tissue-type.

A limitation of this sub-study is the number of subjects included (only 1 subject) which is, however, sufficient under the light of previous studies, to draw a basic conclusion about brain tissues' small capacitive effects in living humans. By including several patients, further studies would be able to investigate the statistical difference between frequency, quantifying and generalizing the frequency effect and qualifying if the capacitive effect can be neglected or, contrariwise, need to be considered.

Still, it is possible to conclude that iEF magnitudes in the deep brain structures at 300 Hz are representative of the fields generated by low frequency tACS.

b. Influence of tACS intensity

This study is the first to mathematically quantify the influence of tACS intensity on iEF magnitude in human *in-vivo*. The quasi-linear relationship between stimulation intensity and iEF magnitude confirm experimentally biophysics theory. Also, this experimental proof will allow further

studies to assume, with a high confidence rate, that iEF generated during a stimulation at an intensity of *k*-mA is about *k* times the value reported in this chapter for a 1 mA stimulation. For stimulation at high intensity (e.g., 4 mA) iEF magnitude at the vicinity of the Amygdala-hippocampus complex can reach 1 $V \cdot m^{-1}$ which can be considerably interesting for potential clinical application of TES

c. Influence of tACS montage

The current study is also the first to explore iEF for different TES montages in human *in-vivo*. Results show that montage, for which stimulation electrodes are the most remote, generates the strongest iEF. However, a variability exists between montages and the iEF magnitude linear changes as a function of the inter-electrode distance reported by (Faria, Hallett and Miranda, 2011) which wasn't observed here. One explanation is because of the single-component calculation constrained by SEEG orientation and the spatial coverage of the SEEG implantation constrained by clinical investigation. Still, maximum iEF is generated when stimulation electrodes are the most distant and minimum iEF values were reported for the least inter-electrode distance montage (Fz-Cz). This was also confirmed through the multi-component iEF calculation which indirectly highlights the scalp-shunt phenomenon.

The scarcity of this quasi-symmetrical implantation exploring the amygdala and cingulate gyrus (one in 3 1/2 years) didn't allow other inclusion. Thus, this single case inclusion is one limitation of the sub-study. Another limitation is related to the SEEG implantation and the multi-component iEF calculation both described earlier.

Thus, the presented results need to be confirmed and extended with additional subjects. In doing so, this investigation would help validate computational studies and establish guidelines for bipolar TES electrodes placement. Data are available online for further computational studies at https://data.mendeley.com/datasets/sk279ktjv3/3.

d. Influence of depth

Huang *et al.*,2017 reported a decrease of iEF magnitude as a function of the depth in their entire cohort (hybrid ECoG/SEEG investigation and exclusive SEEG investigation). In the present study, influence of depth on iEF magnitude was studied in the entire cohort with the same investigational method (exclusive SEEG investigation) and was quantified. The high variability in first segments (smallest distance) are mainly led by the SEEG orientation issue regarding the main EF component. Still, results show a decrease which follows an inverse squared law tendency which confirm physics theory. These findings may seem trivial at first glance but are of capital importance. Indeed, it is the first time that the influence of depth on iEF magnitude was quantified in human *in-vivo* during a tACS. Combined with the knowledge given by the other parameters mentioned above (influence of frequency, intensity, and montage) this gives fundamental knowledge on TES and on the intracerebral electric field behavior in human *in-vivo*.

4. In general

Overall, this intracerebral electric field study in human *in-vivo* should encourage further studies including more patients and more intracerebral structures explored. Also, it could give fundamental insight for more realistic approach of computational modeling by adjusting parameters to fit empirical results and validate computational models.

From a clinical point of view, iEF values reported in the limbic system can be used as a ground truth for prospective TES clinical studies investigating the numerous neurological disorders involving the limbic system. Certainly, under the light of the literature, this study can provide to clinical investigators a base knowledge of iEF achievable in the limbic system using the right montage, intensity, and frequency. Retrospectively, the reported results can also enforce some previous clinical findings on TES or help to improve ongoing protocols.

Chapter III:

Electrophysiological effects of TES in epilepsy: intracerebral human in-vivo investigation

About 25 % to 30 % of epilepsy patients are resistant to pharmacological treatments (Assenza *et al.*, 2017; Fregni *et al.*, 2021) which represents around 200,000 patients in France. One solution is the removal of the epileptogenic zone or, at least, the reduction of the underlying network involved in seizure propagation by surgical intervention. Epilepsy surgery requires a pre-surgical evaluation during which patients undergo several procedures, including SEEG investigation (Kwan *et al.*, 2009; Brodie *et al.*, 2012; Isnard *et al.*, 2018; Salado *et al.*, 2018). However, about 50 % of focal refractory epilepsy patients are not eligible to surgery (Assenza *et al.*, 2017; Fregni *et al.*, 2021). This is because the epileptogenic zone: (1) is located in the eloquent cortex where resection can cause deficit or (2) is not focal or (3) is inaccessible to surgery. Also, a non-negligible amount of focal refractory epilepsy patients don't have access to medical centers where epilepsy surgery is performed (Auvichayapat *et al.*, 2013).

Electrical stimulation such as Deep Brain Stimulation (DBS) (Fisher *et al.*, 2010) or Vagus Nerve Stimulation (VNS) (Toffa *et al.*, 2020) offer interesting alternatives for treating refractory epilepsy. Other techniques such as Transcranial Magnetic Stimulation (TMS) or Transcranial Electrical Stimulation (TES, especially direct current stimulation: tDCS), still under scientific investigations, have the advantage of being non-invasive and present encouraging results. In addition, the ease of use and the affordability of TES constitute a big advantage for this technique to be widely used in the future.

In the past two decades it has been assumed in the community that cathodal tDCS (c-tDCS, injection of a negative current over the epileptogenic focus and/or irritative zone) would hyperpolarize the pathological zone inducing, therefore, a control on cortical hyperexcitability. Five major reviews addressed clinical trials exploring tDCS in epilepsy (San-Juan *et al.*, 2015; Lefaucheur, 2016; Lefaucheur *et al.*, 2017; Regner *et al.*, 2018; Fregni *et al.*, 2021). To date, 12 clinical studies investigated tDCS in epilepsy (Regner *et al.*, 2018) which falls to 7, when excluding single cases (Fregni *et al.*, 2006; Auvichayapat *et al.*, 2013, 2016; Tekturk *et al.*, 2016; Assenza *et al.*, 2017; San-Juan *et al.*, 2017) (for a review see Fregni et al., 2021). Chapter I provides a detailed overview of these studies.

Concerning evidence-based guidelines of tDCS in epilepsy, Lefaucheur et al., (2017) gave no recommendation, whereas Fregni et al., (2021) gave a level B recommendation (probably effective). This discrepancy resides in their judgement criteria differences: Lefaucheur et al., (2017) assessed tDCS effects based on IED and seizure frequency (from studies which included more than 10 subjects) whereas Fregni *et al.*, (2021) assessed tDCS effects based only on seizure frequency (from studies which can have less than 10 subjects). This means that tDCS has a level B recommendation only for seizure frequency reduction, but there is no consensus about the effect on IED. However, a recent study reported a significant effect on IED and on seizure frequency (sham-controlled crossover study) including 15 patients and performing repeated cathodal tDCS (Kaufmann *et al.*, 2021).

IED and seizures are dissociable (Gotman, 1991; Baud *et al.*, 2018), but IED activity is still a non-negligible part of epilepsy disease, which induces cognitive comorbidities (Van Bogaert *et al.*, 2012; Horak *et al.*, 2017; Ung *et al.*, 2017). Therefore, including IED modulation in judgement criteria, as Lefaucheur and colleague (2017) did, seems to be a more precise and complete way to evaluate tDCS effects. Thus, modulating IED activity could have a real clinical impact and/or on patients' everyday life. Furthermore, because of their high daily occurrence and their stability, IEDs are relevant biomarkers of brain irritability (Baud *et al.*, 2018) which is interesting to investigate for assessing the direct and short-term effects of tDCS. To date, only scalp EEG was used to study IED before and after tDCS. Nonetheless, activities located in some brain areas such as mesial temporal sources, are invisible to visual study and automated detection, unless the right analysis technique is used (Koessler *et al.*, 2015). Thus, because of EEG methodology, a substantial part of IED activity can be neglected, which can bias observations and conclusions about tDCS effect on IED.

Thus, after having validated the possibility of TES to generate an electric field in the limbic system in the previous chapter, this one will attempt to explore TES as an application to focal refractory epilepsy. The study will be performed thanks to intracerebral investigation of two epileptic biomarkers: (1) IED activity and (2) seizure activity -- which are very different regarding their electrical and spatio-temporal properties. Thus, this chapter will be divided into two sub-studies (Study 1 and Study 2).

Study 1: tDCS effects on interictal epileptiform discharges (IED)

By placing tDCS electrodes to optimally stimulate the irritative zone, this sub-study will investigate IED activity before during and after tDCS. The hypothesis was that tDCS modifies IED number of apparition and amplitude measured on intracerebral SEEG contacts within the irritative zone.

I. Materials and method

1. Patients

Twelve patients (8 females and 4 males; age: 34 ± 12 years old) with focal drug-resistant epilepsy were prospectively included in this study.

The presurgical evaluation included neuropsychological tests and long-term (5-day period) high-resolution electroencephalographic (EEG) video recordings combined with electrical source imaging analysis, positron emission tomography (PET) and 2 high-resolution magnetic resonance imaging (MRI at 1.5 Tesla. Including one with gadolinium injection to map the vascular network) and SEEG investigation (Abdallah *et al.*, 2017; Rikir *et al.*, 2020) (for more details, refer to Chapter II, part II.1.a).

Inclusion criteria were:

- Age > 18 years old
- Presence of IED
- No SEEG post-implantation complications
- No epileptic seizure occurred hours before the experiment

2. IED and irritative zone detection

Irritative and epileptogenic zones are defined as “the site of cortical tissue that generates interictal discharges” and “the site of the beginning of the epileptic seizures and of their primary organization”, respectively (Talairach and Bancaud, 1966a; Kahane *et al.*, 2006).

Several hours of SEEG signals recorded during the week were analyzed to find the irritative zone. This analysis was performed with an unsupervised automated spike detector, removing potential human biases (Gotman, 1999). The algorithm was designed and published by Janca et al., (2018, 2014, 2013). This algorithm was chosen because it was developed with and for intracerebral recordings (SEEG and ECoG). In addition, the algorithm is available online, easy to use and, robust.

The principle of the spike detector algorithm is based on the detection of events above a specific threshold value which is adapting as a function of the background activity (see Figure 48, full method detailed in (Janca *et al.*, 2014):

First, the algorithm converted the referential SEEG signal into a bipolar signal: to measure an electrophysiological voltage, all SEEG contacts are subtracted to a referential potential (usually set in the white matter far from the epileptogenic zone) which give global information of the intracerebral electrophysiological activity. A bi-polar configuration consists of subtracting intracerebral neighboring contacts of a same SEEG electrode to remove LFP activities contribution from distant sources (for an electrode A, we have A1; A2; A3 …, the bipolar configuration will be A1 − A2; A2 − A3; …).

Then, the signal was filtered by a band-pass filter 10 Hz to 60 Hz (considered as IED frequency band), and its envelope was obtained after performing a Hilbert transform. Next, a 5 second sliding window was applied with an 80 % overlapping in which the amplitude distribution was calculated. After that, a log-normal distribution was fitted by a Maximum-Likelihood Estimation (MLE) method on the amplitude distribution. Then, threshold values were calculated by k·(Mode + Median) of the log-normal distribution (with k a factor determined empirically from a gold standard evaluation). Threshold values were calculated for each 5 second window and interpolated to make a threshold curve. Finally, IED were detected when the signal envelope was above the threshold curve.

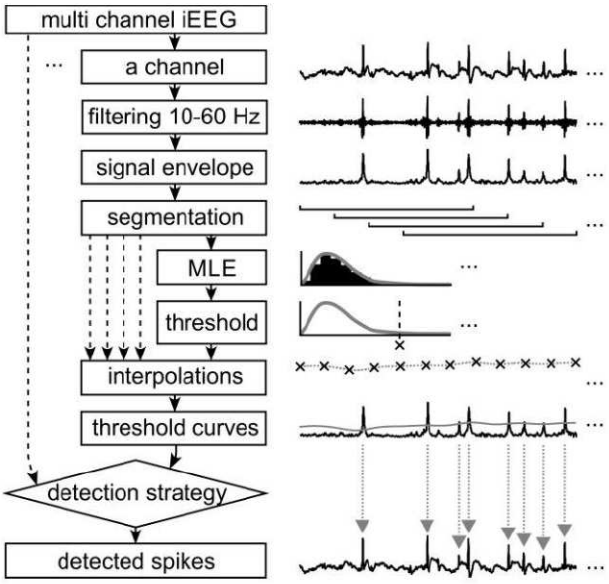

Figure 48: Schematics of detection algorithm. First, the signal was filtered by a band-pass filter 10 Hz to 60 Hz. Then the signal envelope was obtained after performing a Hilbert transform. After that, a 5 second sliding window was applied with an 80 % overlapping. In each window, the amplitude distribution was plotted (x axis amplitude, y axis number of sample). For each distribution, a log-normal distribution was fitted by MLE: Maximum-Likelihood Estimation method. Then threshold values were calculated by doing k·(Mode + Median) of the log-normal distribution (with k a factor determined empirically from a gold standard evaluation). Threshold values were calculated for each 5 second window and interpolated to make the threshold curve. Finally, spikes were detected when the envelope was above the threshold curve. From Detection of Interictal Epileptiform Discharges Using Signal Envelope Distribution Modelling: Application to Epileptic and Non-Epileptic Intracranial Recordings. *Brain Topography*, *28*(1), 172–183 by Janca, R., Jezdik, P., Cmejla, R., Tomasek, M., Worrell, G. A., Stead, M., Wagenaar, J., Jefferys, J. G. R., Krsek, P., Komarek, V., Jiruska, P., & Marusic, P. (2014). © 2014 by SPRINGER NEW YORK LLC. Reproduced with permission of SPRINGER NEW YORK LLC under license number 1201191-2 in the format of print and electronic via Copyright Clearance Center.

Multi-channel events detection

When a spike was detected on a channel, all spikes detected on other channels within 5 milliseconds were considered as a multi-channel event. Then, if the multi-channel detected spikes belonged to the same cluster they were considered as a same event and its origin was the channel where the first detection occurred.

3. Optimal TES electrode placement based on computational model

Dmochowski *et al.*, (2011) proposed an interesting mathematical approach to calculate the optimal position for a TES electrode to obtain the maximum electric field on the desired target. It uses solutions obtained from Finite Element Method (FEM).

a. Realistic vOlumetric Approach to Simulate Transcranial electric stimulation (ROAST,)(Huang *et al.*, 2019)

ROAST is a pipeline to realistically simulate the electric field propagation in the brain during TES (see Chapter I) from a head model based on the subject's MRI (Huang *et al.*, 2019):

1. The operator sets the desired TES electrode position (montage) according to the 10-10 international system (e.g., F8-T7) and their respective intensity values (the sum of all intensities on all electrodes must be equal to zero).
2. Then, based on the patient MRI, the pipeline performs an automated segmentation ("Unified Segmentation" algorithm implemented in SPM12)(Ashburner and Friston, 2005; Huang *et al.*, 2013) to discriminate 6 different compartments (skin, skull, CSF, air, gray matter, white matter).
3. From the segmented compartments, an algorithm (iso2mesh)(Fang and Boas, 2009) generates a FEM 3D mesh (volume).
4. A FEM solver (getDP)(Dular *et al.*, 1998) solves Laplace's equation:

$$\vec{\nabla}\vec{J} = \vec{\nabla}\left(\sigma\vec{\nabla}V\right) = \vec{\nabla}\left(\sigma\vec{E}\right) = 0 \qquad (46)$$

where σ is the medium electrical conductivity.

Therefore, at each node of the FEM, the electric field is calculated:

$$\mathbf{E} = \boldsymbol{\gamma}\, J$$

Where $\mathbf{E}$ and $\boldsymbol{\gamma}$ are $N \times 1$ matrices of the electric field magnitude and the effective resistivity at each node of the mesh (from 1 to N), respectively. J is the current density generated by the stimulation (scalar magnitude normal to the TES electrode).

b. Optimized electrode placement: maximum intensity method (Dmochowski *et al.*, 2011)

Linearity of Laplace's equation makes possible to sum FEM solutions from different montages and constitute the base of their approach: In the case of a system with 72 electrode positions based on the 10-10 system, the FEM solver is ran 71 times to generate 71 solutions for 71 different bipolar configurations by placing the cathode (considered as a reference) at a fixed point (Iz) and the anode at the 71 other positions on the scalp for a given intensity (+ 1 mA). Next, by summing the 71 solutions, we obtain one electric field distribution **E** which is the linear combination of all bipolar stimulation called the lead field. At a node p (the desired target), the expression $\mathbf{j} = \mathbf{E}^T \cdot \boldsymbol{\gamma}(\boldsymbol{p})$ gives the current density required at each TES electrode position to obtain an electric field along the desired direction $\mathbf{E}^T$ at the desired target p. Finally, the 2 extremes values of **j** give the best position for a bi-polar tDCS to generate the maximum intracerebral electric field (iEF) at the desired location.

4. A full MRI-based program to target the irritative zone

During this thesis I developed a program which gathers all published algorithms used to: (1) automatically target the irritative zone, (2) perform realistic EF simulations, (3) find the optimal tDCS electrode position to target the detected irritative zone. The purpose was to create a user-friendly program which prepares a tDCS-SEEG experiment by removing a numerous tasks and processes. With this algorithm the operator will only need the patient's MRI, one hour of SEEG signal, and the intracerebral contacts coordinates detected previously thanks to the MRI-CT co-registration. From these three inputs, the pipeline will deliver the three best montages to optimally target the irritative zone with maximum intensity. It considerably reduces the time needed to prepare the experiments. The different algorithms used are explained in the following lines trying to avoid mathematical formalism, when possible, but which is fully detailed in their respective referenced articles.

Full pipeline (Figure 49)

From the patient's MRI, the pipeline uses ROAST (V2.0) (Huang *et al.*, 2019) to build the lead field based on the electric field linear combination when summing solutions from several simulations (Dmochowski *et al.*, 2011). In parallel, the Spike detector (Janca *et al.*, 2013, 2014, 2018) identifies the SEEG contact (or group of contacts) where the IED occurrence is the highest. Then, the "Fetch" algorithm finds the coordinates of the SEEG contact identified by the Spike detector. Finally, the optimization algorithm `roast_target` finds the optimal bi-polar montage to generate the maximum electric field with a component along the targeted SEEG.

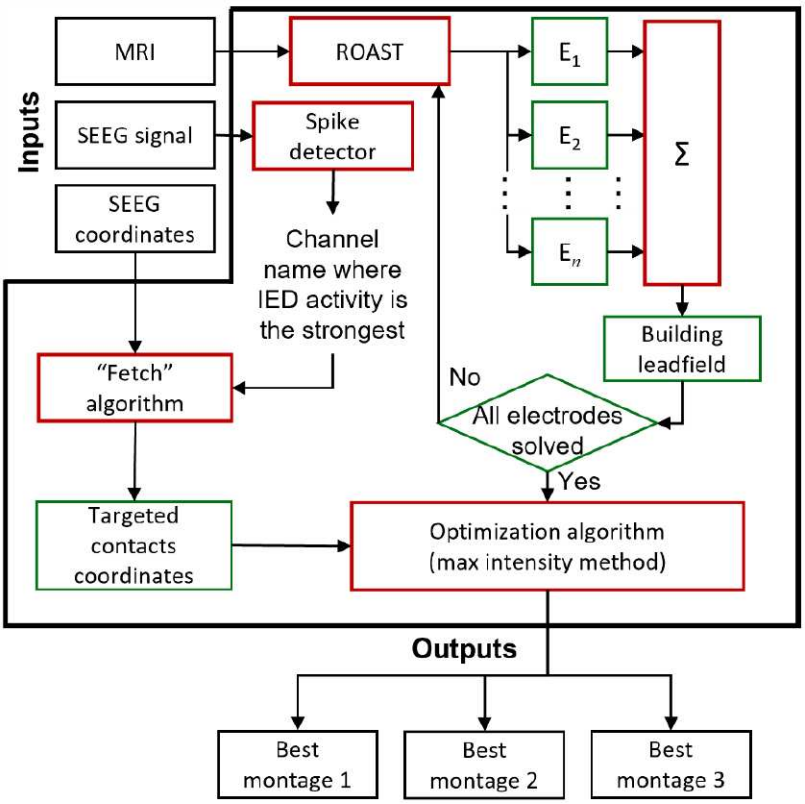

Figure 49: Full MRI-based pipeline implemented during this PhD for stimulating the irritative zone. The pipeline was coded to give 3 optimal montages from a realistic approach (3 different solutions because the first solution for electrodes placement is sometime impossible due to SEEG implantation site) by giving 3 input files: MRI (in NIFTI format), 1 hour of SEEG recording (in TRC format) and the SEEG contact coordinates from the CT-MRI co-registration (in XLS format). Red boxes are algorithms, green boxes are output matrices from algorithms, thin line black boxes are input/output files and the thick line black box is the pipeline coded. The pipeline uses ROAST (Huang *et al.*, 2019), Spike detector (Janca *et al.*, 2013, 2014, 2018), and an optimization algorithm based on max intensity method (Dmochowski *et al.*, 2011, 2013).

The irritative zone detection was then confirmed by visual expertise by trained and experienced epileptologists. In a case of multiple irritative zones detected, the choice of a unique brain target was determined after a collegial decision between the research and the medical teams. The choice of the target was also conditioned by some factors such as the laterality of the irritative zone, the intensity of the activity and the frequency of apparition of IED events. Thus, preferred zones were on the neocortex and/or delivering the strongest IED amplitudes and/or with the most frequent IED events.

5. TDCS protocol

Stimulation devices and electrodes used were the same as those described in Chapter II. Experiments took place on Fridays at 9:00 am and finished at 11:00 am. Therefore, all patients included in the cohort are tested in the same time window in order to remove bias induced by the circadian fluctuation of IEDs (Baud *et al.*, 2018).

The experiments were organized into 3 phases of 20 minutes each (Figure 50):

- **Phase 1** (in green in Figure 50), Sham phase "pre-tDCS": At the beginning, the stimulation current increases for 30 seconds until reaching the nominal intensity then

directly decreases for 30 seconds until 0 mA. Then, for 18 minutes the stimulation current stays at 0 mA. After that, the current increases again then decreases (30 seconds each ramp).

- **Phase 2** (in red in Figure 50), stimulation phase: The current increases for 30 seconds until reaching the nominal intensity, then stays for 19 minutes and starts decreasing 30 seconds before the end of the timer.
- **Phase 3** (in blue in Figure 50), Sham phase "post-tDCS": same as phase 1.

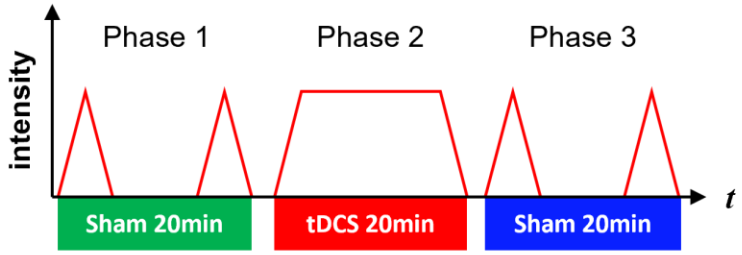

Figure 50:Protocol design for the tDCS experiment. The protocol is divided by 3 phases: 2 phases with a sham stimulation and one phase with an actual stimulation. Red lines show how the stimulator intensity varies over time.

In this study, because of the DC parameter, the 2 electrodes were named "Active" electrode and "Return" electrode (Bikson *et al.*, 2019).

The active electrode is the one placed the closest to the brain target (irritative zone) and on which the tDCS parameters were set:

- Current polarity: positive (anodal stimulation) or negative (cathodal stimulation) current
- Intensity: 1 or 2 mA
- Stimulation duration: 20 min

6. Data analysis

The amplitude of each IED on each contact within the irritative zone was measured. Mean, standard-deviation and median of IEDs' amplitude were calculated for each phase (pre-tDCS, tDCS, and post tDCS).

Qualitatively, data seemed to follow a log-normal distribution. To verify the hypothesis, a log function was applied to the data, then the distribution normality was tested with an algorithm (which uses 10 well-known normality tests) (Öner and Deveci Kocakoç, 2017). It appeared that data doesn't follow a log-normal or normal distribution. So, because the sample size was different (number of IEDs detected) between the 3 phases and because of the non-normal distribution, a Wilcoxon-Mann-Whitney test was performed when comparing IEDs amplitude measured in the three phases:

For a distribution X and a distribution Y, the null hypothesis H_0 for a probability P was $P(X > Y) = P(Y > X)$. This was done by paired comparison: Phase1 *versus* Phase2, Phase1 *versus*

Phase3 and Phase2 *versus* Phase3. First, comparisons were performed on all spike's amplitudes detected in each patient regardless of the intracerebral contact. Paired comparisons were also done on the mean amplitude value for each phase for all patients with:

$$\Delta average = \frac{1}{n}\sum_{i=1}^{n}\left|\mu_x(i) - \mu_y(i)\right|$$

Where n is the total number of patients μ_x (i) and μ_y (i) the mean IED amplitude during a Phase x and a Phase y measured in a patient i (Figure 51).

Next, to test the global effect of tDCS on IED amplitude across patients, a binomial test was performed with the null hypothesis H_0: $\pi = \pi_0$ with π the proportion of patients who had a significant amplitude modulation and π_0 the number of patients who had not. H_0 was rejected when $p < 0.05$.

For each phase, the number of IED was measured. Because the number of samples were equal between phases and data were not normally distributed, a non-parametric ANOVA test (Friedman's test) was performed with the null hypothesis H_0 that the different samples come from the same population and was rejected when $p < 0.05$. This was done to assess tDCS global effect on spike occurrence between phases. To do so, patients were sorted in 2 groups: anodal and cathodal stimulation and comparisons were done for each group.

II. Results

Overall, twelve patients were included. Table 6 gives a summary of patients' epilepsy type.

Table 6: Summary of cohort's epilepsy characteristics. R: Right, L: Left.

Patient #	Gender	Epilepsy duration (years)	Location	MRI
1	M	29	R. temporal	R. ulegyria sequelae of head trauma
2	F	22	L. frontal-temporal	Dysplasia R. frontal orbital
3	M	21	L. temporal	Normal
4	F	19	L. temporal	L. Hippocampal sclerosis
5	M	20	L. temporal	Normal
6	F	46	L. temporal	Normal
7	M	13	R frontal-orbital	Dysplasia R. frontal orbital
8	F	36	L. parietal-occipital	Corpus callosum and fornix dysplasia, L. parietal-occipital ulegyria
9	F	30	L. temporal	L. Hippocampal sclerosis
10	F	28	R frontal-orbital	R Frontal orbital dysplasia
11	F	N.C	L. occipital-parietal	Normal
12	F	11	L. frontal	Dysplasia L frontal gyrus

Considering the entire cohort, IEDs amplitudes were significantly modulated between at least two phases ($p < 0.05$ Wilcoxon-Mann-Witney test) in 7 patients (Patients #1-5, Patient #9, and Patient #11, green in Table 8, see also Figure 52). Mean absolute differences of mean IED amplitudes ($\Delta average$) between phases for significant patients are 25 ± 24 µV, 22 ± 22 µV and 26 ± 43 µV for Phase1 – Phase2, Phase1 – Phase3, and Phase2 – Phase3 respectively (red in Figure 51). For the entire cohort, the chance of tDCS to modulate IED amplitudes is not statistically significant ($p = 0.24$ proportion binomial test). Mean amplitude values, standard deviation and median for every patient are displayed in Table 7.

Table 7: Summary of tDCS parameters for the cohort.

Patient #	Montage	Target	Stimulation
1	FT10-Cz	Right hippocampus	Cathodal 1 mA
2	AF8-P3	Right temporal pole	Anodal 1 mA
3	FT9-F4	Left hippocampus	Cathodal 2 mA
4	FT9-FT10	Left hippocampus	Cathodal 1 mA
5	FT9-FT10	Left temporal pole	Cathodal 1 mA
6	F5-FC6	Left insula	Cathodal 2 mA
7	F4-F3	Right frontal gyrus	Anodal 2 mA
8	CP5-FT8	Left precuneus	Cathodal 1 mA
9	FC5-FT10	Left hippocampus	Cathodal 2 mA
10	FP2-FT9	Right frontal-orbital gyrus	Cathodal 1 mA
11	PO7-TP8	Left cuneus	Cathodal 1 mA
12	F7-O10	Middle frontal gyrus	Anodal 1 mA

Two groups were defined: cathodal group (C group) and anodal group (A group). Nine patients were included in the C group and 3 patients were included in the A group.

Considering only group C, IEDs amplitudes were significantly modulated between at least two phases ($p < 0.05$ Wilcoxon-Mann-Witney test) in 6 out of 9 patients (Patients #1, Patient #3-5, Patient #9 and Patient #11) and the chance to obtain a modulation during a cathodal tDCS is statistically significant ($p < 0.05$ proportion binomial test). Among them, IEDs amplitudes increase during tDCS with an average of 14 ± 17 % in 4 patients (+ 2 % in Patient #1, + 7 % in Patient #5, + 39 % in Patient #9 and + 8 % in Patient #11). IEDs amplitudes decrease during tDCS in 2 patients with an average of − 21 ± 4 % (− 19 % in Patient #3 and − 24 % in Patient #4). After tDCS, IEDs amplitude increased about 9 ± 3 % in 3 patients (+ 6 % in Patient #1, + 11 % in Patient #5 and + 11 % in Patient #11) but decrease about − 30 ± 1 % in 2 patients (− 31 % in Patient #4 and − 30 % in Patient #9) and no modulation after tDCS for Patient #3.

Considering only group A, IEDs amplitudes were significantly modulated between at least two phases ($p < 0.05$ Wilcoxon-Mann-Witney test) in 1 out of 3 patients (Patients #2). However, it is impossible to assess the effect of anodal tDCS because the 3 patient sample is too small. Considering this only patient, IEDs amplitude decrease during (− 2 %) and after (− 4 %) tDCS.

Considering patients with temporal structures targeted (n = 9), IEDs amplitudes were modulated in 6 of them which represent a statistically significant ($p < 0.05$ proportion binomial test) effect of tDCS when temporal structures are targeted.

Concerning the number of IEDs detected, there is no statistically significant modulation between phases, considering the entire cohort ($p > 0.05$ Friedman's test).

Table 8: Mean amplitude, standard deviation and median of detected IED in each patient. Patients who had a significant amplitude modulation between at least 2 phases are highlighted in green.

Patient #	Mean amplitude values (µV)			Median value of amplitude distribution (µV)		
	Before tDCS	During tDCS	After tDCS	Before tDCS	During tDCS	After tDCS
1	78.35 (± 20.99)	80.19(±23.88)	83.09(±24.07)	72.95	74.06	78.70
2	262.57(±150.32)	257.78(±149.68)	252.26(±139.97)	220.28	216.08	214.02
3	177.47(±62.12)	144.62(±44.09)	177.77(±67.50)	165.99	133.60	161.21
4	168.00(±64.76)	126.89(±49.16)	116.41(±34.46)	154.47	114.97	110.24
5	187.20(±49.67)	200.11(±43.16)	207.78(±55.62)	180.01	195.78	196.54
6	114.20(±47.40)	114.94(±51.34)	113.12(±47.80)	104.32	102.40	103.41
7	174.57(±110.22)	179.47(±114.21)	178.67(±116.12)	145.23	151.52	147.25
8	156.49(±72.52)	152.22(±67.74)	153.98(±70.69)	141.83	142.00	140.26
9	174.51(±176.71)	242.91(±414.20)	122.27(±101.76)	107.56	105.23	87.74
10	205.80(±68.72)	205.81(±66.78)	208.65(±69.12)	193.48	194.73	196.86
11	119.13(±48.79)	128.80(±59.62)	132.10(±66.87)	108.46	110.71	112.11
12	194.03(±58.26)	197.00(±57.83)	198.11(±67.65)	179.55	184.18	176.00

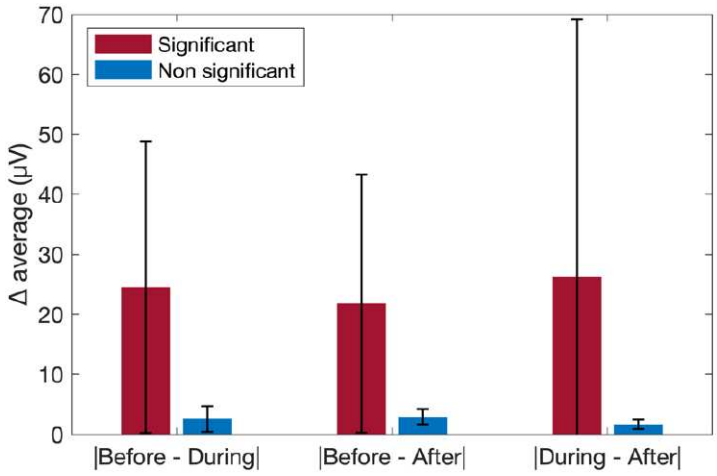

Figure 51: Average of the absolute difference of the mean amplitude between phases for the significant (red) and the non-significant (blue) population. Each phase comparison is represented: Before − During; Before − After; During − After tDCS.

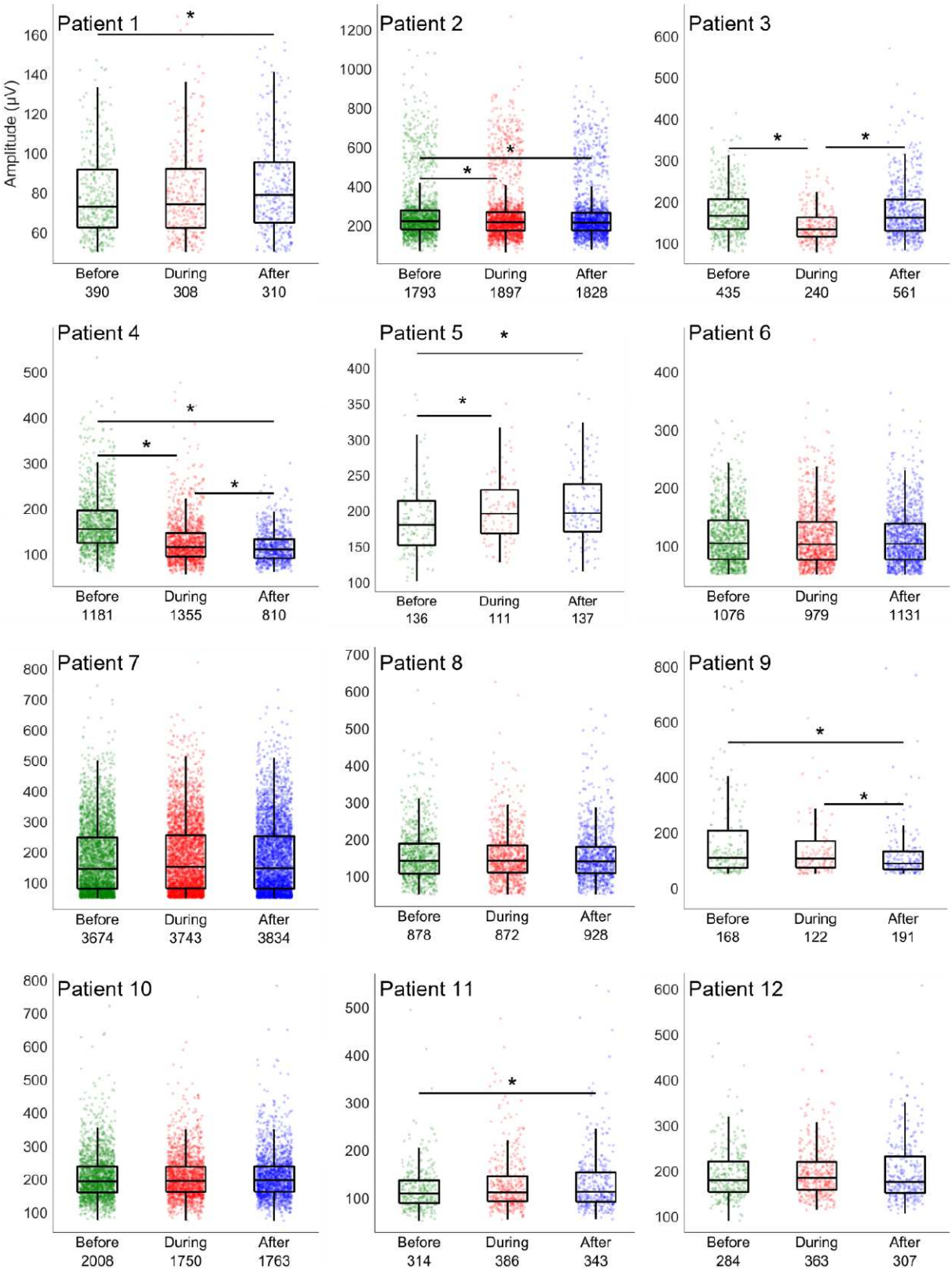

Figure 52: Total IED amplitude distribution during each phase for each patient. Black boxplot represents the distribution's median and inter-quartiles ranges, colored dots are individual IED amplitudes (green: before tDCS, red: during tDCS, blue: after tDCS). Numbers on the *x*-axis are the total number of detected IED for the corresponding phase (e.g. for patient 1, 390 IED were detected before tDCS, 308 during tDCS and 310 after tDCS). Significance bar shows when the distribution is statistically different between 2 phases ($p < 0.05$ Wilcoxon-Mann-Witney test).

III. Conclusions for the first study

The main objective of the first study was to explore the potential application of tDCS in refractory epilepsy through intracerebral investigation of IED including unsupervised detection algorithms.

Designing a TES experiment and analyzing results can be time consuming. Indeed, the steps are (1) studying hours of SEEG traces to define the irritative zone (2) defining the target through co-registration CT-scan/MRI (3) Defining the TES montage and (4) manually detecting all IED occurred during the experiment. In that process there is a high probability to obtain human biased results because of the numerous operator-dependent steps and processes. Therefore, the program developed during this thesis could bring an interesting, automated solution for future large scale clinical studies (in TES applied to epilepsy involving SEEG investigation) to plan robust TES experiments in a reduced amount of time: high precision TES electrode placement thanks to realistic modeling and robust automated IED detection. Moreover, the pipeline offers the option to automatically perform the modelling on a large cohort by allowing the selection of the several individual MRIs. However, robustness can be improved by firstly, implementing the SEEG implantation in the modelling process and, therefore, constraining the model to give more accurate TES montages by defining unavailable scalp zones. Secondly, recent results have been proven that deep learning is a useful tool to detect with a very high precision IEDs (up to 98 % accuracy) (Quon *et al.*, 2022) and can be implemented in the developed pipeline.

Concerning the results on interictal epileptiform discharges in the entire cohort for all structures targeted, there is no evidence that tDCS had an impact on IED amplitude or occurrence regardless of the stimulation polarity.

Considering the cohort's subgroups, it is impossible to conclude on the effect of anodal tDCS because of the sample being too small. However, there is a significant modulation of the IED amplitude during cathodal tDCS. When temporal structures are targeted, there is also a significant modulation of IED amplitude during tDCS no matter the polarity.

Curiously, during tDCS at a given polarity (cathodal) IED amplitude modulation can increase in one patient and decrease in another. This observation is counterintuitive in light of the literature (Faria *et al.*, 2012; San-Juan *et al.*, 2015, 2017; Meiron *et al.*, 2019; Kaufmann *et al.*, 2021). However, it is important to note in these studies that tDCS effects on IED have only been studied in scalp EEG in which only a certain type of IED can be observed (Koessler *et al.*, 2015). Also, the high electric field generated between the scalp and the cortical surface during a tDCS might stop the IED propagation only at the surface where EEG activity is collected. Thus, results presented in the literature may report only an effect on IED propagation to the scalp but not a direct action on pathological sources. In this chapter, IED activity is measured directly at the source and its

surrounding areas thanks to SEEG investigation. Therefore, results observed in this chapter reveal that more complex mechanisms involving IED modulation may exist.

One hypothesis is that the modulation is the result of a chain reaction initiated in the cortical surface where the electric field is the strongest. This would induce either a hyperpolarization or a depolarization in the subcortical area depending on a lot of parameters such as the number of synaptic connections encountered, the induced electric field directionality (Rahman *et al.*, 2013, 2017; Lafon *et al.*, 2017; Farahani *et al.*, 2021), or the number of neurons modulated (Denoyer *et al.*, 2020) *etc*. This means that the outcome from anodal/cathodal tDCS measured in the depth is not as predictable and straightforward as we thought. Cortex folding can play a role in the variability neurons are not exposed the same way to the electric field so inhibitory and excitatory effects can be induced under the same stimulation (Rahman *et al.*, 2013). This non-linearity will be discussed in more details in Chapter V.

The results presented suffer from several weaknesses:

The first concern is the intra-patient IED variation over time. It is difficult to say whether the IED modulation measured within the hour of the experiment is related to the intra-individual variability. Even though the relative stability of IED amplitude has been proven (Baud et al., 2018), there is a need of quantifying the intra-individual variability for each patient who will be included in the future.

The inclusion criteria were deliberately chosen to be the least restrictive possible in order to include numerous patients in a limited time for this exploratory study. This constitutes the second weakness of this chapter: the lack of homogeneity in the inclusion regarding the epilepsy etiology. This was because the study was prospective, and patients were included progressively no matter their epileptogenic zone location. The propensity of IED to be modulated by TES could be related to the location of the irritative zone, its characteristics (dysplasia, lesion) or the epilepsy duration. Therefore, the second suggestion to improve the robustness is to eliminate the inhomogeneity by defining more restrictive inclusion criteria and/or perform subgroups studies in a large cohort which will allow to tackle the question of TES influence according to different epilepsy type and location.

The third weakness is the low number of patients included in the study which weakened the statistical results. Obviously, the resulting suggestion is the inclusion of more patients which can be possible through a multi-centric study or a longer investigation in a mono-centric study.

The fourth weakness is the absence of information about the TES-induced electric field generated on site which could be relevant to quantify the modulation as a function of the electric field strength. Based on results discussed in Chapter II, it is assumed here that with a minimum stimulation intensity of 1 mA, the electric field in the targeted structures are superior to $0.2 V \cdot m^{-1}$ which is strong enough to induce stochastic effects (Liu *et al.*, 2018; Louviot *et al.*, 2022). It would still be relevant to

measure the electric field after each tDCS experiment which is the last suggestion for a robust intracerebral investigation of tDCS-induced modulation of IED.

Study 2: TES effects on an epileptic seizure (single case)

I. Patient and method

1. Patient

The patient was a 19-year-old female who was suffering from left refractory insular-opercular epilepsy which began at 11 years old. She gave her informed consent to take part in the study (NCT03644732). In 2017, five reproducible epileptic seizures were recorded in the epilepsy unit during a long-term video and scalp EEG recording. All of them started with a facial redness, a right motor facial deficit, an anterior flexion of the head and a tonic extension of right upper and lower limbs. On scalp EEG signals, seizures started with a theta rhythm discharge in the left frontal-central regions (F3, C3, FZ and CZ) and shift into ictal discharges several seconds after. The patient had no visible lesion in MRI but PET-scan displayed a hypometabolism on the left temporal pole and the temporal lobe. Several hypotheses of the epileptogenic zone's localization were defined according to the presurgical evaluation: left premotor area, left prefrontal cortex, left frontal pole, left insular cortex or the left anterior temporal lobe.

The patient was stereotactically implanted (for more details, please refer to Chapter II, part II.1.a) with seventeen multi-contact electrodes targeting the left frontal lobe, the left insular cortex and the left anterior temporal lobe (Figure 53 A). Electrodes A', B', C' and P', targeted the temporal pole, the mesial and neocortical temporal lobe. Electrodes H', I', L', O', R', S' and T' targeted the insular cortex and the operculum. Electrodes G', J', K', M', W' and X' targeted the mesial and neocortical frontal lobe. Overall, the patient had 215 intracerebral contacts which represents more than 12 contacts by electrodes (Figure 53 A). Recording reference was set on an intracerebral contact in the white matter (W'8). Long-term SEEG recording, combined with HD-video, was realized 20 hours a day for 5 consecutive days supervised by EEG technicians. Drug treatment remained stable during the SEEG evaluation (Zebinix/Eslicarbazépine: 1.6 g/day and Keppra/Lévétiracétam: 2 g/day). When epileptic seizures occurred, symptoms were verbally described by the EEG technician while keeping patient safety. During seizures, the patient was also asked to do some motor tasks to evaluate the clinical symptoms (smiling, grimacing, sticking the tongue out, raising arms and/or legs *etc.*).

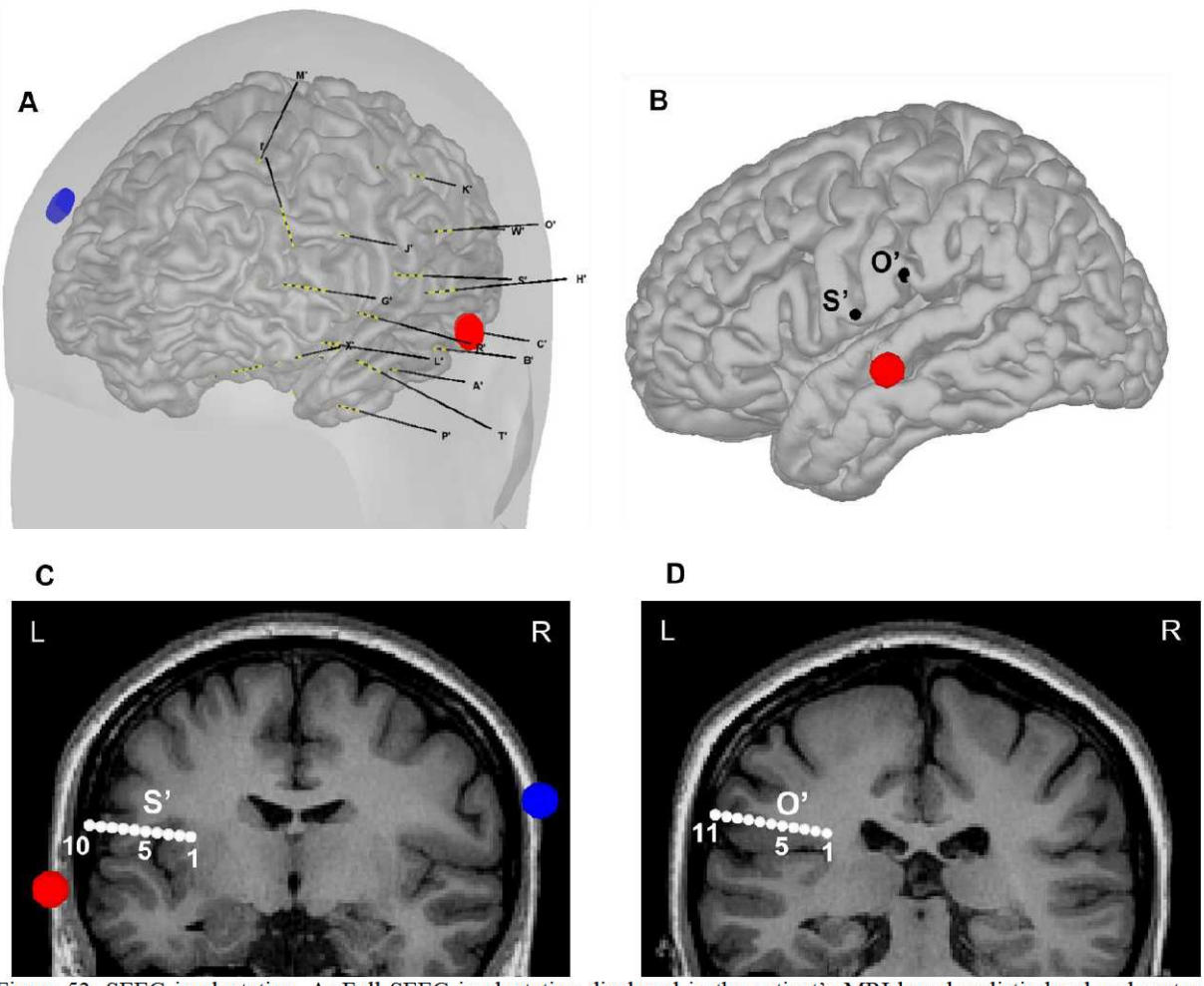

Figure 53: SEEG implantation. A: Full SEEG implantation displayed in the patient's MRI-based realistic head and cortex model. SEEG electrodes are displayed in black, each electrode's intracerebral contacts are displayed in yellow. Real position and size of tDCS electrodes are shown in red (anode) and blue (cathode). B: position of the SEEG electrodes of interest S' and O' on the cortex in relation to the anode (in red). C: coronal anatomical view (MRI) of the intracerebral contacts of S' in relation to tDCS electrodes (red anode, blue cathode) visible in the same slice. D: coronal anatomical view (MRI) of the intracerebral contacts of O'.

2. Stimulation protocol

The same method described in the first study was used to place optimally tDCS electrodes to target the irritative zone detected on the left superior operculum of the insula. Therefore, tDCS electrodes were placed on T7-C6 (anode on T7). A tDCS stimulation at + 1 mA for 20 minutes was preset with the same stimulation device described in Chapter II. After 8 minutes of stimulation, the patient expressed the feeling that a seizure was starting, and the stimulation was aborted right away. The seizure indeed occurred and stopped after 12 seconds.

Patient's SEEG recording of five days before the experiment were taken as a control. The pool of data contained four seizures and IED activities selected by experimented and trained epileptologists and will be compared to the seizure during tDCS.

3. Ictal semiology

Semiological data were retrospectively reviewed by two epileptologists using HD video recordings. All symptoms were analyzed second by second and described sequentially during the entire seizure duration.

4. IEDs and seizure manual detection

The five days of video-SEEG recordings were visually analyzed by two epileptologists blinded to the tDCS experiment. IEDs and seizures were characterized according to their spatial distributions and electrical patterns. Thus, their anatomical localizations were done through SEEG electrophysiological data and individual co-registration of the post-operative CT scan with the preoperative MRI.

The two epileptologists manually selected epochs of signals containing IEDs when the patient was awake and in a resting state. IEDs were divided into 2 groups: The ones that occurred before the stimulation (named hereafter IED) and the ones that occurred during stimulation (named hereafter IED*). Seizure onset time, the end and their durations (defined from the earliest (t0) and latest ictal SEEG patterns) were identified and marked also by trained and experimented epileptologists. Seizures during tDCS is named hereafter S* and seizures occurred during the days prior to the experiment: S.

Two main hypotheses arose:

- The spectral distribution of the seizure during tDCS is statistically different from any interictal activity (without or during tDCS).
- The spectral distribution of the seizure during tDCS is statistically different from the other seizures occurred days before the experiment.

Concerning IEDs, a secondary hypothesis was that the spectral distribution of IEDs during tDCS is statistically different from IEDs without tDCS.

5. IEDs and seizure amplitude spectrum analysis

One way to study the different electrophysiological events is by comparing their amplitude spectrum. The first step was to apply a notch filter at 50 Hz on the signal to remove the hum noise (50 Hz in France), then, an FFT was performed on all data. Next, values in each neuro-electrophysiological frequency band (δ: 1-4 Hz; θ: 4-7 Hz; α: 8-13 Hz; β: 13-30 Hz; γ_1: 30-60 Hz; γ_2 : 60-90 Hz) were compared between the different epileptic events. For visualization purpose only, a moving mean (with a moving window of 256 samples) of the amplitude spectrum was plotted on logarithmic axes (Figure 60 to Figure 65).

a. IEDs *versus* S*

Spectral distribution in each frequency band for all IEDs without tDCS, IEDs during tDCS (called hereafter IEDs*) and S* were compared with Friedman's statistical test, with post-hoc pairwise Bonferonni correction. With H_0 the null hypothesis that values distribution in each frequency band come from the same distribution regardless the electrophysiological event and was rejected when $p < 0.05$.

b. S versus S*

Because seizures are a dynamic process and presented different phases (electrophysiological patterns changing over time), it was necessary to divide them into equal time segments. Comparisons were done segment by segment between all S and S* thanks to a Friedman's statistical test (with post-hoc pairwise Bonferonni correction) with H_0 the null hypothesis that values distribution in each frequency band and for each time segments come from the same distribution regardless of the seizure. H_0 was rejected when $p < 0.05$. Then the global percentage difference at the frequency band F was calculated as follows:

$$\%G\Delta(\mathrm{F}) = \frac{1}{M+N}\sum_{m=1}^{M}\sum_{n=1}^{N}\frac{[\mu S_m^*(\mathrm{F}) - \mu S_{n,m}(\mathrm{F})]100}{\mu S_{n,m}}$$

Where N is the total number of seizures occurring days prior to the tDCS experiment. With M the total number of contacts where the amplitude distribution (within the frequency band F) is significantly different for each comparison n between S* and S_n the n^{th} seizure. $\mu S_m^*(\mathrm{F})$ is the mean of amplitude distribution on the amplitude spectrum of the seizure S* at a frequency band F on the m^{th} significant contact. Finally, $\mu S_{n,m}(\mathrm{F})$ the mean of the amplitude distribution on the amplitude spectrum of S_n (the n^{th} seizure) at a frequency band F on the m^{th} significant contact.

6. Epileptogenicity index

To deepen seizure investigation, an "epileptogenicity index" (EI) (Bartolomei, Chauvel and Wendling, 2008) was calculated on SEEG signals during seizures (Anywave software; Colombet et al., 2015). Briefly, the EI is a normalized quantity computed (ranging from 0 to 1) to objectively quantify and define the neuronal network involved in seizures generation.

EI lies on:

- The detection of the time when abrupt changes in fast frequency/slow frequencies ratio occurs at the seizure onset (from slower background activity to faster frequencies)

The identification of brain structures which generate low amplitude fast discharge (β:13-30 Hz; γ: 30-90 Hz).

High EI values (EI > 0.3) are characteristic of structure onset zones where fast ictal discharges were detected (generally the very first seconds (Bartolomei, Chauvel and Wendling, 2008)). The graphic user interface allows to inspect/validate detected points of abrupt changes (from low to fast frequency), and tune detection parameters in case of false detections. A unique value for the 2 detection parameters was found to perform systematically a good detection of seizures onset (validated by 2 epileptologists) for occurred prior to the tDCS experiment. Then, the algorithm was run on the SEEG trace of the seizure during tDCS with the same parameters.

II. Results

1. Epileptic seizures

During the five days of SEEG investigation, IED (rhythmic spikes and polyspikes) were recorded on S'1-2 to 8-9 and O'5-6 to O'9-10 contacts (for location see Figure 53 B,C and D). These discharges, according to their apparition frequency and electrical patterns, were most likely due to a focal cortical dysplasia.

The irritative zone was localized in the posterior long insular gyrus and the basal part of the parietal operculum. Fifteen datasets of IEDs were randomly manually selected during the week with a duration of 12 seconds. Four datasets of IEDs* were selected during tDCS at their onset time of 56 s, 2min02 s, 5min50 s and 6min35 s after the start of tDCS.

During the five days of SEEG investigation, five epileptic seizures with a duration of 37, 40, 36, 32, and 12 seconds respectively were recorded on the SEEG contacts S'1-2 to 8-9 and O'5-6 to O'9-10 (the other SEEG contacts were considered as non-pathological and, therefore located in healthy and functional areas (e.g., K' electrodes in the motor cortex with a typical beta-gamma activity; (Frauscher *et al.*, 2018)).

The fifth seizure occurred 8 minutes and 03 seconds after the DC stimulation started. Epileptogenic and irritative zones were in the same brain area (i.e., the insula and the parietal operculum) which is a frequent characteristic in focal drug-resistant epilepsy with a focal cortical dysplasia (Chassoux *et al.*, 2012).

All seizures were subdivided into 4 equal segments of 12 seconds each (segment A: 0 to 12 seconds, segment B: 12 to 24 seconds, segment C: 24 to 36 seconds and segment D: 36 to 48 seconds).

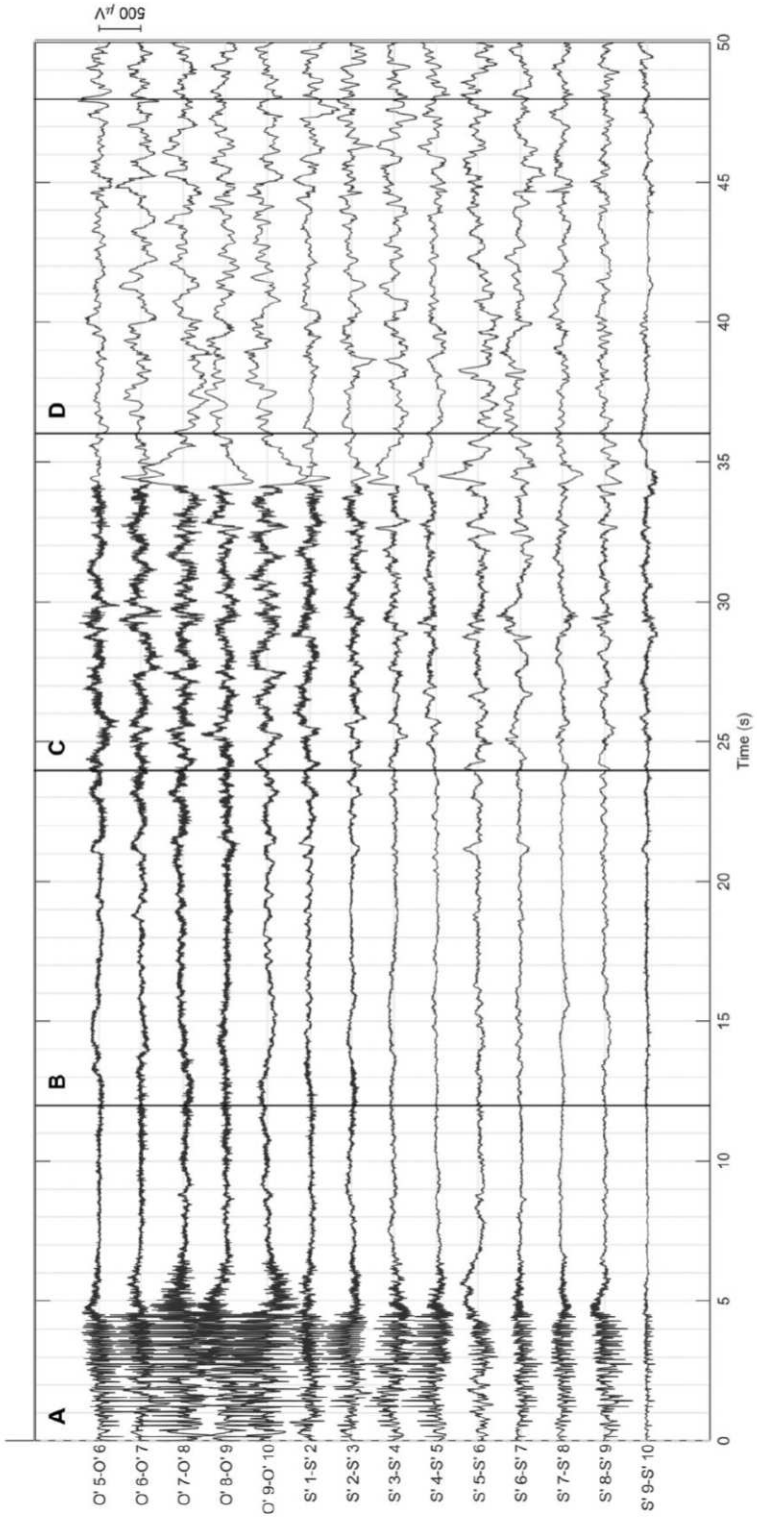

Figure 54: First seizure recorded on intracerebral contacts within the epileptogenic zone. Black vertical lines defined each 12 seconds time segment. A letter was attributed to each segment from A to D.

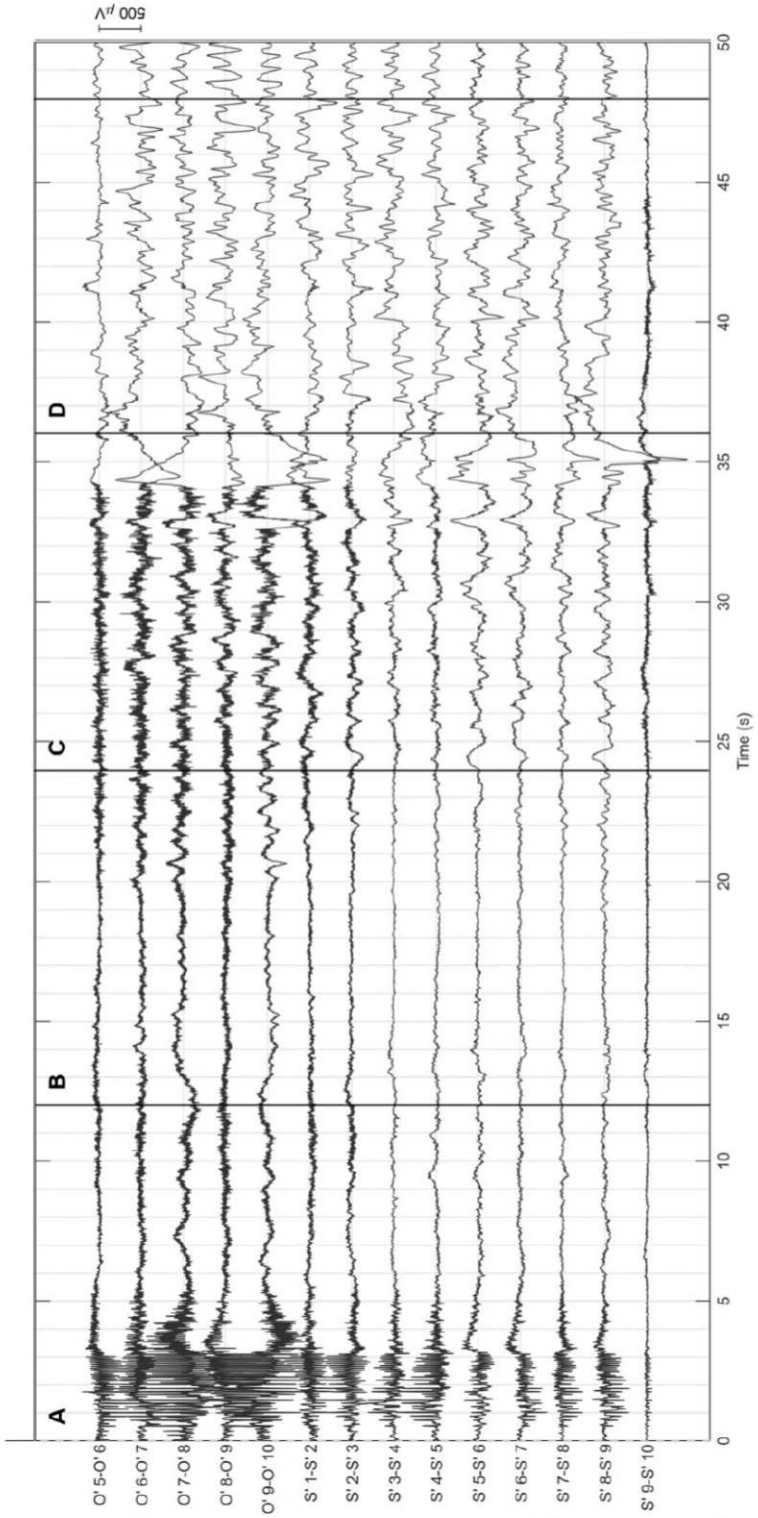

Figure 55: Second seizure recorded on intracerebral contacts within the epileptogenic zone. Black vertical lines defined each 12 seconds time segment. A letter was attributed to each segment from A to D.

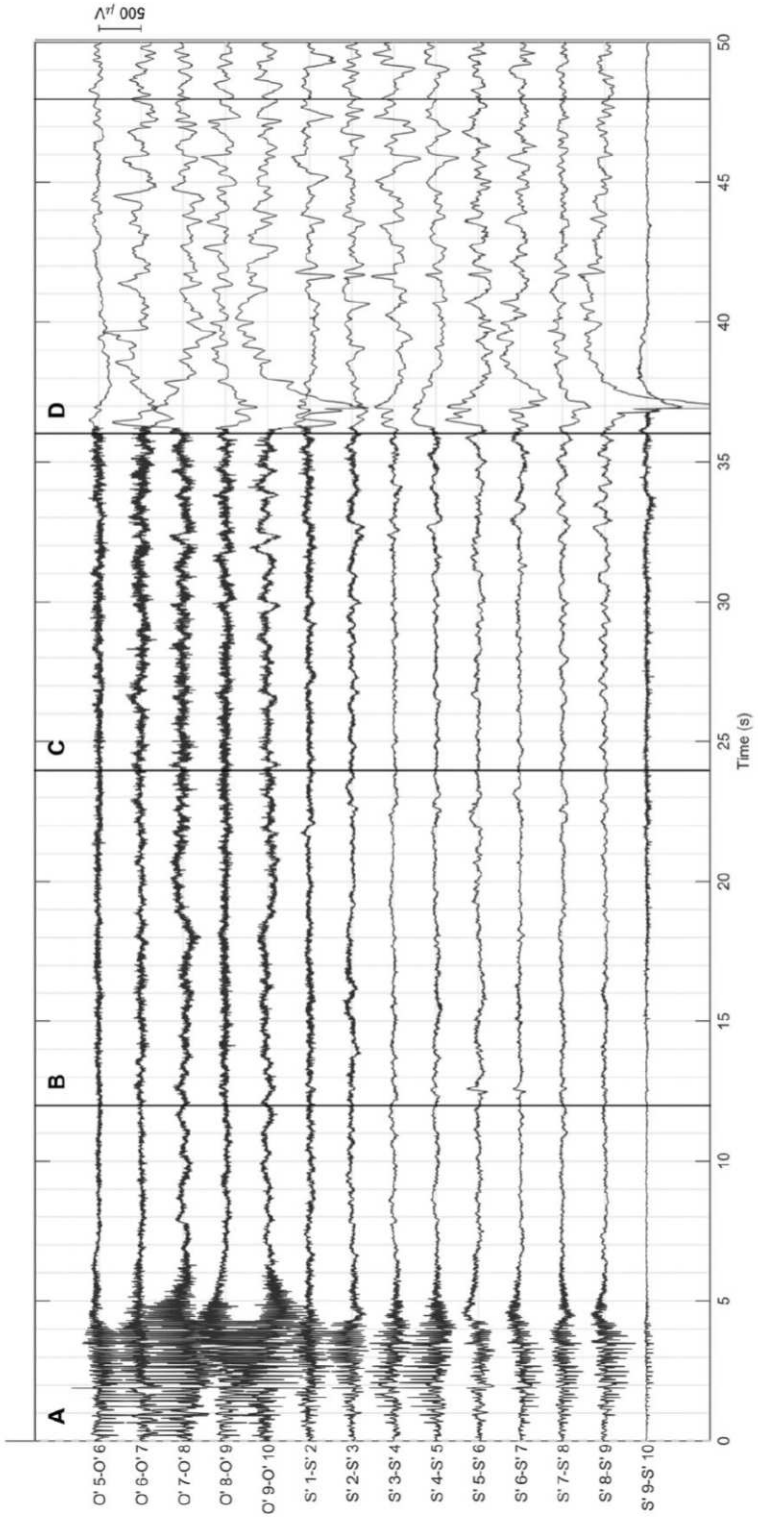

Figure 56: Third seizure recorded on intracerebral contacts within the epileptogenic zone. Black vertical lines defined each 12 seconds time segment. A letter was attributed to each segment from A to D.

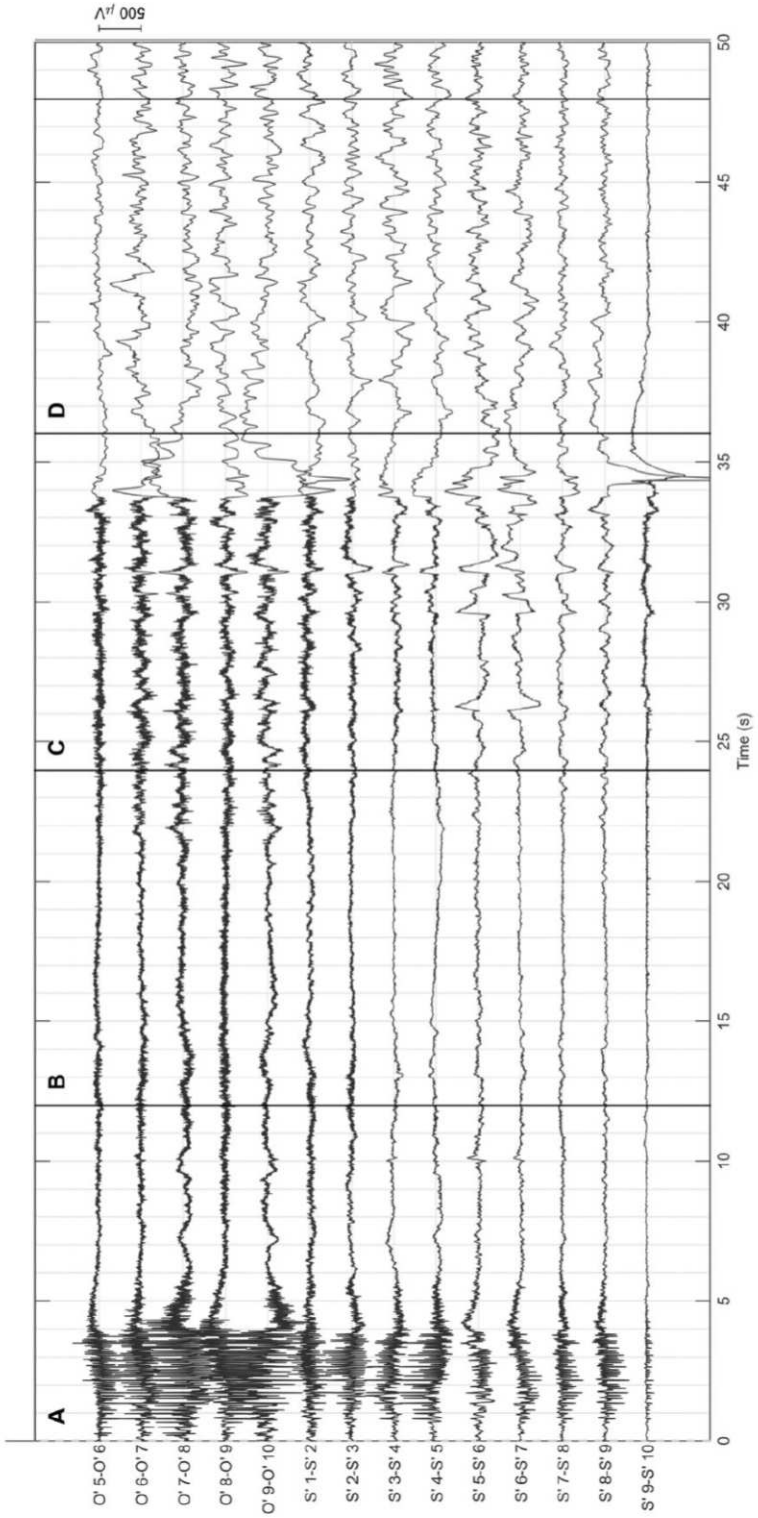

Figure 57: Fourth seizure recorded on intracerebral contacts within the epileptogenic zone. Black vertical lines defined each 12 seconds time segment. A letter was attributed to each segment from A to D.

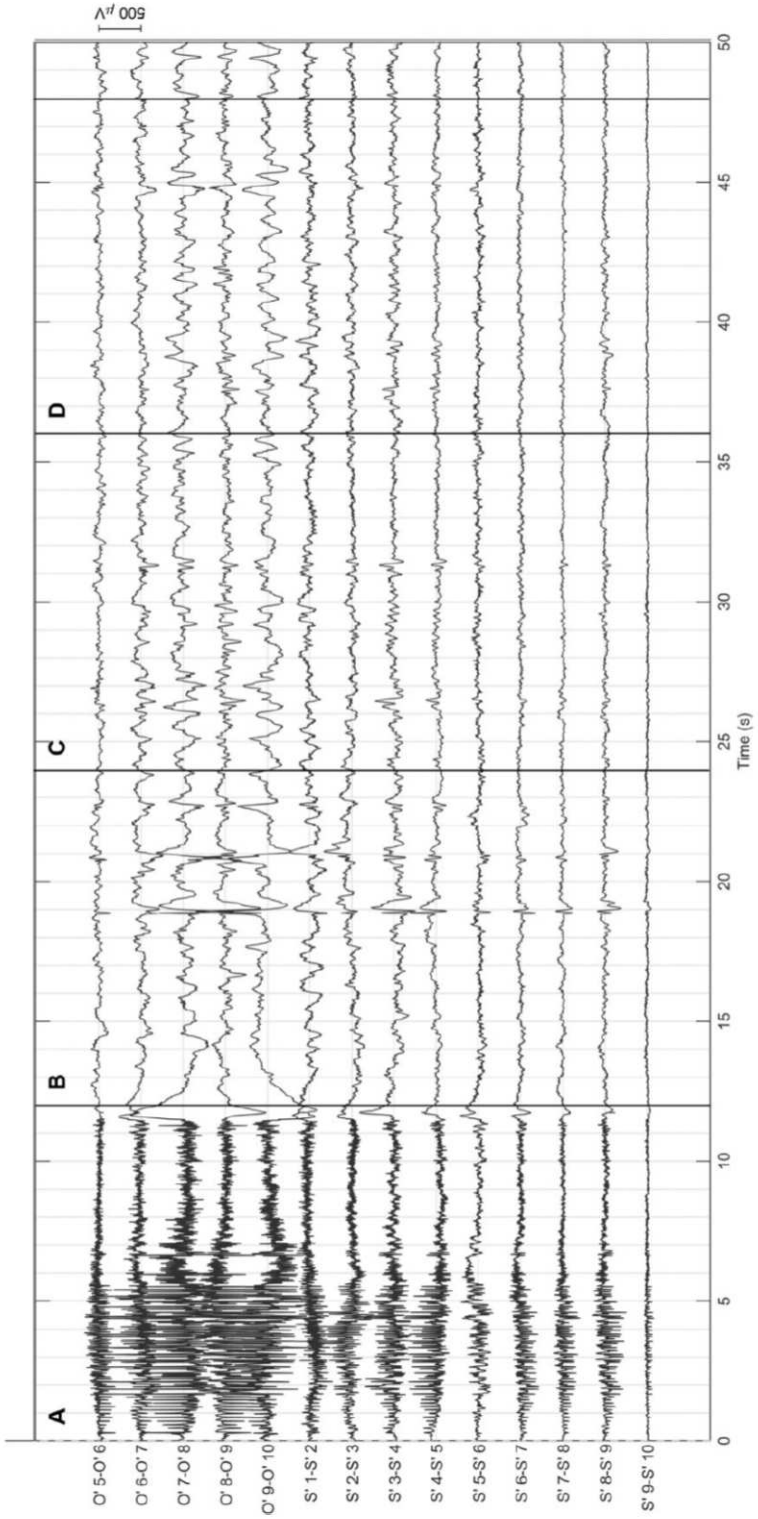

Figure 58: Fifth seizure recorded on intracerebral contacts within the epileptogenic zone. Black vertical lines defined each 12 seconds time segment. A letter was attributed to each segment from A to D.

2. Ictal semiology

The first clinical symptom started with a facial reddening followed (1 second after) (yellow box in Figure 59) by the verbal warning from the patient. Then, the patient had a right upper limb tonic extension (blue box in Figure 59). This extension was followed by a body rotation, a head flexion, a left lower and upper limb tonic extension (red box in Figure 59). Finally, the patient smiled and finally told that the seizure stopped (green box in Figure 59). This semiology was reproducible for the four first seizures (S#1-4 Figure 59).

For the last seizure recorded during tDCS (S#5 Figure 59), the beginning (i.e., the face reddening, the verbal warning and the upper limb extension; yellow and blue boxes) and the end (i.e., the smile; green box) were similar. However, the motor symptoms (i.e. the left limb extension, the head and body rotations, red in Figure 59) completely disappeared.

Figure 59: Semiology of the four partial epileptic seizures (S#1-S#4) and the one recorded during the tDCS (S#5 or S*) using successive views as a function of time. In yellow, the first symptom was a facial reddening. Then, the patient verbally warned about seizure imminence followed by a right upper limb tonic extension (in blue). Other motor symptoms appeared after (in red, left limb extension, the head and body rotation). Finally, in green, patient smiled at the end of the seizure.

3. IEDs and seizures amplitude spectrum analysis

Fifteen datasets containing IEDs and 4 datasets containing IEDs* (IED during tDCS) were collected. On the amplitude spectrum for each dataset (IED, IED* and S*), δ-band (1-4 Hz) and θ-band (4-7 Hz) had 36 samples, α -band (8-13 Hz) 60 samples, β-band (13-30 Hz) 204 samples, γ_1-band (30-60 Hz) and γ_2-band (60-90 Hz) 360 samples each.

a. IEDs *versus* S*

To address the first hypothesis that the seizure during tDCS is not an IED activity, the amplitude spectrums of IEDs and S* were compared.

On electrode O', amplitudes during seizure S* were significantly lower than the IEDs on 2 contacts (O'5-6; O'7-8) with a mean difference of − 46 ± 5 % in δ band only. Amplitudes starts to be significantly higher than the IEDs in θ band (contact O'8-9 ; + 41 %) then, in higher frequency bands on all selected contacts (O'5-6 to O'9-10) with a mean difference of + 127 ± 70 %, + 269 ± 140 %, + 292 ± 105 %, + 324 ± 58 % in α , β, γ_1, γ_2 bands respectively (Table 9 and Figure 60).

On the electrode S', amplitudes during seizure S* are significantly lower than the IEDs on 6 contacts (S'1-2, S'2-3, S'4-5, S'6-7 to S'8-9) in δ band only with a mean difference of − 50 ± 11 %. Amplitudes starts to be significantly higher than the IEDs in θ band on 3 contacts (S'3-4, S'5-6, S'7-8) with a mean difference of + 45 ± 10 %. Then on higher frequency band, all selected contacts (S'1-2 to S'8-9) exhibit a significantly higher amplitude than IEDs with a mean difference of + 124 ± 50 %, + 246 ± 113 %, + 166 ± 42 %, + 132 ± 123 % in α , β, γ_1, γ_2 bands respectively (Table 9 and Figure 60).

Table 9: Difference (in %) of mean amplitudes in all frequency bands between the seizure S* occurred during tDCS and the IED detected days prior the tDCS experiment. Intracerebral contacts selected were in the epileptogenic and irritative zone and so, involved in IED activity and all seizures occurred days before tDCS. Green cells represent a statistically significant difference in the amplitude distribution on the amplitude spectrum ($p < 0.05$, Friedman test)

Contacts	δ-band (%)	θ-band (%)	α -band (%)	β-band (%)	γ_1-band (%)	γ_2-band (%)
O'5-6	−49.91	−13.67	83.00	140.60	170.71	265.89
O'6-7	−10.41	18.58	45.58	119.07	196.20	261.69
O'7-8	−42.19	3.19	166.69	304.62	312.40	344.98
O'8-9	−11.12	40.85	223.06	457.56	378.99	356.35
O'9-10	−38.27	15.31	115.36	324.36	403.97	392.95
S'1-2	−64.46	−16.87	42.14	139.72	173.08	381.18
S'2-3	−47.47	0.28	151.04	203.14	191.69	258.21
S'3-4	11.22	53.94	172.96	473.88	214.92	100.53
S'4-5	−52.45	21.56	163.42	302.98	227.90	102.57
S'5-6	−14.35	46.67	93.87	108.19	119.35	71.19
S'6-7	−32.10	6.01	97.97	226.66	121.84	48.04
S'7-8	−52.79	34.89	183.07	236.17	150.60	43.71
S'8-9	−53.30	9.18	90.64	275.88	129.46	46.68

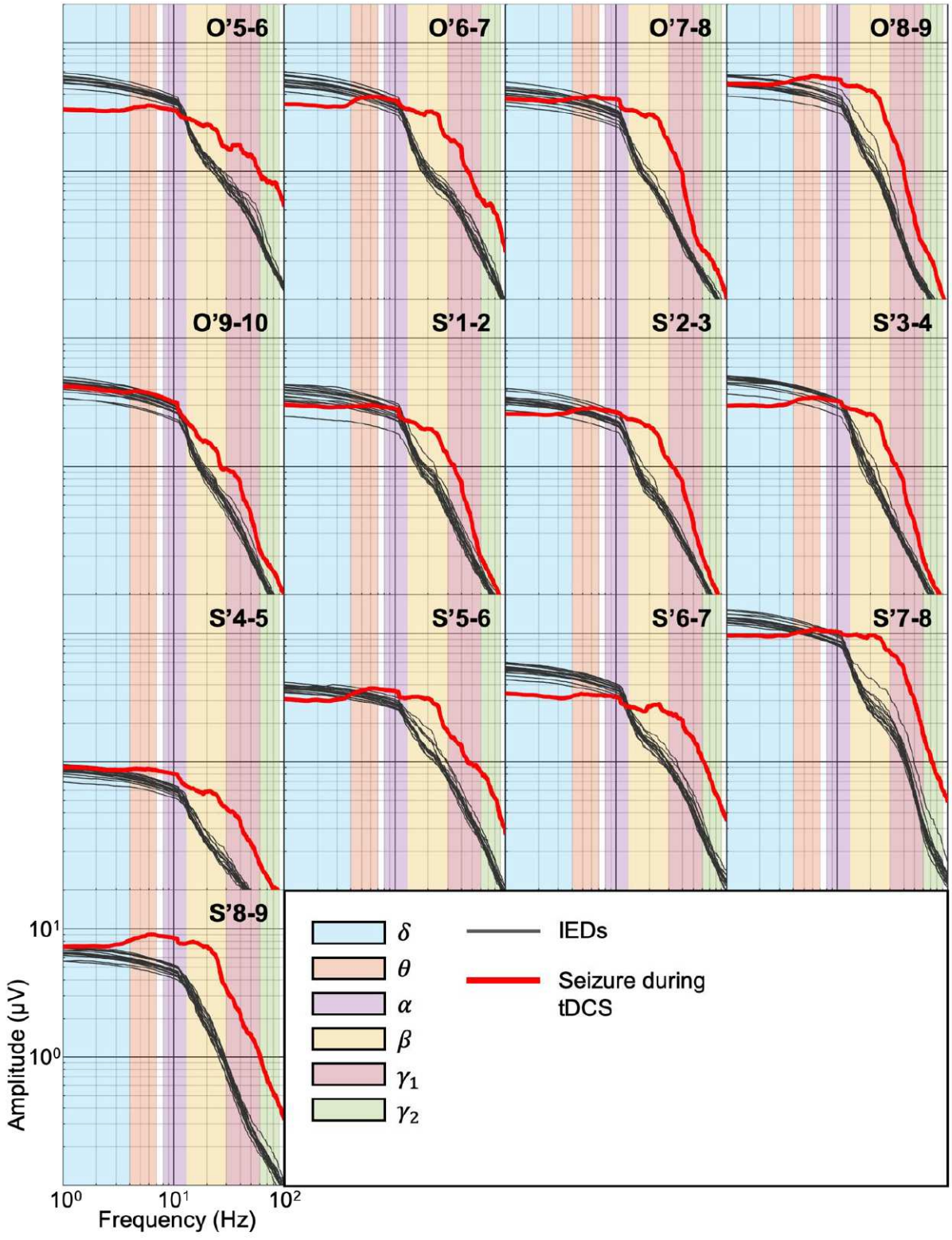

Figure 60: Amplitude spectrum of the seizure occurring during tDCS (red lines) and IEDs detected days prior the experiment (gray lines) on all contacts of interest. The different frequency bands are colored (cyan: δ band; orange: θ band; purple: α band; yellow: β band; red: γ_1 band; green: γ_2 band).

b. IEDs* *versus* S*

Still to address the first hypothesis, the amplitude spectrums of IEDs and S* were compared.

On electrode O', amplitudes during seizure S* were significantly lower than the IEDs* on 3 contacts (O'5-6; O'7-8; O'8-9) with a mean difference of − 39 ± 7 % in δ band only. There is no significant difference between IED* and S* in the θ band. On higher frequency bands, all selected contacts (O'5-6 to O'9-10) show significant higher amplitudes than IEDs* with a mean difference of + 70 ± 26 %, + 155 ± 41 %, + 177 ± 22 %, + 220 ± 24 % in α, β, γ_1, γ_2 bands respectively (Table 10 and Figure 61).

On the electrode S', amplitudes during seizure S* are significantly lower than the IEDs* on 3 contacts (S'1-2, S'2-3, S'4-5) in δ band only with a mean difference of − 45 ± 16 %. In θ band, amplitudes are significantly higher during S* than IEDs* only on contact S'5-6 (64 %). Then, on higher frequency bands, all selected contacts (S'1-2 to S'8-9) exhibit a significantly higher amplitude during S* than IEDs* with a mean difference of + 85 ± 31 %, + 167 ± 52 %, + 140 ± 49 %, + 101 ± 77 % in α, β, γ_1, γ_2 bands respectively (Table 10 and Figure 61).

Table 10: Difference in % of mean amplitude in all frequency bands between the seizure S* occurred during tDCS and IEDs detected during the tDCS experiment (IED*). Intracerebral contacts selected are contacts involved in IED activity and all seizures occurred days before tDCS. Green cells represent a statistically significant difference in the amplitude distribution on the amplitude spectrum ($p < 0.05$ Friedman test)

Contacts	δ-band (%)	θ-band (%)	α-band (%)	β-band (%)	γ_1-band (%)	γ_2-band (%)
O'5-6	−46.55	−19.68	40.99	89.59	166.89	220.11
O'6-7	−11.45	25.78	46.16	140.42	162.90	212.02
O'7-8	−36.86	−8.49	83.21	175.61	183.24	230.83
O'8-9	−32.41	−4.65	102.50	193.38	158.89	186.01
O'9-10	−32.57	14.01	79.15	174.33	212.16	252.62
S'1-2	−63.73	−11.40	23.26	122.72	151.00	233.65
S'2-3	−34.15	−8.05	96.98	151.65	177.54	206.80
S'3-4	−13.71	−14.55	61.22	199.04	161.82	85.65
S'4-5	−36.67	4.53	106.85	222.21	208.63	101.90
S'5-6	7.49	64.34	88.94	63.86	44.57	38.81
S'6-7	37.60	10.40	80.08	188.86	119.21	48.72
S'7-8	−20.10	18.38	123.91	186.36	125.72	44.54
S'8-9	−16.84	24.47	97.38	199.02	128.75	46.65

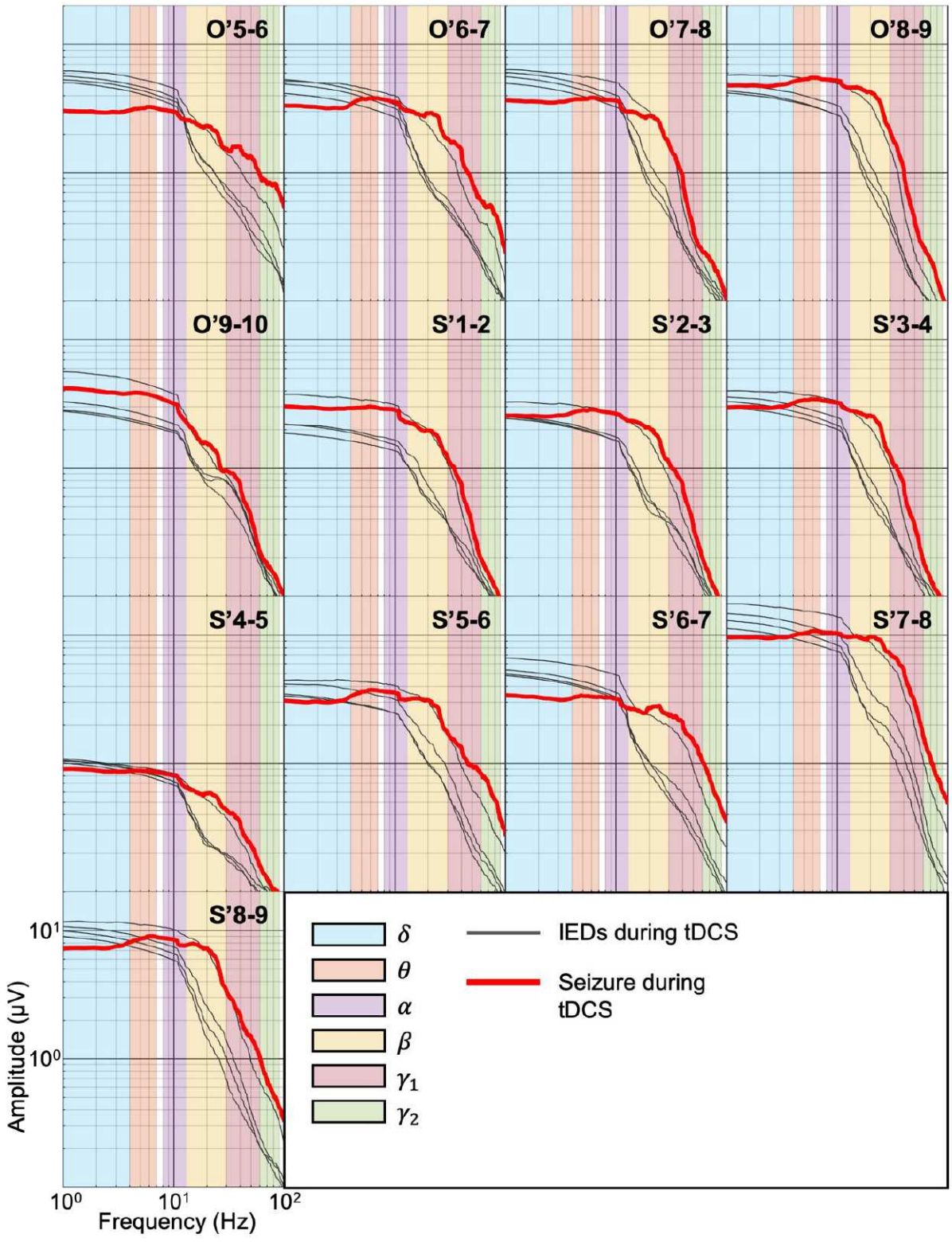

Figure 61: Amplitude spectrum of the seizure occurring during tDCS (red lines) and IEDs detected during tDCS (IEDs* gray lines) on all contacts of interest. The different frequency bands are colored (cyan: δ band; orange: θ band; purple: α band; yellow: β band; red: γ_1 band; green: γ_2 band).

c. IED *versus* IED*

The secondary hypothesis was that the difference on amplitude spectrum of IEDs* is statistically different from IEDs. On electrode O', amplitudes of IEDs* were always significantly higher than the IEDs: one contact (O'8-9) in δ band and θ band, three contacts in α band (O'5-6, O'7-8, O'8-9), on all contacts in β band and finally, 4 contacts in γ_1 (O'5-6, O'7-8 to O'9-10) and γ_2 (O'6-7 to O'9-10) bands. The mean difference values were: 31 %, 48 %, 45 ± 15 %, 42 ± 36 %, 48 ± 35 %, 37 ± 18 % for δ, θ, α, β, γ_1, γ_2 bands respectively (Table 11 and Figure 62).

On the electrode S', IEDs' amplitudes are significantly lower than the IEDs* on 6 contacts (S'2-3 to S'8-9) in δ band with a mean difference of − 33 ± 13 % and higher on 1 contact (S'3-4; 29 %). In θ band, amplitudes are significantly higher during IEDs than IEDs* on one contact S'3-4; 80 % and 11 % lower on S'5-6. Then on higher frequency band, IEDs' amplitudes are significantly higher than IEDs*, with a mean of 48 ± 30 % in α band (2 contacts S'2-3 and S'3-4), of 49 ± 37 % in β band (3 contacts: S'3-4; S'5-6; S'8-9), of 21 ± 22 % in γ_1 band (4 contacts: S'3-4; S'5-6; S'7-8 and S'8-9) and of 16 ± 8 % in γ_2 band (4 contacts: S'1-2 to S'3-4; S'5-6) . (Table 11 and Figure 62).

Table 11: Difference in % of mean amplitude in all frequency bands between the IED detected days prior the tDCS experiment and the IED detected during the tDCS experiment (IED*). Intracerebral contacts selected are contacts involved in IED activity and all seizures occurred days before tDCS. Green cells represent a statistically significant difference in the amplitude distribution on the amplitude spectrum ($p < 0.05$ Friedman test)

Contacts	δ-band (%)	θ-band (%)	α-band (%)	β-band (%)	γ_1-band (%)	γ_2-band (%)
O'5-6	−6.29	7.48	29.80	26.90	1.43	14.30
O'6-7	1.17	−5.72	−0.40	−8.88	12.67	15.92
O'7-8	−8.44	12.76	45.57	46.81	45.60	34.50
O'8-9	31.49	47.71	59.53	90.04	85.02	59.56
O'9-10	−8.45	1.14	20.21	54.69	61.45	39.80
S'1-2	−2.01	−6.18	15.32	7.63	8.80	44.22
S'2-3	−20.23	9.06	27.45	20.46	5.10	16.76
S'3-4	28.90	80.15	69.31	91.91	20.28	8.01
S'4-5	−24.92	16.29	27.35	25.07	6.24	0.33
S'5-6	−20.32	−10.75	2.61	27.05	51.73	23.33
S'6-7	−50.65	−3.98	9.94	13.08	1.20	−0.45
S'7-8	−40.91	13.95	26.42	17.39	11.02	−0.57
S'8-9	−43.85	−12.28	−3.42	25.70	0.31	0.02

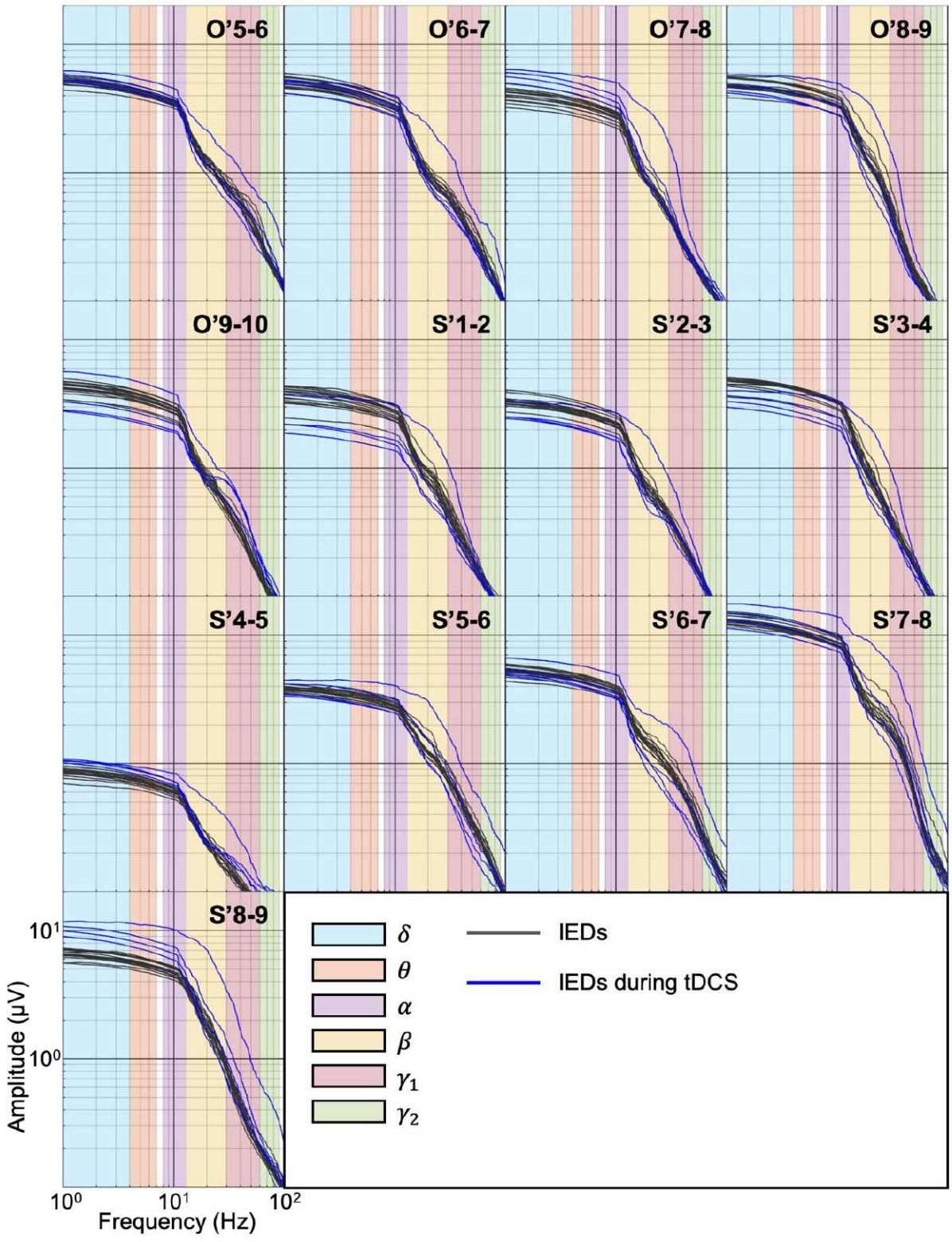

Figure 62: Amplitude spectrum of IEDs occurring during tDCS (blue lines) and IEDs detected days prior the experiment (gray lines) on all contacts of interest. The different frequency bands are colored (cyan: δ band; orange: θ band; purple: α band; yellow: β band; red: γ_1 band; green: γ_2 band).

d. S versus S*

To recall, the hypothesis was that the spectral distribution of the seizure during tDCS is statistically different from the others recorded days prior the experiment. On the SEEG signals, seizures without tDCS (S) were characterized by a polyspike discharge from t = 0 second to t ≈ 8 seconds and then, which evolved into a well-known low amplitude fast discharge until t ≈ 20 seconds. Then, high and low frequency activities composed the last seconds of the seizure (see page 133 to page 136). On the amplitude spectrum seizures "S" were characterized by an amplitude increase in β and γ_1 bands during segment B and D on O'5-6 to O'9-10 and S'1-2 to S'5-6 (Figure 63 to Figure 65). In Figure 63 to Figure 65 one can observe that frequency signatures of all seizures "S" were very similar. This is confirmed by a quantitative analysis of the amplitude spectrum. However, the seizure during tDCS "S*" did not show the same distribution. Therefore:

In delta band, S* amplitude distribution is significantly higher than the amplitude distribution of the other seizures ($p < 0.05$ Friedman's test) on 8 contacts during segment B (from O'5-6 to O'9-10, with %Δ(F) = + 247 ± 64 % and from S'1-2 to S'4-5 with %Δ(F) = + 240 ± 89 %). However, the amplitude distribution is significantly lower on 3 contacts at the end of seizures during segment D (from S'5-6 to S'7-8 with %Δ(F) = − 63 ± 7 %).

In theta band, S* amplitude distribution is significantly higher on 11 contacts during segment B (from O'5-6 to O'9-10 with %Δ(F) = + 363 ± 221 % and from S'1-2 to S'4-5, S'7-8 and S'8-9 with %Δ(F) = + 305 ± 153 %).

In alpha band, S* amplitude distribution is significantly higher on 8 contacts during segment B (O'5-6, from O'7-8 to O'9-10 with %Δ(F) = + 239 ± 123 % and from S'1-2 to S'4-5 with %Δ(F) = + 198 ± 87 %).

Then, in higher frequency band the peak amplitude of the seizures without tDCS shifted the differences making S* amplitude distribution lower than the other seizures:

In beta band, S* amplitude distribution is significantly lower on 3 contacts during segment B (from O'5-6 to O'7-8 with %Δ(F) = − 40 ± 8 %). During segment C the distribution is significantly lower on 11 contacts (from O'5-6 to O'9-10 with %Δ(F) = − 81 ± 3 % and on S'1-2, S'3-4, S'4-5, S'6-7 to S'8-9 with %Δ(F) = − 49 ±11 %).

In gamma1 band, S* amplitude distribution is significantly lower on 6 contacts during segment B (from O'5-6 to O'8-9 with %Δ(F) = − 79 ± 4 % and S'1-2 to S'2-3 with %Δ(F) = − 47 ± 9 %). During segment C, the distribution is significantly lower on 8 contacts (from O'5-6 to O'8-9 with %Δ(F) = − 84 ± 3 % and S'1-2, S'2-3, S'4-5 and S'8-9 with %Δ(F) = − 54 ± 19 %).

In gamma2 band, S* amplitude distribution is significantly lower on 5 contacts during segment B (from O'5-6 to O'8-9 with %Δ(F) = − 68 ± 4 % and S'2-3 with %Δ(F) = − 52 ± 3 %).

During segment C, the distribution is significantly lower on 5 contacts (from O'5-6 to O'8-9 with $\%\Delta(F) = -74 \pm 7$ % and S'1-2 with $\%\Delta(F) = -57 \pm 6$ %).

4. Epileptogenicity index

The algorithm detected significant epileptogenicity indexes (EI > 0.3). on:

- 5 contacts (O'5-6 to O'9-10) for seizure 1
- 4 contacts (O'5-6 to O'8-9) for seizure 2
- 4 contacts (O'5-6, O'7-8 to O'9-10) for seizure 3
- 4 contacts (O'5-6 to O'8-9) for seizure 4

The four seizures occurred days before tDCS experiment had in common 3 contacts on which the algorithm detected a significant EI: O'5-6, O'7-8 and O'8-9.

For the seizure occurred during DC stimulation, there were no detection of seizure onset.

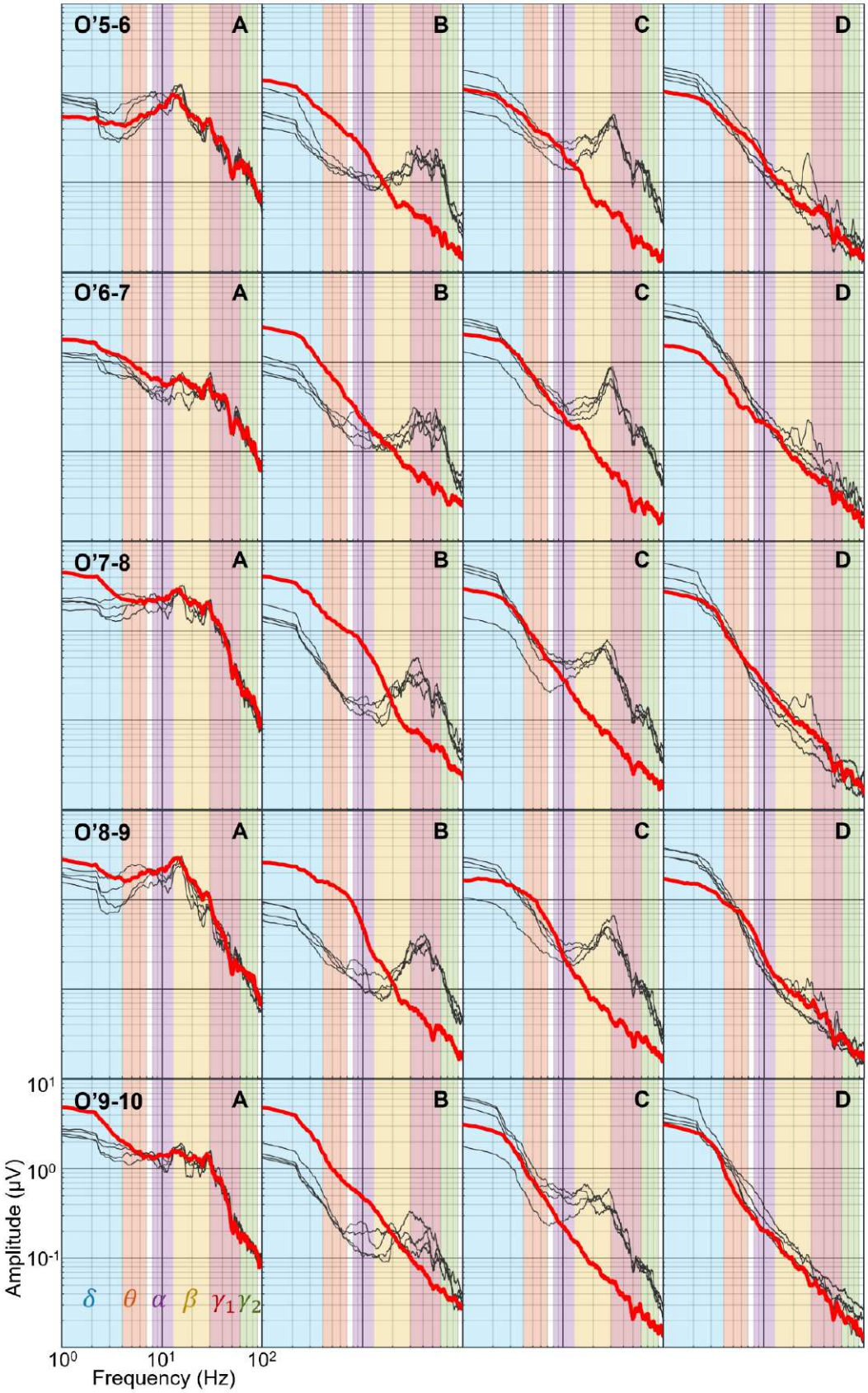

Figure 63: Amplitude spectrum of seizures "S" occurring days prior tDCS experiment (gray lines) and seizure S* occurring during the DC stimulation (red lines) from contacts O'5-6 to O'9-10. Spectrums were plotted for each time segment (columns, A, B, C and D) and for each contact of interest (rows). The different frequency bands are highlighted in cyan: δ band; orange: θ band; purple: α band; yellow: β band; red: γ_1 band; green: γ_2 band.

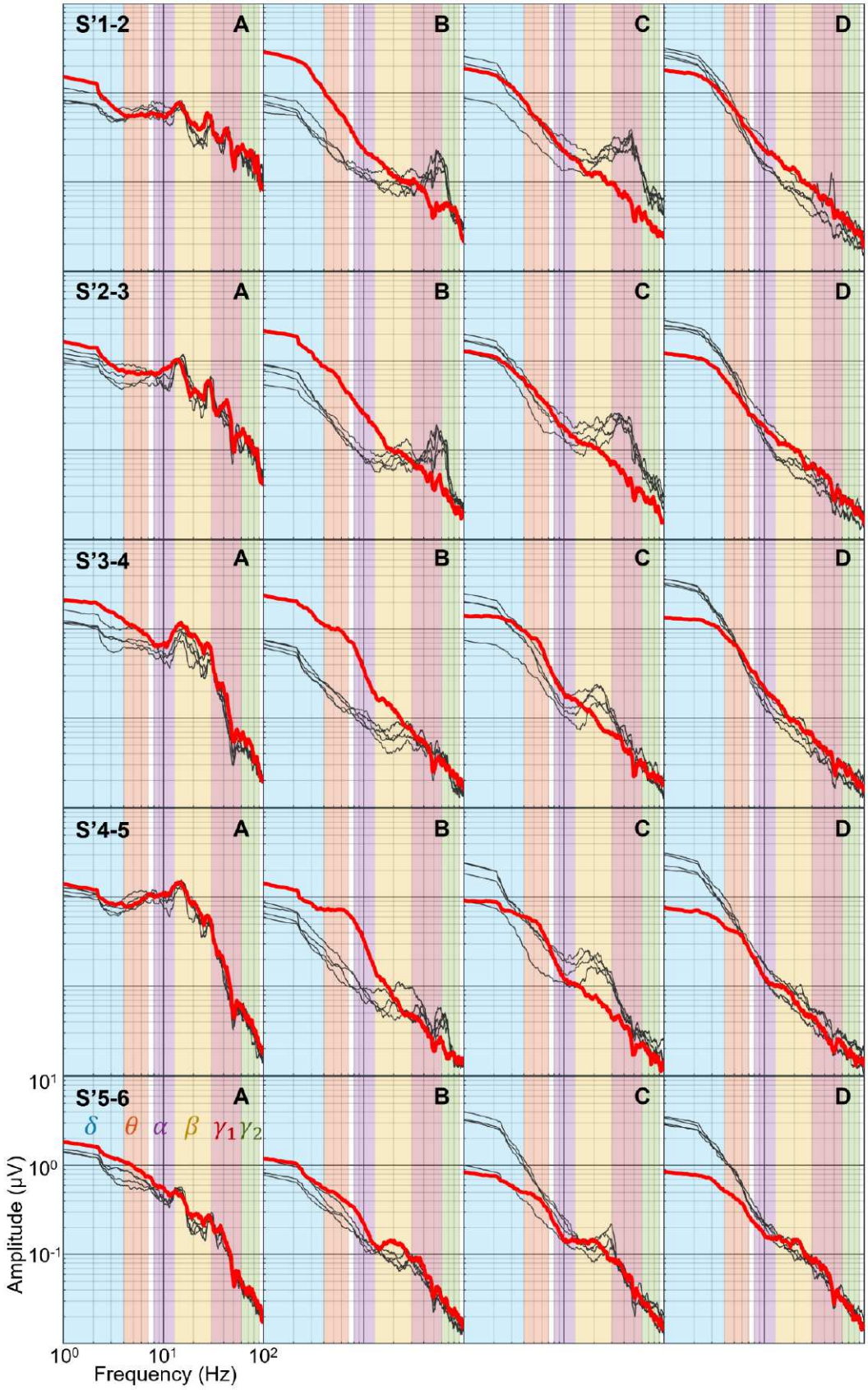

Figure 64: Amplitude spectrum of seizures "S" occurring days prior tDCS experiment (gray lines) and seizure S* occurring during the DC stimulation (red lines) from contacts S'1-2 to S'5-6. Spectrums were plotted for each time segment (columns, A, B, C and D) and for each contact of interest (rows). The different frequency bands are highlighted in cyan: δ band; orange: θ band; purple: α band; yellow: β band; red: γ_1 band; green: γ_2 band.

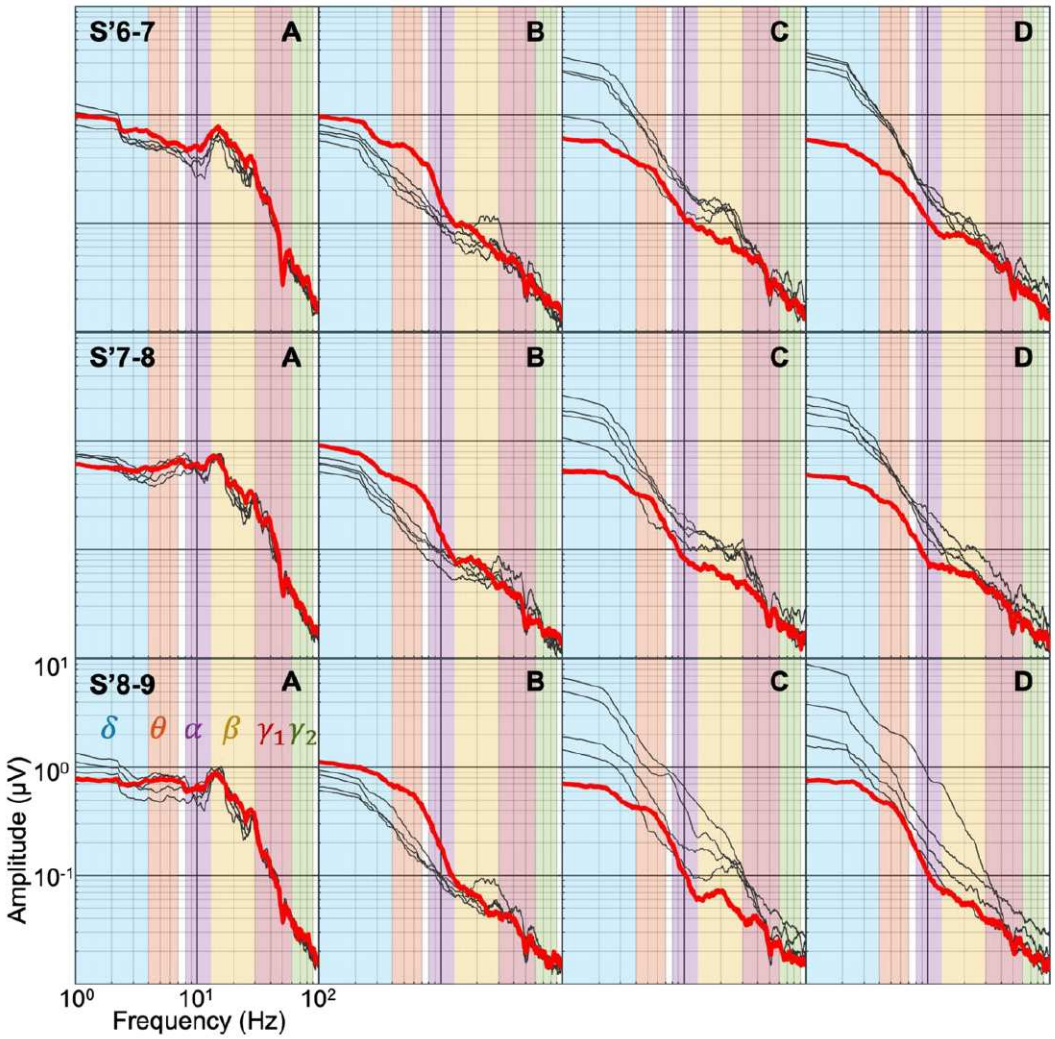

Figure 65: Amplitude spectrum of seizures "S" occurring days prior the tDCS (gray lines) and seizure S* occurring during the DC stimulation (red lines) from contacts S'6-7 to S'8-9. Spectrums were plotted for each time segment (columns, A, B, C and D) and for each contact of interest (rows). The different frequency bands are highlighted in cyan: δ band; orange: θ band; purple: α band; yellow: β band; red: γ_1 band; green: γ_2 band.

III. Conclusion and discussion

The second study presented the first epileptic seizure during a tDCS and measured it with intracerebral electrodes. When qualitatively studying the five seizures' SEEG trace, it is easily noticeable that the seizure during tDCS is different from the others. Indeed, the high frequency phase, which is a typical characteristic of this patient's ictal activity, is not manifesting during tDCS. On the amplitude spectrum the four seizures without tDCS are quite similar and all exhibit a local maximum in gamma1 activity between 12 and 24 seconds which shift into local maximum in beta activity in the next 12 seconds. The amplitude distribution on the spectrum of the seizure during tDCS is significantly lower on several contacts than the other seizures. If we consider only the three contacts on which ictal activity was constantly and systematically detected for the four seizures (contacts on which the epileptogenicity index was superior to 0.3 for the four seizures) the amplitude distribution for the seizure during tDCS is always significantly different from the other seizures.

The occurrence of the seizure couldn't be controlled by the DC stimulation. However, tDCS could influence only weaker and more unstable activities which are the ictal higher frequency/lower phases of the seizures.

For a long time, DC stimulation was applied and investigated on epileptiform activity through *in-vitro* studies (Jefferys, 1995; Ghai, Bikson and Durand, 2000; Durand and Bikson, 2001; Jefferys *et al.*, 2003), and animal studies (for a review: Regner et al., 2018). These studies aimed to control and/or to suppress the epileptiform activity with DC stimulation. Results presented in this chapter could encourage studies to focus only on some ictal activity component (high frequency/low amplitude activities) during a tDCS. Indeed, the stimulation by itself may fail in controlling/suppressing seizures but may succeed in a more subtle way by modulating high frequency/low amplitude dynamics. Because a lot of seizures start with this type of activity (and is even a characteristic to detect seizures onset (Bartolomei, Chauvel and Wendling, 2008)) tDCS could be a useful tool to early abort seizure initiation by suppressing this typical high frequency activity during the first seconds.

Chapter IV:

Electrophysiological effect of TES in cognition: intracerebral human *in-vivo* investigation

In the previous chapter, a study was presented on the application of tDCS in pathology (epilepsy) and its induced effects. This was assessed thanks to the electrophysiological study of epileptic biomarkers both interictal and ictal. In this chapter, a study on the application of tDCS in cognition will be presented. It will be assessed by investigating the electrophysiological responses of a cognitive function: face perception and recognition. This study is subdivided into 2 sub-studies. The first one will explore the electrophysiological responses of the cognitive function through intracerebral investigation (SEEG) in epileptic patients. The second one will explore the electrophysiological responses of the same cognitive function measured on scalp EEG in healthy subjects.

I. State-of-the art and scientific questions

Because the human is a social living being, vision in social interaction is one of the most developed and complex networks. The integration of the visual flow in the human being is done according to two visual pathways (Figure 66):

- The dorsal visual stream (DVS), which starts in the occipital cortex and extends to the parietal lobe, is involved in the processing of spatial vision, allowing the guidance of actions (e.g., finding one's way in relation to an object or reaching an object/location). This pathway is therefore defined as the "where" pathway.
- The ventral visual stream (VVS), which originates in the occipital cortex and extends to the temporal lobe, is involved in the identification and visual recognition of objects, faces and the representation of shapes. It is therefore defined as the "what" pathway.

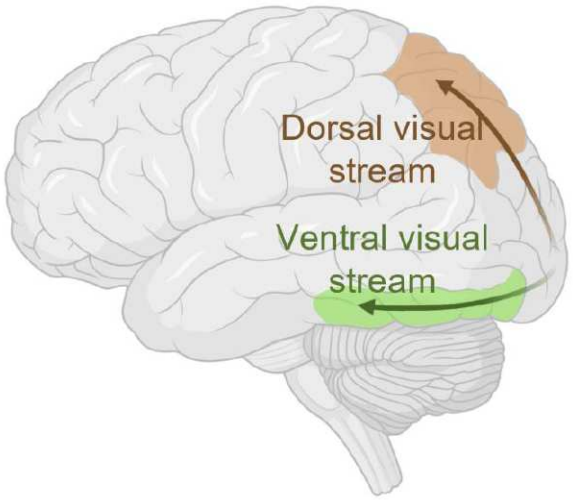

Figure 66: Representation of the two visual pathways. The first visual pathway starts from the occipital lobe and is processed to the parietal lobe (brown), it is the dorsal visual stream which is responsible for object localization and called the “where” pathway. The second visual pathway starts from the occipital lobe and is processed to the temporal lobe, it is the ventral visual stream which is responsible for identifying objects and is called the “what” pathway. Made on biorender.com

Many articles in literature have already demonstrated the importance of the involvement of the VVS in the conscious perception of visual stimuli such as faces (Rossion, 2014a; Grill-Spector *et al.*,

2017) and also words (Reich *et al.*, 2011). An impairment of this brain network induces neurological pathologies like prosopagnosia, which is the inability to recognize faces (Barton *et al.*, 2002; Rossion, 2014b).

1. Behavioral studies of TES applied to face perception/ recognition

Some behavioral studies in face recognition with TES (tDCS, tACS, tRNS) have been performed with various sample sizes, from 16 (Gonzalez-Perez *et al.*, 2019) to 114 participants (Civile *et al.*, 2018). They reported diverse effects on behavior during or after TES: an enhancement of face perception (an increase of + 9.9 % (Gonzalez-Perez *et al.*, 2019) and + 7.1 % (Barbieri, Negrini, Michael A Nitsche, *et al.*, 2016) accuracy compared to sham condition), face memory (Barbieri, Negrini, Michael A. Nitsche, *et al.*, 2016; Brunyé *et al.*, 2017) and humor detection (Manfredi *et al.*, 2017), a decrease of learning effect (Renzi *et al.*, 2015) or even no effect at all (Willis *et al.*, 2019). Behavioral results are sensitive to external parameters, and it is difficult to control all of them (subject's mood, tiredness, environment). Moreover, "sham-controlled experiments" seems to be compromised as Fonteneau et al., (2019) describes: subjects can tell when a stimulation is active or not even during sham and this can induce a non-negligible bias in behavioral data. Poor study design, result inconsistencies, and potential biases led to a lot of questioning and criticism (Bestmann, de Berker and Bonaiuto, 2015; Horvath, Forte and Carter, 2015; Parkin, Ekhtiari and Walsh, 2015). Therefore, measuring the electrophysiological responses could be an interesting solution to study cognitive functions in a more objective way (less influenced by external parameters than behavioral measurements).

2. Electrophysiology of face perception

During a cognitive task, neurons responsible for the specific cognitive function all deliver simultaneous action potentials which results in an EEG evoked related potential (ERP) and was discovered in 1939 by P.A. Davis (Davis, 1939). In the context of face perception, ERPs are generated in the occipital lobe (Bötzel and Grüsser, 1989; Jeffreys, 1989; Bötzel, Schulze and Stodieck, 1995) at a higher amplitude in the right hemisphere (Bentin *et al.*, 1996). This ERP is a negative deflection around 170 milliseconds and is, therefore, called N170 (see Figure 67 (Rossion and Caharel, 2011; Rossion, Hanseeuw and Dricot, 2012)). Neuroimaging studies using PET-scan and functional MRI (fMRI) showed an increase of metabolism and signal bold during face perception/recognition tasks in the right ventral occipital-temporal cortex (VOTC) (Sergent and Signoret, 1992) and more precisely in 2 areas:

- The first one in the inferior occipital gyrus (called "Occipital Face Area" or OFA)
- The second one in the posterior and lateral fusiform gyrus (called "Fusiform Face Area" or FFA)

(Kanwisher, McDermott and Chun, 1997; Gauthier *et al.*, 2000; Rossion, Hanseeuw and Dricot, 2012; Lafer-Sousa, Conway and Kanwisher, 2016). The OFA is sensitive to stimuli presenting a face but also when face fragments are presented (eyes, nose, and mouth). The FFA is more responsive to face-object discrimination and to high-level visual cues (Rossion et al., 2012). Thus, basic mechanism of face perception involves 2 structures working in concert: FFA and OFA. The right hemisphere is usually predominant for face perception but also many other cerebral structures are also (many of them located in the limbic system such as the hippocampus and the amygdala). Because the limbic system is also involved in face perception and face recognition, neurologic and psychiatric disorders affecting the limbic system can impact the N170 ERP and the connectivity between the OFA and FFA functional regions. For instance, it has been reported in schizophrenic patients that the N170 amplitude is lower than in healthy subjects (Feuerriegel *et al.*, 2015). Another example, in the case of anxiety, a higher amplitude of the N170 has been reported interestingly for faces displaying anger (O'Toole *et al.*, 2013).

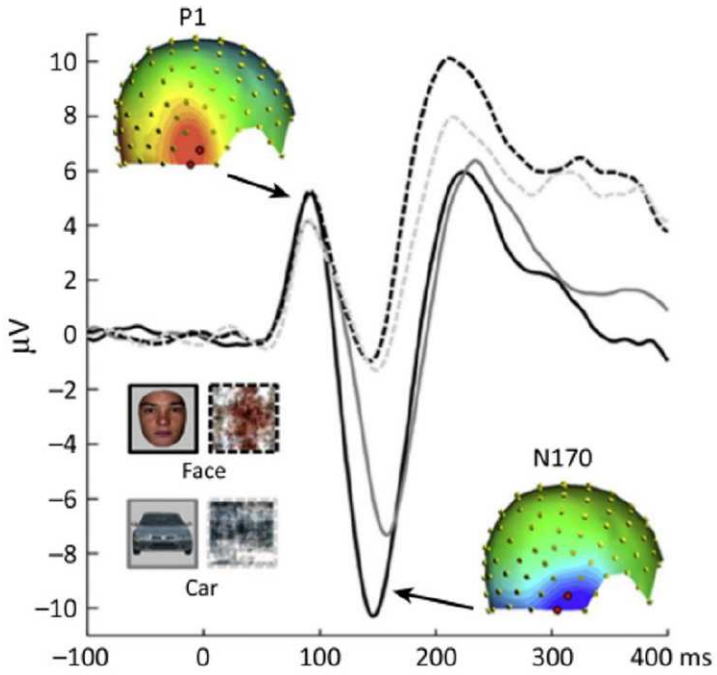

Figure 67: Evoked Related Potential responses recorded on scalp EEG during a cognitive stimulus. Evoked related potentials showing 2 components: P1 and N170. The N170 negative deflection is stronger when faces are presented (plain black line) than when an object is presented (here a car: plain gray line). Scrambled images don't generate an N170 deflection (dashed gray and black lines). Adapted from ERP evidence for the speed of face categorization in the human brain: Disentangling the contribution of low-level visual cues from face perception. *Vision Research*, *51*(12), 1297–1311 by Rossion, B., & Caharel, S. (2011) © 2011 by Elsevier. Reproduced with permission of Elsevier under license number 5267011408712 in the format of print and electronic via Copyright Clearance Center.

3. The use of fast periodic visual stimulation (FPVS) in face perception and recognition

The fast periodic visual stimulation (FPVS) is a paradigm defined by Rossion, 2014c. FPVS is the generic term for a principle introduced by David Regan in 1966 which is steady state visual

evoked potentials (SSVEP). In that case a visual stimulus is presented periodically at a fixed frequency inducing evoked potentials synchronized to that periodical stimulus (Regan, 1966; Morgan, Hansen and Hillyard, 1996; Norcia, Wesemann and Manny, 1999; Wang and Wade, 2011; Andersen, Muller and Martinovic, 2012; Rossion, 2014b; Norcia *et al.*, 2015). After performing a Fourier transform, the frequency spectrum of the EEG signal exhibits an activity at the exact frequency of the stimulus whose amplitude can be measured. This approach usually used for low level cognitive functions (light and basic color perceptions) can also be applied to high level functions such as face perception and face recognition (B. Rossion and Boremanse, 2011; Rossion, 2014a, 2014c). This approach presents numerous advantages: the deterministic nature of the data (electrophysiological responses at the exact frequency set by the experimenter), the simplicity of the responses' quantification (just measuring the peak value on the frequency spectrum), the high signal/noise ratio (SNR) and the high immunity to artifacts make FPVS a robust and easy solution to assess cognitive functions through electrophysiological studies (Rossion *et al.*, 2015).

FPVS was also used to perform anatomical mapping of face-selective areas thanks to intracerebral investigation by stereo-EEG (SEEG) (Jonas *et al.*, 2016). This study showed that face-selective electrophysiological responses are mainly located within the right lateral fusiform gyrus but also in a wider area notably the ventromedial occipital region, medial fusiform gyrus, medial and inferior temporal gyrus and in the anterior temporal lobe.

Thus, FPVS can be used either with scalp EEG or intracerebral EEG (SEEG) and deliver robust and reproducible results while being easy to use.

4. Electrophysiological studies of TES applied to face perception/recognition

Thus, because of its temporal resolution and direct correlation to the cognitive process, the use of electrophysiology is an interesting approach to investigate TES in face perception. As of today, all studies have used EEG recording to assess the electrophysiological response of face perception/recognition with TES.

The first one was performed in 2013 by Lafontaine (Lafontaine *et al.*, 2013). They performed old/new face recognition tasks in 11 healthy subjects before and after tDCS in a sham-controlled study. They placed, according to the 10-10 international system, two tDCS electrodes (saline-soaked sponges 35 cm^2) on F3 and F4 and stimulated for 15 minutes at 1.5 mA. They performed tDCS at 2 different polarities: anodal (+ 1.5 mA on F4) and cathodal (− 1.5 mA on F4). After tDCS, they recorded the N170 on scalp EEG. They reported a non-significant difference of the N170 amplitude up to 2.12 µV between active stimulation (whatever the polarity) and sham. However, they measured a significant difference of the N170 amplitude between cathodal tDCS and anodal tDCS.

Then, in 2014 Yang *et al*. performed tDCS in 39 participants using composite face and face orientation judgement tasks. They placed 2 tDCS electrodes (saline-soaked sponges 35 cm^2) over the occipital lobe at P7 and P8 and stimulated at 1.5 mA for 15 minutes. They measured the N170 after stimulation on scalp EEG and reported a significant amplitude modulation (increase up to 2.01 µV) on the right hemisphere after tDCS.

In 2020, Civile and colleagues performed tDCS in 112 healthy subjects. They placed 2 tDCS electrodes (saline-soaked sponges 35 cm^2 anode on Fp3 and cathode over the right eyebrow) and stimulated at 1.5 mA for 15 minutes. They studied the N170 during inverted/upright face perception tasks (old/new recognition task). They reported the N170 amplitude difference between upright and inverted faces is significantly higher during a tDCS (1.07 ± 0.24 µV) than the sham condition (0.38 ± 0.16 µV).

From the electrophysiological approach, the previous mentioned studies lead to a first conclusion that tDCS induces an electrophysiological effect on face perception/recognition EEG responses.

However, the N170 measurement presents some limitations. First, the evoked related potential (ERP) has a poor signal/noise ratio (SNR) which means it is difficult to extract the N170 component from the background noise, therefore it requires a high number of trials to average the ERP and exhibit the N170 (Jacques, D'Arripe and Rossion, 2007; Rossion, 2014a). Secondly, the real N170 can be misinterpreted from a "N170-like component" and can induce some bias in the interpretation and quantifications of the results (Suzuki and Noguchi, 2013; Rossion, 2014a). Finally, the N170 is sensitive to the test-retest effect and could also influence results and induce confusion between tDCS effects and test-retest effects.

To overcome the limitation of the N170 measurement, one solution is to use fast periodic visual stimulation (FPVS) paradigms. But to date, there are no studies assessing the effect of TES on face perception/recognition by using FPVS. Therefore, this chapter will tackle this topic by studying TES-induced effects through a multi-scale study involving surface and intracerebral EEG investigations by leveraging FPVS paradigms coupled with tDCS. This study will attempt to answer the question: is it possible to modulate the cognitive electrophysiological response with tDCS?

II. Materials and methods

1. Intracerebral investigation

a. Patients and SEEG recording

Six (5 females 1 male) patients with focal refractory epilepsy candidates for a presurgical evaluation were prospectively included in this study. Their standard presurgical evaluation and their

SEEG investigation was according to the process described in Chapter II and III. The inclusion criteria were (according to the anatomo-functional areas described by (Jonas *et al.*, 2016)):

1. The fusiform gyrus explored by the SEEG.
2. The presence of electrodes exploring at least one of these areas:
    a. The anterior segment of the collateral sulcus (anterior temporal lobe).
    b. The anterior segment of the occipito-temporal sulcus (anterior temporal lobe).
    c. The posterior segment of the middle and inferior temporal gyri (posterior temporal lobe)
    d. The ventral part of the occipital lobe.

SEEG signals were recorded on the same device used in clinical routine, 4×64 channels amplifiers (LTM 256 Micromed®, Treviso, Italy) at the sampling rate of 1,024 Hz and with an analog high pass filter at 0.15 Hz. The reference chosen was the same as the one set by the epileptologists for clinical routine: on an intracerebral contact within the white matter.

b. FPVS paradigms

The FPVS paradigm chosen aims to exhibit face selective responses (face perception) and will be called hereafter "Faceloc" for "Face Localizer". It consists of presenting images on a screen placed at 80 cm from the subject eyes. Images are composed of single non-face objects (everyday objects, animals, fruits, vegetables) and faces presented at the frequency of 6 Hz (also called the "base" frequency which has been proven to be the one generating the best SNR (Alonso-Prieto *et al.*, 2013)). Images are presented successively by modulating the contrast from 0 % to 100 % sinusoidally (Figure 68). Faces appear periodically every 5 images, which represent an apparition frequency of $\frac{5}{6} = 1.2$ Hz also called the "oddball" frequency. Thus, it will be possible to discriminate high level cognitive responses (face perception at 1.2 Hz) from low level responses (basic visual responses from the image presentation/the flickering at 6 Hz). One FPVS sequence is 70 seconds long with 2s of contrast ramp-up (fade in) at the beginning and 2s contrast ramp-down (fade out) at the end which results in 66s full contrast amplitude stimulation (0-100 %). This paradigm has been chosen because it generates face selective responses in the visual ventral stream of both hemispheres which was demonstrated intracerebrally by Jonas et al. (2016). Commonly, SEEG investigation explores either the right or the left ventral visual stream, therefore for the SEEG inclusion, this FPVS paradigm is convenient.

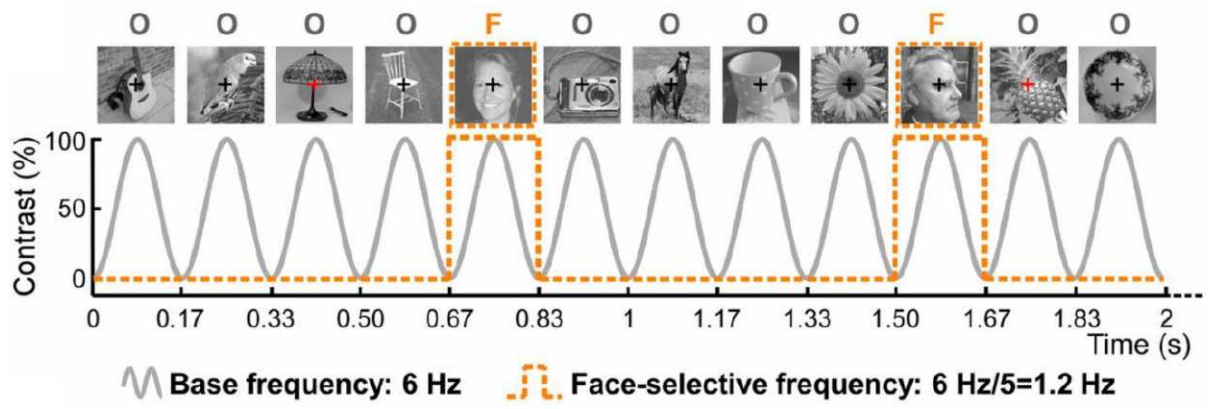

Figure 68: (previous page): FPVS paradigm for the face perception investigation. A visual stimulus presents 6 images per second (frequency 6 Hz) with the contrast modulated sinusoidally. Two types of images are presented during the stimulus: object (gray O) and faces (orange F). Faces are presented periodically every 5 images (at the frequency of 1.2 Hz). This difference in frequency will make possible to discriminate the high-level cognitive responses at 1.2 Hz (called the oddball frequency, highlighted in orange dashed line, which correspond to the face perception task) from the low-level cognitive responses at 6 Hz (called the base frequency, which is the basic visual response from the image presentation). To monitor subject's attention, a black cross in the middle of the image turns pseudo-randomly into a red cross. When the cross' color changes, the subject must press a button. From Jonas et al., 2016.

c. Stimulation

The direct-current (DC) stimulation was delivered with the same device and same electrodes presented in previous chapters. TDCS montages were set to target the explored fusiform gyrus and the contralateral temporal lobe. Thus, electrodes were placed either on P10-FT9 or P9-FT10. Stimulation amplitudes were − 2 mA or + 2 mA. Sham stimulations consisted of a 30-second amplitude increase from 0 to 2 mA followed by a 30-second amplitude decrease (from 2 mA to 0) to "fool" the subject. Two distinct sub-groups were defined:

- The cathodal group in which patients had the electrode over the explored (right or left depending on the implantation) occipito-temporal area injecting a negative current.
- The anodal group in which patients had the electrode over the explored (right or left depending on the implantation) occipito-temporal area injecting a positive current.

d. Experimental design

The sham-controlled experiment is divided into 3 phases.

- Phase 1: Four faceloc sessions of 70 seconds each (for a total duration of 4 min 40 sec, purple in Figure 69) are presented during a sham stimulation (green in Figure 69).
- Phase 2: Four faceloc sessions of 70 seconds each are presented during a DC stimulation (red in Figure 69), 10 minutes after its start (which is the minimum DC stimulation duration to induce potential modulation (Antal, Kincses, *et al.*, 2004)).
- Phase 3: Four faceloc sessions of 70 seconds each are presented during a sham stimulation (blue in Figure 69).

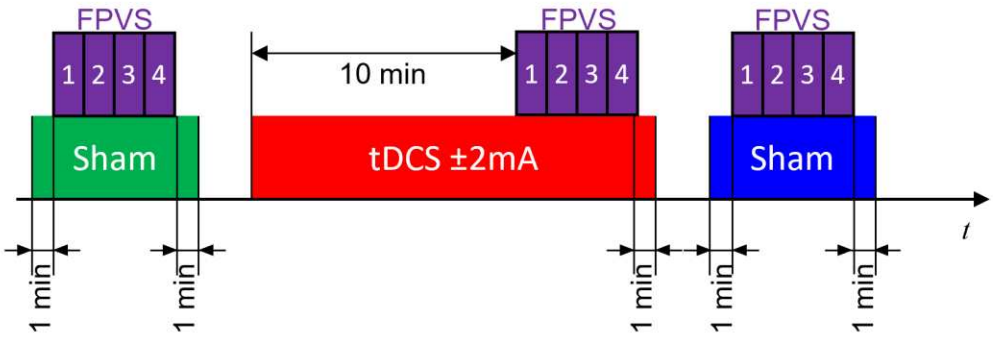

Figure 69: Experimental design of tDCS during FPVS paradigms. Sham stimulations (green and blue) consists of fooling the subject by injecting a current with an increasing then decreasing amplitude for 1 minute at the beginning and at the end of the phase. For more details see Chapter III. Four sessions of a same FPVS paradigm (purple boxes) are presented during each phase.

e. Data processing

Data were analyzed with a Matlab®-based software toolbox "letswave" (https://letswave.cn)

First, SEEG signal was down sampled from 1,024 Hz to 512 Hz. Then, only SEEG signals during FPVS at full contrast's amplitude (contrast from 0 to 100 % without fade-in and fade-out) was selected while ensuring to include 75 face apparition cycles. Second, the four SEEG signal segments of the four FPVS sessions (purple boxes in Figure 69) were averaged. Third, a fast Fourier transform (FFT) was performed on the averaged signal and the amplitude spectrum was obtained (for more details about the amplitude spectrum see Chapter II) for each intracerebral contact within the areas of interest. Because of the sampling rate and the discretized signal, frequencies of interests were actually 1.176 Hz (instead of 1.2) (and its harmonics: all frequencies multiple of 1.176) for face selective responses and 5.88 Hz for base response (instead of 6 Hz) (and its harmonics: all frequencies multiple of 5.88).

Baseline correction of amplitude spectrum.

The baseline correction was performed by subtracting the average amplitude of the baseline interval within the 25 samples before and after the frequency of interest (or the n^{th} harmonic) (Hu *et al.*, 2013; Dzhelyova and Rossion, 2014; Jonas *et al.*, 2016).

Z-score calculation

Z-score was calculated:

$$Zscore = \frac{x - \mu}{\sigma}$$

Where x is the amplitude at each frequency sample, μ the mean amplitude calculated within the 25 samples before and after the frequency of interest (or its harmonic) and σ the standard-deviation calculated within the 25 samples before and after the frequency of interest (or its harmonic). On a chosen intracerebral contact, a z-score > 3.1 at the frequency of interest suggests that a statistically significant response ($p < 0.001$) is recorded on that contact (Jonas *et al.*, 2016).

Signal/noise ratio (SNR) calculation

SNR was calculated:

$$SNR = \frac{x}{\mu}$$

Where x is the amplitude at each frequency sample and μ the mean amplitude calculated within the 25 samples before and after the frequency of interest (or its harmonic)(Jonas *et al.*, 2016).

Response amplitude quantification

Amplitudes at the fundamental and at the different harmonics were summed to quantify the response's amplitude.

Regions Of Interest (ROI)

Thanks to the MRI-CT scan co-registration (more details in Chapter II) intracerebral contacts were located within the brain anatomy. Amplitudes measured on intracerebral contacts within three anatomical regions were analyzed. The regions chosen for this investigation were based on the results of the anatomical study by Jonas et al. (2016) and called hereafter Region of Interest (ROI):

- The ventral occipito-temporal area explored (VOT area, including the fusiform gyrus)
- The ipsilateral temporal lobe (Temporal lobe (TL) area, anterior and posterior including amygdala and hippocampus)

The ROI lateralization was according to the structures targeted by the tDCS montage (e.g. for a subject with whom a tDCS was performed on P9-FT10, ROIs will be (1) the right TL (2) the left VOT which are structures just under the stimulation electrodes). Also, the contralateral temporal lobe was individually considered (making the third ROI), investigating the impact of tDCS on the cognitive network by assuming that the pathway can be changed if the electrophysiological environment is disorganized.

Statistical study

All intracerebral contacts exhibiting a significant response (Z-score > 3.1) during, at least, one phase and within each mentioned ROI were included in the study. To assess amplitude difference between phases, a statistical Friedman's test was performed on all contacts within the same ROI across all patients. The null hypothesis was that amplitudes between phases come from the same distribution and was rejected when $p < 0.05$.

Then, for visualization purposes only, amplitudes were averaged across patients in the same sub-group and on all contacts within the same ROI. Standard error (SE) was calculated for each phase (before, during and after tDCS):

$$SE = \frac{\sigma}{\sqrt{n}}$$

Where σ is the standard deviation calculated on all contacts within the ROI across subjects in the same sub-group and n the number of observations (number of intracerebral contacts within the ROI and for all subjects in the same subgroup).

2. Surface EEG investigation

a. Subjects and EEG recording

Fourteen healthy voluntary subjects were included in the study (6 females, 8 males) all right-handed, equipped with a 10-10 Biosemi® (Amsterdam, Netherland) EEG cap 64-electrodes. The Biosemi® recording system was sampled at 512 Hz and with a 24-bit resolution. The recording device reference was set on Fpz.

b. FPVS paradigms

In these experiments, 3 different paradigms were used:

A. **Faceloc:** as explained before, this paradigm comprises presenting images of non-face objects and faces at 6 Hz (base frequency). Face apparition frequency was at 1.2 Hz (oddball frequency) which will exhibit the face selective function.

B. **Idedis upright:** comprises of presenting unknown faces (Figure 70) at the frequency of 6 Hz. One image over five presents another identity which will exhibit the electrophysiological activity associated with the identity discrimination function.

C. **Idedis inverted:** same as Idedis upright, but faces are presented upside-down (Figure 70). This paradigm is known to impair partially the face discrimination and generates a lower amplitude of the cognitive response (Rossion, 2008, 2009; Liu-Shuang, Norcia and Rossion, 2014).

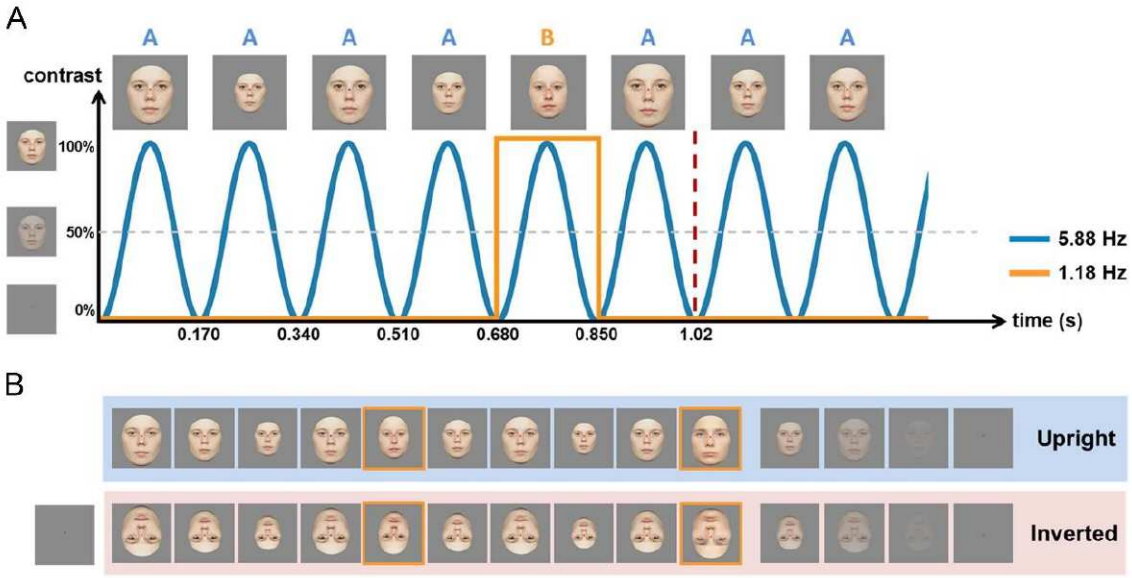

Figure 70: FPVS paradigm for the identity discrimination (Idedis). A: visual stimulus presents faces periodically at the frequency of 5.88 Hz (base) with the contrast modulated sinusoidally. Every 5 images, identity changed from blue A face to another identity (orange B). The identity change occurred at the frequency of 1.176 Hz (oddball). The paradigm can be performed with upright faces (B blue) and inverted faces (B red). From An objective index of individual face discrimination

in the right occipito-temporal cortex by means of fast periodic oddball stimulation. *Neuropsychologia*, *52*(1), 57–72 by Liu-Shuang, J., Norcia, A. M., & Rossion, B. (2014). © 2014 by Elsevier. Reproduced with permission of Elsevier under license number 5283730805423 in the format of print and electronic via Copyright Clearance Center.

c. Transcranial electrical Stimulation

All subjects received a tDCS at + 2 mA on P10-FT9 with the anode next to P10 (Figure 72). Sham stimulations consisted of a 30-second amplitude increase from 0 to 2 mA followed by a 30-second amplitude decrease (from 2 mA to 0) to "fool" the subject. The experiment was subdivided into 3 phases: Phase1 (before tDCS): Sham stimulation, Phase2 (during tDCS): tDCS stimulation, and Phase3 (after tDCS): Sham stimulation.

d. Experimental design

The sham-controlled experiment consists of presenting FPVS paradigms (Faceloc (**A**) Idedis upright (**B**) and Idedis inverted (**C**), male ♂ and female ♀ faces 70-second sessions each) according to 2 pre-defined sequences:

A B (♀) **A C** (♂) **B** (♂) **C** (♀)

A C (♂) **A B** (♀) **C** (♀) **B** (♂)

FPVS paradigms following sequence 1 or 2 (depending on the inclusion order: subjects with an odd inclusion number had sequence 1, subjects with a pair inclusion number had sequence 2) were presented before (during a sham stimulation), during and after tDCS (during a sham stimulation). An example of the experimental design for a patient who had sequence 1 is displayed in Figure 71.

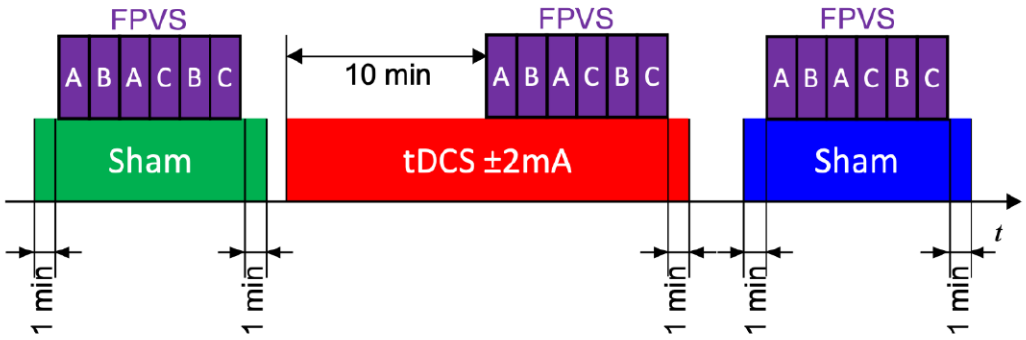

Figure 71: Experimental design of EEG investigation of tDCS applied to face perception (A in purple boxes) and identity discrimination (B and C in purple boxes) in healthy subjects. FPVS paradigms are presented following a pre-determined sequence (ABACBC sequence #1 in that case). Sham stimulations (green and blue) consist of fooling the subject by injecting current with an increasing then decreasing amplitude for 1 minute at the beginning and at the end of the phase.

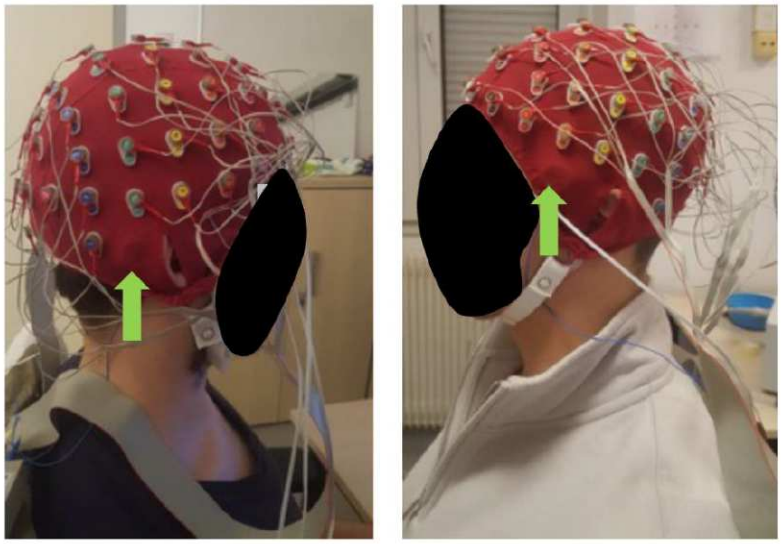

Figure 72: tDCS electrodes placement (green) with the 64-Biosemi EEG cap in two different subjects. Left image displays where the anode is placed (P10 electrode), right image displays where cathode is placed (FT9 electrode). Anode and cathode were placed the same way in every subject.

e. Data processing

Data were analyzed with a Matlab®-based software toolbox "letswave".

EEG signal only during FPVS at full contrast's amplitude (contrast from 0 to 100 % without fade-in and fade-out) were selected while ensuring to include 75 face apparition cycles. Secondly, the EEG during corresponding FPVS sessions (A or B or C in Figure 71) were averaged (e.g EEG signal during A boxes during sham were averaged). Thirdly a fast Fourier transform (FFT) was performed on the averaged signal and the amplitude spectrum was obtained (for more details about the amplitude spectrum see Chapter II) for all EEG electrodes. Because of the sampling rate and the discretized signal, frequencies of interests were actually 1.176 Hz (instead of 1.2) (and its harmonics: all frequencies multiple of 1.176) for face selective responses and 5.88 Hz for base response (instead of 6 Hz) (and its harmonics: all frequencies multiple of 5.88).

Baseline correction of amplitude spectrum.

The baseline correction was performed by subtracting the average amplitude of the baseline interval within the 25 samples before and after the frequency of interest (or the n^{th} harmonic) (Hu *et al.*, 2013; Dzhelyova and Rossion, 2014; Jonas *et al.*, 2016).

Signal/noise ratio (SNR) calculation

SNR was calculated as follow:

$$SNR = \frac{x}{\mu}$$

Where x is the amplitude at each frequency sample and μ the mean amplitude calculated within the 25 samples before and after the frequency of interest (or its harmonic)(Jonas *et al.*, 2016).

Response amplitude quantification

Amplitudes at the fundamental and at their different respective harmonics (until the seventh for the base frequency $7f_{base}$ = 41.15 Hz, and until the fourteenth for the oddball frequency $14f_{oddball}$ = 14 f_{base} / 5 = 16.46 Hz considered as all significant harmonics (Rossion *et al.*, 2015)) were summed to quantify the response's amplitude.

Region Of Interest (ROI) selection

For statistical comparison, regions of interest (ROI) were selected following the same selection from studies with the same channel configuration (Alonso-Prieto et al., 2013; Rossion et al., 2012b; Rossion and Boremanse, 2011) wich are EEG electrodes of the right occipito-temporal area: PO8, P10, P8, P6.

Individual EEG electrodes were averaged across subjects and topographical maps were plotted with Brainstorm (Tadel *et al.*, 2011).

For statistical comparison, amplitudes measured on EEG electrodes within ROIs for all subjects were compared between phases with a Friedman's statistical test where the null hypothesis H_0 was that the amplitudes measured in each phase come from the same population. H_0 was rejected when $p < 0.05$.

Then, amplitude and SNR values on individual EEG electrodes within ROI were averaged. Next, ROIs were averaged across patient. Standard error (SE) for each phase was calculated as follow:

$$SE = \frac{\sigma}{\sqrt{n}}$$

Where σ is the standard deviation calculated on electrodes within the ROI across subjects and n the number of observations (number of EEG electrodes within the ROI times the number of subjects). Amplitude across patient for ROIs were plotted.

Percentage of amplitude difference between phases was calculated as follow:

$$\%modulation = \frac{\mu_n - \mu_m}{\mu_m} 100$$

With μ the mean amplitude calculated within the ROI across subjects during the phase n and m.

III. Results

1. Intracerebral investigation

Subjects had a total of 1,093 intracerebral contacts (mean of 156 ± 21 contacts per subjects). A total of 568 contacts sampled the two ROI: 80 sampling the VOT area (40 in each hemisphere), 245 and 243 sampling the left and right TL, respectively. Three subjects received anodal tDCS and the three others received cathodal tDCS.

As expected, all subjects felt a mild ticklish sensation during sham and stimulation.

a. At the oddball frequency (1.176 Hz)

Cathodal sub-group

At the oddball frequency, for the cathodal sub-group a total of 80 intracerebral contacts exhibited a significant face selective response (Z-score > 3.1) during, at least, one phase (i.e., before or during or after): Thirty-one (31) in the ipsilateral VOT, 9 in the ipsilateral TL and 40 in the contralateral TL.

Face selective responses' amplitudes did not change significantly across phases in any ROIs, even though an increase (non-significant p = 0.61 between Phase 1 and Phase 2, p = 0.47 between Phase 1 and Phase 3, p = 0.96 between Phase 2 and Phase 3) is noticeable within the temporal lobe (Figure 73) (where was the anode). In the ipsilateral TL, amplitudes, and standard error (SE) went from 2.01 ± 0.52 (SE) µV to 3.36 ± 0.68 (SE) µV and 4.53 ± 1.05 (SE) µV, during Phase 1 (before tDCS), Phase 2 (during tDCS) and Phase 3 (after tDCS) respectively (Figure 73). In parallel, a decrease during tDCS is noticeable within the contralateral TL (Figure 73). Indeed, amplitudes in this ROI went from 3.20 ± 0.31 (SE) µV to 2.52 ± 0.35 (SE) µV during Phase 1 and Phase 2 respectively, and back to 2.83 ± 0.42 (SE) µV during Phase 3.

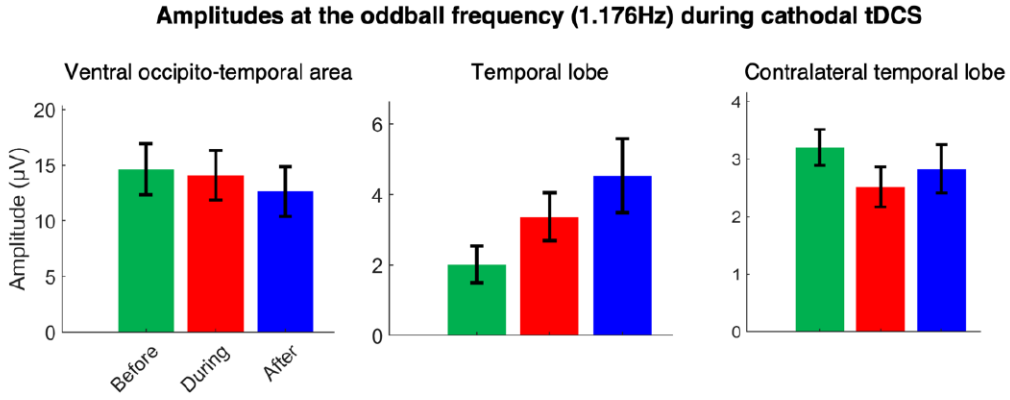

Figure 73: Face selective response amplitudes (± SE) at the oddball frequency (1.176 Hz) in each ROI for the cathodal sub-group. All phases are represented: green: Phase 1 before tDCS, red: Phase 2 during tDCS and blue: Phase 3 after tDCS.

Anodal sub-group

At the oddball frequency, for the anodal sub-group a total of 43 intracerebral contacts exhibited a significant face selective response (Z-score > 3.1) during, at least, one phase: Nineteen (19) in the VOT, 14 in the ipsilateral TL and 10 in the contralateral TL.

Face selective response amplitudes did not change significantly in any ROIs, even though a decrease (non-significant p = 0.20 between Phase 1 and Phase 2, p = 0.06 between Phase 1 and Phase 3, p = 0.84 between Phase 2 and Phase 3) is noticeable within the temporal lobe (Figure 74) (where the cathode is located). In this ROI, amplitudes went from 5.01 ± 1.04 (SE) µV to 2.40 ± 0.52 (SE) µV and 2.14 ± 0.40 (SE) µV, during Phase 1, Phase 2, and Phase 3 respectively. Also, slight decreases but

less obvious are noticeable during and after tDCS within the VOT area and the contralateral TL (Figure 74). Indeed, amplitudes in these ROIs went from 12.06 ± 2.28 (SE) µV to 10.56 ± 2.26 (SE) µV and 10.70 ± 2.06 (SE) µV during Phase 1, Phase 2, and Phase 3 respectively in the VOT area, and from 3.87 ± 0.90 (SE) µV to 3.36 ± 0.91 (SE) µV and 3.46 ± 1.10 (SE) µV during Phase 1, Phase 2, and Phase 3 respectively in the contralateral TL.

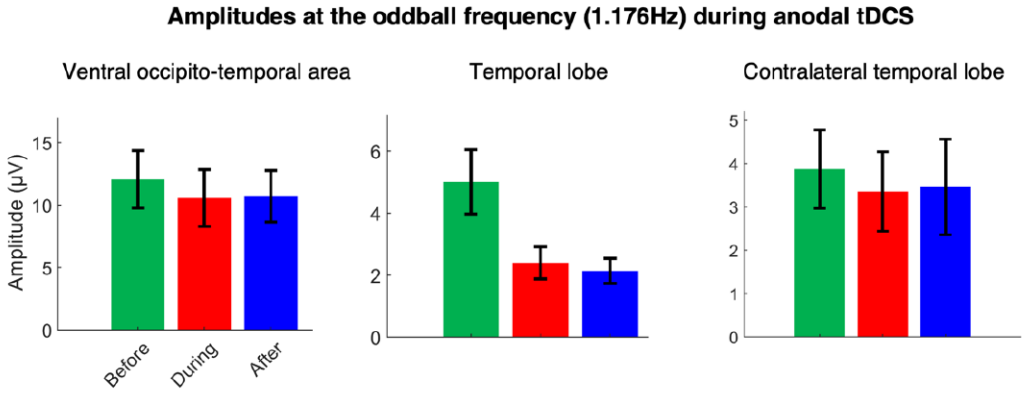

Figure 74: Face selective response amplitudes (± SE) at the oddball frequency (1.176 Hz) in each ROI for the anodal sub-group. All phases are represented: green: Phase 1 before tDCS, red: Phase 2 during tDCS and blue: Phase 3 after tDCS.

b. At the base frequency (5.88 Hz)

Cathodal sub-group

At the base frequency, for the cathodal sub-group a total of 137 intracerebral contacts exhibited a significant low level visual response (Z-score > 3.1) during, at least, one phase: Thirty-one (31) in the VOT, 30 in the TL and 76 in the contralateral TL.

Visual response amplitudes during Phase 3 were significantly ($p < 0.05$) lower within the contralateral temporal lobe with values varying from 1.13 ± 0.10 (SE) µV to 0.73 ± 0.10 (SE) µV between Phase 1 and Phase 3 which represent a difference of − 0.39 µV (− 35 %) and from 1.16 ± 0.12 (SE) µV to 0.73 ± 0.10 (SE) µV between Phase 2 and Phase 3 which represent a difference of − 0.43 µV (− 37 %). Also, a slight but non-significant decrease is noticeable within the VOT area with amplitudes varying from 3.86 ± 0.60 (SE) µV to 3.22 ± 0.57 (SE) µV between Phase 1 and Phase 2 ($p = 0.08$) and from 3.86 ± 0.60 (SE) µV to 3.33 ± 0.55 (SE) µV between phase 1 and Phase 3 ($p = 0.64$).

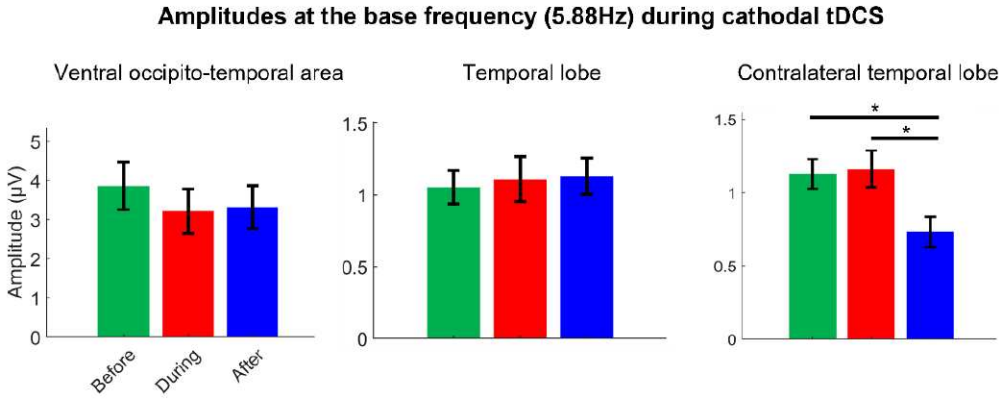

Figure 75: Face selective response amplitudes (± SE) at the base frequency (5.88 Hz) in each ROI for the cathodal sub-group. All phases are represented: green: Phase 1 before tDCS, red: Phase 2 during tDCS and blue: Phase 3 after tDCS. Significant signs: $p < 0.05$ Friedman's test.

Anodal sub-group

At the base frequency, for the anodal sub-group a total of 91 intracerebral contacts exhibited a significant low level visual response (Z-score > 3.1) during, at least, one phase: Twenty-five (25) in the VOT, 13 in the TL and 53 in the contralateral TL.

Amplitudes decrease continuously from Phase 1 to Phase 3 in all ROIs. Noticeably, significant amplitude reduction ($p < 0.05$) occurred in all ROIs between Phase 1 and Phase 3 with values varying from 3.88 ± 0.61 (SE) µV to 2.40 ± 0.57 (SE) µV in the VOT area, from 1.99 ± 0.42 (SE) µV to 0.11 ± 0.09 (SE) µV in the ipsilateral TL and 1.70 ± 0.19 (SE) µV to 0.61 ± 0.11 (SE) µV in the contralateral TL. This represents a decrease of − 1.47 µV (− 38 %), − 1.89 µV (− 95 %), − 1.08 µV (− 64 %) in the VOT area, TL, and contralateral TL, respectively (Figure 76).

Also, in the VOT area the amplitudes decrease significantly between Phase 2 and Phase 3 by − 0.52 µV (− 18 %). Then, within the contralateral TL, amplitudes decrease significantly between Phase 1 and Phase 2 by − 0.85 µV (− 50 %). In the TL, there is no significant difference between Phase 1 and Phase 2 ($p = 0.08$) or between Phase 2 and Phase 3 ($p = 0.08$) but still shows a noticeable drop of − 1.26 µV (− 63 %) and − 0.63 µV (− 85 %) between Phase 1 and Phase 2 and between Phase 2 and Phase 3, respectively (Figure 76).

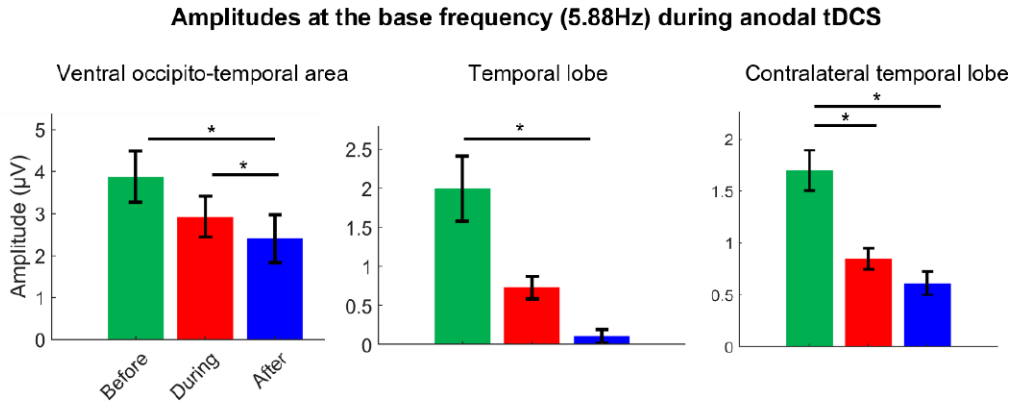

Figure 76: Face selective response amplitudes (± SE) at the base frequency (5.88 Hz) in each ROI for the anodal sub-group. All phases are represented: green: Phase 1 before tDCS, red: Phase 2 during tDCS and blue: Phase 3 after tDCS. Significant signs: $p < 0.05$ Friedman's test.

2. Surface EEG investigation in healthy subjects

a. At the oddball frequency (1.176 Hz)

Cognitive responses of face perception and identity discrimination before tDCS exhibited a topographical distribution on the right occipito-temporal area as expected (Figure 77).

Amplitude study

Mean amplitudes before tDCS in face selective ROI were 1.97 ± 0.17 (SE) µV, 0.7 1± 0.09 (SE) µV and 0.25 ± 0.06 (SE) µV for Faceloc, Idedis upright faces and Idedis inverted faces respectively at the oddball frequency (1.716 Hz) (Figure 78). Amplitude at the oddball frequency during tDCS exhibited a statistically significant difference ($p < 0.05$) with, at least, one phase (before or after) when Idedis paradigm was presented (Figure 78).

For the Idedis paradigm during tDCS, amplitudes at the oddball frequency were 0.48 ± 0.11 (SE) µV and 0.02 ± 0.08 (SE) µV for upright and inverted faces, respectively. Thus, both upright and inverted face paradigms of identity discrimination had an amplitude decrease of − 0.23 µV during tDCS which was statistically significant only for upright faces (decrease of − 32 %) (Figure 78 and Figure 79**A**). When comparing during and after tDCS, the amplitude increased significantly by 0.43 µV (increase of 89 %) and 0.29 µV (increase of 1782 %) for upright and inverted faces, respectively (Figure 78 and Figure 79**B** and **C**). There were no statistically significant differences between before and after tDCS.

Signal noise ratio (SNR) study

SNR decreased significantly by − 17 % during tDCS for Faceloc. There was a significant SNR increase of 14 % between before and after tDCS for Idedis upright only. SNR increased also significantly between during and after tDCS by 17 % and 26 % for Faceloc and Idedis upright, respectively.

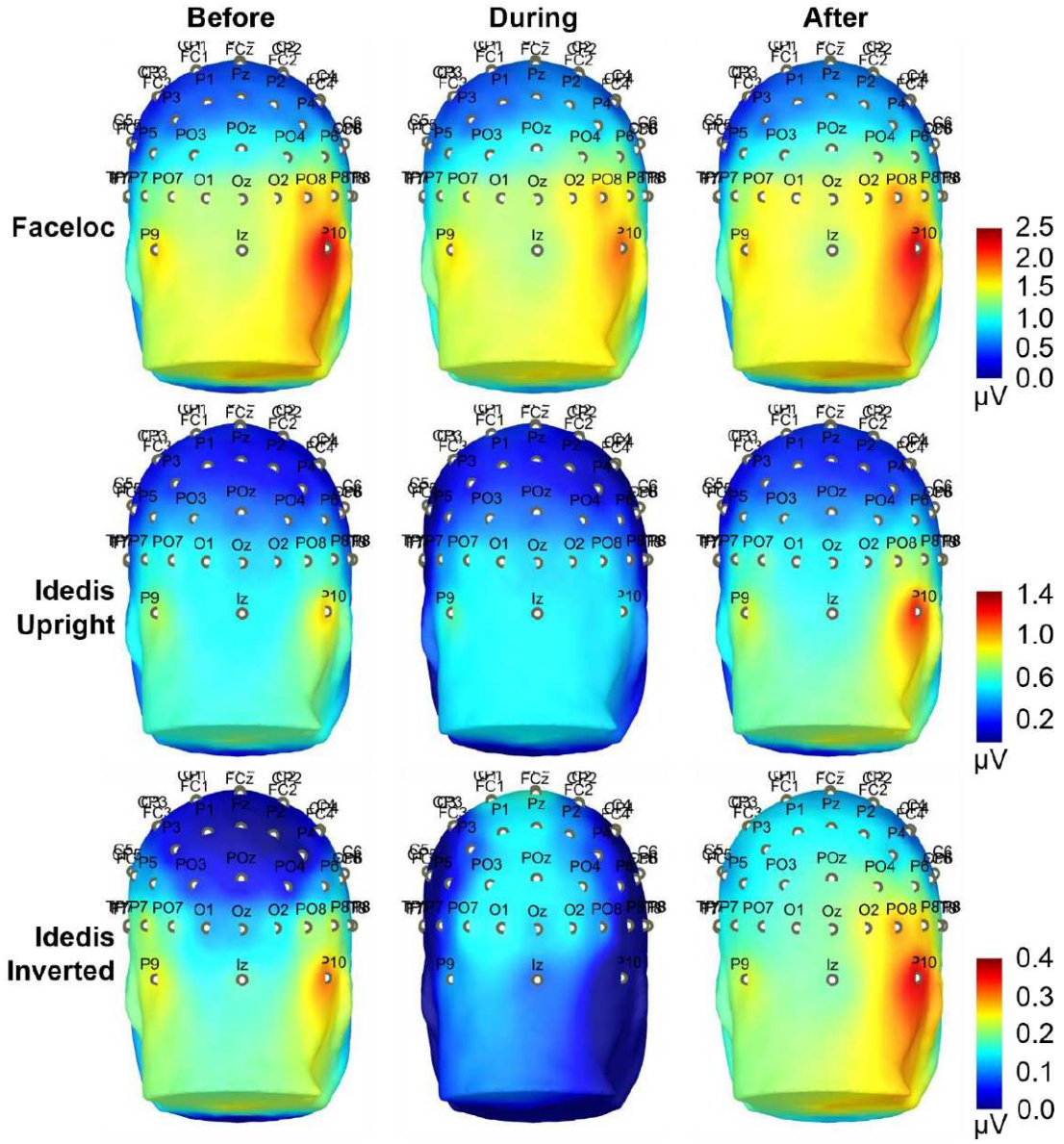

Figure 77: Topographical maps of the cognitive responses' amplitude averaged across subjects for face perception (Faceloc) and identity discrimination (Idedis upright and inverted faces) (second and third rows) at the oddball frequency (1.176 Hz). Each column represents a phase: before, during and after tDCS. Before tDCS topographical distribution were, as expected, mainly localized in the right occipital area.

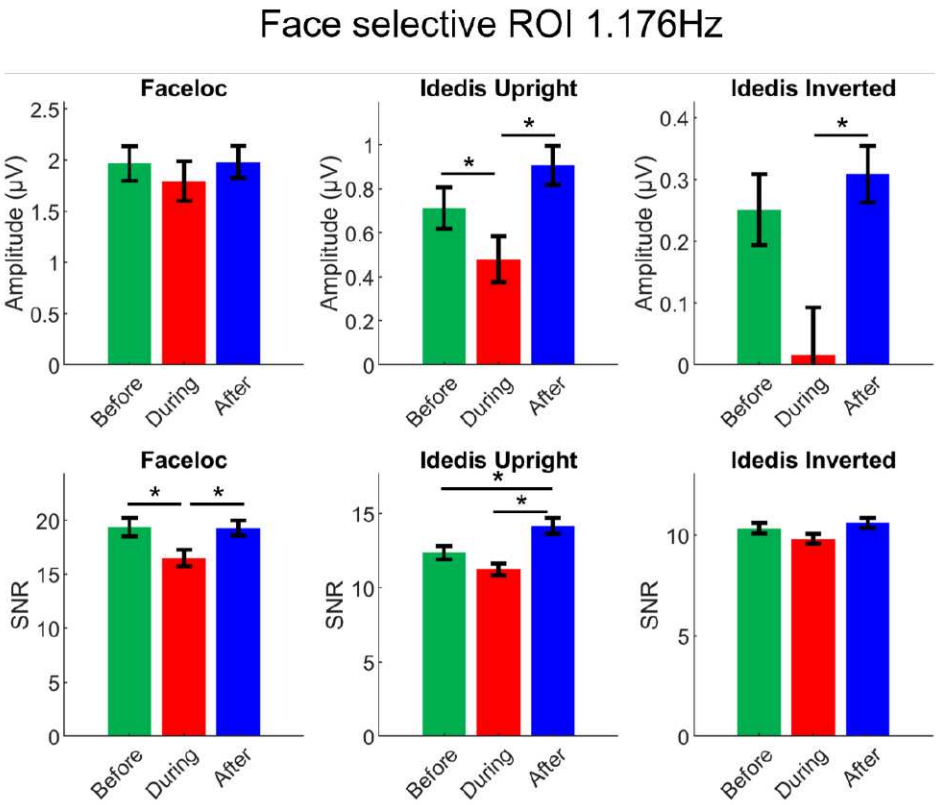

Figure 78: Amplitudes (first row) and SNR (second row) values within the face selective ROI across subjects at the oddball frequency (1.176 Hz). Colors represent experimental phases: green: Phase 1 before tDCS, red: Phase 2 during tDCS and blue: Phase 3 after tDCS. Significant signs: $p < 0.05$ Friedman's test.

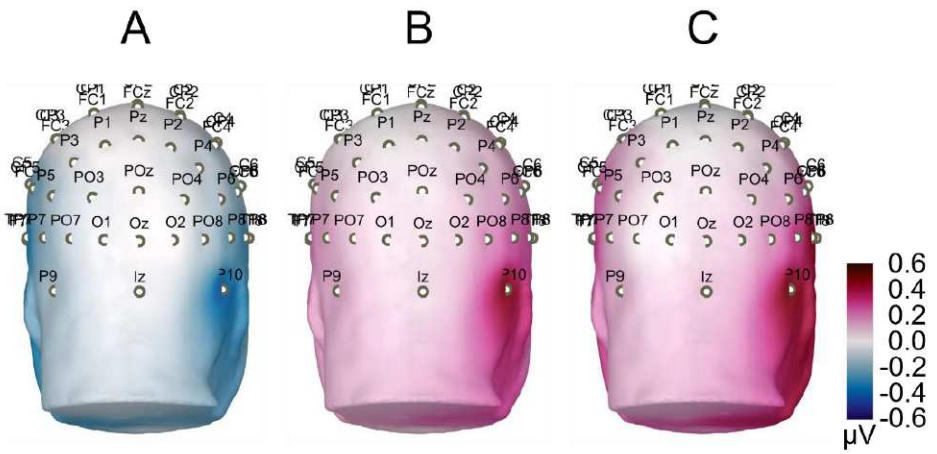

Figure 79: Topographical map of amplitude subtraction between phases at the oddball frequency (1.176 Hz). Only significant differences are shown. **A**: amplitude difference between before and during tDCS when Idedis with upright faces was presented. **B** and **C**: amplitude difference between during and after tDCS when Idedis with upright (**B**) and inverted (**C**) faces were presented.

b. At the base frequency (5.88 Hz)

Basic visual responses before tDCS exhibited a topographical distribution on the occipital area as expected (Figure 80) with a small predominance on the right when identity discrimination (Idedis) paradigms were presented.

Amplitude study

Mean amplitudes before tDCS in face selective ROI were 1.25 ± 0.13 (SE) µV, 1.05 ± 0.10 (SE) µV and 0.78 ± 0.09 (SE) µV for Faceloc, Idedis upright and inverted faces respectively at the base frequency (5.88 Hz) (Figure 81). Amplitude at base frequency during tDCS exhibited a statistically significant difference ($p < 0.05$ Friedman's test) with, at least, one phase (before or after) when Faceloc and Idedis inverted faces were presented.

For Faceloc and Idedis (inverted faces only) paradigms during tDCS, amplitudes at the base frequency were 1.46 ± 0.14 (SE) µV and 0.94 ± 0.09 (SE) µV, respectively (Figure 81). This represents a significant increase of 0.21 µV (17 %) and 0.16 µV (20 %) during tDCS for Faceloc and Idedis (inverted faces only), respectively (Figure 82 **A** and **C**). When comparing during and after tDCS, the amplitude decreases significantly by − 0.22 µV (− 24 %) for Idedis (face inverted only) (Figure 82**D**). When comparing before and after tDCS there was a significant amplitude increase of 0.18 µV (14 %) for Faceloc paradigm only (Figure 82**B**).

SNR study

Interestingly, SNR during tDCS was significantly higher than before tDCS by 25 % and 23 % for Faceloc and Idedis respectively. Also, SNR during tDCS was significantly higher than after tDCS by 14 %, 19 % and 24 % for Faceloc, Idedis upright and inverted, respectively.

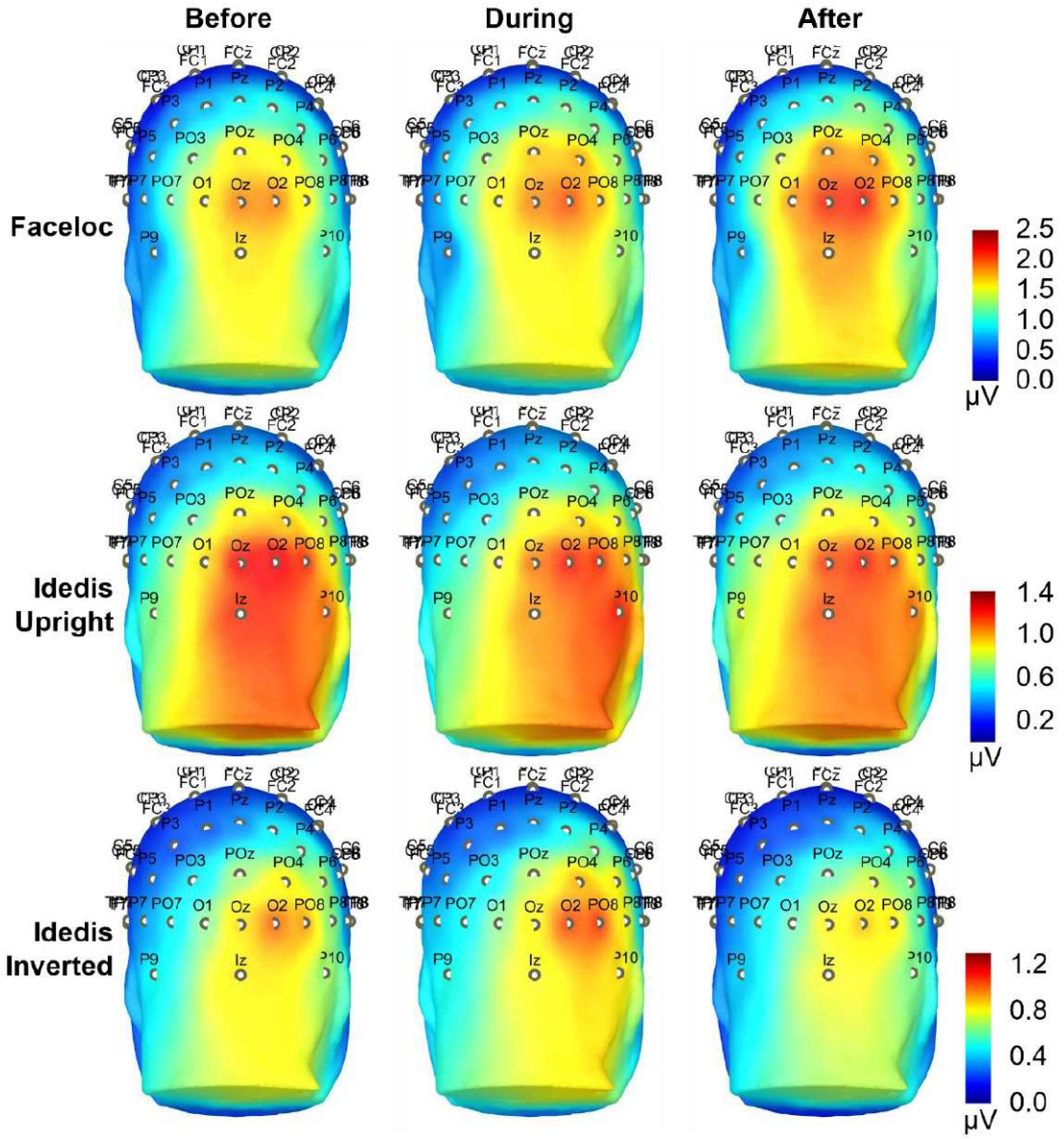

Figure 80: Topographical maps of the basic visual responses' amplitude averaged across subject for face perception (Faceloc) and identity discrimination (Idedis upright and inverted faces) (second and third rows) at the base frequency (5.88 Hz). Each column represents a phase: before, during and after tDCS.

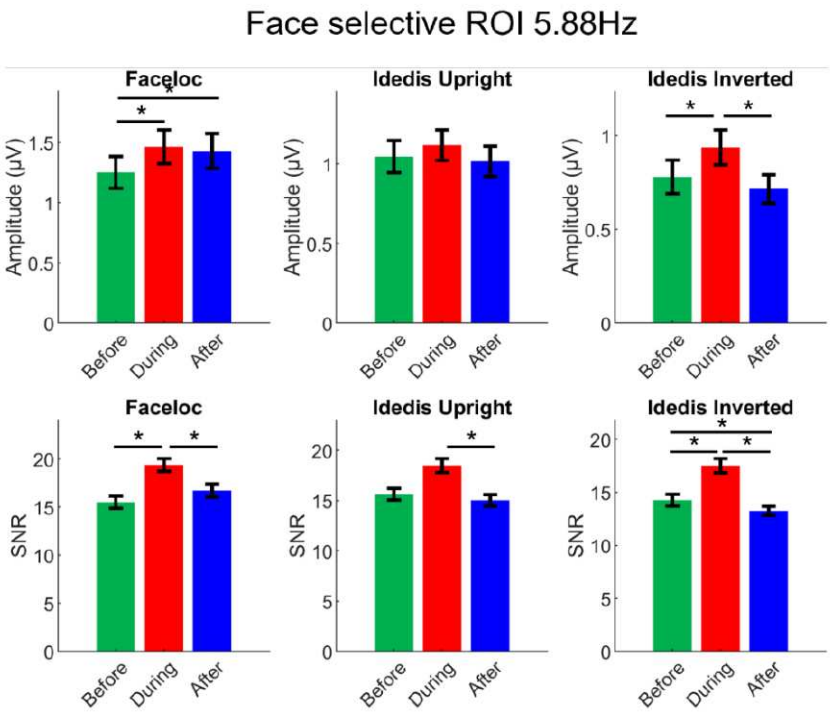

Figure 81: Amplitudes (first row) and SNR (second row) values within the face selective ROI across subjects at the base frequency (5.88 Hz). Colors represent experimental phases: green: before tDCS, red: during tDCS and blue: after tDCS. Significant signs: $p < 0.05$ Friedman's test.

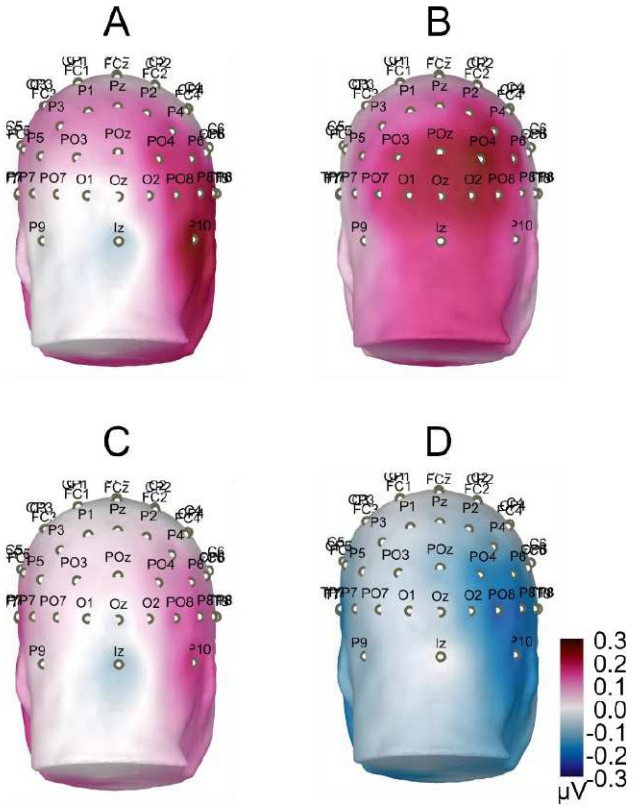

Figure 82: Topographical map of amplitude subtraction between phases at the base frequency (5.88 Hz). Only significant differences are shown. **A** and **B**: amplitude difference between before and during (**B**) tDCS and between before and after (**C**) tDCS when Faceloc was presented. **C** and **D**: amplitude difference between before and during (**C**) tDCS and between during and after (**D**) tDCS when Idedis with inverted faces was presented.

IV. Conclusion and discussion

This study was the first to combine tDCS and FPVS at a multi-scale level (intracerebral and scalp) and shows that there are significant differences of cognitive responses amplitudes before, during and after tDCS.

Intracerebral investigation showed that low level cognitive responses only (visual responses) are systematically and significantly modulated after an anodal tDCS in all ROI studied with a maximum of − 95 %. Cathodal stimulation also exhibits a possible influence on the ROI by showing a modulation within the contralateral temporal lobe up to − 37 %. This quasi-systematical modulation of low-level visual functions are in line with previous studies showing the same result during tDCS (Antal, Kincses, *et al.*, 2004; Stagg, Antal and Nitsche, 2018).

While the findings from the intracerebral study might suggest that only low-level responses can be modulated by tDCS, surface EEG investigation suggests otherwise by adding further information regarding the modulation of some high-level responses. Indeed, by exploring other cognitive tasks such as identity discrimination, a modulation on surface EEG is observed during tDCS for this specific task. We can easily be led to think that there are only certain high level cognitive processes affected by tDCS such as face discrimination rather than face perception. If it were the case, tDCS would have reduced only the amplitude for upright faces and not for inverted faces. Indeed, it is known that the inverted face paradigm drastically alters the holistic representation and forces the brain to analyze face's differently (by taking features individually (nose, mouth, eyes *etc.*)) (Rossion, 2008, 2009; Liu-Shuang, Norcia and Rossion, 2014). Therefore, instead of modulating a specific cognitive function, tDCS would rather induces effect depending on the amplitude generated by the high-level cognitive task response: lower is the amplitude, stronger the modulation would be.

Even though behavioral effect wasn't measured in the present study, it is safe to say that behavior wasn't affected at a significant level. What behavior would induce a few more micro-volts during tDCS? Will the subject be able to "better recognize" a face or an identity? Would an amplitude decrease generate a transient loss of cognitive functions? It is hard to answer positively. To illustrate, transient prosopagnosia (the inability to recognize a face) was induced by intracerebral electrical stimulation of the face sensitive area with an intensity from 1 to 1.8 mA applied directly on the cortical area (through 2 adjacent SEEG contacts) (Jonas et al. 2012). Intensities generated by tDCS on the cortex are far from the mentioned quantities and couldn't induce any direct behavioral impairment at 2 mA on the scalp. But tDCS-induced modulation showed in the present study could induce second plan modulation by stochastic phenomenon (e.g. effect involving memory encoding).

In the literature, some articles concluded that cathodal tDCS lowers amplitudes and anodal tDCS increases it. The findings presented in this chapter could raise a more complex question which

can challenge the well-established belief of anodal/cathodal dichotomy already pointed out by other studies in the past (Batsikadze *et al.*, 2013; Bestmann, de Berker and Bonaiuto, 2015). In the present study, intracerebral results show that anodal stimulation systematically lowers the low-level visual response amplitudes but from a surface EEG point of view, and the same response is raised. First, these results could suggest that tDCS effects depends on the depth which has been theorized by Das et al. (2016) and it would be interesting to empirically investigate this point in futures studies which will be further discussed in the next chapter. Secondly, it highlights the difference between intracerebral and surface investigation which is, sometimes, difficult to put in relation (Jacques *et al.*, 2019, 2020). Amplitudes collected on surface EEG give a global view of the wide-spread network involved in the cognitive process whereas activity measured on intracerebral contacts give information only on an isolated part of this network. Therefore, measured effects induced by tDCS would be different regarding the investigation technique. This might also highlight the difference in terms of cognitive processes between epilepsy and healthy subjects which may give two different results and, therefore, two different conclusions. These differences are the first limitation of this study: the intracerebral and surface investigations didn't include the same population. Futures studies should include EEG studies with epileptic patients before SEEG implantation using the same paradigm, montage, stimulation intensity and polarity. Then, thanks to multi-scale recording performed in Nancy (concomitant surface and intracerebral EEG recording) it would be possible to repeat the protocol. That way, amplitudes will be measured before and during SEEG implantation increasing robustness and conclusions strength.

The second limitation is the number of subjects included in the intracerebral investigation given the recent sanitary context and the scarcity of occipito-temporal implantation (with SEEG electrode sampling the fusiform gyrus).

Still, this is proof of concept that activity recorded from robust cognitive paradigm of FPVS can be modulated during and after tDCS. These results should encourage further studies in the field of cognition and clinical application of cognitive rehabilitation with TES.

Chapter V:
General conclusions & discussions

I. On the electric field generated in the brain

1. Reaching an intense electric field…

To recall, the purpose of this study was to answer the question: "is it possible to measure a sufficient electric field in human in-vivo during a transcranial electrical stimulation?" which was the very first essential step before investigating potential effects induced by TES. Indeed, this question was fundamental, and the answers constituted the cornerstones of this thesis constraining the direction took in the presented research work. The main findings showed an electric field superior or equal to 0.14 $V \cdot m^{-1}$ achievable in the limbic system for a 1 mA tACS. These findings have been recently confirmed at a larger scale (Wang *et al.*, 2022). This value of 0.14 $V \cdot m^{-1}$ is the lower bound of electric field influence on neural activity (Francis, Gluckman and Schiff, 2003) and effects that may ensue are qualified as stochastic (Liu *et al.*, 2018) or as Stochastic resonance ("injection of subthreshold noise into a system can serve to enhance signal detection") (Stacey and Durand, 2000; van der Groen and Wenderoth, 2016; Fertonani and Miniussi, 2017). Among the community, an electric field of 1 $V \cdot m^{-1}$ is generally considered as a critical value inducing an effect 100 % of the time based on the works of Terzuolo and Bullock (1956). From the electric field values presented in chapter II and their relationship to the stimulation intensity (almost perfectly linear), it would be possible to get closer to 1 $V \cdot m^{-1}$ in the limbic system by multiplying the stimulation intensity by 5 or 6.

2. … At what price?

However, the quest to 1 $V \cdot m^{-1}$ in deep brain structure comes with a price and raises other questions concerning, for example, the intensity of the electric field on neighboring structures or on the cortex, and the cutaneous pain (patient's tolerability) during stimulation at such high intensities. TES safety and tolerability has been assessed at 4 mA (Nitsche and Bikson, 2017), 10 mA (Kunz *et al.*, 2017) and higher intensities (Paneri *et al.*, 2016). Two of the mentioned studies (Paneri *et al.*, 2016; Kunz *et al.*, 2017) had to use high frequency alternating or pulsed current to minimize skin pain (as described Antal et al. (2017)) and one reported that DC stimulations induces more adverse effects (Paneri *et al.*, 2016). Another important parameter to optimize high-intensity 2-electrode TES is the stimulated surface area. It has been demonstrated computationally that the bigger the stimulation surface is, the deeper the electric field penetrates (Faria, Leal and Miranda, 2009; Miranda, Faria and Hallett, 2009; Faria, Hallett and Miranda, 2011) and milder is the skin sensation due to lower current density applied (Minhas, Datta and Bikson, 2011). Knowing that the tolerability question of conventional TES at high intensity has been explored, what about iEF strength generated on the cortex while targeting deep brain structures? To date, as far as I know, there is no human *in-vivo* study assessing this question. Therefore, basic multiplication of TES intensities, to reach 1$V \cdot m^{-1}$ in deep structures, could generate unwanted neuromodulation of neighboring structures.

3. Other ways to attempt generating a strong intracerebral electric field and overcoming adverse effects

Some studies have developed other ways to generate a focal iEF on target such as HD-TES theorized by Dmochowski *et al.*, (2011) and others (Edwards *et al.*, 2013; Ruffini *et al.*, 2014) focusing iEF on cortical surfaces by the mean of stimulation currents summation through several small electrodes (the same size used in this thesis). Then HD-TES became mainly known through one aspect of it: the use of the "4×1 montage" where one active electrode is surrounded by four return electrodes placed at an equal distance to each other. But another interesting HD-TES approach has been studied notably by leveraging on the reciprocity principle introduced by Helmholtz in 1853. With this approach, in theory, it would be possible to target with HD-TES an intracerebral electrical source detected on surface EEG. Indeed, the current path taken from the intracerebral source to the EEG electrodes is the same than the one from TES electrodes to the source (Rush and Driscoll, 1969). With this statement, the idea of naively reinjecting back the current detected on surface EEG has been studied by some teams (Cancelli *et al.*, 2016; Fernández-Corazza *et al.*, 2016). However, this naive implementation of reciprocal stimulation failed to deliver an intense and focal electric field on target. To overcome the spatial blurring, Dmchowski and colleagues (2017) proposed a new mathematical solution, based on their previous fundamental work (Dmochowski *et al.*, 2011), to generate a focal electric field at an intensity 163 % higher than the naive reciprocity (Figure 83 (Dmochowski *et al.*, 2017)). Even though optimized reciprocity generates an electric field more intense than the naive reciprocity, the main limitation of HD-TES is the tradeoff between focality, intensity and depth which is impossible to obtain altogether (Dmochowski, Bikson and Parra, 2012; Huang and Parra, 2019).

Temporal interference (TI) stimulation re-introduced by (Grossman *et al.*, 2017) proposes an elegant way to generate a deep, strong, and focal electric field in the brain. Its principle is based on the generation of two different kHz tACS, resulting in an amplitude modulated signal (AM) when the two currents overlap in brain depth (Figure 84). The high frequency would reduce skin sensation and would not induce any neuronal effect on lateral structures due to brain tissue low-pass behavior. The signal generated in the depth, however, has a low frequency envelope which could induce neural effects on site only (Figure 84). The elegance of this approach led to a certain excitement toward the method and maybe prompt conclusions. In fact, mitigated results deriving from computational, and animal studies are presented and highlight the need for empirical results from intracerebral Human *in-vivo* studies (Cao and Grover, 2018; Vöröslakos *et al.*, 2018; Rampersad *et al.*, 2019; Mirzakhalili *et al.*, 2020; Esmaeilpour *et al.*, 2021; Howell and McIntyre, 2021). One future perspective would address iEF generated by the mentioned methods by using the intracerebral methodology presented in this thesis.

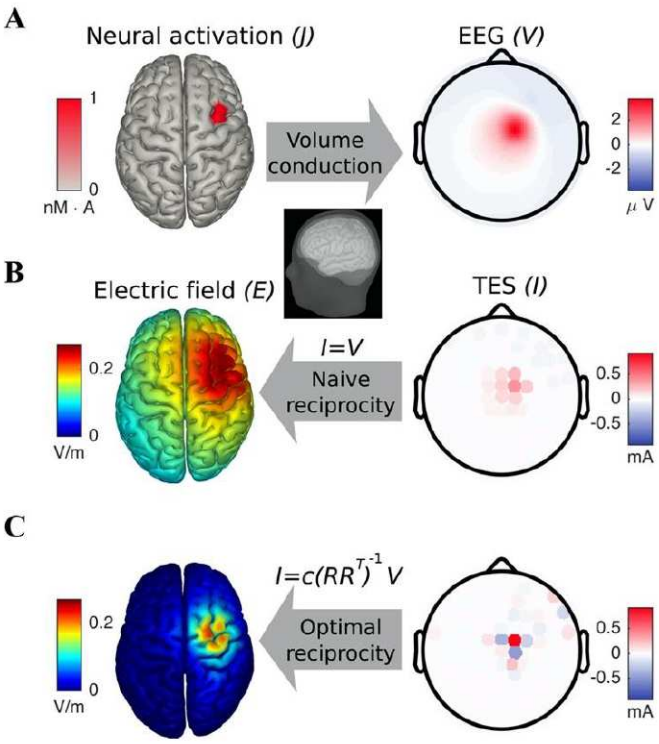

Figure 83: From Optimal use of EEG recordings to target active brain areas with transcranial electrical stimulation. *NeuroImage*, *157*(May), 69–80 by Dmochowski, J. P., Koessler, L., Norcia, A. M., Bikson, M., & Parra, L. C. (2017). under the CC BY-NC-ND license. Reciprocal stimulation. (A) Focal neural activation of the right frontocentral cortex produces a radially symmetric pattern of electric potentials on the scalp. (B) By patterning the stimulation currents according to the observed scalp activity, "naive" reciprocity generates a diffuse electric field that is strong at the site of activation but also over expansive regions of cortex. (C) Applying TES in proportion to the spatially decorrelated EEG.

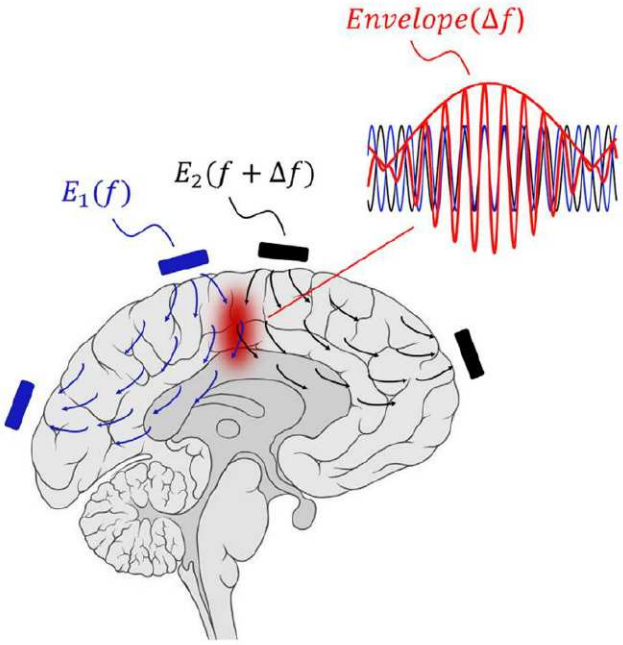

Figure 84: Temporal interference stimulation from Grossman *et al.*, (2017) under **CC-BY-4.0** license. Two couples of electrodes inject an alternative current at a frequency f (tACS electrodes in blue) and at $f + \Delta f$ (tACS electrode in black) resulting into an amplitude modulated (AM) electric field at the overlapping point (Envelop Δf).

4. The question of the frequency

Temporal interference stimulation usually uses frequencies in the kHz range. But a recurrent topic in TES and or EEG/SEEG recordings is the signal attenuation as a function of the frequency. The pioneer works of Gabriel et al., (1996) show in *ex-vivo* tissues a frequency-dependance of the permittivity and conductivities notably in brain tissues. Then, temporal interferences can be challenged and even some conventional tACS performed in the literature (40 Hz, 80 Hz,140 Hz or even 250 Hz (Moliadze, Antal and Paulus, 2010; Moliadze *et al.*, 2012; Antal *et al.*, 2017; Krause *et al.*, 2019; Jones *et al.*, 2020)) could raise questions about the penetration of such frequencies while it has been demonstrated that brain tissues don't act as a purely resistive medium. On the other hand, *Vöröslakos et al.*, (2018) showed, in their *post-mortem* study that frequency under 1 kHz might have a negligible impact on the intracerebral electric field generated. Of course, knowing their limitations (Opitz *et al.*, 2017) these *ex-vivo* statements needed to be found in Human *in-vivo*. With this aim, this thesis presented the first quantification of frequency dependency on intracerebral electric field and the presented results showed that the frequency has, indeed, a negligible impact which was then confirmed later in a recent study (Wang *et al.*, 2022). Therefore, it is possible to state that brain tissues can be considered as a purely resistive medium for TES at frequencies below 1 kHz.

5. The limitation of intracerebral investigation (SEEG)

Despite the numerous advantages of SEEG such as being mini-invasive or its good space (in depth only) and time resolution, some limitations remain. The first one is related to the voltage measurement and iEF calculation which was done along SEEG electrode's orientation only. Even though iEF magnitudes from full tensor calculation were not statistically different from the measured ones (along the SEEG electrode orientation), the full tensor still relies on amplitudes' gross interpolation done on scattered values whose spacing varies a lot. Indeed, intracerebral contact distribution within the volume is non-homogeneously distributed and depends on the implantation: for a temporal lobe implantation, scattered values' spatial distribution would be denser along the right-left orientation than along the antero-posterior orientation, leading to a less precise approximation along the latter. Reasoning by *reductio ad absurdum*, there is a need of a 3D grid of equally spaced measurement points within the entire brain parenchyma which would make a perfect configuration to investigate electric field in all direction. This configuration is, of course, impossible in *in-vivo* brains.

Even though SEEG is less traumatic and invasive than ECoG, it still requires a surgical intervention and modifies the head surface geometry, conductivities and the intracerebral medium (a foreign body in the brain parenchyma). Concerning the head surface geometry and conductivities, special attention has been paid to put TES far from the implantation site to avoid modification in the current flow as it was discussed in Chapter II (Datta, Bikson and Fregni, 2010). Concerning the intracerebral medium, the presence of SEEG electrodes may alter the electric field distribution due to

their shape-related behavior: if an SEEG electrode is put inside a uniformly distributed electric field, the alternating disposition of conducting (higher conductivity) and insulating (lower conductivity) materials will create interferences in the electric field lines. These interferences will result in an increase of electric field magnitude at the edges of the electrode's conductive parts (edge effects) and create a wavy electric field distribution (Figure 85). Finally, only focal refractory epilepsy patients can be included in SEEG procedures, and it is known that some discrepancies exist in brain conductivity within specific area such as the epilepsy foci (Koessler *et al.*, 2017).

Despites the weaknesses mentioned, SEEG is still, for now, the most optimal solution for intracerebral electric field investigation.

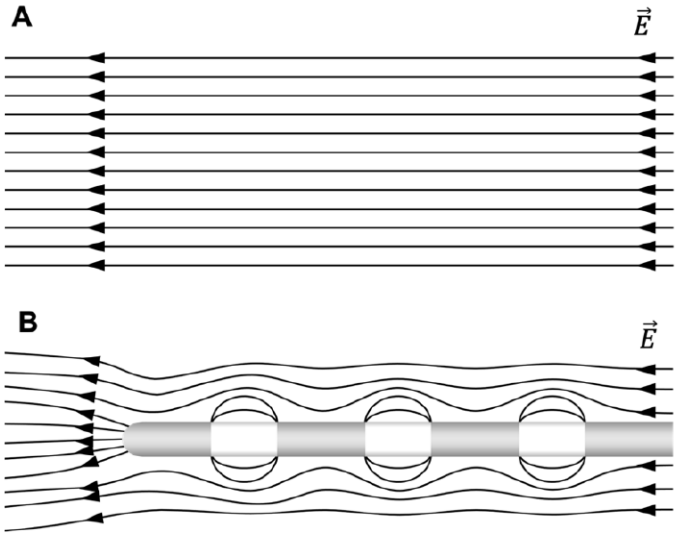

Figure 85: Schematical representation of a uniform electric field without (**A**) and with an SEEG electrode within (**B**). Electric field lines are bent as a function of the material conductivity: inward when the conductivity is higher (conductive parts in gray), outward when the conductivity is lower (insulating part in white).

6. Future perspective to investigate the intracerebral electric field generated during a TES

The next step for measuring TES-induced electric field in human brain in-vivo is without interfering with the intracerebral medium. One interesting way to do it is by using MR imaging/spectroscopy. The most known way is to leverage on Magnetic Resonance Electrical Impedance Tomography (MREIT) to measure (1) brain tissues conductivities σ, (2) the magnetic flux density distribution during TES and then reconstructing current density j. Then, with those two quantities, the electric field E can be calculated ($E = \sigma j$) (Kwon *et al.*, 2016; Kasinadhuni *et al.*, 2017; Chauhan *et al.*, 2018; Lee *et al.*, 2018; Sajib *et al.*, 2021). Other studies rely on MRI field mapping to detect the magnetic field generated by a tDCS (Jog *et al.*, 2016, 2020) and include simultaneous BOLD signal measurement which give the unique opportunity to quantify directly and concurrently tDCS-induced electric field and its related physiological effects in the entire brain. These MRI and MREIT based methodologies offer the possibility to measure (1) in human *in-vivo*, (2) in the

entire brain, (3) along every direction of the electric field generated by a TES and can become the new ground truth upon which models can be validated and/or improved. In addition, individual brain tissues conductivities measured from MREIT can be implemented in realistic modeling workflows and add another level of precision. Also, the possibility to include healthy subjects as well as patients with neurological pathologies would provide groundbreaking knowledge of iEF distribution characteristics during a TES as a function of the presence and the type of pathology. In the same vein we can find the Magnetic Resonance Electrical Properties Tomography (MREPT) which can provide other information such as the conductivities (Zhang, Liu and He, 2014; Soullié *et al.*, 2021).

The MR-based electromagnetic field measurement is mainly limited by the signal artifacts generated by the scanner itself and requires finding a good tradeoff between removing the artifacts by smoothing too much data or keeping the artifacts (Sajib *et al.*, 2021). Also, electric field extraction from these methods is not straightforward, demanding sometimes complex machine learning implementation which may discourage the use of these methods by clinicians. Overall MR-based approaches seem very promising but need wider investigations and improvement for potential larger scale multi-centric studies.

II. On the application of TES (the case of tDCS)

Results from electrophysiological studies in this thesis suggest that tDCS might affect both pathological and physiological activities. Mainly, biomarker amplitudes and/or frequency signature are significantly different during a tDCS compared to a sham session.

However, there is still a long way to go between these results and a precise knowledge of TES' effects to master them and make a solid clinical application.

1. Improving experiment designs

There is a need for further research using intracerebral investigation methods to address tDCS in epilepsy and/or cognition. First, investigations need to be done in a larger cohort to improve the potential statistical significance. Secondly, inclusion criterion needs to be more selective or sub-group studies need to be performed to focus on only one neuropathological condition (only hippocampal sclerosis or cortical dysplasia or lesions). Next, as it was mentioned in previous chapters, experiments need to be improved by performing double-blinded studies.

To study the tDCS effects on interictal epileptiform discharges, the experimental design could be organized into 2 segments: the control segment and the stimulation segment. Control segments would contain 3 blocks of 20 minutes of sham stimulation to obtain an hour of electrophysiological activity used as a control. The stimulation segment would be the 3-blocks protocol already used in the thesis (Phase 1: sham stimulation; Phase 2: tDCS; Phase 3: sham stimulation) and would provide another hour of electrophysiological activity during which a stimulation is done (Figure 86.C). With

this design, it is possible to measure interictal activity fluctuation within an entire hour without stimulation and to compare to the other interictal activity fluctuation during another hour when a 20-minute stimulation is done. Finally, this single-arm study will have to be double-blinded.

However, this experimental design can't be implemented for the study of tDCS effects on an electrophysiological response of cognitive function. Indeed, the time of the experiment is too long to perform cognitive tasks and could induce a fatigue after more than an hour of visual stimulus. Thus, a shorter experiment can be done in a double-blinded two-arm study with an active group and a placebo group. For the active group, the "classic" 3-block protocol already used in the thesis (Phase 1: sham stimulation; Phase 2: tDCS; Phase 3: sham stimulation, Figure 86.A) would be executed, and for the placebo group a 3-blocks protocol with only sham stimulation would be performed (Figure 86.B).

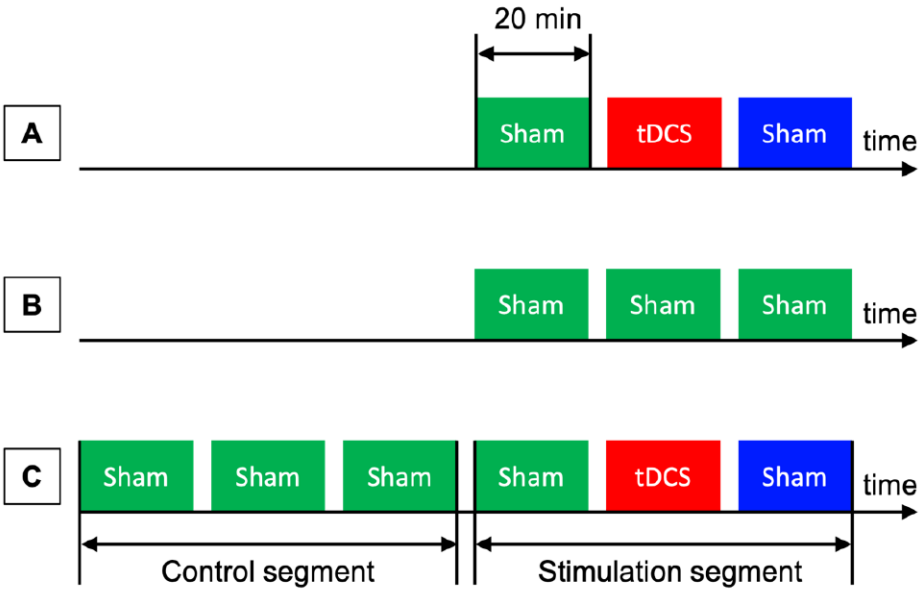

Figure 86: Experimental design to study tDCS effects on electrophysiology. **A.** Experimental design already used in this thesis in the study of epilepsy and cognition. **B.** Experimental design proposed for the placebo group in the case of a two-arm study preferably to investigate tDCS effects on electrophysiological responses of cognitive function. **C.** Experimental design proposed in the case of a single-arm study to investigate tDCS effect on interictal activity.

Because SEEG patients are included for an entire week, another solution would be to perform Fast Periodic Visual Stimulation (FPVS) during days before the tDCS experiment (which usually takes place on Fridays). This will give a better baseline of electrophysiological responses of cognitive functions to compare with those during tDCS.

2. The issue of sham stimulation

A potential weakness is regarding the sham stimulation. It is not adequately discussed in the literature, but an interesting study suggests that "blinding" is compromised because the subject can tell if it is a sham or a real stimulation (Turi *et al.*, 2019). Despite that, sham-controlled studies are still published, and we still consider this configuration a standard. It is a difficult question: how can we obtain a robust control condition? A solution would be to use different waveforms and to compare the differences between them. For instance, in FPVS configuration, sham sessions could be replaced by a tRNS stimulation during visual stimulation. Or we could think about a phase-locked tACS stimulation synchronized with the visual stimulus frequency in phased and/or 180° phase shifted. This has been explored in an article investigating speech comprehension during a tACS performed with different lags, or during anodal and cathodal tDCS (Wilsch *et al.*, 2018). Then, they compared the behavioral response for each stimulation lag and polarity. Despite the main message presented in the article which can be widely discussed, they used an interesting method to remove the sham session from their experiments.

3. Factors that could influence the results

Results are mitigated, notably when it comes to the stimulation polarity's effects. It has been reported in this thesis that amplitude modulation is not directly related to stimulation polarity: for instance, cathodal tDCS can either increase or decrease significantly electrophysiological biomarker amplitudes. These observations are in contradiction with the general opinion and observation that cathodal/anodal tDCS inducing hyperpolarization/depolarization would decrease/increase neuronal excitability and, therefore, decrease/increase electrophysiological biomarkers' amplitudes. This opinion is based on results from early animal studies (Creutzfeldt, Fromm and Kapp, 1962; Bindman, Lippold and Redfearn, 1964; Purpura and McMurtry, 1965), and human studies investigating motor evoked potentials (Nitsche and Paulus, 2000, 2001; Nitsche, Nitsche, *et al.*, 2003), visual evoked potential (Antal, Nitsche and Paulus, 2001; Antal, Kincses, *et al.*, 2004; Antal, Varga, *et al.*, 2004) and in cognition (Kincses *et al.*, 2003; Nitsche, Schauenburg, *et al.*, 2003; Nitsche *et al.*, 2010). Then, in a will of simplification and generalization, it has been assumed that the relationship between cathodal (anodal), inhibitory(excitatory), and hyperpolarizing(depolarizing) effects would be the same at any scale for any other application in Humans. And so, cathodal tDCS was quasi-systematically performed in neuronal excitability disorders such as epilepsy (San-Juan *et al.*, 2015; Lefaucheur, 2016; Lefaucheur *et al.*, 2017; Regner *et al.*, 2018; Fregni *et al.*, 2021) assuming its inhibitory effects.

However, it is inaccurate to state that cathodal (anodal) stimulation generates simple hyperpolarization (depolarization) at any level and condition. Some stimulation parameters could induce polarity-reversal without changing stimulation polarity. One of these parameters is the stimulation duration. While a 13-min anodal tDCS significantly enhances motor cortical excitability

(Nitsche and Paulus, 2000; Monte-Silva *et al.*, 2013), a twice longer anodal stimulation (26 min) decreases it (Monte-Silva *et al.*, 2013; Yavari *et al.*, 2018). The second parameter to consider is the stimulation intensity. The same non-linear effect as stimulation duration has been reported when stimulation intensity is increased: a 2-mA cathodal tDCS induced the same effects as a 2 mA anodal tDCS namely an excitability enhancement of the motor cortex (Batsikadze *et al.*, 2013).

At the neuronal scale, complexity in observed results challenges the simplistic polarity approach, as it has been stated that there are the same number of cells/compartments which are depolarized and hyperpolarized for a same stimulation (Bikson *et al.*, 2004; Joucla and Yvert, 2009; Rahman *et al.*, 2013; Woods *et al.*, 2016; Yavari *et al.*, 2018). Also, neurons morphology and their orientation regarding to the current flow play an important role shown in *in-vitro* and *in-silico* studies (Bindman, Lippold and Redfearn, 1964; Chan and Nicholson, 1986; Chan, Hounsgaard and Nicholson, 1988; Radman *et al.*, 2009; Kabakov *et al.*, 2012). Thus, effects measured on neocortical pyramidal cells population can be totally different from those measured in hippocampal cells population. This could be the case of intracerebral investigation presented in this thesis performed in human in-vivo, where 2 contacts within the hippocampus could exhibit 2 different effects due to neurons population orientation having a 180° difference from one contact to another. Also at the cortical level, gyrification exposes differently neurons population to the electric field, even under the stimulation electrode, inducing simultaneous hyper and depolarization (Datta *et al.*, 2009; Woods *et al.*, 2016).

Another factor to consider is related to the depth. An in-vitro study showed that inhibitory (excitatory) effects of cathodal (anodal) tDCS were inverted for neurons located in subcortical layers (Purpura and McMurtry, 1965). One hypothesis of this phenomenon was the non-linear effect of the intensity described above. Because current intensity is correlated to the depth, the effect induced would, therefore, be different. This hypothesis was challenged in other in-vitro studies showing a linear effect of the intensity instead (Chan, Hounsgaard and Nicholson, 1988; Bikson *et al.*, 2004; Fröhlich and Mccormick, 2010). Another hypothesis is proposed by Das and colleagues (Das *et al.*, 2016): polarity-reversal effects as a function of the depth would be induced by a difference in neurons' lateral connection or cortical current density distribution (CSD) (Rappelsberger, Pockberger and Petsche, 1982). CSD is characterized by a maximum output current occurring in layer I (positive current) which is sunk in layer II and III (negative current) creating a dipole during electrophysiological activity (Csercsa *et al.*, 2010). This dipole can be enforced by anodal tDCS and induce, therefore, an increase in negative current in layer II and III and positive current in layer I (Das *et al.*, 2016).

A last factor, but not the least, is related to the brain network. It is more and more accepted that tDCS is network-dependent (Peña-Gómez *et al.*, 2012; Kunze *et al.*, 2016) and a hint of this phenomenon has been observed in the cognitive investigation section (Chapter IV). In that study,

contralateral structures exhibited an amplitude increase while structures directly under stimulation's electrodes exhibited a decrease. This underlines the necessity to consider more seriously brain networks when performing a TES and should encourage further study in this direction. Indeed, instead of developing TES technique focused on the depth, considering networks may be an answer for reaching some deep structures. This consideration could be interesting for TES applied to neurological diseases involving a network such as epilepsy. The potential opportunity to disorganize pathological networks could already be a big step toward clinical application of TES.

This thesis, which explored an affordable and easy-to-use non-invasive neuromodulation technique, unveils more questions than answers but still provides a proof of concept of biophysics TES intracerebral investigation and its application in epilepsy and cognition. Materials, methodology and results from this research work should establish the foundations and guidelines paving the way for future intracerebral investigation of TES in the lab.

References

Abdallah, C. *et al.* (2017) "Localizing value of electrical source imaging: Frontal lobe, malformations of cortical development and negative MRI related epilepsies are the best candidates," *NeuroImage: Clinical*, 16, pp. 319–329. doi:10.1016/j.nicl.2017.08.009.

Aggleton, J.P. (ed.) (1992) *The amygdala: Neurobiological aspects of emotion, memory, and mental dysfunction.*, *The amygdala: Neurobiological aspects of emotion, memory, and mental dysfunction*. New York, NY, US: Wiley-Liss.

Aldini, G. (1803) *An account of the late improvements in galvanism : with a series of curious and interesting experiments performed before the commissioners of the French National Institute, and repeated lately in the anatomical theatres of London*. London: Wilks and Taylor.

Aldini, G. (1804) *Essai théorique et expérimental sur le galvanisme avec une série d'expériences faites en présence des Commissaires de l'Institut national de France et en divers amphithéatres anatomiques de Londres*. Paris: De l'Imprimerie de Fournier fils. doi:10.5479/sil.166863.39088003171683.

Almukhtar, A. *et al.* (2014) "Comparison of the accuracy of voxel based registration and surface based registration for 3D assessment of surgical change following orthognathic surgery," *PLoS ONE*, 9(4), pp. 1–6. doi:10.1371/journal.pone.0093402.

Alonso-Prieto, E. *et al.* (2013) "The 6Hz fundamental stimulation frequency rate for individual face discrimination in the right occipito-temporal cortex," *Neuropsychologia*, 51(13), pp. 2863–2875. doi:10.1016/j.neuropsychologia.2013.08.018.

Amaral, D.G. *et al.* (1992) "Anatomical organization of the primate amygdaloid complex.," *The Amygdala: Neurobiological Aspects of Emotion, Memory, and Mental Dysfunction*, pp. 1–66.

Amidror, I. (2002) "Scattered data interpolation methods for electronic imaging systems: a survey," *Journal of Electronic Imaging*, 11(2), p. 157. doi:10.1117/1.1455013.

Andersen, S.K., Muller, M.M. and Martinovic, J. (2012) "Bottom-Up Biases in Feature-Selective Attention," *Journal of Neuroscience*, 32(47), pp. 16953–16958. doi:10.1523/JNEUROSCI.1767-12.2012.

Andreasen, M. and Nedergaard, S. (1996) "Dendritic electrogenesis in rat hippocampal CA1 pyramidal neurons: functional aspects of Na+ and Ca2+ currents in apical dendrites," *Hippocampus*, 6(1), pp. 79–95. doi:10.1002/(SICI)1098-1063(1996)6:1<79::AID-HIPO13>3.0.CO;2-H.

Antal, A., Kincses, T.Z., *et al.* (2004) "Excitability Changes Induced in the Human Primary Visual Cortex by Transcranial Direct Current Stimulation: Direct Electrophysiological Evidence," *Investigative Opthalmology & Visual Science*, 45(2), p. 702. doi:10.1167/iovs.03-0688.

Antal, A., Varga, E.T., *et al.* (2004) "Oscillatory brain activity and transcranial direct current stimulation in humans," *NeuroReport*, 15(8), pp. 1307–1310. doi:10.1097/01.wnr.0000127460.08361.84.

Antal, A. *et al.* (2015) "Conceptual and Procedural Shortcomings of the Systematic Review "Evidence That Transcranial Direct Current Stimulation (tDCS) Generates Little-to-no Reliable Neurophysiologic Effect Beyond MEP Amplitude Modulation in Healthy Human Subjects: A Systematic R," *BRS*, 8, pp. 846–849. doi:10.1016/j.brs.2015.05.009.

Antal, A. *et al.* (2017) "Low intensity transcranial electric stimulation: Safety, ethical, legal regulatory and application guidelines," *Clinical Neurophysiology*, pp. 1774–1809. doi:10.1016/j.clinph.2017.06.001.

Antal, A., Nitsche, M.A. and Paulus, W. (2001) "External modulation of visual perception in humans," *NeuroReport*, 12(16), pp. 3553–3555. doi:10.1097/00001756-200111160-00036.

Arfai, E. *et al.* (1970) "A Controlled Study of Polarization in Depression," *British Journal of Psychiatry*, 116(533), pp. 433–434. doi:10.1192/bjp.116.533.433.

Arndt, R. (1870) "Die Electricität in der Psychiatrie," *Archiv für Psychiatrie und Nervenkrankheiten*, 2(3), pp. 546–600. doi:10.1007/BF02046767.

Asan, A.S., Gok, S. and Sahin, M. (2019) "Electrical fields induced inside the rat brain with skin, skull, and dural placements of the current injection electrode," *PLoS ONE*. Edited by M. Bikson, 14(1), p. e0203727. doi:10.1371/journal.pone.0203727.

Ashburner, J. and Friston, K.J. (2005) "Unified segmentation," *NeuroImage*, 26(3), pp. 839–851. doi:10.1016/j.neuroimage.2005.02.018.

Assenza, G. *et al.* (2017) "Cathodal transcranial direct current stimulation reduces seizure frequency in adults with drug-resistant temporal lobe epilepsy: A sham controlled study," *Brain Stimulation*, 10(2), pp. 333–335. doi:10.1016/j.brs.2016.12.005.

Auvichayapat, N. *et al.* (2013) "Transcranial direct current stimulation for treatment of refractory childhood focal epilepsy," *Brain Stimulation*, 6(4), pp. 696–700. doi:10.1016/j.brs.2013.01.009.

Auvichayapat, N. *et al.* (2016) "Transcranial direct current stimulation for treatment of childhood pharmacoresistant lennox-gastaut syndrome: A pilot study," *Frontiers in Neurology*, 7(MAY), pp. 1–8. doi:10.3389/fneur.2016.00066.

Azevedo, F.A.C. *et al.* (2009) "Equal numbers of neuronal and nonneuronal cells make the human brain an isometrically scaled-up primate brain," *Journal of Comparative Neurology*, 513(5), pp. 532–541. doi:10.1002/cne.21974.

Barbieri, M., Negrini, M., Nitsche, Michael A, *et al.* (2016) "Anodal-tDCS over the human right occipital cortex enhances the perception and memory of both faces and objects," *Neuropsychologia*, 81, pp. 238–244. doi:10.1016/j.neuropsychologia.2015.12.030.

Barbieri, M., Negrini, M., Nitsche, Michael A., *et al.* (2016) "Anodal-tDCS over the human right occipital cortex enhances the perception and memory of both faces and objects," *Neuropsychologia*, 81, pp. 238–244. doi:10.1016/j.neuropsychologia.2015.12.030.

von Bartheld, C.S., Bahney, J. and Herculano-Houzel, S. (2016) "The search for true numbers of neurons and glial cells in the human brain: A review of 150 years of cell counting," *Journal of Comparative Neurology*, pp. 3865–3895. doi:10.1002/cne.24040.

Bartolomei, F., Chauvel, P. and Wendling, F. (2008) "Epileptogenicity of brain structures in human temporal lobe epilepsy: a quantified study from intracerebral EEG," *Brain*, 131(7), pp. 1818–1830. doi:10.1093/brain/awn111.

Barton, J.J.S. *et al.* (2002) "Lesions of the fusiform face area impair perception of facial configuration in prosopagnosia," *Neurology*, 58(1), pp. 71–78. doi:10.1212/WNL.58.1.71.

Batsikadze, G. *et al.* (2013) "Partially non-linear stimulation intensity-dependent effects of direct current stimulation on motor cortex excitability in humans," *Journal of Physiology*, 591(7), pp. 1987–2000. doi:10.1113/jphysiol.2012.249730.

Baud, M.O. *et al.* (2018) "Multi-day rhythms modulate seizure risk in epilepsy," *Nature Communications*, 9(1), p. 88. doi:10.1038/s41467-017-02577-y.

Baulac, M. *et al.* (2015) "Epilepsy priorities in Europe: A report of the ILAE-IBE Epilepsy Advocacy Europe Task Force," *Epilepsia*, 56(11), pp. 1687–1695. doi:10.1111/epi.13201.

Bawin, S.M. *et al.* (1986) "Long-term effects of sinusoidal extracellular electric fields in penicillin-treated rat hippocampal slices," *Brain Research*, 399(1), pp. 194–199. doi:10.1016/0006-8993(86)90619-0.

Beaudreau, S.A. and Finger, S. (2006) "Medical electricity and madness in the 18th century: the legacies of Benjamin Franklin and Jan Ingenhousz.," *Perspectives in biology and medicine*, 49(3), pp. 330–45. doi:10.1353/pbm.2006.0036.

Benar, C.G. and Gotman, J. (2000) "Modeling of post-surgical brain and skull defects in the EEG inverse problem with boundary element models," *NeuroImage*, 11(5 PART II). doi:10.1016/s1053-8119(00)91564-7.

Bentin, S. *et al.* (1996) "Electrophysiological studies of face perception in humans," *Journal of Cognitive Neuroscience*, 8(6), pp. 551–565. doi:10.1162/jocn.1996.8.6.551.

Bertucci, P. (2007) "Therapeutic attractions: Early applications of electricity to the art of healing," in Whitaker, H., Smith, C.U.M., and Finger, S. (eds) *Brain, Mind and Medicine: Essays in Eighteenth-Century Neuroscience*. Boston, MA: Springer US, pp. 271–283. doi:10.1007/978-0-387-70967-3.

Bestmann, S., de Berker, A.O. and Bonaiuto, J. (2015) "Understanding the behavioural consequences of noninvasive brain stimulation," *Trends in Cognitive Sciences*, pp. 13–20. doi:10.1016/j.tics.2014.10.003.

Bikson, M. *et al.* (2004) "Effect of uniform extracellular DC electric fields on excitability in rat hippocampal slices in vitro," *Journal of Physiology*, 557(1), pp. 175–190. doi:10.1113/jphysiol.2003.055772.

Bikson, M. *et al.* (2019) "Transcranial electrical stimulation nomenclature," *Brain Stimulation*, 12(6), pp. 1349–1366. doi:10.1016/j.brs.2019.07.010.

Bikson, M., Radman, T. and Datta, A. (2006) "Rational modulation of neuronal processing with applied electric fields," in *2006 International Conference of the IEEE Engineering in Medicine and Biology Society*. IEEE, pp. 1616–1619. doi:10.1109/IEMBS.2006.259548.

Bindman, L.J., Lippold, O.C.J. and Redfearn, J.W.T. (1964) "The action of brief polarizing currents on the cerebral cortex of the rat (1) during current flow and (2) in the production of long-lasting after-effects," *The Journal of Physiology*, 172(3), pp. 369–382. doi:10.1113/jphysiol.1964.sp007425.

Birch, J. (1792) "A letter to Mr. George Adams, on the subject of medical electricity," in Adams, G. (ed.) *An essay on electricity*. 4th edn. London: Hindmarsh, pp. 519–573.

Van Bogaert, P. *et al.* (2012) "Impact of focal interictal epileptiform discharges on behaviour and cognition in children," *Neurophysiologie Clinique/Clinical Neurophysiology*, 42(1–2), pp. 53–58. doi:10.1016/j.neucli.2011.11.004.

Bötzel, K. and Grüsser, O.J. (1989) "Electric brain potentials evoked by pictures of faces and non-faces: a search for 'face-specific' EEG-potentials," *Experimental Brain Research*, 77(2), pp. 349–360. doi:10.1007/BF00274992.

Bötzel, K., Schulze, S. and Stodieck, S.R.G. (1995) "Scalp topography and analysis of intracranial sources of face-evoked potentials," *Experimental Brain Research*, 104(1), pp. 135–143. doi:10.1007/BF00229863.

Brigo, F. *et al.* (2011) "The breach rhythm," *Clinical Neurophysiology*. Clin Neurophysiol, pp. 2116–2120. doi:10.1016/j.clinph.2011.07.024.

Brodie, M.J. *et al.* (2012) "Patterns of treatment response in newly diagnosed epilepsy," *Neurology*, 78(20), pp. 1548–1554. doi:10.1212/WNL.0b013e3182563b19.

Brunyé, T.T. *et al.* (2017) "Non-invasive brain stimulation targeting the right fusiform gyrus selectively increases working memory for faces," *Brain and Cognition*, 113, pp. 32–39. doi:10.1016/j.bandc.2017.01.006.

Cancelli, A. *et al.* (2016) "A simple method for EEG guided transcranial electrical stimulation without models," *Journal of neural engineering*, 13(3). doi:10.1088/1741-2560/13/3/036022.

Cao, J. and Grover, P. (2018) "Do single neuron models exhibit temporal interference stimulation?," *2018 IEEE Biomedical Circuits and Systems Conference, BioCAS 2018 - Proceedings*, pp. 1–4. doi:10.1109/BIOCAS.2018.8584745.

Carlson, C. and Devinsky, O. (2009) "The excitable cerebral cortex," *Epilepsy & Behavior*, 15(2), pp. 131–132. doi:10.1016/j.yebeh.2009.03.002.

Carney, M.W.P., Cashman, M.D. and Sheffield, B.F. (1970) "Polarization in Depression," *British Journal of Psychiatry*, 117(539), pp. 474–475. doi:10.1192/bjp.117.539.474.

Catani, M., Dell'Acqua, F. and Thiebaut de Schotten, M. (2013) "A revised limbic system model for memory, emotion and behaviour," *Neuroscience & Biobehavioral Reviews*, 37(8), pp. 1724–1737. doi:10.1016/j.neubiorev.2013.07.001.

Chan, C.Y., Hounsgaard, J. and Nicholson, C. (1988) "Effects of electric fields on transmembrane potential and excitability of turtle cerebellar Purkinje cells in vitro.," *The Journal of Physiology*, 402(1), pp. 751–771. doi:10.1113/jphysiol.1988.sp017232.

Chan, C.Y. and Nicholson, C. (1986) "Modulation by applied electric fields of Purkinje and stellate cell activity in the isolated turtle cerebellum.," *The Journal of Physiology*, 371(1), pp. 89–114. doi:10.1113/jphysiol.1986.sp015963.

Chassoux, F. *et al.* (2012) "Type II focal cortical dysplasia: Electroclinical phenotype and surgical outcome related to imaging," *Epilepsia*, 53(2), pp. 349–358. doi:10.1111/j.1528-1167.2011.03363.x.

Chauhan, M. *et al.* (2018) "Low-Frequency Conductivity Tensor Imaging of the Human Head In Vivo Using DT-MREIT: First Study," *IEEE Transactions on Medical Imaging*, 37(4), pp. 966–976. doi:10.1109/TMI.2017.2783348.

Chhatbar, P.Y. *et al.* (2018) "Evidence of transcranial direct current stimulation-generated electric fields at subthalamic level in human brain in vivo," *Brain Stimulation*, 11, pp. 727–733. doi:10.1016/j.brs.2018.03.006.

Civile, C. *et al.* (2018) "The effect of scrambling upright and inverted faces on the N170," *Quarterly Journal of Experimental Psychology*, 71(11), pp. 2464–2476. doi:10.1177/1747021817744455.

Civile, C. *et al.* (2020) "Testing the effects of transcranial direct current stimulation (tDCS) on the face inversion effect and the N170 event-related potentials (ERPs) component," *Neuropsychologia*, 143, p. 107470. doi:10.1016/j.neuropsychologia.2020.107470.

Colombet, B. *et al.* (2015) "AnyWave: A cross-platform and modular software for visualizing and processing electrophysiological signals," *Journal of Neuroscience Methods*, 242, pp. 118–126. doi:10.1016/j.jneumeth.2015.01.017.

Costain, R., Redfearn, J.W.T. and Lippold, O.C.J. (1964) "A Controlled Trial of the Therapeutic Effects of Polarization of the Brain in Depressive Illness," *British Journal of Psychiatry*, 110(469), pp. 786–799. doi:10.1192/bjp.110.469.786.

Creutzfeldt, O.D., Fromm, G.H. and Kapp, H. (1962) "Influence of transcortical d-c currents on cortical neuronal activity," *Experimental Neurology*, 5(6), pp. 436–452. doi:10.1016/0014-4886(62)90056-0.

Csercsa, R. *et al.* (2010) "Laminar analysis of slow wave activity in humans," *Brain*, 133(9), pp. 2814–2829. doi:10.1093/brain/awq169.

Csifcsák, G. *et al.* (2018) "Effects of transcranial direct current stimulation for treating depression: A modeling study," *Journal of Affective Disorders*, 234, pp. 164–173. doi:10.1016/j.jad.2018.02.077.

de Curtis, M., Jefferys, J.G.R. and Avoli, M. (2012) "Interictal Epileptiform Discharges in Partial Epilepsy," in *Jasper's Basic Mechanisms of the Epilepsies*, pp. 213–227. doi:10.1093/med/9780199746545.003.0017.

Das, S. *et al.* (2016) "Impact of Transcranial Direct Current Stimulation (tDCS) on Neuronal Functions," *Frontiers in Neuroscience*, 10(NOV), p. 550. doi:10.3389/fnins.2016.00550.

Datta, A. *et al.* (2008) "Transcranial current stimulation focality using disc and ring electrode configurations: FEM analysis," *Journal of Neural Engineering*, 5(2), pp. 163–174. doi:10.1088/1741-2560/5/2/007.

Datta, A. *et al.* (2009) "Gyri-precise head model of transcranial direct current stimulation: Improved spatial focality using a ring electrode versus conventional rectangular pad," *Brain Stimulation*, 2(4). doi:10.1016/j.brs.2009.03.005.

Datta, A. *et al.* (2011) "Individualized model predicts brain current flow during transcranial direct-current stimulation treatment in responsive stroke patient," *Brain Stimulation*, 4(3), pp. 169–174. doi:10.1016/j.brs.2010.11.001.

Datta, A. *et al.* (2012) "Inter-individual variation during transcranial direct current stimulation and normalization of dose using MRI-derived computational models," *Frontiers in Psychiatry*, 3(OCT). doi:10.3389/fpsyt.2012.00091.

Datta, A., Bikson, M. and Fregni, F. (2010) "Transcranial direct current stimulation in patients with skull defects and skull plates: High-resolution computational FEM study of factors altering cortical current flow," *NeuroImage*, 52(4), pp. 1268–1278. doi:10.1016/j.neuroimage.2010.04.252.

Davis, P.A. (1939) "Effects of Acoustic Stimuli on the Waking Human Brain," *Journal of Neurophysiology*, 2(6), pp. 494–499. doi:10.1152/jn.1939.2.6.494.

Dawson, J. and Montagu, J.D. (1965) "Small Direct Currents and the Human Brain," *British Journal of Psychiatry*, 111(473), pp. 368–368. doi:10.1192/bjp.111.473.368.

Deans, J.K., Powell, A.D. and Jefferys, J.G.R. (2007) "Sensitivity of coherent oscillations in rat hippocampus to AC electric fields," *Journal of Physiology*, 583(2), pp. 555–565. doi:10.1113/jphysiol.2007.137711.

Denoyer, Y. *et al.* (2020) "Modelling acute and lasting effects of tDCS on epileptic activity," *Journal of Computational Neuroscience*, 48(2), pp. 161–176. doi:10.1007/s10827-020-00745-6.

Dieleman, J.L. *et al.* (2020) "US Health Care Spending by Payer and Health Condition, 1996-2016," *JAMA - Journal of the American Medical Association*, 323(9), pp. 863–884. doi:10.1001/jama.2020.0734.

Dmochowski, J.P. *et al.* (2011) "Optimized multi-electrode stimulation increases focality and intensity at target," *Journal of Neural Engineering*, 8(4). doi:10.1088/1741-2560/8/4/046011.

Dmochowski, J.P. *et al.* (2013) "Targeted transcranial direct current stimulation for rehabilitation after stroke," *NeuroImage*, 75, pp. 12–19. doi:10.1016/j.neuroimage.2013.02.049.

Dmochowski, J.P. *et al.* (2017) "Optimal use of EEG recordings to target active brain areas with transcranial electrical stimulation," *NeuroImage*, 157(May), pp. 69–80. doi:10.1016/j.neuroimage.2017.05.059.

Dmochowski, J.P., Bikson, M. and Parra, L.C. (2012) "The point spread function of the human head and its implications for transcranial current stimulation," *Physics in Medicine and Biology*, 57(20), pp. 6459–6477. doi:10.1088/0031-9155/57/20/6459.

Ten Donkelaar, H.J. *et al.* (2020) "The Limbic System," in Springer (ed.) *Clinical Neuroanatomy: Brain Circuitry and Its Disorders*. 2nd 2020. Berlin: Springer International Publishing, pp. 1–981. doi:10.1007/978-3-030-41878-6.

Dular, P. *et al.* (1998) "A general environment for the treatment of discrete problems and its application to the finite element method," *IEEE Transactions on Magnetics*, 34(5), pp. 3395–3398. doi:10.1109/20.717799.

Durand, D.M. and Bikson, M. (2001) "Suppression and control of epileptiform activity by electrical stimulation: A review," *Proceedings of the IEEE*, 89(7), pp. 1065–1081. doi:10.1109/5.939821.

Dzhelyova, M. and Rossion, B. (2014) "Supra-additive contribution of shape and surface information to individual face discrimination as revealed by fast periodic visual stimulation," *Journal of Vision*, 14(14), pp. 15–15. doi:10.1167/14.14.15.

Edwards, D. *et al.* (2013) "Physiological and modeling evidence for focal transcranial electrical brain stimulation in humans: A basis for high-definition tDCS," *NeuroImage*, 74, pp. 266–275. doi:10.1016/j.neuroimage.2013.01.042.

Eickhoff, S.B. *et al.* (2005) "A new SPM toolbox for combining probabilistic cytoarchitectonic maps and functional imaging data." doi:10.1016/j.neuroimage.2004.12.034.

Eickhoff, S.B. *et al.* (2006) "Testing anatomically specified hypotheses in functional imaging using cytoarchitectonic maps." doi:10.1016/j.neuroimage.2006.04.204.

Eickhoff, S.B. *et al.* (2007) "Assignment of functional activations to probabilistic cytoarchitectonic areas revisited." doi:10.1016/j.neuroimage.2007.03.060.

Esmaeilpour, Z. *et al.* (2021) "Temporal interference stimulation targets deep brain regions by modulating neural oscillations," *Brain Stimulation*, 14(1), pp. 55–65. doi:10.1016/j.brs.2020.11.007.

Evans, C. (1757) "A relation of a cure performed by electricity," *Medical Observations and Inquiries*, 1, pp. 83–86.

Fang, Q. and Boas, D.A. (2009) "Tetrahedral mesh generation from volumetric binary and grayscale images," in *Proceedings - 2009 IEEE International Symposium on Biomedical Imaging: From Nano to Macro, ISBI 2009*, pp. 1142–1145. doi:10.1109/ISBI.2009.5193259.

Farahani, F. *et al.* (2021) "Effects of direct current stimulation on synaptic plasticity in a single neuron," *Brain Stimulation*, 14(3), pp. 588–597. doi:10.1016/j.brs.2021.03.001.

Faria, P. *et al.* (2012) "Feasibility of focal transcranial DC polarization with simultaneous EEG recording: Preliminary assessment in healthy subjects and human epilepsy," *Epilepsy & Behavior*, 25(3), pp. 417–425. doi:10.1016/j.yebeh.2012.06.027.

Faria, P., Hallett, M. and Miranda, P.C. (2011) "A finite element analysis of the effect of electrode area and inter-electrode distance on the spatial distribution of the current density in tDCS," *Journal of Neural Engineering*, 8(6). doi:10.1088/1741-2560/8/6/066017.

Faria, P., Leal, A. and Miranda, P.C. (2009) "Comparing different electrode configurations using the 10-10 international system in tDCS: A finite element model analysis," in *Proceedings of the 31st Annual International Conference of the IEEE Engineering in Medicine and Biology Society: Engineering the Future of Biomedicine, EMBC 2009*. IEEE Computer Society, pp. 1596–1599. doi:10.1109/IEMBS.2009.5334121.

Fernández-Corazza, M. *et al.* (2016) "Transcranial electrical neuromodulation based on the reciprocity principle," *Frontiers in Psychiatry*, 7(MAY), pp. 1–19. doi:10.3389/fpsyt.2016.00087.

Fertonani, A. and Miniussi, C. (2017) "Transcranial electrical stimulation: What we know and do not know about mechanisms," *Neuroscientist*, 23(2), pp. 109–123. doi:10.1177/1073858416631966.

Feuerriegel, D. *et al.* (2015) "The N170 and face perception in psychiatric and neurological disorders: A systematic review," *Clinical Neurophysiology*, 126(6), pp. 1141–1158. doi:10.1016/j.clinph.2014.09.015.

Fiest, K.M. *et al.* (2017) "Prevalence and incidence of epilepsy," *Neurology*, pp. 296–303. doi:10.1212/WNL.0000000000003509.

Finger, S. (2007) "Benjamin Franklin and the Electrical Cure for Disorders of the Nervous System," in Whitaker, H., Smith, C.U.M., and Finger, S. (eds) *Brain, Mind and Medicine: Essays in Eighteenth-Century Neuroscience*. Boston, MA: Springer US, pp. 245–256. doi:10.1007/978-0-387-70967-3_18.

Fisher, R. *et al.* (2010) "Electrical stimulation of the anterior nucleus of thalamus for treatment of refractory epilepsy," *Epilepsia*, 51(5), pp. 899–908. doi:10.1111/j.1528-1167.2010.02536.x.

Fonteneau, C. *et al.* (2019) "Sham tDCS: A hidden source of variability? Reflections for further blinded, controlled trials," *Brain Stimulation*, 12(3), pp. 668–673. doi:10.1016/j.brs.2018.12.977.

Francis, J.T., Gluckman, B.J. and Schiff, S.J. (2003) "Sensitivity of Neurons to Weak Electric Fields," *The Journal of Neuroscience*, 23(19), pp. 7255–7261. doi:10.1523/JNEUROSCI.23-19-07255.2003.

Franklin, B. (1785) *Franklin, Benjamin to Ingenhousz, Jan, Passy, April 29, 1785*, *The Papers of Benjamin Franklin, Vol. (Unpublished) edited by The Packard Humanities Institute*.

Frauscher, B. *et al.* (2018) "High-Frequency Oscillations in the Normal Human Brain," *Annals of Neurology*, 84(3), pp. 374–385. doi:10.1002/ana.25304.

Fregni, F. *et al.* (2006) "A controlled clinical trial of cathodal DC polarization in patients with refractory epilepsy," *Epilepsia*, 47(2), pp. 335–342. doi:10.1111/j.1528-1167.2006.00426.x.

Fregni, F. *et al.* (2021) "Evidence-Based Guidelines and Secondary Meta-Analysis for the Use of Transcranial Direct Current Stimulation in Neurological and Psychiatric Disorders," *International Journal of Neuropsychopharmacology*, 24(4), pp. 256–313. doi:10.1093/ijnp/pyaa051.

Frigo, M. and Johnson, S.G. (2005) "The design and implementation of FFTW3," in *Proceedings of the IEEE*, pp. 216–231. doi:10.1109/JPROC.2004.840301.

Fröhlich, F. and Mccormick, D.A. (2010) "Endogenous Electric Fields May Guide Neocortical Network Activity," *Neuron*, 67, pp. 129–143. doi:10.1016/j.neuron.2010.06.005.

Gabriel, S., Lau, R.W. and Gabriel, C. (1996) "The dielectric properties of biological tissues: II. Measurements in the frequency range 10 Hz to 20 GHz," *Physics in Medicine and Biology*, 41(11), pp. 2251–2269. doi:10.1088/0031-9155/41/11/002.

Gale, T. (1802) *Electricity, or the ethereal fire, considered.* Troy [NY]: Moffitt & Lyon.

Galvani, L. (1791) *De viribus electricitatis in motu musculari. Commentarius*. Bononiae (Bologna): Institutus Scientiarium.

Gardiol, F. (2002) *Traité d'électricité, volume 3 : Electromagnétisme*. Presses Po.

Gaser, C. and Dahnke, R. (2016) "CAT-A Computational Anatomy Toolbox for the Analysis of Structural MRI Data," *Human Brain Mapping*, 32(7), pp. 336–348.

Gauthier, I. *et al.* (2000) "The fusiform 'face area' is part of a network that processes faces at the individual level," *Journal of Cognitive Neuroscience*, 12(3), pp. 495–504. doi:10.1162/089892900562165.

Geuzaine, C. and Remacle, J.-F. (2009) "Gmsh: A 3-D finite element mesh generator with built-in pre- and post-processing facilities," *International Journal for Numerical Methods in Engineering*, 79(11), pp. 1309–1331. doi:10.1002/nme.2579.

Ghai, R.S., Bikson, M. and Durand, D.M. (2000) "Effects of Applied Electric Fields on Low-Calcium Epileptiform Activity in the CA1 Region of Rat Hippocampal Slices," *Journal of Neurophysiology*, 84(1), pp. 274–280. doi:10.1152/jn.2000.84.1.274.

Gluckman, Bruce J. *et al.* (1996) "Electric field suppression of epileptiform activity in hippocampal slices," *Journal of Neurophysiology*, 76(6), pp. 4202–4205. doi:10.1152/jn.1996.76.6.4202.

Gluckman, Bruce J *et al.* (1996) "Stochastic Resonance in a Neuronal Network from Mammalian Brain," *Physical Review Letters*, 77(19), pp. 4098–4101. doi:10.1103/PhysRevLett.77.4098.

Gonzalez-Perez, M. *et al.* (2019) "Transcranial alternating current stimulation (tACS) at 40 Hz enhances face and object perception," *Neuropsychologia*, 135, p. 107237. doi:10.1016/J.NEUROPSYCHOLOGIA.2019.107237.

Gotman, J. (1991) "Relationships Between Interictal Spiking and Seizures: Human and Experimental Evidence," *Canadian Journal of Neurological Sciences / Journal Canadien des Sciences Neurologiques*, 18(S4), pp. 573–576. doi:10.1017/S031716710003273X.

Gotman, J. (1999) "Automatic detection of seizures and spikes.," *Journal of clinical neurophysiology : official publication of the American Electroencephalographic Society*, 16(2), pp. 130–40. doi:10.1097/00004691-199903000-00005.

Grill-Spector, K. *et al.* (2017) "The Functional Neuroanatomy of Human Face Perception," *Annual Review of Vision Science*, pp. 167–196. doi:10.1146/annurev-vision-102016-061214.

Grill-Spector, K. and Weiner, K.S. (2014) "The functional architecture of the ventral temporal cortex and its role in categorization," *Nature Reviews Neuroscience*, pp. 536–548. doi:10.1038/nrn3747.

van der Groen, O. and Wenderoth, N. (2016) "Transcranial random noise stimulation of visual cortex: Stochastic resonance enhances central mechanisms of perception," *Journal of Neuroscience*, 36(19), pp. 5289–5298. doi:10.1523/JNEUROSCI.4519-15.2016.

Grossman, N. *et al.* (2017) "Noninvasive Deep Brain Stimulation via Temporally Interfering Electric Fields," *Cell*, 169(6), pp. 1029-1041.e16. doi:10.1016/j.cell.2017.05.024.

Helmholtz, H. (1853) "Ueber einige Gesetze der Vertheilung elektrischer Ströme in körperlichen Leitern, mit Anwendung auf die thierisch-elektrischen Versuche (Schluss.)," *Annalen der Physik*, 165(7), pp. 353–377. doi:10.1002/andp.18531650702.

Hippocrate (1849) *De la Maladie Sacrée, livre 6*. Edited by E. Littré. Paris: Baillière.

Hofmanis, J. *et al.* (2011) "Automatic depth electrode localization in intracranial space," in *4th International Conference on Bio-inspired Systems and Signal Processing, Biosignals 2011*. Rome, Italy, p. CDROM. Available at: https://hal.archives-ouvertes.fr/hal-00605570.

Horak, P.C. *et al.* (2017) "Interictal epileptiform discharges impair word recall in multiple brain areas," *Epilepsia*, 58(3), pp. 373–380. doi:10.1111/epi.13633.

Horvath, J.C., Forte, J.D. and Carter, O. (2014) "Evidence that transcranial direct current stimulation (tDCS) generates little-to-no reliable neurophysiologic effect beyond MEP amplitude modulation in healthy human subjects: A systematic review," *Neuropsychologia*, 66, pp. 213–236. doi:10.1016/j.neuropsychologia.2014.11.021.

Horvath, J.C., Forte, J.D. and Carter, O. (2015) "Quantitative Review Finds No Evidence of Cognitive Effects in Healthy Populations From Single-session Transcranial Direct Current Stimulation (tDCS)," *Brain Stimulation*, 8, pp. 535–550. doi:10.1016/j.brs.2015.01.400.

Howell, B. and McIntyre, C.C. (2021) "Feasibility of Interferential and Pulsed Transcranial Electrical Stimulation for Neuromodulation at the Human Scale," *Neuromodulation*, 24(5), pp. 843–853. doi:10.1111/ner.13137.

Hu, L. *et al.* (2013) "Single-trial time-frequency analysis of electrocortical signals: Baseline correction and beyond," *NeuroImage*, 84. doi:10.1016/j.neuroimage.2013.09.055.

Huang, Y. *et al.* (2013) "Automated MRI segmentation for individualized modeling of current flow in the human head," *Journal of Neural Engineering*, 10(6), p. 066004. doi:10.1088/1741-2560/10/6/066004.

Huang, Y. *et al.* (2017) "Measurements and models of electric fields in the in vivo human brain during transcranial electric stimulation," *eLife*, 6, pp. 1–27. doi:10.7554/eLife.18834.

Huang, Y. *et al.* (2019) "Realistic volumetric-approach to simulate transcranial electric stimulation - ROAST - a fully automated open-source pipeline," *Journal of Neural Engineering*, 16(5), p. 056006. doi:10.1088/1741-2552/ab208d.

Huang, Y. and Parra, L.C. (2019) "Can transcranial electric stimulation with multiple electrodes reach deep targets?," *Brain Stimulation*, pp. 30–40. doi:10.1016/j.brs.2018.09.010.

Huang, Y., Parra, L.C. and Haufe, S. (2016) "The New York Head—A precise standardized volume conductor model for EEG source localization and tES targeting," *NeuroImage*, 140, pp. 150–162. doi:10.1016/j.neuroimage.2015.12.019.

Ingenhousz, J. (1783) *Ingenhousz, Jan to Franklin, Benjamin, Vienna, August 15, 1783*, *The Papers of Benjamin Franklin, Vol. (Unpublished)The Papers of Benjamin Franklin, Vol. (Unpublished) edited by The Packard Humanities Institute*.

Isnard, J. *et al.* (2018) "French guidelines on stereoelectroencephalography (SEEG)," *Neurophysiologie Clinique*, 48(1), pp. 5–13. doi:10.1016/j.neucli.2017.11.005.

Jacques, C. *et al.* (2019) "The inferior occipital gyrus is a major cortical source of the face-evoked N170: Evidence from simultaneous scalp and intracerebral human recordings," *Human Brain Mapping*, 40(5), pp. 1403–1418. doi:10.1002/HBM.24455.

Jacques, C. *et al.* (2020) "Fast periodic visual stimulation to highlight the relationship between human intracerebral recordings and scalp electroencephalography," *Human Brain Mapping*, 41(September 2019), pp. 2373–2388. doi:10.1002/hbm.24952.

Jacques, C., D'Arripe, O. and Rossion, B. (2007) "The time course of the inversion effect during individual face discrimination," *Journal of Vision*, 7(8), pp. 3–3. doi:10.1167/7.8.3.

Jaeger, D. *et al.* (1987) "The effects of externally applied transcephalic weak direct currents on lateralization in choice reaction tasks," *Journal of Psychophysiology*, 1(2), pp. 127–133.

Janca, R. *et al.* (2013) "Automatic detection and spatial clustering of interictal discharges in invasive recordings," in *2013 IEEE International Symposium on Medical Measurements and Applications (MeMeA)*. IEEE, pp. 219–223. doi:10.1109/MeMeA.2013.6549739.

Janca, R. *et al.* (2014) "Detection of Interictal Epileptiform Discharges Using Signal Envelope Distribution Modelling: Application to Epileptic and Non-Epileptic Intracranial Recordings," *Brain Topography*, 28(1), pp. 172–183. doi:10.1007/s10548-014-0379-1.

Janca, R. *et al.* (2018) "The sub-regional functional organization of neocortical irritative epileptic networks in pediatric epilepsy," *Frontiers in Neurology*, 9(MAR), pp. 1–11. doi:10.3389/fneur.2018.00184.

Jefferys, J.G. (1981) "Influence of electric fields on the excitability of granule cells in guinea-pig hippocampal slices.," *The Journal of Physiology*, 319(1), pp. 143–152. doi:10.1113/jphysiol.1981.sp013897.

Jefferys, J.G. (1995) "Nonsynaptic modulation of neuronal activity in the brain: electric currents and extracellular ions," *Physiol Rev*, 75(4), pp. 689–723. doi:10.1152/physrev.1995.75.4.689.

Jefferys, J.G.R. *et al.* (2003) "Effects of weak electric fields on the activity of neurons and neuronal networks," *Radiation Protection Dosimetry*, 106(4), pp. 321–323. doi:10.1093/oxfordjournals.rpd.a006367.

Jeffreys, D.A. (1989) "A face-responsive potential recorded from the human scalp," *Experimental Brain Research*, 78(1), pp. 193–202. doi:10.1007/BF00230699.

Jog, M. *et al.* (2020) "Concurrent Imaging of Markers of Current Flow and Neurophysiological Changes During tDCS," *Frontiers in Neuroscience*, 14, p. 374. doi:10.3389/fnins.2020.00374.

Jog, M. v. *et al.* (2016) "In-vivo imaging of magnetic fields induced by Transcranial Direct Current Stimulation (tDCS) in human brain using MRI," *Scientific Reports*, 6(1), p. 34385. doi:10.1038/srep34385.

Jonas, J. *et al.* (2012) "Focal electrical intracerebral stimulation of a face-sensitive area causes transient prosopagnosia," *Neuroscience*, 222, pp. 281–288. doi:10.1016/j.neuroscience.2012.07.021.

Jonas, J. *et al.* (2016) "A face-selective ventral occipito-temporal map of the human brain with intracerebral potentials," *Proceedings of the National Academy of Sciences of the United States of America*, 113(28), pp. E4088–E4097. doi:10.1073/pnas.1522033113.

Jones, K.T. *et al.* (2020) "Modulation of auditory gamma-band responses using transcranial electrical stimulation," *Journal of Neurophysiology*, 123(6), pp. 2504–2514. doi:10.1152/JN.00003.2020.

Joucla, S. and Yvert, B. (2009) "Improved focalization of electrical microstimulation using microelectrode arrays: A modeling study," *PLoS ONE*. Edited by H.D. Mansvelder, 4(3), p. e4828. doi:10.1371/journal.pone.0004828.

Jumah, F.R. and Dossani, R.H. (2021) "Neuroanatomy, Cingulate Cortex," *StatPearls* [Preprint]. Available at: https://www.ncbi.nlm.nih.gov/books/NBK537077/ (Accessed: March 13, 2022).

Jürgens, U. (1974) "The Hypothalamus and Behavioral Patterns," *Progress in Brain Research*, 41(C), pp. 445–463. doi:10.1016/S0079-6123(08)61925-1.

Kabakov, A.Y. *et al.* (2012) "Contribution of axonal orientation to pathway-dependent modulation of excitatory transmission by direct current stimulation in isolated rat hippocampus," *Journal of Neurophysiology*, 107(7), pp. 1881–1889. doi:10.1152/jn.00715.2011.

Kahane, P. *et al.* (2006) "The Bancaud and Talairach view on the epileptogenic zone: A working hypothesis," in *Epileptic Disorders*, pp. S16-26. Available at: https://www.hal.inserm.fr/inserm-00388256 (Accessed: January 10, 2022).

Kahane, P. and Bartolomei, F. (2010) "Temporal lobe epilepsy and hippocampal sclerosis: Lessons from depth EEG recordings," in *Epilepsia*, pp. 59–62. doi:10.1111/j.1528-1167.2009.02448.x.

Kaiboriboon, K. *et al.* (2013) "Incidence and prevalence of treated epilepsy among poor health and low-income Americans," *Neurology*, 80(21), pp. 1942–1949. doi:10.1212/WNL.0b013e318293e1b4.

Kanwisher, N., McDermott, J. and Chun, M.M. (1997) "The Fusiform Face Area: A Module in Human Extrastriate Cortex Specialized for Face Perception," *The Journal of Neuroscience*, 17(11), pp. 4302–4311. doi:10.1523/JNEUROSCI.17-11-04302.1997.

Kar, K., Duijnhouwer, J. and Krekelberg, B. (2017) "Transcranial Alternating Current Stimulation Attenuates Neuronal Adaptation," *The Journal of Neuroscience*, 37(9), pp. 2325–2335. doi:10.1523/JNEUROSCI.2266-16.2016.

Kasinadhuni, A.K. *et al.* (2017) "Imaging of current flow in the human head during transcranial electrical therapy," *Brain Stimulation*, 10(4), pp. 764–772. doi:10.1016/j.brs.2017.04.125.

Kaufmann, E. *et al.* (2021) "Acute effects of spaced cathodal transcranial direct current stimulation in drug resistant focal epilepsies," *Clinical Neurophysiology*, 132(7), pp. 1444–1451. doi:10.1016/j.clinph.2021.03.048.

Kellaway, P. (1946) "The part played by electric fish in the early history of bioelectricity and electrotherapy," *Bulletin of the History of Medicine*, 20(2), pp. 112–137.

Kim, J.J. *et al.* (2000) "An MRI-based parcellation method for the temporal lobe," *NeuroImage*, 11(4), pp. 271–288. doi:10.1006/nimg.2000.0543.

Kincses, T.Z. *et al.* (2003) "Facilitation of probabilistic classification learning by transcranial direct current stimulation of the prefrontal cortex in the human," *Neuropsychologia*, 42, pp. 113–117. doi:10.1016/S0028-3932(03)00124-6.

Kling, A., Steklis, H.D. and Deutsch, S. (1979) "Radiotelemetered activity from the amygdala during social interactions in the monkey," *Experimental Neurology*, 66(1), pp. 88–96. doi:10.1016/0014-4886(79)90065-7.

Kling, A.S. and Brothers, L.A. (1992) "The amygdala and social behavior.," in *The amygdala: Neurobiological aspects of emotion, memory, and mental dysfunction.* New York, NY, US: Wiley-Liss, pp. 353–377.

Koessler, L. *et al.* (2009) "Automated cortical projection of EEG sensors: Anatomical correlation via the international 10-10 system," *NeuroImage*, 46(1), pp. 64–72. doi:10.1016/j.neuroimage.2009.02.006.

Koessler, L. *et al.* (2015) "Catching the Invisible: Mesial Temporal Source Contribution to Simultaneous EEG and SEEG Recordings," *Brain Topography*, 28(1), pp. 5–20. doi:10.1007/s10548-014-0417-z.

Koessler, L. *et al.* (2017) "In-vivo measurements of human brain tissue conductivity using focal electrical current injection through intracerebral multicontact electrodes," *Human Brain Mapping*, 38(2), pp. 974–986. doi:10.1002/hbm.23431.

Krause, M.R. *et al.* (2019) "Transcranial alternating current stimulation entrains single-neuron activity in the primate brain," *Proceedings of the National Academy of Sciences of the United States of America*, 116(12), pp. 5747–5755. doi:10.1073/pnas.1815958116.

Kunz, P. *et al.* (2017) "5 kHz transcranial alternating current stimulation: Lack of cortical excitability changes when grouped in a theta burst pattern," *Frontiers in Human Neuroscience*, 10, p. 683. doi:10.3389/fnhum.2016.00683.

Kunze, T. *et al.* (2016) "Transcranial direct current stimulation changes resting state functional connectivity: A large-scale brain network modeling study," *NeuroImage*, 140, pp. 174–187. doi:10.1016/j.neuroimage.2016.02.015.

Kwan, P. *et al.* (2009) "Definition of drug resistant epilepsy: Consensus proposal by the ad hoc Task Force of the ILAE Commission on Therapeutic Strategies," *Epilepsia*, 51(6), pp. 1069–1077. doi:10.1111/j.1528-1167.2009.02397.x.

Kwon, O.I. *et al.* (2016) "Current density imaging during transcranial direct current stimulation using DT-MRI and MREIT: Algorithm development and numerical simulations," *IEEE Transactions on Biomedical Engineering*, 63(1), pp. 168–175. doi:10.1109/TBME.2015.2448555.

Labat, René. (1951) *Traité akkadien de diagnostics et pronostics médicaux.* Paris: Académie internationale d'histoire de sciences (Collection de travaux de l'Académie internationale d'histoire des sciences ;no. 7).

Ladino, L.D. and Moien-afshari, F. (2011) "A Comprehensive Review of Temporal lobe epilepsy," in *Neurological Disorders. Clinical Methods*. 1st edn. iConcept Press Ltd. Available at: https://www.researchgate.net/publication/263965704 (Accessed: March 14, 2022).

Lafer-Sousa, R., Conway, B.R. and Kanwisher, N.G. (2016) "Color-Biased Regions of the Ventral Visual Pathway Lie between Face- and Place-Selective Regions in Humans, as in Macaques," *The Journal of Neuroscience*, 36(5), pp. 1682–1697. doi:10.1523/JNEUROSCI.3164-15.2016.

Lafon, B. *et al.* (2017) "Direct Current Stimulation Alters Neuronal Input/Output Function," *Brain Stimulation*, 10(1), pp. 36–45. doi:10.1016/j.brs.2016.08.014.

Lafontaine, M.P. *et al.* (2013) "Transcranial Direct Current Stimulation of the Dorsolateral Prefrontal Cortex Modulates Repetition Suppression to Unfamiliar Faces: An ERP Study," *PLoS ONE*. Edited by G. Yovel, 8(12), p. e81721. doi:10.1371/journal.pone.0081721.

Lau, S. *et al.* (2016) "Skull defects in finite element head models for source reconstruction from magnetoencephalography signals," *Frontiers in Neuroscience*, 10(APR), p. 141. doi:10.3389/fnins.2016.00141.

LeDoux, J.E. (1992) "Emotion and the amygdala.," in *The amygdala: Neurobiological aspects of emotion, memory, and mental dysfunction.* New York, NY, US: Wiley-Liss, pp. 339–351.

Lee, M.B. *et al.* (2018) "Anisotropic conductivity tensor imaging for transcranial direct current stimulation (tDCS) using magnetic resonance diffusion tensor imaging (MR-DTI)," *PLOS ONE*. Edited by T. Yuan, 13(5), p. e0197063. doi:10.1371/journal.pone.0197063.

Leech, R. and Sharp, D.J. (2014) "The role of the posterior cingulate cortex in cognition and disease," *Brain*, 137(1), pp. 12–32. doi:10.1093/brain/awt162.

Lefaucheur, J.P. (2016) "A comprehensive database of published tDCS clinical trials (2005–2016)," *Neurophysiologie Clinique*, 46(6), pp. 319–398. doi:10.1016/j.neucli.2016.10.002.

Lefaucheur, J.P. *et al.* (2017) "Evidence-based guidelines on the therapeutic use of transcranial direct current stimulation (tDCS)," *Clinical Neurophysiology*. International Federation of Clinical Neurophysiology, pp. 56–92. doi:10.1016/j.clinph.2016.10.087.

Lifshitz, K. and Harper, P. (1968) "A Trial of Transcranial Polarization in Chronic Schizophrenics," *British Journal of Psychiatry*, 114(510), pp. 635–637. doi:10.1192/bjp.114.510.635.

Lippold, O.C.J. and Redfearn, J.W.T. (1964) "Mental Changes Resulting from the Passage of Small Direct Currents Through the Human Brain," *British Journal of Psychiatry*, 110(469), pp. 768–772. doi:10.1192/bjp.110.469.768.

Liu, A. *et al.* (2018) "Immediate neurophysiological effects of transcranial electrical stimulation," *Nature Communications*, 9(1), p. 5092. doi:10.1038/s41467-018-07233-7.

Liu-Shuang, J., Norcia, A.M. and Rossion, B. (2014) "An objective index of individual face discrimination in the right occipito-temporal cortex by means of fast periodic oddball stimulation," *Neuropsychologia*, 52(1), pp. 57–72. doi:10.1016/j.neuropsychologia.2013.10.022.

Lohse, M. *et al.* (2016) "Effective connectivity from early visual cortex to posterior occipitotemporal face areas supports face selectivity and predicts developmental prosopagnosia," *Journal of Neuroscience*, 36(13), pp. 3821–3828. doi:10.1523/JNEUROSCI.3621-15.2016.

Louviot, S. *et al.* (2022) "Transcranial Electrical Stimulation generates electric fields in deep human brain structures," *Brain Stimulation*, 15(1), pp. 1–12. doi:10.1016/j.brs.2021.11.001.

Magiorkinis, E., Sidiropoulou, K. and Diamantis, A. (2010) "Hallmarks in the history of epilepsy: Epilepsy in antiquity," *Epilepsy and Behavior*, 17(1), pp. 103–108. doi:10.1016/j.yebeh.2009.10.023.

Maillard, L. *et al.* (2004) "Semiologic and electrophysiologic correlations in temporal lobe seizure subtypes," *Epilepsia*, 45(12), pp. 1590–1599. doi:10.1111/j.0013-9580.2004.09704.x.

Manfredi, M. *et al.* (2017) "tDCS application over the STG improves the ability to recognize and appreciate elements involved in humor processing," *Experimental Brain Research*, 235(6), pp. 1843–1852. doi:10.1007/s00221-017-4932-5.

Medina, J. and Cason, S. (2017) "No evidential value in samples of transcranial direct current stimulation (tDCS) studies of cognition and working memory in healthy populations," *Cortex*, 94, pp. 131–141. doi:10.1016/j.cortex.2017.06.021.

Meiron, O. *et al.* (2019) "Antiepileptic effects of a novel noninvasive neuromodulation treatment in a subject with early-onset epileptic encephalopathy: Case report with 20 sessions of HDTDCS intervention," *Frontiers in Neuroscience*, 13(MAY), p. 547. doi:10.3389/FNINS.2019.00547/BIBTEX.

Mikkonen, M. *et al.* (2020) "Cost of focality in TDCS: Interindividual variability in electric fields," *Brain Stimulation*, 13(1), pp. 117–124. doi:10.1016/j.brs.2019.09.017.

Minhas, P. *et al.* (2012) "Transcranial direct current stimulation in pediatric brain: A computational modeling study," in *Proceedings of the Annual International Conference of the IEEE Engineering in Medicine and Biology Society, EMBS*. IEEE, pp. 859–862. doi:10.1109/EMBC.2012.6346067.

Minhas, P., Datta, A. and Bikson, M. (2011) "Cutaneous perception during tDCS: Role of electrode shape and sponge salinity," *Clinical Neurophysiology*, 122(4), pp. 637–638. doi:10.1016/j.clinph.2010.09.023.

Miranda, P.C., Faria, P. and Hallett, M. (2009) "What does the ratio of injected current to electrode area tell us about current density in the brain during tDCS?," *Clinical Neurophysiology*, 120(6), pp. 1183–1187. doi:10.1016/j.clinph.2009.03.023.

Miranda, P.C., Lomarev, M. and Hallett, M. (2006) "Modeling the current distribution during transcranial direct current stimulation," *Clinical Neurophysiology*, 117(7), pp. 1623–1629. doi:10.1016/j.clinph.2006.04.009.

Mirzakhalili, E. *et al.* (2020) "Biophysics of Temporal Interference Stimulation," *Cell Systems*, 11(6), pp. 557-572.e5. doi:10.1016/J.CELS.2020.10.004.

Moliadze, V. *et al.* (2012) "Close to threshold transcranial electrical stimulation preferentially activates inhibitory networks before switching to excitation with higher intensities," *Brain Stimulation*, 5(4), pp. 505–511. doi:10.1016/j.brs.2011.11.004.

Moliadze, V., Antal, A. and Paulus, W. (2010) "Boosting brain excitability by transcranial high frequency stimulation in the ripple range," *The Journal of Physiology*, 588(24), pp. 4891–4904. doi:10.1113/jphysiol.2010.196998.

Monte-Silva, K. *et al.* (2013) "Induction of late LTP-like plasticity in the human motor cortex by repeated non-invasive brain stimulation," *Brain Stimulation*, 6(3), pp. 424–432. doi:10.1016/j.brs.2012.04.011.

Morgan, S.T., Hansen, J.C. and Hillyard, S.A. (1996) "Selective attention to stimulus location modulates the steady-state visual evoked potential.," *Proceedings of the National Academy of Sciences*, 93(10), pp. 4770–4774. doi:10.1073/pnas.93.10.4770.

Nitsche, M.A., Liebetanz, D., *et al.* (2003) "Chapter 27 Modulation of cortical excitability by weak direct current stimulation - technical, safety and functional aspects," *Supplements to Clinical Neurophysiology*, 56(C), pp. 255–276. doi:10.1016/S1567-424X(09)70230-2.

Nitsche, M.A., Schauenburg, A., *et al.* (2003) "Facilitation of Implicit Motor Learning by Weak Transcranial Direct Current Stimulation of the Primary Motor Cortex in the Human," *Journal of Cognitive Neuroscience*, 15(4), pp. 619–626. doi:10.1162/089892903321662994.

Nitsche, M.A., Nitsche, M.S., *et al.* (2003) "Level of action of cathodal DC polarisation induced inhibition of the human motor cortex," *Clinical Neurophysiology*, 114(4), pp. 600–604. doi:10.1016/S1388-2457(02)00412-1.

Nitsche, M.A. *et al.* (2010) "Contribution of the Premotor Cortex to Consolidation of Motor Sequence Learning in Humans During Sleep," *Journal of Neurophysiology*, 104(5), pp. 2603–2614. doi:10.1152/jn.00611.2010.

Nitsche, M.A. and Bikson, M. (2017) "Extending the parameter range for tDCS: Safety and tolerability of 4 mA stimulation," *Brain Stimulation*, pp. 541–542. doi:10.1016/j.brs.2017.03.002.

Nitsche, M.A. and Paulus, W. (2000) "Excitability changes induced in the human motor cortex by weak transcranial direct current stimulation," *Journal of Physiology*, 527(3), pp. 633–639. doi:10.1111/j.1469-7793.2000.t01-1-00633.x.

Nitsche, M.A. and Paulus, W. (2001) "Sustained excitability elevations induced by transcranial DC motor cortex stimulation in humans," *Neurology*, 57(10), pp. 1899–1901. doi:10.1212/WNL.57.10.1899.

Norcia, A.M. *et al.* (2015) "The steady-state visual evoked potential in vision research: A review," *Journal of Vision*, 15(6), p. 4. doi:10.1167/15.6.4.

Norcia, A.M., Wesemann, W. and Manny, R.E. (1999) "Electrophysiological correlates of vernier and relative motion mechanisms in human visual cortex," *Visual Neuroscience*, 16(6), pp. 1123–1131. doi:10.1017/S0952523899166124.

Öner, M. and Deveci Kocakoç, İ. (2017) "JMASM 49: A Compilation of Some Popular Goodness of Fit Tests for Normal Distribution: Their Algorithms and MATLAB Codes (MATLAB)," *Journal of Modern Applied Statistical Methods*, 16(2), pp. 547–575. doi:10.22237/jmasm/1509496200.

Opitz, A. *et al.* (2015) "Determinants of the electric field during transcranial direct current stimulation," *NeuroImage*, 109, pp. 140–150. doi:10.1016/j.neuroimage.2015.01.033.

Opitz, A. *et al.* (2016) "Spatiotemporal structure of intracranial electric fields induced by transcranial electric stimulation in humans and nonhuman primates," *Scientific Reports*, 6(1), pp. 1–11. doi:10.1038/srep31236.

Opitz, A. *et al.* (2017) "Limitations of ex vivo measurements for in vivo neuroscience," *Proceedings of the National Academy of Sciences of the United States of America*, 114(20), pp. 5243–5246. doi:10.1073/pnas.1617024114.

Opitz, A. *et al.* (2018) "On the importance of precise electrode placement for targeted transcranial electric stimulation," *NeuroImage*, 181, pp. 560–567. doi:10.1016/j.neuroimage.2018.07.027.

O'Toole, L.J. *et al.* (2013) "The N170 to angry faces predicts anxiety in typically developing children over a two-year period," *Developmental Neuropsychology*, 38(5), pp. 352–363. doi:10.1080/87565641.2013.802321.

Ozen, S. *et al.* (2010) "Transcranial electric stimulation entrains cortical neuronal populations in rats," *Journal of Neuroscience*, 30(34), pp. 11476–11485. doi:10.1523/JNEUROSCI.5252-09.2010.

Palejwala, A.H. *et al.* (2020) "Anatomy and white matter connections of the fusiform gyrus," *Scientific Reports*, 10(1), p. 13489. doi:10.1038/s41598-020-70410-6.

Paneri, B. *et al.* (2016) "Tolerability of Repeated Application of Transcranial Electrical Stimulation with Limited Outputs to Healthy Subjects," *Brain Stimulation*, 9(5), pp. 740–754. doi:10.1016/j.brs.2016.05.008.

Parazzini, M. *et al.* (2011) "tDCS Estimation of the electric field and of the current density in an anatomical human head model," *IEEE Transactions on Biomedical Engineering*, 58(6), pp. 1773–1780. doi:10.1109/TBME.2011.2116019.

Parazzini, M. *et al.* (2015) "Effect of the Interindividual Variability on Computational Modeling of Transcranial Direct Current Stimulation," *Computational Intelligence and Neuroscience*, 2015(3), pp. 1–9. doi:10.1155/2015/963293.

Parent, A. (2004) "Giovanni Aldini: From animal electricity to human brain stimulation," *Canadian Journal of Neurological Sciences*, 31(4), pp. 576–584. doi:10.1017/S0317167100003851.

Parent, A. (2009) *Histoire du cerveau : de l'Antiquité aux neurosciences*. Québec, Lyon: Presses de l'université Laval Chronique sociale.

Parkin, B.L., Ekhtiari, H. and Walsh, V.F. (2015) "Non-invasive Human Brain Stimulation in Cognitive Neuroscience: A Primer," *Neuron*, pp. 932–945. doi:10.1016/j.neuron.2015.07.032.

Peelen, M. v. and Downing, P.E. (2005) "Selectivity for the human body in the fusiform gyrus," *Journal of Neurophysiology*, 93(1), pp. 603–608. doi:10.1152/jn.00513.2004.

Peña-Gómez, C. *et al.* (2012) "Modulation of large-scale brain networks by transcranial direct current stimulation evidenced by resting-state functional MRI," *Brain Stimulation*, 5(3), pp. 252–263. doi:10.1016/j.brs.2011.08.006.

Priori, A. *et al.* (1998) "Polarization of the human motor cortex through the scalp," *NeuroReport*, 9(10), pp. 2257–2260. doi:10.1097/00001756-199807130-00020.

Priori, A. (2003) "Brain polarization in humans: A reappraisal of an old tool for prolonged non-invasive modulation of brain excitability," *Clinical Neurophysiology*, 114(4), pp. 589–595. doi:10.1016/S1388-2457(02)00437-6.

Przybylowski, C.J. *et al.* (2021) "Anatomical Subpial Resection of Tumors in the Amygdala and Hippocampus," *World Neurosurgery*, 151, pp. e652–e662. doi:10.1016/j.wneu.2021.04.100.

Puonti, O. *et al.* (2020) "Value and limitations of intracranial recordings for validating electric field modeling for transcranial brain stimulation," *NeuroImage*, 208(November 2019), p. 116431. doi:10.1016/j.neuroimage.2019.116431.

Purpura, D.P. and McMurtry, J.G. (1965) "Intracellular Activities and Evoked Potential Changes During Polarization of Motor Cortex," *Journal of neurophysiology*, 28(1), pp. 166–185. doi:10.1152/jn.1965.28.1.166.

Quon, R.J. *et al.* (2022) "AiED: Artificial intelligence for the detection of intracranial interictal epileptiform discharges," *Clinical Neurophysiology*, 133, pp. 1–8. doi:10.1016/j.clinph.2021.09.018.

Radman, T. *et al.* (2007) "Spike Timing Amplifies the Effect of Electric Fields on Neurons: Implications for Endogenous Field Effects," *Journal of Neuroscience*, 27(11), pp. 3030–3036. doi:10.1523/JNEUROSCI.0095-07.2007.

Radman, T. *et al.* (2009) "Role of cortical cell type and morphology in subthreshold and suprathreshold uniform electric field stimulation in vitro," *Brain Stimulation*, 2(4), pp. 215-228.e3. doi:10.1016/j.brs.2009.03.007.

Rahman, A. *et al.* (2013) "Cellular effects of acute direct current stimulation: Somatic and synaptic terminal effects," *Journal of Physiology*, 591(10), pp. 2563–2578. doi:10.1113/jphysiol.2012.247171.

Rahman, A. *et al.* (2017) "Direct current stimulation boosts synaptic gain and cooperativity in vitro," *The Journal of Physiology*, 595(11), pp. 3535–3547. doi:10.1113/JP273005.

Rampersad, S. *et al.* (2019) "Prospects for transcranial temporal interference stimulation in humans: A computational study," *NeuroImage*, 202, p. 116124. doi:10.1016/j.neuroimage.2019.116124.

Ramsay, John.C. and Schlagenhauf, G. (1966) "Treatment of Depression with Low Voltage Direct Current," *Southern Medical Journal*, 59(8), pp. 932–934. doi:10.1097/00007611-196608000-00013.

Rangarajan, V. *et al.* (2014) "Electrical stimulation of the left and right human fusiform gyrus causes different effects in conscious face perception," *Journal of Neuroscience*, 34(38), pp. 12828–12836. doi:10.1523/JNEUROSCI.0527-14.2014.

Rappelsberger, P., Pockberger, H. and Petsche, H. (1982) "The contribution of the cortical layers to the generation of the EEG: Field potential and current source density analyses in the rabbit's visual cortex," *Electroencephalography and Clinical Neurophysiology*, 53(3), pp. 254–269. doi:10.1016/0013-4694(82)90083-9.

Reato, D. *et al.* (2010) "Low-Intensity Electrical Stimulation Affects Network Dynamics by Modulating Population Rate and Spike Timing," *Journal of Neuroscience*, 30(45), pp. 15067–15079. doi:10.1523/JNEUROSCI.2059-10.2010.

Reato, D. *et al.* (2013) "Effects of weak transcranial alternating current stimulation on brain activity—a review of known mechanisms from animal studies," *Frontiers in Human Neuroscience*, 7(October), pp. 1–8. doi:10.3389/fnhum.2013.00687.

Regan, D. (1966) "Some characteristics of average steady-state and transient responses evoked by modulated light," *Electroencephalography and Clinical Neurophysiology*, 20(3), pp. 238–248. doi:10.1016/0013-4694(66)90088-5.

Regner, G.G. *et al.* (2018) "Preclinical to Clinical Translation of Studies of Transcranial Direct-Current Stimulation in the Treatment of Epilepsy: A Systematic Review," *Frontiers in Neuroscience*, 12. doi:10.3389/fnins.2018.00189.

Reich, L. *et al.* (2011) "A ventral visual stream reading center independent of visual experience," *Current Biology*, 21(5), pp. 363–368. doi:10.1016/j.cub.2011.01.040.

Renzi, C. *et al.* (2015) "The role of the occipital face area in holistic processing involved in face detection and discrimination: A tDCS study," *Neuropsychology*, 29(3), pp. 409–416. doi:10.1037/neu0000127.

Rikir, E. *et al.* (2020) "Respective Contribution of Ictal and Inter-ictal Electrical Source Imaging to Epileptogenic Zone Localization," *Brain Topography*, 33(3), pp. 384–402. doi:10.1007/s10548-020-00768-3.

Roberts, D.J. *et al.* (2013) "Efficient visual object and word recognition relies on high spatial frequency coding in the left posterior fusiform gyrus: Evidence from a case-series of patients with ventral occipito-temporal cortex damage," *Cerebral Cortex*, 23(11), pp. 2568–2580. doi:10.1093/cercor/bhs224.

Rossion, B. (2008) "Picture-plane inversion leads to qualitative changes of face perception," *Acta Psychologica*, 128(2), pp. 274–289. doi:10.1016/j.actpsy.2008.02.003.

Rossion, B. (2009) "Distinguishing the cause and consequence of face inversion: The perceptual field hypothesis," *Acta Psychologica*, 132(3), pp. 300–312. doi:10.1016/j.actpsy.2009.08.002.

Rossion, B. *et al.* (2012) "A steady-state visual evoked potential approach to individual face perception: Effect of inversion, contrast-reversal and temporal dynamics," *NeuroImage*, 63(3), pp. 1585–1600. doi:10.1016/j.neuroimage.2012.08.033.

Rossion, B. (2014a) "Understanding face perception by means of human electrophysiology," *Trends in Cognitive Sciences*, 18(6), pp. 310–318. doi:10.1016/j.tics.2014.02.013.

Rossion, B. (2014b) "Understanding face perception by means of prosopagnosia and neuroimaging," *Frontiers in Bioscience*, 6(2), p. 706. doi:10.2741/e706.

Rossion, B. (2014c) "Understanding individual face discrimination by means of fast periodic visual stimulation," *Experimental Brain Research*, 232(6), pp. 1599–1621. doi:10.1007/s00221-014-3934-9.

Rossion, B. *et al.* (2015) "Fast periodic presentation of natural images reveals a robust face-selective electrophysiological response in the human brain," *Journal of Vision*, 15(1), pp. 1–18. doi:10.1167/15.1.18.

Rossion, B. and Boremanse, A. (2011) "Robust sensitivity to facial identity in the right human occipito-temporal cortex as revealed by steady-state visual-evoked potentials," *Journal of Vision*, 11(2), pp. 16–16. doi:10.1167/11.2.16.

Rossion, Bruno and Boremanse, A. (2011) "Robust sensitivity to facial identity in the right human occipito-temporal cortex as revealed by steady-state visual-evoked potentials," *Journal of Vision*, 11(2), pp. 16–16. doi:10.1167/11.2.16.

Rossion, B. and Caharel, S. (2011) "ERP evidence for the speed of face categorization in the human brain: Disentangling the contribution of low-level visual cues from face perception," *Vision Research*, 51(12), pp. 1297–1311. doi:10.1016/j.visres.2011.04.003.

Rossion, B., Hanseeuw, B. and Dricot, L. (2012) "Defining face perception areas in the human brain: A large-scale factorial fMRI face localizer analysis," *Brain and Cognition*, 79(2), pp. 138–157. doi:10.1016/j.bandc.2012.01.001.

Ruffini, G. *et al.* (2014) "Optimization of multifocal transcranial current stimulation for weighted cortical pattern targeting from realistic modeling of electric fields," *NeuroImage*, 89, pp. 216–225. doi:10.1016/j.neuroimage.2013.12.002.

Ruhnau, P. *et al.* (2018) "Sailing in a sea of disbelief: In vivo measurements of transcranial electric stimulation in human subcortical structures," *Brain Stimulation*, 11(1), pp. 241–243. doi:10.1016/j.brs.2017.09.015.

Rush, S. and Driscoll, D.A. (1968) "Current Distribution in the Brain From Surface Electrodes," *Anesthesia & Analgesia*, 47(6), pp. 717–723. doi:10.1213/00000539-196811000-00016.

Rush, S. and Driscoll, D.A. (1969) "EEG Electrode Sensitivity-An Application of Reciprocity," *IEEE Transactions on Biomedical Engineering*, BME-16(1), pp. 15–22. doi:10.1109/TBME.1969.4502598.

Sadleir, R.J. *et al.* (2010) "Transcranial direct current stimulation (tDCS) in a realistic head model," *NeuroImage*, 51(4), pp. 1310–1318. doi:10.1016/j.neuroimage.2010.03.052.

Sajib, S.Z.K. *et al.* (2021) "Magnetic-resonance-based measurement of electromagnetic fields and conductivity in vivo using single current administration—A machine learning approach," *PLoS ONE*, 16(7 July), p. e0254690. doi:10.1371/journal.pone.0254690.

Salado, A.L. *et al.* (2018) "sEEG is a safe procedure for a comprehensive anatomic exploration of the insula: A retrospective study of 108 procedures representing 254 transopercular insular electrodes," *Operative Neurosurgery*, 14(1), pp. 1–8. doi:10.1093/ons/opx106.

San-Juan, D. *et al.* (2015) "Transcranial direct current stimulation in epilepsy," *Brain Stimulation*, 8(3), pp. 455–464. doi:10.1016/j.brs.2015.01.001.

San-Juan, D. *et al.* (2017) "Transcranial Direct Current Stimulation in Mesial Temporal Lobe Epilepsy and Hippocampal Sclerosis," *Brain Stimulation*, 10(1), pp. 28–35. doi:10.1016/j.brs.2016.08.013.

San-juan, D. *et al.* (2019) "Neuromodulation techniques for status epilepticus: A review," *Brain Stimulation*, 12(4), pp. 835–844. doi:10.1016/j.brs.2019.04.005.

Sarmast, S.T., Abdullahi, A.M. and Jahan, N. (2020) "Current Classification of Seizures and Epilepsies: Scope, Limitations and Recommendations for Future Action," *Cureus* [Preprint]. doi:10.7759/cureus.10549.

Saturnino, G.B., Antunes, A. and Thielscher, A. (2015) "On the importance of electrode parameters for shaping electric field patterns generated by tDCS," *NeuroImage*, 120, pp. 25–35. doi:10.1016/j.neuroimage.2015.06.067.

Scheffer, I.E. *et al.* (2017) "ILAE classification of the epilepsies: Position paper of the ILAE Commission for Classification and Terminology," *Epilepsia*, 58(4), pp. 512–521. doi:10.1111/epi.13709.

Schultz, C. and Engelhardt, M. (2014) "Anatomy of the Hippocampal Formation," in *Frontiers of neurology and neuroscience*, pp. 6–17. doi:10.1159/000360925.

Schumann, C.M., Bauman, M.D. and Amaral, D.G. (2011) "Abnormal structure or function of the amygdala is a common component of neurodevelopmental disorders," *Neuropsychologia*, 49(4), pp. 745–759. doi:10.1016/j.neuropsychologia.2010.09.028.

Seeck, M. *et al.* (2017) "The standardized EEG electrode array of the IFCN," *Clinical Neurophysiology*, pp. 2070–2077. doi:10.1016/j.clinph.2017.06.254.

Sergent, J. and Signoret, J.L. (1992) "Functional and anatomical decomposition of face processing: evidence from prosopagnosia and PET study of normal subjects.," *Philosophical transactions*

of the Royal Society of London. Series B, Biological sciences, 335(1273), pp. 55–62. doi:10.1098/rstb.1992.0007.

Sibson, R. (1981) "A Brief Description of Natural Neighbour Interpolation," in *Interpolating Multivariate Data*. V. Barnett. New York: John Wiley & Sons, Ltd, pp. 21–36.

Soullié, P. *et al.* (2021) "MR electrical properties imaging using a generalized image-based method," *Magnetic Resonance in Medicine*, 85(2), pp. 762–776. doi:10.1002/MRM.28458.

Spector, R., Robert Snodgrass, S. and Johanson, C.E. (2015) "A balanced view of the cerebrospinal fluid composition and functions: Focus on adult humans," *Experimental Neurology*. Academic Press, pp. 57–68. doi:10.1016/j.expneurol.2015.07.027.

Stacey, W.C. and Durand, D.M. (2000) "Stochastic resonance improves signal detection in hippocampal CA1 neurons," *Journal of Neurophysiology*, 83(3), pp. 1394–1402. doi:10.1152/jn.2000.83.3.1394.

Stagg, C.J., Antal, A. and Nitsche, M.A. (2018) "Physiology of Transcranial Direct Current Stimulation," *Journal of ECT*, 34(3), pp. 144–152. doi:10.1097/YCT.0000000000000510.

Strick, P.L., Dum, R.P. and Picard, N. (1998) "Motor areas on the medial wall of the hemisphere," *Novartis Foundation Symposium*, 218(218), pp. 64–80. doi:10.1002/9780470515563.ch5.

Suzuki, M. and Noguchi, Y. (2013) "Reversal of the face-inversion effect in N170 under unconscious visual processing," *Neuropsychologia*, 51(3), pp. 400–409. doi:10.1016/j.neuropsychologia.2012.11.021.

Tadel, F. *et al.* (2011) "Brainstorm: A user-friendly application for MEG/EEG analysis," *Computational Intelligence and Neuroscience*, 2011, p. 13. doi:10.1155/2011/879716.

Talairach, J. and Bancaud, J. (1966a) "Lesion, 'Irritative' Zone and Epileptogenic Focus," *Stereotactic and Functional Neurosurgery*, 27(1–3), pp. 91–94. doi:10.1159/000103937.

Talairach, J. and Bancaud, J. (1966b) "Lesion, 'irritative' zone and epileptogenic focus.," *Confinia neurologica*, 27(1), pp. 91–94. doi:10.1159/000103937.

Talairach, J., Bancaud, J. and Szikla, G. (1974) "Approche nouvelle de la neurochirurgie de l'epilepsie. Methodologie stereotaxique et resultats therapeutiques.," *Neurochirurgie*, 20(1 sup.).

Tekturk, P. *et al.* (2016) "The effect of transcranial direct current stimulation on seizure frequency of patients with mesial temporal lobe epilepsy with hippocampal sclerosis," *Clinical Neurology and Neurosurgery*, 149, pp. 27–32. doi:10.1016/j.clineuro.2016.07.014.

Terzuolo, C.A. and Bullock, T.H. (1956) "Measurement of Imposed Voltage Gradient Adequate to Modulate Neuronal Firing," *Proceedings of the National Academy of Sciences*, 42(9), pp. 687–694. doi:10.1073/pnas.42.9.687.

Thielscher, A., Antunes, A. and Saturnino, G.B. (2015) "Field modeling for transcranial magnetic stimulation: A useful tool to understand the physiological effects of TMS?," in *Proceedings of the Annual International Conference of the IEEE Engineering in Medicine and Biology Society, EMBS*. IEEE, pp. 222–225. doi:10.1109/EMBC.2015.7318340.

Thomas, P. and Arzimanoglou, A. (2003) *Épilepsies*. Elsevier M.

Toffa, D.H. *et al.* (2020) "Learnings from 30 years of reported efficacy and safety of vagus nerve stimulation (VNS) for epilepsy treatment: A critical review," *Seizure*, 83, pp. 104–123. doi:10.1016/j.seizure.2020.09.027.

Turi, Z. *et al.* (2019) "Blinding is compromised for transcranial direct current stimulation at 1 mA for 20 min in young healthy adults," *European Journal of Neuroscience*, 50(8), pp. 3261–3268. doi:10.1111/ejn.14403.

Underwood, E. (2016) “Cadaver study challenges brain stimulation methods: Unusual test of transcranial stimulation shows that little electrical current penetrates the skull,” *Science*, 352(6284), p. 397. doi:10.1126/science.352.6284.397.

Ung, H. *et al.* (2017) “Interictal epileptiform activity outside the seizure onset zone impacts cognition,” *Brain*, 140(8), pp. 2157–2168. doi:10.1093/brain/awx143.

Vogt, B.A. *et al.* (1995) “Human cingulate cortex: Surface features, flat maps, and cytoarchitecture,” *The Journal of Comparative Neurology*, 359(3), pp. 490–506. doi:10.1002/cne.903590310.

Vogt, B.A. (2016) “Midcingulate cortex: Structure, connections, homologies, functions and diseases,” *Journal of Chemical Neuroanatomy*, pp. 28–46. doi:10.1016/j.jchemneu.2016.01.010.

Vogt, B.A. and Laureys, S. (2005) “Posterior cingulate, precuneal and retrosplenial cortices: Cytology and components of the neural network correlates of consciousness,” *Progress in Brain Research*. Prog Brain Res, pp. 205–217. doi:10.1016/S0079-6123(05)50015-3.

Vöröslakos, M. *et al.* (2018) “Direct effects of transcranial electric stimulation on brain circuits in rats and humans,” *Nature Communications*, 9(1). doi:10.1038/s41467-018-02928-3.

Wagner, T. *et al.* (2007) “Transcranial direct current stimulation: A computer-based human model study,” *NeuroImage*, 35(3), pp. 1113–1124. doi:10.1016/j.neuroimage.2007.01.027.

Wang, J. and Wade, A.R. (2011) “Differential attentional modulation of cortical responses to S-cone and luminance stimuli,” *Journal of Vision*, 11(6), pp. 1–15. doi:10.1167/11.6.1.

Wang, M. *et al.* (2022) “In vivo Measurements of Electric Fields During Cranial Electrical Stimulation in the Human Brain,” *Frontiers in Human Neuroscience*, 16, p. 41. doi:10.3389/fnhum.2022.829745.

Weiner, K.S. and Grill-Spector, K. (2012) “The improbable simplicity of the fusiform face area,” *Trends in Cognitive Sciences*. Elsevier, pp. 251–254. doi:10.1016/j.tics.2012.03.003.

WHO (2018) *Principaux repères sur l’épilepsie*, *Organisation mondiale de la Santé*. Available at: https://www.who.int/fr/news-room/fact-sheets/detail/epilepsy (Accessed: September 19, 2021).

Willis, M.L. *et al.* (2019) “Anodal tDCS and high-frequency TRNs targeting the occipitotemporal cortex do not always enhance face perception,” *Frontiers in Neuroscience*, 13(FEB). doi:10.3389/fnins.2019.00078.

Wilsch, A. *et al.* (2018) “Transcranial alternating current stimulation with speech envelopes modulates speech comprehension,” *NeuroImage*, 172, pp. 766–774. doi:10.1016/j.neuroimage.2018.01.038.

Wilson, J. V and Reynolds, E.H. (1990) “Texts and documents. Translation and analysis of a cuneiform text forming part of a Babylonian treatise on epilepsy.,” *Medical history*, 34(2), pp. 185–98. doi:10.1017/s0025727300050651.

Windhoff, M., Opitz, A. and Thielscher, A. (2013) “Electric field calculations in brain stimulation based on finite elements: An optimized processing pipeline for the generation and usage of accurate individual head models,” *Human Brain Mapping*, 34(4), pp. 923–935. doi:10.1002/hbm.21479.

Wong, R.K. and Stewart, M. (1992) “Different firing patterns generated in dendrites and somata of CA1 pyramidal neurones in guinea-pig hippocampus.,” *The Journal of Physiology*, 457(1), pp. 675–687. doi:10.1113/jphysiol.1992.sp019401.

Woods, A.J. *et al.* (2016) *A technical guide to tDCS, and related non-invasive brain stimulation tools*, *Clinical Neurophysiology*. doi:10.1016/j.clinph.2015.11.012.

Yang, L.-Z. *et al.* (2014) “Electrical Stimulation over Bilateral Occipito-Temporal Regions Reduces N170 in the Right Hemisphere and the Composite Face Effect,” *PLoS ONE*. Edited by J. Hsiao, 9(12), p. e115772. doi:10.1371/journal.pone.0115772.

Yavari, F. *et al.* (2018) "Basic and functional effects of transcranial Electrical Stimulation (tES)—An introduction," *Neuroscience & Biobehavioral Reviews*, 85(July 2017), pp. 81–92. doi:10.1016/j.neubiorev.2017.06.015.

Yilmazer-Hanke, D.M. (2012) "Amygdala," in Mai, J.K. and Paxinos, G. (eds) *The Human Nervous System*. Third edit. Amsterdam: Elsevier, pp. 401–424.

Zago, S. *et al.* (2016) "Historical Aspects of Transcranial Electric Stimulation," in Brunoni, A., Nitsche, M., and Loo, C. (eds) *Transcranial Direct Current Stimulation in Neuropsychiatric Disorders: Clinical Principles and Management*. Springer International Publishing, pp. 3–19. doi:10.1007/978-3-319-33967-2.

Zhang, X., Liu, J. and He, B. (2014) "Magnetic Resonance Based Electrical Properties Tomography: A Review," *IEEE reviews in biomedical engineering*, 7, p. 87. doi:10.1109/RBME.2013.2297206.

Table of figures

Appendix

Brain Stimulation 15 (2022) 1–12

Contents lists available at ScienceDirect

Brain Stimulation

journal homepage: http://www.journals.elsevier.com/brain-stimulation

Transcranial Electrical Stimulation generates electric fields in deep human brain structures

Samuel Louviot [a], Louise Tyvaert [a, b], Louis G. Maillard [a, b], Sophie Colnat-Coulbois [a, c], Jacek Dmochowski [d], Laurent Koessler [a, *]

[a] Université de Lorraine, CNRS, CRAN, F-54000, Nancy, France
[b] Université de Lorraine, CHRU-Nancy, Service de Neurologie, F-54000, Nancy, France
[c] Université de Lorraine, CHRU-Nancy, Service de Neurochirurgie, F-54000, Nancy, France
[d] Department of Biomedical Engineering, City College of New York, New York, NY, USA

ARTICLE INFO

Article history:
Received 5 March 2021
Received in revised form
21 October 2021
Accepted 1 November 2021
Available online 4 November 2021

Keywords:
Transcranial electrical stimulation
Human *in-vivo*
Stereoelectroencephalography
Electric field
HD electrodes
Hippocampus

ABSTRACT

Background: Transcranial electrical stimulation (TES) efficiency is related to the electric field (EF) magnitude delivered on the target. Very few studies (n = 4) have estimated the *in-vivo* intracerebral electric fields in humans. They have relied mainly on electrocorticographic recordings, which require a craniotomy impacting EF distribution, and did not investigate deep brain structures.
Objective: To measure the electric field in deep brain structures during TES in humans *in-vivo*. Additionally, to investigate the effects of TES frequencies, intensities, and montages on the intracerebral EF.
Methods: Simultaneous bipolar transcranial alternating current stimulation and intracerebral recordings (SEEG) were performed in 8 drug-resistant epileptic patients. TES was applied using small high-definition (HD) electrodes. Seven frequencies, two intensities and 15 montages were applied on one, six and one patients, respectively.
Results: At 1 mA intensity, we found mean EF magnitudes of 0.21, 0.17 and 0.07 $V \cdot m^{-1}$ in the amygdala, hippocampus, and cingulate gyrus, respectively. An average of 0.14 ± 0.07 $V \cdot m^{-1}$ was measured in these deep brain structures. Mean EF magnitudes in these structures at 1Hz were 11% higher than at 300Hz ($+0.03$ $V \cdot m^{-1}$). The EF was correlated with the TES intensities. The TES montages that yielded the maximum EF in the amygdalae were T7-T8 and in the cingulate gyri were C3-FT10 and T7-C4.
Conclusion: TES at low intensities and with small HD electrodes can generate an EF in deep brain structures, irrespective of stimulation frequency. EF magnitude is correlated to the stimulation intensity and depends upon the stimulation montage.
© 2021 The Authors. Published by Elsevier Inc. This is an open access article under the CC BY-NC-ND license (http://creativecommons.org/licenses/by-nc-nd/4.0/).

1. Introduction

Transcranial Electrical Stimulation (TES) is one of the most developed non-invasive brain stimulation technique. Both transcranial direct current stimulation (tDCS) [1] and transcranial alternating current stimulation (tACS) [2] have shown promise to understand brain function [3] and as an investigational treatment for neurological [4,5] and psychiatric [6,7] disorders. At the neuronal scale (*in-vitro* experiments), the mechanism underlying the beneficial effects of TES relates to the modulation of the neuronal membrane potential by the electric field (EF) applied, and potentially the plastic changes that may ensue [2,8–16]. Under the ideal conditions of *in-vitro* experiments, an EF as low as 0.2–0.5 $V \cdot m^{-1}$ can shift spike timing [11,14,17–19]. Our understanding of the EF generated in the brain when delivering low-frequency electric currents with scalp electrodes has been derived from computational models of the current flow [20–22]. The type of electrodes, their montages and the current intensities applied, which are crucial to generate a sufficient EF to modulate the neuronal population, are still a matter of debate [23–26]. One of the biggest challenges in TES is generating an EF in deep brain structures such as the limbic system [27,28] that would have a truly significant impact at the clinical level (e.g., improvement of Epilepsy or Alzheimer's diseases conditions) and at the fundamental level (e.g., understanding of memory processes, including learning).

* Corresponding author.
E-mail address: laurent.koessler@univ-lorraine.fr (L. Koessler).

https://doi.org/10.1016/j.brs.2021.11.001
1935-861X/© 2021 The Authors. Published by Elsevier Inc. This is an open access article under the CC BY-NC-ND license (http://creativecommons.org/licenses/by-nc-nd/4.0/).

TES effects in deep brain structures have generated two major issues in the scientific community.

The first issue concerns the mechanisms underlying the beneficial effects of TES in deep brain structures. In-vivo non-human primate studies have found spike timing changes induced by tACS in the hippocampus and basal ganglia and measured EF (peak field strengths of 0.3 $V \cdot m^{-1}$) in these structures [29,30]. Clinical studies have also shown [31–33] encouraging results in mesial temporal lobe epilepsy (i.e., decrease of seizure and interictal discharge frequencies). However, currently, the ability to directly neuromodulate (i.e., without other indirect activations) deep brain structures is under considerable debate, especially since several studies in humans and non-human animal models suggest alternative peripheral mechanisms [34–37].

The second issue concerns the ability of electric currents to penetrate tissues to reach deep brain regions at low TES intensities (safety issue). Several TES studies did not induce volume conduction and little to no EF magnitudes within the brain volume [38–40]. The most frequent reasons advanced for this lack of findings are the decrease of the EF due to the depth between the stimulation electrodes and the anatomical target [41], and the head tissue resistivities-especially the skull's high resistivity [42]. Yet, computational studies have found deep brain EF hotspots with realistic MRI-based modelling [27,43–45]. Moreover, other recent studies reported an electric field induced by TES using *in-vivo* human investigations [41,46–48]. Opitz et al. reported EF magnitudes up to 0.5 V m^{-1} in the superficial cortex for a 1 mA tACS using saline soaked sponge electrodes (25 cm^2) and Huang et al. presented an EF of 0.4 $V \cdot m^{-1}$ in cortical structures for a 2 mA tACS using rubber electrodes (4 cm^2). These results can be biased because they relied on combined stereoelectroencephalographic (SEEG) and electrocorticographic (ECoG) investigation in which large skull defects were performed that can affect these intracerebral EF magnitudes [49]. In a computational study, it was demonstrated that conductivity of large skull defects increased and current were concentrated in cortex underlying the defect area (Datta et al., 2010).

Using deep brain stimulation electrodes, two studies estimated the global electric fields achieved in subthalamic nuclei and internal globus pallidus using two distant electrodes (2 cm–4 cm) and a DC experiment (n = 2 patients; EF ranged from 0.19 to 0.26 $V \cdot m^{-1}$ at 4 mA intensity) [47] or an AC experiment [48] (n = 1 patient; EF_{max}: 0.08 $V \cdot m^{-1}$ for an intensity of 1 mA).

Considering these limited and variable observations, which leave the two issues mentioned above wide open, the main objective of the present study was to measure the intracerebral EF during TES with an emphasis on deep brain structures. To do so, we leveraged the unique ability to record the EF *in-vivo* in humans using depth electrodes implanted in drug-resistant epileptic patients (SEEG) by applying TES using small high-definition (HD) electrodes and low intensity ($\leq$1 mA). Our secondary objectives were, first, to investigate the influence of TES frequency, intensity, and montages on EF magnitudes and second, to investigate the influence of the depth (i.e., the distance between the depth electrodes and the TES electrodes) on EF magnitudes.

2. Materials & methods

2.1. Patients

Eight patients (4 females and 4 males; age: 30 ± 11 years old) with focal drug-resistant epilepsy were prospectively included in this study. Patients were informed early and gave their consent prior to participation (NCT03644732). Patients were instructed to report any discomfort during TES and were told that the stimulation could be stopped if they felt pain at any time. They were all candidates for presurgical evaluation. Their standard presurgical evaluation included: neuropsychological tests and long-term (5-day period) high-resolution electroencephalographic (EEG) video recordings combined with electrical source imaging analysis, positron emission tomography (PET) and high-resolution magnetic resonance imaging (MRI). SEEG was performed in these patients to complete the presurgical evaluation to better define the epileptogenic zone and the surrounding functional area [50]. In all included patients, SEEG allowed delineating a single and spatially limited epileptogenic zone.

2.2. Stereoelectroencephalography

For each patient, an individual SEEG implantation scheme was defined according to the presurgical evaluation and epileptogenic zone hypotheses.

Under general anesthesia, the intracerebral multi-contact electrodes (0.8 mm-diameter, from 5 to 18 Platinum/Iridium contacts with 2 mm length separated by 1.5 mm insulator; Dixi Medical®, Besançon, France) were implanted according to a standard stereotactic procedure [51]. The SEEG electrodes were inserted into a screw (2.45 mm-diameter) and secured with a tight seal to prevent cerebrospinal fluid leak. Immediately after the implantation, patients underwent a postoperative CT-scan. Using a co-registration of the CT-scan with the preoperative high-resolution MRI (voxel-based registration; SPM 8 toolbox for Matlab; MathWorks, Natick, Massachusetts), the anatomical positions of each electrode contact were determined, and potential surgical complications were inspected. Due to the minimally invasive procedure used for SEEG investigation, anatomical structures did not move in the intracranial volume (no CSF leakage and no brain swelling) and MR-CT co-registration can be assumed as very precise (<1 mm [52]).

In addition to the intracerebral multi-contact electrodes, 27 scalp electrodes were placed according to an adapted 10/20 system [53]. Visual review of the simultaneous EEG-SEEG recordings was done prior to the tACS experiments. Moreover, the visual review checked for unusual electrophysiological activity such as breach rhythm which is defined as a focal increase in the amplitude activity of alpha, beta and mu rhythms which tends to develop over or near the area of a bony skull defect, such as after craniotomy or cranial surgery [54]. In our study, no breach rhythm was observed.

During tACS experiments, SEEG signals were recorded with a 256-channel (2 × 128 channels) amplifier with a 10 kHz sampling rate, 16 bits resolution at 0.25 μV/bit, a high-pass filter 1st order at 0.3 Hz, an input impedance superior to 10 GΩ and an input signal range ± 8.191 mV (NeuroPort™ System by Blackrock® Microsystems, Salt Lake City, UT, USA). The recording device's ground was set on the right foot, away from the TES electrodes and the recording reference, which was set on a deep SEEG contact.

2.3. Transcranial electrical stimulation

Before the intracerebral electrode withdrawal, tACS were performed using two HD electrodes (12 mm external diameter; Soterix Medical®, New York, NY, USA). Both were inserted in an electrode-holder (24 mm diameter) filled with a conductive gel, creating a 4.52 cm^2 stimulation area on the scalp for each electrode. The impedances were checked before, during, and after each stimulation and were always inferior or equal to 5kΩ. According to the HD electrodes' geometry, current densities generated on site were 0.11 $mA \cdot cm^{-2}$ and 0.22 $mA \cdot cm^{-2}$ for 0.5 mA and 1 mA intensities, respectively. The stimulation was delivered through these

electrodes using a multichannel TES stimulator MxN-9 (Soterix Medical®, New York, NY, USA). TACS was a bipolar sinusoidal waveform which can be expressed by:

$$s(t) = I.\sin(2\pi ft)$$

where I is the stimulation intensity in milli-Ampere (mA) (i.e., the peak to baseline value of the intensity) and f the stimulation frequency in Hertz (Hz).

A stimulation design (Fig. 1) was defined by its frequency, intensity, and montage. A typical session had a 2-min duration (30-s ramp up, 1-min full intensity, 30-s ramp down) at a given intensity and frequency. Each session was separated by a 1-min resting state, tACS off. During all sessions, patients were in a resting state with eyes open. For data analysis, the most superficial SEEG contacts (outside of the brain) were discarded to avoid aberrant values.

For one patient (Patient #0), tACS experiment was done using seven different frequencies (1 Hz; 3 Hz; 7 Hz; 35 Hz; 71 Hz; 140 Hz and 300 Hz). For the other patients (Patient #1–7), tACS was applied at 300 Hz only. This frequency of interest was between the large-amplitude LFP oscillations and the spiking activity i.e., in a frequency band with low neuro-electrophysiological activity. For a detailed analysis regarding the reliability of our stimulation and acquisition systems at the frequency used, see Supplementary Material (Supplementary data 1, Figs. 1–2). Finally, the TES electrode coordinates were numerically collected by fitting in Brainstorm [55] a Colin27 generic 10-10 EEG cap on the individual patient's head model.

2.4. Intracerebral electric field

This study included all eight patients. They had an average of 14 (±3) SEEG electrodes and 170 (±35) intracerebral contacts. TACS montages were defined using the MRI-CT co-registrations which showed the positions and trajectories of each intracerebral multi-contact electrode [51] and thus allowed cranio-anatomical correlations [56]. To guarantee asepsis conditions, a minimum distance of at least 5 cm was maintained between the closest implanted SEEG electrodes and the TES electrodes. To target both the hippocampus/amygdala complex and the cingulate gyri, an FT9-FT10 or T7-C4 or C3-FT10 montage was chosen. These montages were chosen to (1) get the EF's largest component along the SEEG electrodes' direction, (2) reach the deep targeted structures and (3) place as far as possible the two stimulation electrodes to maximize the current flowing inside the brain (minimizing the scalp shunt) [57,58].

Bipolar alternative current stimulations were done at two different intensities: 0.5 mA and 1 mA. The first objective was to investigate the intracerebral electric field specifically in deep brain structures such as the hippocampus, amygdala, and cingulate gyrus.

In theory, the EF is the electric potential gradient in the three directions of space (x,y,z):

$$\vec{E} = -\overrightarrow{grad}\,\vec{V} = -\left(\frac{\partial V}{\partial x}\,\vec{u_x} + \frac{\partial V}{\partial y}\,\vec{u_y} + \frac{\partial V}{\partial z}\,\vec{u_z}\right) \quad (1)$$

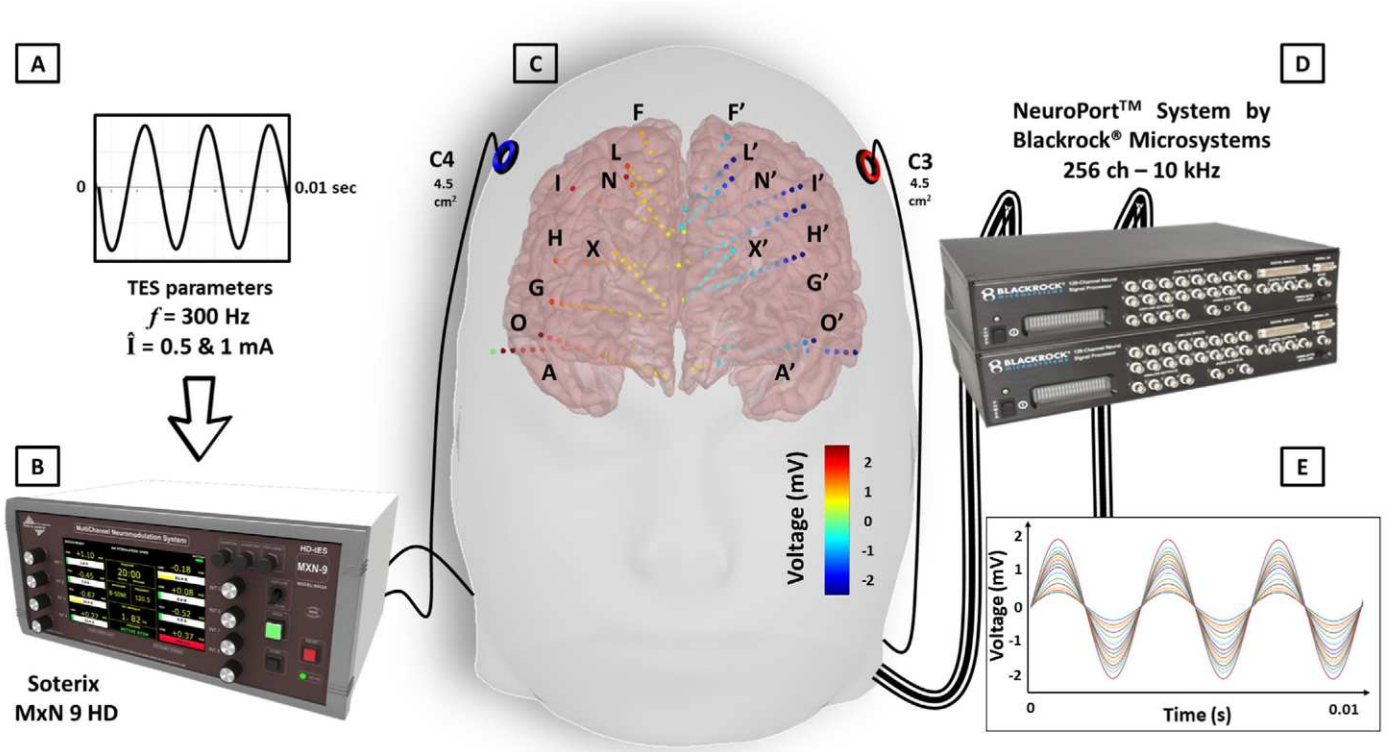

Fig. 1. Title: Simultaneous combination of transcranial alternative current stimulations (tACS) and SEEG recordings.
Caption: Bipolar sinusoidal signals at 300 Hz (part A) were delivered using a Soterix MxN stimulator (part B), and two HD ring electrodes (4.5 cm^2, active electrode in red, neutral electrode in blue) (Part C). A 256-channel amplifier (NeuroPort™ System by Blackrock® Microsystems, Salt Lake City, UT, USA) (part D) was used to record the sinusoidal signals in all intracerebral multi-contact electrodes (superimposed SEEG signals are represented in colored lines) (part E). In part C, colors represent the *in-vivo* measured voltage in all intracerebral contacts (n = 140; colored dots) using a realistic head model (patient 7) with a C3–C4 stimulation at 300 Hz and 1 mA intensity. (For interpretation of the references to color in this figure legend, the reader is referred to the Web version of this article.)

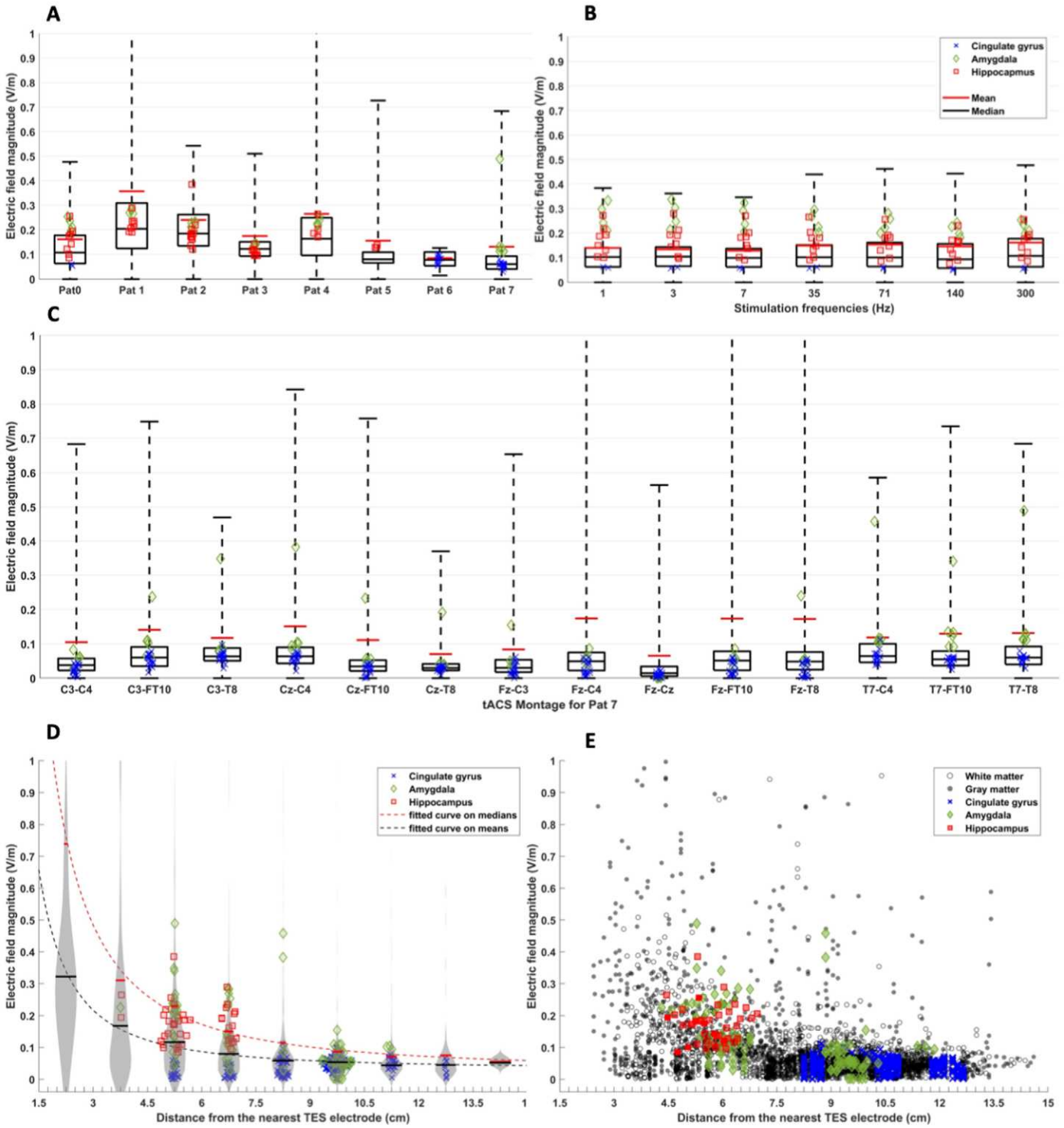

Fig. 2. Title: Electric field magnitude distribution in the cohort according to different tACS frequencies, montages, and the distance from the nearest TES electrode.
For all figures, the EF magnitudes in deep cortical structures are displayed with symbols (hippocampus: red squares, amygdala: green diamonds, cingulate gyrus: blue crosses). **A:** Electric field magnitude in the entire brain for all patients for a tACS at 300Hz and 1 mA. **B:** Electric field magnitude in the entire brain for every frequency tested in Pat 0 at 1 mA. **C:** Electric field magnitude in the entire brain for all montages tested in Pat 7 at 300Hz and 1 mA. For A, B and C: whiskers, considered as minimum and maximum values, represent 2.5 the standard-deviation of every EF magnitude distribution and boxes represent the 25th and 75th percentiles values of EF magnitudes. Black lines inside the box are the median values of the EF magnitude distribution and red lines indicate the means. **D:** Density of the EF magnitude distribution against the distance from the nearest TES electrode. Dashed lines represent the fitted power-curves from a non-linear regression on means values (in red; $R^2 = 0.99$) and median values (in black; $R^2 = 0.99$). **E:** Scattered representation of EF magnitudes against the distance from the nearest TES electrode. Gray and white dots are EF in the gray and white matter, respectively. (For interpretation of the references to color in this figure legend, the reader is referred to the Web version of this article.)

The EF along the direction x is expressed:

$$\overrightarrow{E}(x) = -\frac{dV}{dx}\overrightarrow{u_x} \quad 2$$

with $\overrightarrow{u_x}$ the unit vector along the direction x and the EF magnitude:

$$\left|\overrightarrow{E_x}\right| = -\frac{dV}{dx} \quad 3$$

Also, using $\overrightarrow{u_p}$ the unit vector, which has its module and its directionality given by 2 contiguous SEEG contacts on the same electrode, we can express the electric field along that SEEG electrode by

$$\overrightarrow{E}(p) = -\frac{dV}{dp}\overrightarrow{u_p} \quad 4$$

With dp the distance between the 2 contiguous contacts.

Thus, the EF was obtained by calculating the gradient of the voltage measured on each contact of a same SEEG electrode.

First, a baseline correction was performed. It was executed by performing a manual selection of the analysis window of the SEEG signal under stimulation, while avoiding potential DC offset and artifacts (see supplementary data 1, Fig. 3A). To do so, the raw SEEG signal was subtracted by the mean of the signal calculated in a 2-s window right before the stimulation, when patients were in a resting state (see supplementary data 1, Figs. 3 and 4).

Every baseline correction window of raw SEEG signals was visually checked, and no artifact observed.

Second, all SEEG signals were superimposed upon each other to facilitate the selection of the time window analysis (after the ramp up and before the ramp down of the tACS).

Third, a Fast Fourier Transform was computed on the SEEG signal in each contact using Matlab `fft()` function [59]. The two-sided power spectrum of the FFT was converted to a single-sided power spectrum. Then, the amplitude spectrum was obtained by calculating the square root of this single-sided power spectrum's absolute value (Bessel-Parseval theorem). Finally, to obtain our voltage values (V), the maximum value (peak) was searched in the amplitude spectrum between 297 Hz and 303 Hz with a frequency resolution of 0.016 Hz. The baseline correction (0 Hz) did not influence the voltage amplitude V at these high frequencies.

The Matlab (The MathWorks®) gradient function was used for calculating the gradient of V along a multi-contact SEEG electrode to get the EF module. This calculation was repeated for all SEEG electrodes.

For each patient and all SEEG electrodes, the mean electric field and its standard deviation were calculated (Table 1). The mean EF values for the entire brain were calculated by:

$$\overline{|E|} = \frac{1}{n}\sum_{j=1}^{n}|E|_j \quad 5$$

where n is the number of SEEG contacts and $|E|_j$ the EF magnitude calculated on a contact j.

EF distributions according to all patients, the TES frequencies and montages were displayed using boxplots with boxes represented the 25th and the 75th percentiles and whiskers showed the EF magnitude values spread with a coverage of 2.5 the standard deviation.

The position of each intracerebral contact was automatically detected in the individual CT-scan [60] and visually defined using patients' MRI-CT co-registration. Automatic segmentation method (CAT12, SPM12 toolbox; [61]) allowed to identify gray and white matters.

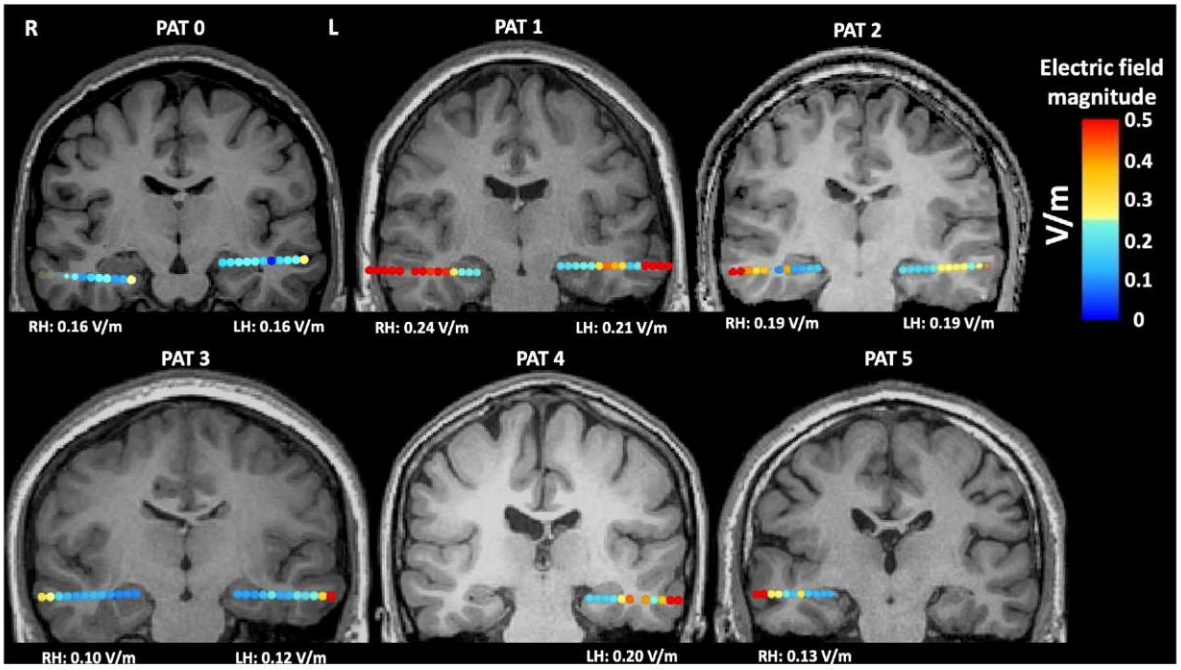

Fig. 3. Title: Empirical electric fields (EF) in the hippocampi.
Caption: Empirical electric fields (EF) in the hippocampi for a 1 mA tACS using FT9-FT10 montage. Below each individual MRI with the reconstructed SEEG electrodes, the mean EF values of SEEG contacts within the deep structures was indicated. (L: left, R: right, H: Hippocampus). (For interpretation of the references to color in this figure legend, the reader is referred to the Web version of this article.)

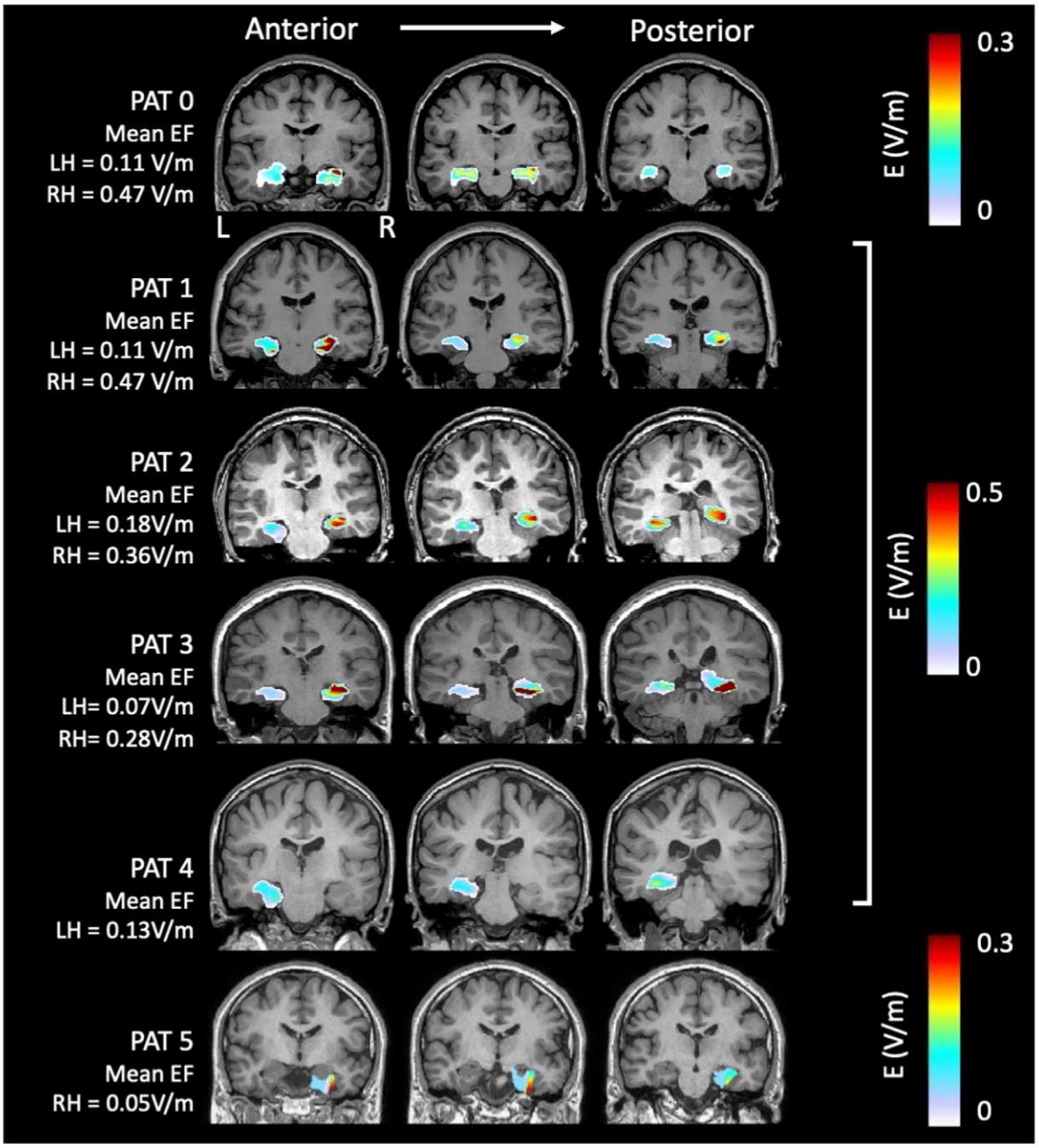

Fig. 4. Title: Spatial distribution of the electric field magnitudes in hippocampi using the full tensor calculation.
Caption: Coronal view of spatial distribution of the electric field magnitudes in hippocampi after calculating the full electric field (EF) tensor overlayed on individual patients' MRI. EF tensors were computed from the empirical values measured in SEEG contacts within the hippocampus. For each patient, three slices of interest are displayed (From left to right: anterior to posterior). (L: left, R: right, H: Hippocampus). (For interpretation of the references to color in this figure legend, the reader is referred to the Web version of this article.)

Table 1
Title : Means and standard deviations of the electric field magnitudes at 0.5 and 1 mA intensities in our cohort (EF: Electric field ; SEEG : stereoelectroencephalographic).

Patient	Nb of SEEG contacts	Mean EF at 0.5 mA ($V \cdot m^{-1}$)	Mean EF at 1 mA ($V \cdot m^{-1}$)
0	172	NA	0.16 (±0.19)
1	162	0.18 (±0.29)	0.36 (±0.58)
2	101	0.13 (±0.11)	0.24 (±0.22)
3	151	0.09 (±0.1)	0.17 (±0.20)
4	89	0.14 (±0.29)	0.26 (±0.58)
5	155	0.08 (±0.14)	0.16 (±0.29)
6	149	0.04 (±0.02)	0.08 (±0.04)
7	166	NA	0.13 (±0.27)

2.4.1. Deep brain structures investigation

We visually selected, thanks to the CT-MR co-registrations, SEEG contacts within the deep brain structures to study the EF in these regions. Electrophysiological data were checked by neurologists to confirm the previous selection and to determine boundaries between gray and white matter. Intracerebral SEEG contacts which recorded physiological brain activity were considered within the gray matter, and those which did not, were considered within the white matter [62]. Then, we calculated the mean and the standard deviation of the EF magnitudes in the deep brain structures (both right and left): amygdala, hippocampus, and cingulate gyrus. The mean was obtained by doing the same equation as (Eq. (5)) where n is the number of SEEG contacts within the deep structures and Ej the EF in the SEEG contact j (in the structures).

To estimate the EF in the entire volume of the deep brain structures, we calculated the EF tensors using the five following steps:

1. On the individual patient's MRI, anatomy was automatically labelled with CAT12 (a SPM12 toolbox) [63]. Thanks to this segmentation and labelling, different masks were generated: amygdala mask, hippocampus mask, cingulum mask (depending on the patient).
2. An interpolant F was calculated with the Matlab® function `F=scatteredInterpolant(x,y,z,v)` using all SEEG contacts (where x,y,z are the SEEG contact coordinates and v the measured voltage amplitudes) using a natural neighbor method [64].
3. The interpolated amplitudes were evaluated at the query points for each anatomical mask by calling F (qx,qy,qz) (where qx, qy and qz are the mask's voxel coordinates).
4. Then, the full gradient was calculated using the Matlab® function `gradient()`) on the evaluated interpolated amplitudes within each mask, which gave the electric field in the 3D space Ex, Ey, Ez.
5. The electric field magnitude was calculated in each voxel of the mask using $|E| = \sqrt{Ex^2 + Ey^2 + Ez^2}$. The mean and maximum interpolated EF were measured in each anatomical mask (hippocampus, amygdala, and in the cingulate gyrus).

Finally, a paired student's test was performed to compare the mean EF magnitudes and the mean tensor-based EF magnitudes in our population with the hypothesis H_0: the mean difference of mean EF magnitudes and mean tensor-based EF magnitudes is null.

2.5. Influence of tACS parameters

2.5.1. Influence of tACS frequency

To investigate the frequency dependence of the EF, we calculated the percentages of variation between the EF magnitudes obtained at different TES frequencies (1 Hz; 3 Hz; 7 Hz; 35 Hz; 71 Hz; 140 Hz) with the magnitudes obtained at the TES frequency of interest used in this study (i.e., 300 Hz). We calculated these variations as follows:

$$\%Variation(f) = \frac{1}{n}\sum_{i=1}^{n}\left(\frac{EF_i(f) - EF_i(f=300)}{EF_i(f=300)} \cdot 100\right)$$

With f the frequency tested, n the total number of intracerebral contacts.

This variation was calculated on all intracerebral contacts. Then, we calculated the difference (in $V \cdot m^{-1}$ and in percentage) of the mean EF magnitudes in the entire brain and the deep structures between the lowest (1 Hz) and the highest (300 Hz) frequencies.

2.5.2. Influence of tACS intensity

To investigate the impact of the tACS intensity, we calculated the EF values obtained at 0.5 mA and those obtained at 1 mA in all SEEG contacts. In order to discard SEEG contacts that could be saturated (especially at 1 mA), we used the `isoutlier()` Matlab function to remove the outliers which were over three standard deviations away from the mean of the error (i.e., the difference between measured and expected EF values).

A 1st degree polynomial linear regression was executed on the data ($E_1 = f(E_{0.5})$ with $E_{0.5}$ and E_1 the electric field distribution at 0.5 mA and at 1 mA, respectively) to estimate the coefficient of the given function. The fitted 1st degree polynomial curve can be expressed by:

$$E_1 = f(E_{0.5}) = p1 \cdot E_{0.5} + p2$$

where p1 (the slope) and p2 are the coefficients obtained from the model.

Then, we compared the empirical values E_1 with the predicted values E_{1th} (with a slope at exactly 2.00) by calculating the mean of the absolute difference (error) between E_1 and E_{1th} which can be considered as the Mean Absolute Error (MAE).

2.5.3. Influence of tACS montages

To investigate the impact of the tACS montage, a study was conducted with patient #7 (male 27 years old). Eighteen SEEG electrodes were implanted symmetrically in the same brain structures in both hemispheres (9 electrodes in each hemisphere) for a total of 203 intracerebral contacts (Fig. 1). SEEG electrodes sampled mainly the frontal lobe structures (cingulate gyri, supplementary motor areas, superior, middle, and inferior frontal gyri *e*tc.) and also both amygdalae. The principal objective was to investigate the impact of different tACS montages on the intracerebral EF values in deep brain structures.

Fifteen different montages based on the 10-10 system were used: C3-FT10; C3-T8; C3—C4; Cz-FT10; Cz-T8; Cz-C4; Fz-FT10; Fz-T8; Fz-C4; Fz-Cz; Fz-C3; Fz-T7, T7-FT10; T7-T8; T7-C4. Among these TES montages, we searched for those which gave the maximum mean EF value in the deep brain structures using empirical and tensor-based investigations (SEEG contacts in both hemispheres for amygdalae, anterior cingulate gyri, and middle cingulate gyri).

2.6. Influence of the depth

For every patient, the Euclidean distances between each intracerebral contact and the nearest TES electrode were measured. To study the influence of distance on EF magnitudes, we segmented the total distance in similarly sized segments and grouped EF magnitudes according to these segments. Then, we calculated the mean and median of the EF in each distance group. Next, assuming that the mean and median values would decrease as a function of the distance according to the inverse-square law, we performed a non-linear regression on those values by fitting a power curve expressed by:

$$f(d) = a \cdot \frac{1}{d^b} + c$$

where a, b and c are the non-linear regression coefficients and d the distance from the nearest TES electrode. Groups of EF magnitudes were displayed in violin plots by computing the density of the data distribution as a function of the depth.

3. Results

As expected, during TES, patients reported mild skin sensations (tickling) at both 0.5 mA and 1 mA intensities. No other side effects were noticed. No epileptic seizure was induced by the tACS experiments.

Altogether, patients had 1360 intracerebral SEEG contacts. The most superficial SEEG contacts, in addition to 21 SEEG contacts (which were detected as outliers) were discarded (n = 215). Therefore, this intracerebral EF study relied on 1145 SEEG contacts (average: 143 contacts/patient).

3.1. Intracerebral electric fields

Original data of this study, including individual anonymized MRI, SEEG electrode coordinates and EF magnitudes are available at Mendeley Data at: https://data.mendeley.com/datasets/sk279ktjv3/3.

Fig. 2A displays global EF distributions in our cohort (Patient #0–7).

In this population, 102 SEEG contacts sampled the deep brain structures: 42 were in the hippocampi, 28 in the amygdalae and 32 in the cingulate gyri (Table 2).

The mean and standard deviation (SD) of the EF in these deep brain structures were 0.14 ± 0.08 V·m^{-1}.

The mean and SD of the EF in the hippocampi were 0.17 ± 0.06 V·m^{-1} with a maximum of 0.38 V·m^{-1} for a 1 mA stimulation (Fig. 3).

The mean and SD of the EF in the amygdala were 0.21 ± 0.08 V·m^{-1} with a maximum of 0.49 V·m^{-1} for a 1 mA stimulation.

The mean and SD of the EF in the cingulate gyri were 0.07 ± 0.02 V·m^{-1} with a maximum of 0.11 V·m^{-1} for a 1 mA stimulation.

The mean and SD of the tensor-based EF magnitudes were 0.16 ± 0.14 V·m^{-1}, 0.19 ± 0.09 V·m^{-1} and 0.10 ± 0.07 V·m^{-1} for the hippocampi, amygdalae, and cingulate gyri, respectively (Fig. 4 for the spatial distribution in the hippocampus. For the full tensor, see supplementary data 2,3,4). There was no significant difference between the empirical mean EF values and the tensor-based mean EF values (paired student's t-test $p = 0.88$).

Table 2
Title : Electric field magnitudes in the deep brain structures.

Patient	Deep brain structures	Nb of SEEG contacts	Mean EF at 1 mA (V·m^{-1})	Mean tensor-based EF (V·m^{-1})	Max EF at 1 mA (V·m^{-1})	EF Value 1 (V·.m^{-1})	EF Value 2 (V·.m^{-1})	EF Value 3 (V·.m^{-1})	EF Value 4 (V·.m^{-1})	EF Value 5 (V·.m^{-1})
0	R Hippocampus	4	0.16	0.09	0.26	0.26	0.10	0.09	0.19	*NA*
	L Hippocampus	4	0.16	0.06	0.18	0.12	0.14	0.18	0.18	*NA*
	L Amygdala	4	0.22	0.09	0.25	0.25	0.24	0.21	0.20	*NA*
	L. Post Cingulate gyrus	2	0.06	*NA*	0.06	0.05	0.06	*NA*	*NA*	*NA*
1	R Hippocampus	4	0.24	0.47	0.29	0.21	0.23	0.24	0.29	*NA*
	L Hippocampus	4	0.21	0.11	0.23	0.19	0.19	0.21	0.23	*NA*
	L Amygdala	4	0.28	0.30	0.29	0.28	0.29	0.27	0.27	*NA*
2	L Hippocampus	5	0.19	0.07	0.22	0.20	0.19	0.18	0.17	0.22
	R Hippocampus	5	0.19	0.28	0.38	0.17	0.16	0.14	0.12	0.38
	L Amygdala	5	0.22	0.34	0.23	0.23	0.23	0.21	0.20	0.23
3	L Hippocampus	4	0.12	0.07	0.14	0.12	0.12	0.11	0.14	*NA*
	R Hippocampus	4	0.10	0.28	0.11	0.10	0.10	0.10	0.11	*NA*
	L Amygdala	4	0.14	0.10	0.14	0.14	0.14	0.14	0.13	*NA*
4	L Hippocampus	5	0.20	0.13	0.26	0.19	0.17	0.17	0.20	0.26
	L Amygdala	5	0.23	0.13	0.25	0.25	0.24	0.22	0.22	0.23
5	R Hippocampus	3	0.13	0.07	0.14	0.13	0.13	0.14	*NA*	*NA*
6	L. Ant Cingulate gyrus 1	2	0.09	0.08	0.1	0.08	0.10	*NA*	*NA*	*NA*
	L. Ant Cingulate gyrus 2	3	0.08		0.9	0.09	0.08	0.08	*NA*	*NA*
	L. mid Cingulate gyrus	2	0.06		0.06	0.05	0.06	*NA*	*NA*	*NA*
	R ant. Cingulate gyrus 1	2	0.10	0.08	0.1	0.09	0.10	*NA*	*NA*	*NA*
	R ant. Cingulate gyrus 2	2	0.09		0.09	0.08	0.09	*NA*	*NA*	*NA*
	R. mid Cingulate gyrus	2	0.07		0.06	0.06	0.07	*NA*	*NA*	*NA*
7	L ant. Cingulate gyrus	3	0.06	0.18	0.07	0.07	0.06	0.06	*NA*	*NA*
	L mid. Cingulate gyrus 1	3	0.07		0.08	0.07	0.07	0.08	*NA*	*NA*
	L mid. Cingulate gyrus 2	2	0.06		0.07	*NA*	0.05	0.07	*NA*	*NA*
	R ant. Cingulate gyrus	3	0.05	0.14	0.07	0.04	0.05	0.07	*NA*	*NA*
	R mid. Cingulate gyrus 1	3	0.07		0.07	0.07	0.06	0.07	*NA*	*NA*
	R mid. Cingulate gyrus 2	3	0.09		0.11	0.11	0.09	0.07	*NA*	*NA*
	L Amygdala	3	0.13	0.20	0.13	0.13	0.13	0.12	*NA*	*NA*
	R Amygdala	3	0.24	0.18	0.49	0.11	0.11	0.49	*NA*	*NA*

3.2. Influence of tACS parameters

3.2.1. Influence of tACS frequency

Fig. 2B and supplementary data 4 display global EF distributions of patient #0 according to tACS frequencies. In the entire brain and in the deep brain structures, compared to EF magnitudes at 300 Hz, global EF magnitudes varied around of 9 ± 8% and 5 ± 7%. Overall, the mean EF magnitudes at 1 Hz were 15% lower than at 300 Hz (i.e., −0.02 $V \cdot m^{-1}$). In opposition, in the deep brain structures, the mean EF magnitudes at 1Hz were 11% higher than at 300Hz (i.e., +0.03 $V \cdot m^{-1}$).

3.2.2. Influence of tACS intensity

6 patients were included for the EF magnitude comparison between a 0.5 mA and a 1 mA stimulation (2 datasets of 807 values; Patients #1–6). The measured slope (p1) from the linear regression varied from 2 (Patient #1–5) to 2.2 (Patient #6), and the determination coefficients ranged from $R^2 = 0.98$ (Patient #6) to $R^2 = 1.00$ (Patients #3–5) (see supplementary data 1 Fig. 6). Finally, the comparison of the empirical values to the predicted ones (with a slope exactly at 2.00) showed a MAE from 0.0003 (Patient #6) to 0.0174 (Patient #1). These values demonstrated EF is doubled when stimulation intensity is doubled.

3.2.3. Influence of tACS montage

Fig. 2C displays global EF distributions of patient #7 according to tACS montages. 166 SEEG contacts in patient #7 were used to analyze the influence of the TES montages. Fourteen montages were included in the analysis, and one was discarded (Fz-T7: noisy data). Seventeen contacts were in the cingulate gyri and 6 contacts in the amygdalae. There was no contact in the hippocampus.

In these deep brain structures, the TES montage which yielded the highest mean EF in the amygdalae was T7-T8 (0.24 $V \cdot m^{-1}$) and in the cingulate gyri was T7-C4 (0.09 $V \cdot m^{-1}$) (Table 3). The TES montage, which yielded the lowest mean EF was Fz-Cz for the deep brain structures investigated.

The highest tensor-based mean EF estimations showed the same effective montage (T7-T8) for the amygdalae (0.41 $V \cdot m^{-1}$) and Fz-C4 for the cingulate gyri (0.42 $V \cdot m^{-1}$) (supplementary data 3). Fz-Cz montage was also the montage which yielded the lowest mean EF.

3.3. Influence of the depth

The maximum distance from the nearest TES electrode and a SEEG contact was 14.6 cm. Ten segments of 1.5 cm were defined from 0 cm to 15 cm and EF magnitudes were grouped according to these segments. No EF magnitudes were found between 0 cm and 1.5 cm.

The measured coefficients from the non-linear regression on the median (black dashed line in Fig. 2D) EF distribution across groups were: $a = 1.28$ (0.92, 1.63), $b = -1.76$ (with −2.13 and −1.39 as the 95% confidence bounds), $c = 0.03$ (0.01, 0.05) and a determination coefficient of $R^2 = 0.99$.

The measured coefficients from the non-linear regression on the mean (red dashed line in Fig. 2D) EF distribution across groups were: $a = 2.8$ (2.1, 3.51); $b = -1.65$ (−1.99, −1.31); $c = 0.03$ (−0.02, 0.07) and a determination coefficient of $R^2 = 0.99$.

Fig. 2E displays global distribution of the EF magnitudes in the entire brain and the deep brain structures in our cohort.

4. Discussion

The human *in-vivo* estimation of electric field during TES poses great technical and methodological challenges. While the simultaneous combination of intracerebral human EEG recordings with TES could greatly contribute to this endeavor, it is rare - only a few clinical contexts require intracerebral recordings in humans such as Parkinson's disease or drug-resistant epilepsies [41,46–48] - and also highly challenging. To the best of our knowledge, compared to previous *in-vivo* human studies, our study included a higher number of patients and is the first to measure the intracerebral EF with a high number of SEEG contacts generated by low intensity-tACS using small HD electrodes.

SEEG is particularly relevant for the intracerebral EF investigation. First, it offers a high spatial resolution in depth, which makes the EF investigation from superficial to deep brain structures possible. Second, it relies on the implantation of depth electrodes through very small guide screws inserted into the skull, which do not require craniotomy where a bone flap is temporally removed from the skull to access the brain. Computational studies have shown that skull defects from craniotomies impact brain sources stimulations [49] or localizations [65,66]. For instance, in the TES context, Datta et al. demonstrated that a craniotomy (moderate/large skull defect) leads to an increase of peak cortical EF, especially when one stimulating electrode was placed over the skull defects [49]. In our study, the size of the skull defect (2.45 mm-diameter) is at least 30 times smaller than the size of a craniotomy (around 7-10 cm-diameter) performed during epilepsy surgery. In addition, craniotomy induces breach rhythms, which cause an increase in the amplitude of alpha, beta, and mu rhythms, leading to the breach effect [54]. In tACS studies at low frequencies in patients with craniotomy (e.g., electrocorticography investigation), the high voltage of breach rhythms can induce artifacts on the signal and so mis-estimation of the EF. In contrast, in the present study, thanks to simultaneous EEG-SEEG recording performed before the tACS investigation, there was no breach rhythm detected. Further, compared to Opitz et al. [46], who placed TES electrodes (25 cm^2) over both temples close to SEEG electrodes' holes (right and left temporal lobes), our study placed small TES electrodes far (at least 5 cm) from the first holes performed for the SEEG investigation. Thus, the impact of the "craniotomy" performed during the SEEG implantation in our study should be low, if not negligible, in the EF measurement. It is also worth mentioning that, according to

Table 3
Title : Electric field magnitudes according to differents tACS montages in patient #7.

Mean EF magnitudes ($V \cdot m^{-1}$)	Cz-FT10	Cz-T8	Cz-C4	C3-FT10	C3-T8	C3–C4	T7-FT10	T7-T8	T7-C4	Fz-FT10	Fz-T8	Fz-C4	Fz-Cz	Fz-C3
L ant. cingulate gyrus	0.03	0.03	0.06	0.06	0.05	0.04	0.06	0.05	0.05	0.05	0.04	0.05	0.01	0.01
L mid. cingulate gyrus 1	0.04	0.04	0.07	0.07	0.07	0.04	0.06	0.06	0.05	0.05	0.05	0.05	0.02	0.01
L mid. cingulate gyrus 2	0.03	0.03	0.06	0.06	0.06	0.02	0.04	0.05	0.05	0.04	0.05	0.04	0.02	0.00
R ant. cingulate gyrus	0.01	0.02	0.04	0.03	0.04	0.01	0.04	0.05	0.05	0.01	0.02	0.01	0.00	0.02
R mid. cingulate gyrus 1	0.02	0.03	0.06	0.05	0.06	0.01	0.05	0.06	0.07	0.01	0.02	0.01	0.01	0.04
R mid. cingulate gyrus 2	0.00	0.02	0.05	0.04	0.08	0.02	0.05	0.06	0.09	0.02	0.00	0.02	0.00	0.05
L Amygdala	0.05	0.04	0.10	0.11	0.09	0.06	0.13	0.12	0.11	0.06	0.05	0.06	0.00	0.05
R Amygdala	0.11	0.09	0.18	0.12	0.17	0.05	0.17	0.24	0.22	0.05	0.11	0.05	0.00	0.08

simultaneous EEG-SEEG studies of brain source detections, the volume conduction can be considered as being normal (i.e., without currents leakage and breach rhythms) [67–69].

Two previous studies investigated the global intracerebral EF using only SEEG recordings ([46], n = 1 patient; [41], n = 1 patient) and two studies investigated the intracerebral EF in the subthalamic nuclei and internal globus pallidus ([47], n = 3 patients; [48], n = 1). However, the methodology and objectives of these four studies (regarding both recording and stimulating) differed substantially from ours. First, our study used SEEG recording coupled with low intensity tACS, small electrodes, and no craniotomy. Second, we showed the ability of TES to reach the deep limbic structures (cingulate gyrus, hippocampus, and amygdala) with a mean electric field of 0.14 $V \cdot m^{-1}$ at 1 mA intensity. Despite the relatively low numbers of SEEG contacts, which were not homogeneously located (on a 3D grid) in the deep structures due to clinical constraints, the tensors-based EF magnitude confirmed our results. Thus, pending further validation of our results in a larger cohort, our study suggests that low-intensity TES can be proposed for neuromodulation of deep brain structures.

Interestingly, our findings showed values higher than those required to induce neural entrainment and stochastic effects (at lower frequency TES) [11,14,18,19,70]. Our results bring fundamental biophysical evidence supporting the promising results of deep structure neuromodulation using TES [31,32,71,72]. In a previous paper, we demonstrated that the volume conduction laws applied from deep electrical brain sources (epileptic focus) to scalp electrodes [68]. Therefore, we expected that the volume conduction laws applied from a scalp electrical source (TES electrodes) to the deep brain structures.

Our current study provides empirical evidence that the reciprocity principle used in few TES studies [73,74] can also apply to deep brain sources. From a biophysical point of view, we also showed that the EF magnitudes in the entire brain, according to the depth, followed the same distribution as Huang et al. [41]. As expected, because of the biophysical properties, EF magnitudes decreased as a function of the depth following a power-curve with coefficients close to the inverse-square law value (theoretically $b = 2$). The presence of low EF magnitudes in the most external parts of the brain can be explained by the positions between the current sources (i.e., the stimulating scalp electrodes) and the SEEG contacts.

In the present study, we found a strong correlation between the intracerebral electric field magnitude and the TES intensity at 300 Hz. As expected, when the stimulation intensity doubles, the electric field strength doubles as well. Huang et al. qualitatively reported this linearity on the intracerebral voltage measurements [41]. Assuming the purely resistive nature of the head tissues (quasi-static assumption), which was confirmed by our results on the tACS frequency investigation, this linear relationship between stimulation intensity and EF magnitudes can be extrapolated for other TES frequency stimulations. In addition, we did not observe body resistance reduction, contrary to Chhatbar et al. who used tDCS and demonstrated this phenomenon when stimulation intensity increased [47]. One plausible account of this discrepancy could be that the alternative current of tACS does not polarize the tissues as tDCS does. Therefore, the body resistance would be less affected by tACS. Considering both the recent tDCS studies which used 4 mA [47,75–77] and our own observations (i.e., a mean of 0.14 $V \cdot m^{-1}$ EF in the deep brain structures and the linear relationship between intensity and EF magnitudes), we would expect higher electric fields.

Computational studies have demonstrated the importance of the target's orientation regarding the current flow [78,79], the stimulation electrodes' position [26,57,80,81], and a detailed head tissues modeling [27,82–85]. The two studies which compared, predicted and measured EF in humans reported good correlations ($0.70 \leq r \leq 0.75$) but not perfect predictions ($0.50 \leq r^2 \leq 0.58$) [41,85]. The extrapolation of these studies needs further investigation and validation using human *in-vivo* datasets. In our study, we showed that the TES montages producing the strongest EF in deep brain structures were those with the longest distance between the TES electrodes (i.e., minimal scalp shunt). The smaller EF magnitudes in the cingulate gyri (by comparison to the complex amygdala/hippocampus) can be explained by the orientation of the SEEG electrodes. Also, the low empirical EF magnitudes found with TES montages of the closest electrodes (such as Fz-Cz) seem to reflect the scalp shunt phenomenon. These results are in line with a recent computational study [57].

Despite its original contribution and strengths, our study also has limitations. First, due to the rare and challenging combination of TES and SEEG recordings, the study still includes a relatively low number of patients (especially for the influence of TES montages). Our findings should therefore encourage additional research in the field of intracerebral EF estimation in human *in-vivo* for both methodological and fundamental (neuromodulation) purposes. The second limitation is that the influence of TES frequency was evaluated in one subject only, while the tACS parameters were limited to 300 Hz and 1 min stimulation in all other individual brains tested. However, the choice of 300 Hz was particularly adapted to this methodological study of intracerebral EF investigation because it falls in a frequency band where electrophysiological activity of the human brain is low. In the entire brain, we observed an increase (15%) of the mean EF magnitudes in function of the frequency. This finding is in opposition to the one from Opitz *et al.* This difference could be explained by some discrepancies. First, the anatomical and biophysical properties between species (humans versus monkeys) differ. Second, the number and the positions of the intracerebral contacts in the brain volume differ: 172 contacts with a perpendicular implantation (left to right) in our study versus 64 contacts with a tangential implantation (posterior to anterior) in Opitz *et al.* Third, we calculated the raw electric fields at the difference to Opitz *et al.*, who calculated the mean normalized voltages. Contrary to our finding in the entire brain, our experiment (Patient #0) exhibited mean EF magnitudes in deep brain structures at 1 Hz 11% higher than at 300 Hz. So, our EF magnitudes in the deep brain structures at 300 Hz are representative of the fields generated by low frequency tACS [86,87] or tDCS studies [7].

Finally, the influence of TES montage was also evaluated in one patient only. Thus, our data showing different EF magnitudes according to TES montages need to be confirmed and extended with additional individual brain tested. In doing so, this investigation would help validate computational studies and establish guidelines for bipolar TES electrodes placement.

CRediT authorship contribution statement

Samuel Louviot: Methodology, Software, Investigation, Formal analysis, Writing – original draft. **Louise Tyvaert:** Resources, Writing – review & editing, Clinical, Validation. **Louis G. Maillard:** Resources, Writing – review & editing, Clinical, Validation. **Sophie Colnat-Coulbois:** Resources, Writing – review & editing, Clinical, Validation. **Jacek Dmochowski:** Conceptualization, Methodology, Software, Resources, Formal analysis, Writing – review & editing, Funding acquisition. **Laurent Koessler:** Conceptualization, Methodology, Resources, Validation, Writing – review & editing, Funding acquisition, Supervision.

Declaration of competing interest

We wish to draw the attention of the Editor to the following facts which may be considered as potential conflicts of interest: Jacek Dmochowski has patent rights to HD-tDCS technology.

We confirm that the manuscript has been read and approved by all named authors and that there are no other persons who satisfied the criteria for authorship but are not listed. We further confirm that the order of authors listed in the manuscript has been approved by all of us.

Acknowledgements

This study was funded by grants from the Lorraine University of Excellence Initiative (France) and the City College of New-York (USA) (DrEAM mobility grant) and the Rotary Club of Nancy (France). The authors thank Mr. Pierre Riff for the data acquisition and Bruno Rossion for his comments.

Appendix A. Supplementary data

Supplementary data to this article can be found online at https://doi.org/10.1016/j.brs.2021.11.001.

References

[1] Stagg CJ, Nitsche MA. Physiological basis of transcranial direct current stimulation. Neuroscientist 2011;17:37–53. https://doi.org/10.1177/1073858410386614.
[2] Reato D, Rahman A, Bikson M, Parra LC. Effects of weak transcranial alternating current stimulation on brain activity—a review of known mechanisms from animal studies. Front Hum Neurosci 2013;7:1–8. https://doi.org/10.3389/fnhum.2013.00687.
[3] Filmer HL, Dux PE, Mattingley JB. Applications of transcranial direct current stimulation for understanding brain function. Trends Neurosci 2014;37:742–53. https://doi.org/10.1016/j.tins.2014.08.003.
[4] Boggio PS, Ferrucci R, Rigonatti SP, Covre P, Nitsche M, Pascual-Leone A, et al. Effects of transcranial direct current stimulation on working memory in patients with Parkinson's disease. J Neurol Sci 2006;249:31–8. https://doi.org/10.1016/j.jns.2006.05.062.
[5] Schlaug G, Renga V, Nair D. Transcranial direct current stimulation in stroke recovery. Arch Neurol 2008;65:1571–6. https://doi.org/10.1001/archneur.65.12.1571.
[6] Tortella G. Transcranial direct current stimulation in psychiatric disorders. World J Psychiatr 2015;5:88. https://doi.org/10.5498/wjp.v5.i1.88.
[7] Lefaucheur JP. A comprehensive database of published tDCS clinical trials (2005–2016). Neurophysiol Clin 2016;46:319–98. https://doi.org/10.1016/j.neucli.2016.10.002.
[8] Jackson MP, Rahman A, Lafon B, Kronberg G, Ling D, Parra LC, et al. Animal models of transcranial direct current stimulation: methods and mechanisms. Clin Neurophysiol 2016;127:3425–54. https://doi.org/10.1016/j.clinph.2016.08.016.
[9] Bikson M, Inoue M, Akiyama H, Deans JK, Fox JE, Miyakawa H, et al. Effect of uniform extracellular DC electric fields on excitability in rat hippocampal slices in vitro. J Physiol 2004;557:175–90. https://doi.org/10.1113/jphysiol.2003.055772.
[10] Jefferys JG. Influence of electric fields on the excitability of granule cells in Guinea-pig hippocampal slices. J Physiol 1981;319:143–52. https://doi.org/10.1113/jphysiol.1981.sp013897.
[11] Francis JT, Gluckman BJ, Schiff SJ. Sensitivity of neurons to weak electric fields. J Neurosci 2003;23:7255–61. https://doi.org/10.1523/JNEUROSCI.23-19-07255.2003.
[12] Rahman A, Reato D, Arlotti M, Gasca F, Datta A, Parra LC, et al. Cellular effects of acute direct current stimulation: somatic and synaptic terminal effects. J Physiol 2013;591:2563–78. https://doi.org/10.1113/jphysiol.2012.247171.
[13] Reato D, Bikson M, Parra LC. Lasting modulation of in vitro oscillatory activity with weak direct current stimulation. J Neurophysiol 2015;113:1334–41. https://doi.org/10.1152/jn.00208.2014.
[14] Reato D, Rahman A, Bikson M, Parra LC. Low-intensity electrical stimulation affects network dynamics by modulating population rate and spike timing. J Neurosci 2010;30:15067–79. https://doi.org/10.1523/JNEUROSCI.2059-10.2010.
[15] Gluckman BJ, Neel EJ, Netoff TI, Ditto WL, Spano ML, Schiff SJ. Electric field suppression of epileptiform activity in hippocampal slices. J Neurophysiol 1996;76:4202–5. https://doi.org/10.1152/jn.1996.76.6.4202.
[16] Parra LC, Bikson M. Model of the effect of extracellular fields on spike time coherence. In: Annu. Int. Conf. IEEE Eng. Med. Biol. - Proc., vol. 26 VI, Conf Proc IEEE Eng med Biol Soc; 2004. p. 4584–7. https://doi.org/10.1109/iembs.2004.1404271.
[17] Terzuolo CA, Bullock TH. Measurement of imposed voltage gradient adequate to modulate neuronal firing. Proc Natl Acad Sci Unit States Am 1956;42:687–94. https://doi.org/10.1073/pnas.42.9.687.
[18] Deans JK, Powell AD, Jefferys JGR. Sensitivity of coherent oscillations in rat hippocampus to AC electric fields. J Physiol 2007;583:555–65. https://doi.org/10.1113/jphysiol.2007.137711.
[19] Liu A, Vöröslakos M, Kronberg G, Henin S, Krause MR, Huang Y, et al. Immediate neurophysiological effects of transcranial electrical stimulation. Nat Commun 2018;9. https://doi.org/10.1038/s41467-018-07233-7.
[20] Miranda PC, Lomarev M, Hallett M. Modeling the current distribution during transcranial direct current stimulation. Clin Neurophysiol 2006;117:1623–9. https://doi.org/10.1016/j.clinph.2006.04.009.
[21] Wagner T, Fregni F, Fecteau S, Grodzinsky A, Zahn M, Pascual-Leone A. Transcranial direct current stimulation: a computer-based human model study. Neuroimage 2007;35:1113–24. https://doi.org/10.1016/j.neuroimage.2007.01.027.
[22] Datta A, Bansal V, Diaz J, Patel J, Reato D, Bikson M. Gyri-precise head model of transcranial direct current stimulation: improved spatial focality using a ring electrode versus conventional rectangular pad. Brain Stimul 2009;2. https://doi.org/10.1016/j.brs.2009.03.005.
[23] Ruffini G, Wendling F, Merlet I, Molaee-Ardekani B, Mekonnen A, Salvador R, et al. Transcranial current brain stimulation (tCS): models and technologies. IEEE Trans Neural Syst Rehabil Eng 2013;21:333–45. https://doi.org/10.1109/TNSRE.2012.2200046.
[24] Saturnino GB, Antunes A, Thielscher A. On the importance of electrode parameters for shaping electric field patterns generated by tDCS. Neuroimage 2015;120:25–35. https://doi.org/10.1016/j.neuroimage.2015.06.067.
[25] Ramaraju S, Roula MA, McCarthy PW. Modelling the effect of electrode displacement on transcranial direct current stimulation (tDCS). J Neural Eng 2018;15. https://doi.org/10.1088/1741-2552/aa8d8a.
[26] Opitz A, Yeagle E, Thielscher A, Schroeder C, Mehta AD, Milham MP. On the importance of precise electrode placement for targeted transcranial electric stimulation. Neuroimage 2018;181:560–7. https://doi.org/10.1016/j.neuroimage.2018.07.027.
[27] Huang Y, Parra LC. Can transcranial electric stimulation with multiple electrodes reach deep targets? Brain Stimul 2019;12:30–40. https://doi.org/10.1016/j.brs.2018.09.010.
[28] Bikson M, Dmochowski J. What it means to go deep with non-invasive brain stimulation. Clin Neurophysiol 2020;131:752–4. https://doi.org/10.1016/j.clinph.2019.12.003.
[29] Krause MR, Vieira PG, Csorba BA, Pilly PK, Pack CC. Transcranial alternating current stimulation entrains single-neuron activity in the primate brain. Proc Natl Acad Sci U S A 2019;116:5747–55. https://doi.org/10.1073/pnas.1815958116.
[30] Vieira PG, Krause MR, Pack CC. tACS entrains neural activity while somatosensory input is blocked. PLoS Biol 2020;18. https://doi.org/10.1371/journal.pbio.3000834.
[31] Tekturk P, Erdogan ET, Kurt A, Vanli-yavuz EN, Ekizoglu E, Kocagoncu E, et al. The effect of transcranial direct current stimulation on seizure frequency of patients with mesial temporal lobe epilepsy with hippocampal sclerosis. Clin Neurol Neurosurg 2016;149:27–32. https://doi.org/10.1016/j.clineuro.2016.07.014.
[32] San-Juan D, Espinoza López DA, Vázquez Gregorio R, Trenado C, Fernández-González Aragón M, Morales-Quezada L, et al. Transcranial direct current stimulation in mesial temporal lobe epilepsy and hippocampal sclerosis. Brain Stimul 2017;10:28–35. https://doi.org/10.1016/j.brs.2016.08.013.
[33] Assenza G, Campana C, Assenza F, Pellegrino G, Di Pino G, Fabrizio E, et al. Cathodal transcranial direct current stimulation reduces seizure frequency in adults with drug-resistant temporal lobe epilepsy: a sham controlled study. Brain Stimul 2017;10:333–5. https://doi.org/10.1016/j.brs.2016.12.005.
[34] Khatoun A, Asamoah B, Laughlin MM. How does transcranial alternating current stimulation entrain single-neuron activity in the primate brain? Proc Natl Acad Sci U S A 2019;116:22438–9. https://doi.org/10.1073/pnas.1912927116.
[35] Asamoah B, Khatoun A, Mc Laughlin M. tACS motor system effects can be caused by transcutaneous stimulation of peripheral nerves. Nat Commun 2019;10:266. https://doi.org/10.1038/s41467-018-08183-w.
[36] Adair D, Truong D, Esmaeilpour Z, Gebodh N, Borges H, Ho L, et al. Electrical stimulation of cranial nerves in cognition and disease. Brain Stimul 2020;13:717–50. https://doi.org/10.1016/j.brs.2020.02.019.
[37] Vanneste S, Mohan A, Yoo H Bin, Huang Y, Luckey AM, Lauren McLeod S, et al. The peripheral effect of direct current stimulation on brain circuits involving memory. Sci Adv 2020;6:1–19. https://doi.org/10.1126/SCIADV.AAX9538.
[38] Underwood E. Cadaver study challenges brain stimulation methods: unusual test of transcranial stimulation shows that little electrical current penetrates the skull. Science 2016;352(80):397. https://doi.org/10.1126/science.352.6284.397.
[39] Vöröslakos M, Takeuchi Y, Brinyiczki K, Zombori T, Oliva A, Fernández-Ruiz A, et al. Direct effects of transcranial electric stimulation on brain circuits in rats and humans. Nat Commun 2018;9. https://doi.org/10.1038/s41467-018-02928-3.
[40] Lafon B, Henin S, Huang Y, Friedman D, Melloni L, Thesen T, et al. Low frequency transcranial electrical stimulation does not entrain sleep rhythms

measured by human intracranial recordings. Nat Commun 2017;8:1199. https://doi.org/10.1038/s41467-017-01045-x.
[41] Huang Y, Liu AA, Lafon B, Friedman D, Dayan M, Wang X, et al. Measurements and models of electric fields in the in vivo human brain during transcranial electric stimulation. Elife 2017;6:1–27. https://doi.org/10.7554/eLife.18834.
[42] Akhtari M, Bryant HC, Mamelak AN, Flynn ER, Heller L, Shih JJ, et al. Conductivities of three-layer line human skull. Brain Topogr 2002;14:151–67. https://doi.org/10.1023/A:1014590923185.
[43] Dasilva AF, Mendonca ME, Zaghi S, Lopes M, Dossantos MF, Spierings EL, et al. TDCS-induced analgesia and electrical fields in pain-related neural networks in chronic migraine. Headache 2012;52:1283–95. https://doi.org/10.1111/j.1526-4610.2012.02141.x.
[44] DaSilva AF, Truong DQ, DosSantos MF, Toback RL, Datta A, Bikson M. State-of-art neuroanatomical target analysis of high-definition and conventional tDCS montages used for migraine and pain control. Front Neuroanat 2015;9:89. https://doi.org/10.3389/fnana.2015.00089.
[45] Gomez-Tames J, Asai A, Hirata A. Significant group-level hotspots found in deep brain regions during transcranial direct current stimulation (tDCS): a computational analysis of electric fields. Clin Neurophysiol 2020;131:755–65. https://doi.org/10.1016/j.clinph.2019.11.018.
[46] Opitz A, Falchier A, Yan CG, Yeagle EM, Linn GS, Megevand P, et al. Spatiotemporal structure of intracranial electric fields induced by transcranial electric stimulation in humans and nonhuman primates. Sci Rep 2016;6:1–11. https://doi.org/10.1038/srep31236.
[47] Chhatbar PY, Kautz SA, Takacs I, Rowland NC, Revuelta GJ, George MS, et al. Evidence of transcranial direct current stimulation-generated electric fields at subthalamic level in human brain in vivo. Brain Stimul 2018;11:727–33. https://doi.org/10.1016/j.brs.2018.03.006.
[48] Ruhnau P, Rufener KS, Heinze HJ, Zaehle T. Sailing in a sea of disbelief: in vivo measurements of transcranial electric stimulation in human subcortical structures. Brain Stimul 2018;11:241–3. https://doi.org/10.1016/j.brs.2017.09.015.
[49] Datta A, Bikson M, Fregni F. Transcranial direct current stimulation in patients with skull defects and skull plates: high-resolution computational FEM study of factors altering cortical current flow. Neuroimage 2010;52:1268–78. https://doi.org/10.1016/j.neuroimage.2010.04.252.
[50] Isnard J, Taussig D, Bartolomei F, Bourdillon P, Catenoix H, Chassoux F, et al. French guidelines on stereoelectroencephalography (SEEG). Neurophysiol Clin 2018;48:5–13. https://doi.org/10.1016/j.neucli.2017.11.005.
[51] Salado AL, Koessler L, DeMijolla G, Schmitt E, Vignal JP, Civit T, et al. sEEG is a safe procedure for a comprehensive anatomic exploration of the insula: a retrospective study of 108 procedures representing 254 transopercular insular electrodes. Oper Neurosurg 2018;14:1–8. https://doi.org/10.1093/ons/opx106.
[52] Almukhtar A, Ju X, Khambay B, McDonald J, Ayoub A. Comparison of the accuracy of voxel based registration and surface based registration for 3D assessment of surgical change following orthognathic surgery. PLoS One 2014;9:1–6. https://doi.org/10.1371/journal.pone.0093402.
[53] Jacques C, Jonas J, Maillard L, Colnat-Coulbois S, Rossion B, Koessler L. Fast periodic visual stimulation to highlight the relationship between human intracerebral recordings and scalp electroencephalography. Hum Brain Mapp 2020;41:2373–88. https://doi.org/10.1002/hbm.24952.
[54] Brigo F, Cicero R, Fiaschi A, Bongiovanni LG. The breach rhythm. Clin Neurophysiol 2011;122:2116–20. https://doi.org/10.1016/j.clinph.2011.07.024.
[55] Tadel F, Baillet S, Mosher JC, Pantazis D, Leahy RM. Brainstorm: a user-friendly application for MEG/EEG analysis. Comput Intell Neurosci 2011;2011:13. https://doi.org/10.1155/2011/879716.
[56] Koessler L, Maillard L, Benhadid A, Vignal JP, Felblinger J, Vespignani H, et al. Automated cortical projection of EEG sensors: anatomical correlation via the international 10-10 system. Neuroimage 2009;46:64–72. https://doi.org/10.1016/j.neuroimage.2009.02.006.
[57] Faria P, Hallett M, Miranda PC. A finite element analysis of the effect of electrode area and inter-electrode distance on the spatial distribution of the current density in tDCS. J Neural Eng 2011;8. https://doi.org/10.1088/1741-2560/8/6/066017.
[58] Datta A, Elwassif M, Battaglia F, Bikson M. Transcranial current stimulation focality using disc and ring electrode configurations: FEM analysis. J Neural Eng 2008;5:163–74. https://doi.org/10.1088/1741-2560/5/2/007.
[59] Frigo M, Johnson SG. The design and implementation of FFTW3. Proc IEEE 2005;93:216–31. https://doi.org/10.1109/JPROC.2004.840301.
[60] Hofmanis J, Caspary O, Louis-Dorr V, Maillard L. Automatic depth electrode localization in intracranial space. In: 4th Int. Conf. Bio-inspired Syst. Signal process. Biosignals 2011. Rome, Italy: CDROM; 2011.
[61] Ashburner J, Friston KJ. Unified segmentation. Neuroimage 2005;26:839–51. https://doi.org/10.1016/j.neuroimage.2005.02.018.
[62] Koessler L, Colnat-Coulbois S, Cecchin T, Hofmanis J, Dmochowski JP, Norcia AM, et al. In-vivo measurements of human brain tissue conductivity using focal electrical current injection through intracerebral multicontact electrodes. Hum Brain Mapp 2017;38:974–86. https://doi.org/10.1002/hbm.23431.
[63] Rolls ET, Huang CC, Lin CP, Feng J, Joliot M. Automated anatomical labelling atlas 3. Neuroimage 2020:206. https://doi.org/10.1016/j.neuroimage.2019.116189.
[64] Amidror I. Scattered data interpolation methods for electronic imaging systems: a survey. J Electron Imag 2002;11:157. https://doi.org/10.1117/1.1455013.
[65] Benar CG, Gotman J. Modeling of post-surgical brain and skull defects in the EEG inverse problem with boundary element models. Neuroimage 2000;11. https://doi.org/10.1016/s1053-8119(00)91564-7.
[66] Lau S, Güllmar D, Flemming L, Grayden DB, Cook MJ, Wolters CH, et al. Skull defects in finite element head models for source reconstruction from magnetoencephalography signals. Front Neurosci 2016;10:141. https://doi.org/10.3389/fnins.2016.00141.
[67] Jacques C, Jonas J, Maillard L, Colnat-Coulbois S, Rossion B, Koessler L. Fast periodic visual stimulation to highlight the relationship between human intracerebral recordings and scalp electroencephalography. Hum Brain Mapp 2020:1–16. https://doi.org/10.1002/hbm.24952.
[68] Koessler L, Cecchin T, Colnat-Coulbois S, Vignal JP, Jonas J, Vespignani H, et al. Catching the invisible: mesial temporal source contribution to simultaneous EEG and SEEG recordings. Brain Topogr 2014;28:5–20. https://doi.org/10.1007/s10548-014-0417-z.
[69] Gavaret M, Dubarry AS, Carron R, Bartolomei F, Trébuchon A, Bénar CG. Simultaneous SEEG-MEG-EEG recordings Overcome the SEEG limited spatial sampling. Epilepsy Res 2016;128:68–72. https://doi.org/10.1016/j.eplepsyres.2016.10.013.
[70] Kato I, Innami K, Sakuma K, Miyakawa H, Inoue M, Aonishi T. Frequency-dependent entrainment of spontaneous Ca transients in the dendritic tufts of CA1 pyramidal cells in rat hippocampal slice preparations by weak AC electric field. Brain Res Bull 2019;153:202–13. https://doi.org/10.1016/j.brainresbull.2019.08.009.
[71] Khan A, Wang X, Ti CHE, Tse CY, Tong KY. Anodal transcranial direct current stimulation of anterior cingulate cortex modulates subcortical brain regions resulting in cognitive enhancement. Front Hum Neurosci 2020;14:584136. https://doi.org/10.3389/fnhum.2020.584136.
[72] Verveer I, Hill AT, Franken IHA, Yücel M, van Dongen JDM, Segrave R. Modulation of Control: can HD-tDCS targeting the dACC reduce impulsivity? Brain Res 2021:1756. https://doi.org/10.1016/j.brainres.2021.147282.
[73] Fernández-Corazza M, Turovets S, Luu P, Anderson E, Tucker D. Transcranial electrical neuromodulation based on the reciprocity principle. Front Psychiatr 2016;7:1–19. https://doi.org/10.3389/fpsyt.2016.00087.
[74] Dmochowski JP, Koessler L, Norcia AM, Bikson M, Parra LC. Optimal use of EEG recordings to target active brain areas with transcranial electrical stimulation. Neuroimage 2017;157:69–80. https://doi.org/10.1016/j.neuroimage.2017.05.059.
[75] Nitsche MA, Bikson M. Extending the parameter range for tDCS: safety and tolerability of 4 mA stimulation. Brain Stimul 2017;10:541–2. https://doi.org/10.1016/j.brs.2017.03.002.
[76] Chhatbar PY, Chen R, Deardorff R, Dellenbach B, Kautz SA, George MS, et al. Safety and tolerability of transcranial direct current stimulation to stroke patients – A phase I current escalation study. Brain Stimul 2017;10:553–9. https://doi.org/10.1016/j.brs.2017.02.007.
[77] Khadka N, Borges H, Paneri B, Kaufman T, Nassis E, Zannou AL, et al. Adaptive current tDCS up to 4 mA. Brain Stimul 2020;13:69–79. https://doi.org/10.1016/j.brs.2019.07.027.
[78] Dmochowski JP, Datta A, Bikson M, Su Y, Parra LC. Optimized multi-electrode stimulation increases focality and intensity at target. J Neural Eng 2011;8. https://doi.org/10.1088/1741-2560/8/4/046011.
[79] Rawji V, Ciocca M, Zacharia A, Soares D, Truong D, Bikson M, et al. tDCS changes in motor excitability are specific to orientation of current flow. Brain Stimul 2018;11:289–98. https://doi.org/10.1016/j.brs.2017.11.001.
[80] Faria P, Leal A, Miranda PC. Comparing different electrode configurations using the 10-10 international system in tDCS: a finite element model analysis. In: Proc. 31st Annu. Int. Conf. IEEE Eng. Med. Biol. Soc. Eng. Futur. Biomed. EMBC 2009, vol. 2009. IEEE Computer Society; 2009. p. 1596–9. https://doi.org/10.1109/IEMBS.2009.5334121.
[81] Gomez-Tames J, Asai A, Mikkonen M, Laakso I, Tanaka S, Uehara S, et al. Group-level and functional-region analysis of electric-field shape during cerebellar transcranial direct current stimulation with different electrode montages. J Neural Eng 2019;16. https://doi.org/10.1088/1741-2552/ab0ac5.
[82] Laakso I, Tanaka S, Koyama S, De Santis V, Hirata A. Inter-subject variability in electric fields of motor cortical tDCS. Brain Stimul 2015;8:906–13. https://doi.org/10.1016/j.brs.2015.05.002.
[83] Lee C, Jung YJ, Lee SJ, Im CH. COMETS2: an advanced MATLAB toolbox for the numerical analysis of electric fields generated by transcranial direct current stimulation. J Neurosci Methods 2017;277:56–62. https://doi.org/10.1016/j.jneumeth.2016.12.008.
[84] Saturnino GB, Madsen KH, Thielscher A. Electric field simulations for transcranial brain stimulation using FEM: an efficient implementation and error analysis. J Neural Eng 2019;16. https://doi.org/10.1088/1741-2552/ab41ba.
[85] Puonti O, Saturnino GB, Madsen KH, Thielscher A. Value and limitations of intracranial recordings for validating electric field modeling for transcranial brain stimulation. Neuroimage 2020;208:116431. https://doi.org/10.1016/j.neuroimage.2019.116431.
[86] Elyamany O, Leicht G, Herrmann CS, Mulert C. Transcranial alternating current stimulation (tACS): from basic mechanisms towards first applications in psychiatry. Eur Arch Psychiatr Clin Neurosci 2021;271:135–56. https://doi.org/10.1007/s00406-020-01209-9.
[87] Antal A, Paulus W. Transcranial alternating current stimulation (tACS). Front Hum Neurosci 2013;7:1–4. https://doi.org/10.3389/fnhum.2013.00317.

Abstract

From the electric fish used by the Romans to today's variable current generators, via the Volta battery in the 19th century, human has always spontaneously applied an electric current to the head of patients for therapeutic purposes. However, transcranial electrical stimulation (TES), which consist of applying a weak current through electrodes put on the scalp surface, only became popular at the beginning of the 21st century. The effects of TES are directly related to the electric fields generated, which modify neuronal activity. These effects have been extensively studied in-vitro and intracerebral in-vivo in animals. In humans, effects have also been observed in surface EEG, or at the behavioral level or in the expression of a neurological pathology studied. However, despite these results, there are still debates as to the real effects of TES on cognition or on pathology. One of the main arguments is that the stimulation intensity routinely used (1 to 2 mA) cannot deliver a sufficient electric field on site to induce a modulation of the neuronal electrical activity (1V/m). Another argument is that there are cognitive biases induced by electrical stimulation in behavioral studies. These debates are induced by a lack of knowledge both at the biophysical level (propagation of intracerebral electric fields in humans) and at the level of electrophysiological expression of the pathology or of the intracerebral cognitive response in humans in vivo. This is mainly due to the scientific and technical obstacles which are (1) The difficulty of measuring an intracerebral electric field in humans in-vivo simultaneously with a TES. (2) The intracerebral recording of pathology's electrophysiological expression during a TES. (3) The intracerebral recording of an electrophysiological response associated with a cognitive function during a TES via a robust protocol thus avoiding cognitive biases and test-re test effects.

It is in this context that this thesis will attempt to answer the following three scientific questions: (1) Is it possible to generate a sufficient intracerebral electric field during a TES? (2) Is it possible to modulate the electrophysiological activity of a pathology via TES? (3) Is it possible to modulate the electrophysiological activity associated with a cognitive function (face perception) via a TES?

The strength and originality of this thesis is based on multiscale recordings (surface and intracerebral EEG (SEEG)) concomitant with TES in patients with focal refractory epilepsy. The study will first focus on the intracerebral recording of the signal decay during transcranial alternative current stimulation (tACS) which will allow to calculate the electric field generated in deep structures. In a second step, the study will focus on the intracerebral measurement of epileptic biomarkers (intercritical paroxysmal discharges) before, during and after transcranial direct current stimulation (tDCS). In a third step, the study will focus on the measurement of electrophysiological biomarkers associated with the cognitive task of face recognition during a Fast Periodic Visual Stimulation (FPVS) before, during and after tDCS, thus overcoming the test-retest effect and the cognitive bias generated by the sensation during stimulation.

Résumé

Du poisson électrique utilisé par les Romains aux générateurs de courant variable d'aujourd'hui en passant par la pile de Volta au XIXe siècle, l'Homme a depuis toujours et spontanément appliqué un courant électrique sur la tête de patients dans un but thérapeutique. Cependant, la stimulation électrique transcrânienne (SET), qui consiste à appliquer un faible courant par le biais d'électrodes placées à la surface du cuir chevelu, n'est devenue populaire qu'au début du XXIe siècle. Les effets de la SET sont directement reliés aux champs électriques générés modifiant ainsi l'activité neuronale. Ces effets ont largement été étudiés in-vitro et en intracérébral in-vivo chez l'animal. Chez l'Homme, des effets ont également été observés en EEG de surface, ou au niveau comportemental ou encore au niveau de l'expression d'une pathologie neurologique étudiée. Or, malgré ces résultats, il subsiste des débats quant aux réels effets de la SET en cognition ou en clinique. Un des principaux arguments avancés est que l'intensité de stimulation utilisée en routine (1 à 2 mA) ne peut délivrer un champ électrique suffisant sur site pour induire une modulation de l'activité électrique neuronale (1V/m). Un autre argument consiste à dire qu'il existe des biais cognitifs induit par la stimulation électrique dans les études comportementales. Ces débats sont induits par un manque de connaissances tant au niveau biophysique (propagation des champs électriques intracérébraux chez l'Homme) qu'au niveau de l'expression électrophysiologique de la pathologie ou encore de la réponse cognitive en intracérébral chez l'Homme in-vivo. Cela est principalement dû aux verrous scientifiques et techniques que sont (1) La difficulté de mesurer un champs électrique intracérébral chez l'Homme in-vivo en simultané à une SET. (2) L'enregistrement intracérébral de l'expression électrophysiologique d'une pathologie durant une SET. (3) L'enregistrement intracérébral d'une réponse électrophysiologique associée à une fonction cognitive lors d'une SET via un protocole robuste évitant ainsi les biais cognitifs et les effets test-re test.

Ainsi, c'est dans ce contexte que s'inscrit cette thèse et tentera de répondre aux trois questions scientifiques suivantes : (1) Est-il possible de générer un champ électrique intracérébral suffisant lors d'une SET ? (2) Est-il possible de moduler l'activité électrophysiologique d'une pathologie via une SET ? (3) Est-il possible de moduler l'activité électrophysiologique associée à une fonction cognitive (perception des visages) via une SET ?

La force et l'originalité de la thèse reposent sur l'enregistrement multi-échelle (EEG de surface et intracérébrale (SEEG)) concomitant à la SET chez des patients atteint d'épilepsie focale pharmacorésistante. L'étude portera dans un premier temps sur l'enregistrement en intracérébral de la décroissance du signal lors d'une stimulation transcrânienne à courant alternatif (tACS) qui permettra de calculer le champ électrique généré dans des structures profondes. Dans un deuxième temps, l'étude portera sur la mesure intracérébrale de biomarqueurs épileptiques (décharges paroxystiques intercritiques) avant, pendant et après une stimulation transcrânienne à courant continu (tDCS). Dans un troisième temps, l'étude portera sur la mesure de biomarqueur électrophysiologique associé à la tâche cognitive de reconnaissance des visages lors d'une Fast Periodic Visual Stimulation (FPVS) avant, pendant et après une tDCS permettant ainsi de s'affranchir de l'effet test-retest et du biais cognitif généré par la sensation lors de la stimulation.